Understanding human mononuclear phagocyte ontogeny using human induced pluripotent stem cells (iPSCs)

Julian Buchrieser

Sir William Dunn School of Pathology
Lincoln College

University of Oxford

A thesis submitted for the degree of

Doctor of Philosophy

Michaelmas 2016

Acknowledgements

I would like to give my deepest gratitude to Prof. William James and Dr Kenny Moore, my supervisors, for their help and guidance throughout the course of these four years and for their meticulous and insightful feedback on the writing of this thesis. I would also like to give a special thanks to Dr Quin Wills for his helpful insight in transcriptome analysis, Dr Walther Hänseler for kindly letting me use some of his transcriptomic data, Dr Rowan Flynn for his advice on CRISPR/Cas9 gene knock-out, and Jane Vowles, Cathy Browne and Lilly Couper for their introduction to human stem cell culture.

In addition to already cited laboratory members I would like to express my gratitude to all current and previous members of the James laboratory who have made my day-to-day life in the laboratory very enjoyable and provided invaluable assistance; Dr Sally Cowley, Cecilia Lee, Benjamin Dodsworth, Damien Warner, Dr Maria Jose Oliva Martin, Olga Perestenko, Dr Serena Barral, Dr Darshan Baskaran and Dr Federica Rinaldi.

I am also grateful to the Medical Research Council and the Heatley Merck Sharpe and Dohme studentship for the funding which made this D.Phil. possible. I would also like to thank Keith A. Gillow, Sam Evans and John McManigle for sharing their beautiful LaTeXtemplate.

Finally I would like to express my love to Julie for being by my side and supporting me and thank my parents Carmen and Roland and my sister Yasmin for their support and encouragement throughout my study and life.

Abstract

Tissue-resident macrophages (Mϕ) such as microglia, Kupffer and Langerhans cells derive from Myb-independent yolk sac (YS) progenitors generated before the emergence of hematopoietic stem cells (HSCs). Myb-independent YS-derived resident Mϕs self-renew locally, independently of circulating adult monocytes and HSCs. In contrast, adult blood monocytes as well as infiltrating, gut and dermal Mϕs derive from Myb-dependent HSCs and are less proliferative. These findings are derived from the mouse, using gene knock-outs and lineage tracing, but their applicability to human development has not been formally demonstrated. Here I use a human pluripotent stem cell (hPSC) differentiation model of hematopoiesis, capable of monocyte/Mϕ production over prolonged periods of time, as a tool to investigate human mononuclear phagocyte ontogeny. Using a transcriptomic approach I showed that hiPSC-derived monocytes/Mϕs (iPS-Mo/Mϕs) produced early in differentiation (first weeks) are more proliferative and less immunologically mature than iPS-Mo/Mϕs produced at a later time point. I therefore hypothesised either that iPS-Mo/Mϕs only become fully mature after several weeks of differentiation or that there are two developmentally distinct waves of Mϕs produced over time. By comparing the transcription profile of iPS-Mo/Mϕs to that of primary adult blood monocytes and fetal microglia I then showed that early and late iPS-Mo/Mϕs were transcriptionally closer to fetal microglia than to adult blood monocytes. To further investigate if iPS-Mo/Mϕs are indeed of the same developmental origin as MYB-independent Mϕs such as microglia, I used a CRISPR-Cas9 knock-out strategy to show for the first time, that human iPS-Mo/Mϕs develop in a MYB-independent, RUNX1 and SPI1 (PU.1)-dependent fashion. This result makes human iPS-Mo/Mϕs developmentally related to, and a good model for, MYB-independent tissue-resident Mϕs such as alveolar and kidney Mϕs, microglia, Kupffer and Langerhans cells. Interestingly, while MYB was not required for the generation of iPS-Mo/Mϕs, its knock-out resulted in an increase in iPS-Mo/Mϕ production. To investigate this increase I developed two methods for quantifying the differentiation bottleneck occurring during hiPSC differentiation to iPS-Mo/Mϕs. Those techniques highlighted a potential increase in progenitor cell generation in MYB KO cells and thus lay foundation to improve our technical understanding of EB differentiation and will enable enhanced manipulation of the EB model.

Contents

List of Figures **xiii**

List of Tables **xv**

List of Abbreviations **xvii**

1 Introduction **1**

1.1 Macrophage function and diversity 2

1.2 Mammalian hematopoietic development 4

1.2.1 Mouse hematopoietic development 4

1.2.1.1 *In vivo* studies of mouse hematopoietic development 4

1.2.1.2 Primitive precursors, EMPs and HSCs 6

1.2.1.3 Transcription factors MYB, RUNX1 and PU.1 . . . 7

1.2.1.4 Mouse embryonic stem cells (mESC) differentiation 8

1.2.2 Human hematopoietic development 9

1.2.2.1 *In vivo* 9

1.2.2.2 Human *in vitro* hPSC hematopoietic development . 10

1.2.2.2.1 hPSC as a tool for studying development . 10

1.2.2.2.2 hPSC hematopoiesis - primitive versus definitive 12

1.3 Tissue-resident Mϕ ontogeny in the mouse 17

1.3.1 Early concepts of Mϕ ontogeny - The unified mononuclear phagocytic system 17

1.3.2 Contribution of YS primitive Mϕs to tissue-resident Mϕ populations 17

1.3.3 Contribution of EMP-derived monocytes and Mϕs to tissue-resident Mϕ populations 19

1.3.4 Contribution of fetal HSCs to tissue-Resident Mϕ populations 19

1.3.5 Nomenclature of macrophage development 20

1.3.5.1 MYB-independent and MYB-dependent hematopoiesis 20

1.3.5.2 Monocytes and Mϕs 20

1.3.6 Maintenance of tissue-resident Mϕ populations in disease and homeostasis 22

1.3.6.1 Mϕ proliferation . . . 22
1.3.6.2 Homeostatic control of proliferation and monocyte recruitment . . . 23
1.3.6.2.1 Intestinal, Dermal Mϕs and LCs . . . 23
1.3.6.2.2 Microglia . . . 24
1.3.6.2.3 Alveolar and Cardiac Mϕs and Kupffer cells 24
1.3.7 How different are these Mϕ populations? . . . 25
1.4 Tissue-resident Mϕ ontogeny in the human . . . 27
1.4.1 *In vivo* Mϕ ontogeny . . . 27
1.4.2 hPSC Mϕ protocols . . . 28
1.4.3 Nomenclature - hPSC-derived Monocytes and Mϕs . . . 29
1.4.4 Pluripotent stem cell-derived Mϕ ontogeny . . . 29

2 General Materials and Methods 31
2.1 Ethics Statements for use of Adult Blood and Stem Cell Lines . . . 31
2.2 hESC/hiPSC culture . . . 32
2.3 iPS-Mo/Mϕ differentiation . . . 32
2.3.1 EB formation . . . 32
2.3.2 iPS-Mo/Mϕ differentiation (iPS-Mo/Mϕ Factories) . . . 33
2.4 Cell count and viability . . . 34
2.5 Cell proliferation assay . . . 34
2.6 Eosin and Methylene-Blue staining . . . 34
2.7 Flow cytometry staining and antibodies . . . 34
2.8 Lentiviral production . . . 35
2.9 EB diameter measurement . . . 35

3 Transcriptional & functional characterization of iPS-Mo/Mϕs over time 37
3.1 Introduction . . . 38
3.2 Materials and methods . . . 41
3.2.1 Transcriptome sample preparation . . . 41
3.2.2 Transcriptome analysis . . . 41
3.2.2.1 Data import, log2 transformation and normalization 42
3.2.2.2 Generating a ranked gene list . . . 43
3.2.2.3 Pre-ranked Gene Ontogeny (GO) GSEA . . . 44
3.2.2.4 GSEA result filtering and heatmap generation . . . 44
3.2.2.5 Study of individual genes within a gene set . . . 45
3.2.2.6 Metadata analysis . . . 48
3.3 Results . . . 51
3.3.1 Monocyte production, proliferation and morphology over time 51

3.3.2 Transcriptomic data analysis 56
3.3.2.1 Initial QC of data 56
3.3.2.2 Differential transcript expression study using RP approach 56
3.3.2.3 Closer look at the individual genes in a gene set . . 60
3.3.2.3.1 Cell cycle genes are progressively downregulated between H1 and H5 61
3.3.2.3.2 Viral genome replication related genes are high early on and get downregulated over time 61
3.3.2.3.3 Adaptative immune response genes get progressively upregulated 62
3.3.2.3.4 Summary 63
3.3.3 iPS-Mo/Mϕs are more similar to fetal microglia than adult blood monocytes 69
3.3.3.1 Comparative MDS vs blood monocytes and fetal microglia 69
3.3.3.2 iPS-Mo/Mϕ have higher proliferation gene expression than fetal microglia and blood monocytes . . . 70
3.3.3.3 H1 iPS-Mo/Mϕ have lower adaptative immune gene enrichment than fetal microglia or blood monocytes 72
3.3.3.4 H5 iPS-Mo/Mϕ are very similar to fetal microglia . 73
3.4 Discussion 76

4 hiPSC-derived monocyte & Mϕ ontogeny 79
4.1 Introduction 80
4.2 Materials and Methods 82
4.2.1 shRNA 82
4.2.1.1 shRNA design 82
4.2.1.2 Cloning of the shRNA vectors 83
4.2.1.3 p24 ELISA 83
4.2.1.4 Generation of shRNA-expressing cell lines 85
4.2.2 CRISPR/Cas9 86
4.2.2.1 In-silico design 86
4.2.2.2 High resolution melt analysis (HRM) primer design 87
4.2.2.3 Vector construction 87
4.2.2.4 Gene editing and single-cell cloning 88
4.2.2.5 Clone screening, DNA extraction and HRM 89
4.2.2.6 Screening for WT contamination 91

4.2.2.7 DNA extraction and Illumina SNP array 91
4.2.3 Molecular biology and functional assays 93
4.2.3.1 Phagocytosis assay 93
4.2.3.2 TNFα enzyme-linked immunosorbent assay (ELISA) 93
4.2.3.3 ROS assay 93
4.2.3.4 EB dissociation and colony forming assay 94
4.2.3.5 Western bloting 94
4.2.3.6 RNA extraction, reverse transcription (RT) and quantitative Polymerase Chain Reaction (qPCR) . 95
4.3 Results 96
4.3.1 Using shRNAs to knock-down MYB in hiPSCs 96
4.3.1.1 MYB shRNAs had limited KD efficiency in Jurkat and CCRF-CEM cell lines 96
4.3.1.2 MYB shRNAs had limited KD efficiency in hESC . 98
4.3.1.3 Effect of MYB KD using shRNAs on iPS-Mo/Mϕ differentiation 100
4.3.2 Optimizing the CRISPR-Cas9 protocol to generate hiPSC KO 101
4.3.3 Exon 9 MYB KO 106
4.3.3.1 Structure of MYB and gRNA design 106
4.3.3.1.1 Genomic structure of MYB 106
4.3.3.1.2 Generating MYB Exon 9 KO hiPSCs . . . 106
4.3.3.2 MYB$^{\Delta Ex9}$ hiPSC lines have un-modified iPS-Mo/Mϕ differentiation capacity 109
4.3.4 Generation of the RUNX1, SPI1 and MYB KO hiPSC lines 111
4.3.4.1 Why chose these genes and this location? 111
4.3.4.1.1 Targeting location 111
4.3.4.2 Different generated KO clones 115
4.3.4.3 Quality control of the hiPSCs 115
4.3.4.4 iPS-Mo/Mϕ development is MYB independent but RUNX1 and SPI1 dependent 119
4.3.4.5 MYB$^{\Delta Ex6}$ iPS-Mo/Mϕs display no apparent phenotypic or functional defects 121
4.3.4.6 MYB KO results in increased number of hematopoietic progenitors within the EB 121
4.3.4.7 hiPSC-derived erythrocytes and granulocytes are dependent on MYB, RUNX1 and SPI1 124
4.4 Discussion 124

5 Investigating the differentiation bottleneck 129
5.1 Introduction . . . 129
5.2 Materials and methods . . . 133
5.2.1 Copy number variation (CNV) digital droplet PCR (ddPCR) 133
5.3 Results . . . 134
5.3.1 RFP-GFP statistical model . . . 134
5.3.1.1 Poisson distribution and assumptions . . . 134
5.3.1.2 A dual reporter system to quantify the bottleneck . 136
5.3.1.3 GFP/RFP model confirms GeCKO library results . 138
5.3.1.4 Clonal RFP-GFP experiment . . . 141
5.3.1.4.1 AH016-03 subcloning . . . 141
5.3.1.4.2 AH01603 results . . . 141
5.3.2 Using RUNX1$^{\Delta Ex5}$ hiPSCs to investigate the differentiation bottleneck . . . 144
5.3.2.1 Proof of concept . . . 144
5.3.2.2 Effect of MYB$^{\Delta Ex6}$ on the differentiation bottleneck 146
5.4 Discussion . . . 148

6 Discussion 151
6.1 Summary of results . . . 151
6.2 Implications and perspectives . . . 154

Appendices

A Appendix 163
A.1 EdU staining . . . 163
A.2 Rank Product . . . 164

Bibliography 171

List of Figures

1.1 Macrophage heterogeneity in the human and mouse. 3
1.2 Mouse and Human hematopoietic development 6
1.3 Myeloid development and maintenance in the mouse embryo and adult mouse. 18

2.1 iPS-Mo/Mϕ stepwise differentiation 33

3.1 Transcriptome - Experimental design. 40
3.2 Image of the three hiPSCs lines used in the transcriptome and their differentiation. 52
3.3 Basic experimental study of the iPS-Mo/Mϕ over time. 54
3.4 EdU staining of iPS-Mo/Mϕ over time. 55
3.5 Normalization of transcriptomic expression data 57
3.6 Exploratory MDS plot showing clustering of the 12 different iPS-Mo/Mϕ samples 58
3.7 GSEA clustering heatmap of GO gene sets 60
3.8 Analysis of the cell cycle process gene cluster. 64
3.9 Analysis of the mitosis gene cluster 65
3.10 Analysis of the viral genome replication gene cluster. 66
3.11 Analysis of the response to virus gene cluster 67
3.12 Analysis of the response to virus gene cluster 68
3.13 MDS plot of iPS-Mo/Mϕs, fetal microglia, blood monocytes and hiPSCs 70
3.14 Cell cycle genes are enriched in iPS-Mo/Mϕs. 71
3.15 GSEA analysis of H1-iPS-Mo/Mϕs compared to fetal microglia or blood monocytes. 74
3.16 GSEA analysis of H5-iPS-Mo/Mϕs compared to fetal microglia or blood monocytes 75

4.1 shRNA Target location and design 83
4.2 Plasmid map of the shRNA lentiviral vectors 86
4.3 Schematic representation of the choice of the gRNA target location and primer design 88

4.4 Schematic representation of the CRISPR-Cas9 based KO strategy in iPSCs. . . . 90
4.5 Schematic representation of HRM analysis. . . . 92
4.6 MYB shRNAs had limited KD efficiency in Jurkat and CCRF-CEM cell lines . . . 97
4.7 MYB shRNAs had limited KD efficiency in hESC. . . . 99
4.8 HUES-2$^{\text{shMYB-27}}$ were capable of hES-Mo/Mϕ differentiation while shCTRL$^{\text{27nt}}$ had defective differentiation. . . . 100
4.9 Schematic representation of the optimization of the CRISPR KO protocol in hiPSCs and hESCs. . . . 102
4.10 Genomic structure of MYB and CRISPR/Cas9 targeting of exon 9 . 107
4.11 Quality control of MYB$^{\Delta\text{Ex9}}$ hiPSCs clones. . . . 108
4.12 MYB$^{\Delta\text{Ex9}}$ hiPSC lines have un-modified iPS-Mo/Mϕ differentiation capacity . . . 110
4.13 Genomic structure of MYB and CRISPR/Cas9 targeting of exon 6 . 112
4.14 Genomic structure of SPI1 and CRISPR/Cas9 targeting . . . 113
4.15 Genomic structure of RUNX1 and CRISPR/Cas9 targeting . . . 114
4.16 Gene-KO hiPSC lines maintained pluripotency and karyotype . . . 117
4.17 Gene-KO hiPSC lines maintained pluripotency and karyotype (continued) . . . 118
4.18 iPS-Mo/Mϕ production capacity of WT, MYB$^{\text{-/+ Ex6}}$, MYB$^{\Delta\text{Ex6}}$, RUNX$^{\Delta\text{Ex5}}$ and SPI1$^{\Delta\text{Ex3}}$ hiPSCs. . . . 120
4.19 MYB$^{\Delta\text{Ex6}}$ iPS-Mo/Mϕs display no apparent phenotypic or functional differences compared to WT controls. . . . 123
4.20 Study of the progenitor cells within the hiPSC-derived EBs. . . . 125

5.1 Hematopoietic differentiation bottleneck . . . 132
5.2 CNV analysis using ddPCR . . . 133
5.3 Schematic representation of the GFP/RFP statistical model . . . 137
5.4 HUES-2 polyclonal GFP/RFP model . . . 140
5.5 AH016-03 clonal GFP/RFP model . . . 143
5.6 Using RUNX1$^{\Delta\text{Ex5}}$ hiPSCs to investigate the differentiation bottleneck. 145
5.7 Investigating the role of MYB during cell fate decision in hiPSCs differentiation to Mϕ . . . 147

A.1 Supplementary EdU staining of iPS-Mo/Mϕ over time. . . . 163

List of Tables

1.1 Different protocols described for the generation of mature myloid cells from human PSCs. 15
1.2 Different protocols described for the generation of mature lymphoid cells from human PSCs. 16

3.1 General information on the donors and reprogramming method used for the hiPSCs used for the transcriptome analysis 51

4.1 shRNA oligonucleotides. 84
4.2 CRISPR-Cas9 KO protocol improvement 105

List of Abbreviations

ADA	Adenosine deaminase deficiency
AGM	Aorta-gonad-mesonephros
AMV	Avian myeoloblastosis virus
ANOVA	Analysis of variance
bFGF	Basic fibroblast growth factor
BFU-E	Blast-forming unit erythrocyte
BGA	Between group analysis
BL-CFC	Blast colony-forming cells
BM	Bone marrow
BMP4	Bone morphogenetic protein 4
BP	Biological process
BSA	Bovine serum albumin
CC	Cellular component
CFU-E	Colony-forming unit erythrocyte
CFU-GEMM	Colony-forming unit erythroid, macrophage & megakaryocyte
CFU-GM	Colony-forming unit granulo-monocyte
CFU-M	Colony-forming unit Macrophage
CNV	Copy number variation
CRISPR	Clustered regularly inter-spaced short palindromic repeat
CSF1R	Colony stimulating factor 1 receptor
ddPCR	Digital Droplet PCR

EB	Embryoid body
EDTA	Ethylenediaminetetraacetic acid
EdU	5-ethynyl-2'-deoxyuridine
EHT	Endothelial to hematopoietic transition
ELISA	Enzyme-linked immunosorbent assay
EMP	Erythro-myeloid progenitor
EPO	Erythropoietin
ES	Enrichment score
ETS	E26 transformation-specific
FCS	Fetal calf serum
FDR	False discovery rate
FGF1	Fibroblast growth factor 1
FL	Fetal liver
Flt3-L	Fms-related tyrosine kinase 3 ligand
FSC-H	Forward scatter height
G-CSF	Granulocyte-colony stimulating factor
GeCKO	Genome-scale CRISPR knock-out
GEO	Gene Expression Omnibus
GM-CSF	Granulocyte-macrophage colony-stimulating factor
GO	Gene Ontogeny
gRNA	Guide RNA
GSEA	Gene Set Enrichment Analysis
HBSS	Hank's Balanced Salt Solution
HE	Hemogenic endothelium
HEK-293T	Human Embryonic Kidney 293 expressing SV40 T antigen

hESC	Human embryonic stem cell
hiPSC	Human induced pluripotent stem cell
hPSC	Human pluripotent stem cell
HRM	High-resolution melt analysis
HSC	Hematopoietic stem cell
HU	Hydroxyurea
IGF-1	Insulin-like growth factor-1
IL	Interleukin
iPSC	Induced pluripotent stem cell
iPS-Mo/Mϕ	iPSC-derived monocyte/macrophage
KD	Knock-down
KO	Knock-out
LB	Lysogeny broth
LC	Langerhans cell
LIMMA	Linear Models for Microarray and RNA-Seq data
LPS	Lipopolysaccharide
LT-HSC	Long-term repopulating hematopoietic stem cell
Mϕ	Macrophage
M-CSF	Macrophage colony-stimulating factor
MDS	Multi-dimensional scaling
MEF	Mouse embryonic fibroblast
mESC	Mouse embryonic stem cell
MF	Molecular function
Mk	Megakaryocyte
MOI	Multiplicity of infection

MPO	Myeloperoxidase
MPS	Monouclear phagocytic system
Myb	Mouse V-Myb Avian Myeloblastosis Viral Oncogene Homolog
MYB	Human V-Myb Avian Myeloblastosis Viral Oncogene Homolog
NGS	Next-Generation high throughput deep sequencing
NK cell	Natural killer cell
NMD	Nonsense-mediated mRNA decay
NRD	Negative regulatory domain
nt	Nucleotide
PAM	Protospacer adjacent motif
PBS	Phosphate-buffered saline
PCA	Principal component analysis
PCR	Polymerase chain reaction
PDGFRα	Platelet-derived growth factor receptor-α
PEI	Polyethylenimine
PM	Primitive mesoderm
PMA	Phorbol myristate acetate
PS	Primitive streak
PTC	Premature termination codon
qPCR	Quantitative polymerase chain reaction
ROC	Receiver operating characteristic
RP	Ranked product
RT	Room temperature
Runx1	Mouse runt-related transcription factor 1
RUNX1	Human runt-related transcription factor 1

SAM	Significance analysis of microarrays
SCF	Stem cell factor
SFFV	Spleen focus-forming virus
shRNA	Short hairpin RNA
SNP	Single-nucleotide polymorphism
Spi1	Mouse Spi-1 proto-oncogene
SPI1	Human Spi-1 proto-oncogene
SSC-H	Side scatter height
TAD	Transactivation domain
TBS	Tris-buffered saline
TNF-α	Tumor necrosis factor α
TPO	Thrombopoietin
VEGF	Vascular endothelial growth factor
VSV-g	Vesicular stomatitis virus
Wnt3A	Wnt Family Member 3A
WT	Wild type
WTHG	Wellcome trust for human genetics
YS	Yolk sac

1 Introduction

Contents

1.1 Macrophage function and diversity 2
1.2 Mammalian hematopoietic development 4
1.2.1 Mouse hematopoietic development 4
1.2.1.1 *In vivo* studies of mouse hematopoietic development 4
1.2.1.2 Primitive precursors, EMPs and HSCs 6
1.2.1.3 Transcription factors MYB, RUNX1 and PU.1 7
1.2.1.4 Mouse embryonic stem cells (mESC) differentiation 8
1.2.2 Human hematopoietic development 9
1.2.2.1 *In vivo* 9
1.2.2.2 Human *in vitro* hPSC hematopoietic development 10
1.3 Tissue-resident Mϕ ontogeny in the mouse 17
1.3.1 Early concepts of Mϕ ontogeny - The unified mononuclear phagocytic system 17
1.3.2 Contribution of YS primitive Mϕs to tissue-resident Mϕ populations 17
1.3.3 Contribution of EMP-derived monocytes and Mϕs to tissue-resident Mϕ populations 19
1.3.4 Contribution of fetal HSCs to tissue-Resident Mϕ populations 19
1.3.5 Nomenclature of macrophage development 20
1.3.5.1 MYB-independent and MYB-dependent hematopoiesis 20
1.3.5.2 Monocytes and Mϕs 20
1.3.6 Maintenance of tissue-resident Mϕ populations in disease and homeostasis 22
1.3.6.1 Mϕ proliferation 22

1.3.6.2 Homeostatic control of proliferation and monocyte recruitment 23
1.3.7 How different are these Mϕ populations? 25
1.4 Tissue-resident Mϕ ontogeny in the human 27
1.4.1 *In vivo* Mϕ ontogeny 27
1.4.2 hPSC Mϕ protocols 28
1.4.3 Nomenclature - hPSC-derived Monocytes and Mϕs . . . 29
1.4.4 Pluripotent stem cell-derived Mϕ ontogeny 29

1.1 Macrophage function and diversity

Macrophages (Mϕs), discovered in 1884 by Ilya Mechnikov, are highly plastic multifunctional terminally differentiated immune cells present throughout all tissues of most vertebrates as well as some invertebrates (Okabe and Medzhitov, 2015). As their name suggests (from greek: "big eaters", $\mu\alpha\kappa\rho o\zeta$ (makros) = large, $\varphi\alpha\gamma\varepsilon iv$ (phagein) = to eat) they are best known for their phagocytic function, which is key not only for host defence but also many "housekeeping" functions such as removal of apoptotic cells and remodelling of the extracellular matrix (Wynn et al., 2013; Gordon et al., 2014). In addition to their essential housekeeping and host defence roles many studies have now shown much broader roles of Mϕs in tissue homeostasis, metabolism, development and tissue repair (Wynn et al., 2013; Gordon et al., 2014). They display a wide variety of functions such as neuronal patterning, angiogenesis, adipose tissue generation and bone morphogenesis (Pollard, 2009). In line with their multifunctional nature, the dysregulation of Mϕs is involved in many pathological conditions such as atherosclerosis (Moore and Tabas, 2011), type 2 diabetes (Olefsky and Glass, 2010), fibrosis (Wynn et al., 2011), osteoporosis (Boyle et al., 2003), obesity (Chawla et al., 2011) and cancer (Noy and Pollard, 2014). Mϕs have also been shown to be the host of many viral, bacterial and parasitic pathogens (Klepper and Branch, 2015; Thi et al., 2012).

While Mϕs all share the same core functions, they are very diverse cells. The unique combination of signals in each tissue directs tissue-resident Mϕs to differentiate into various tissue-specific subtypes, some of the major subtypes are

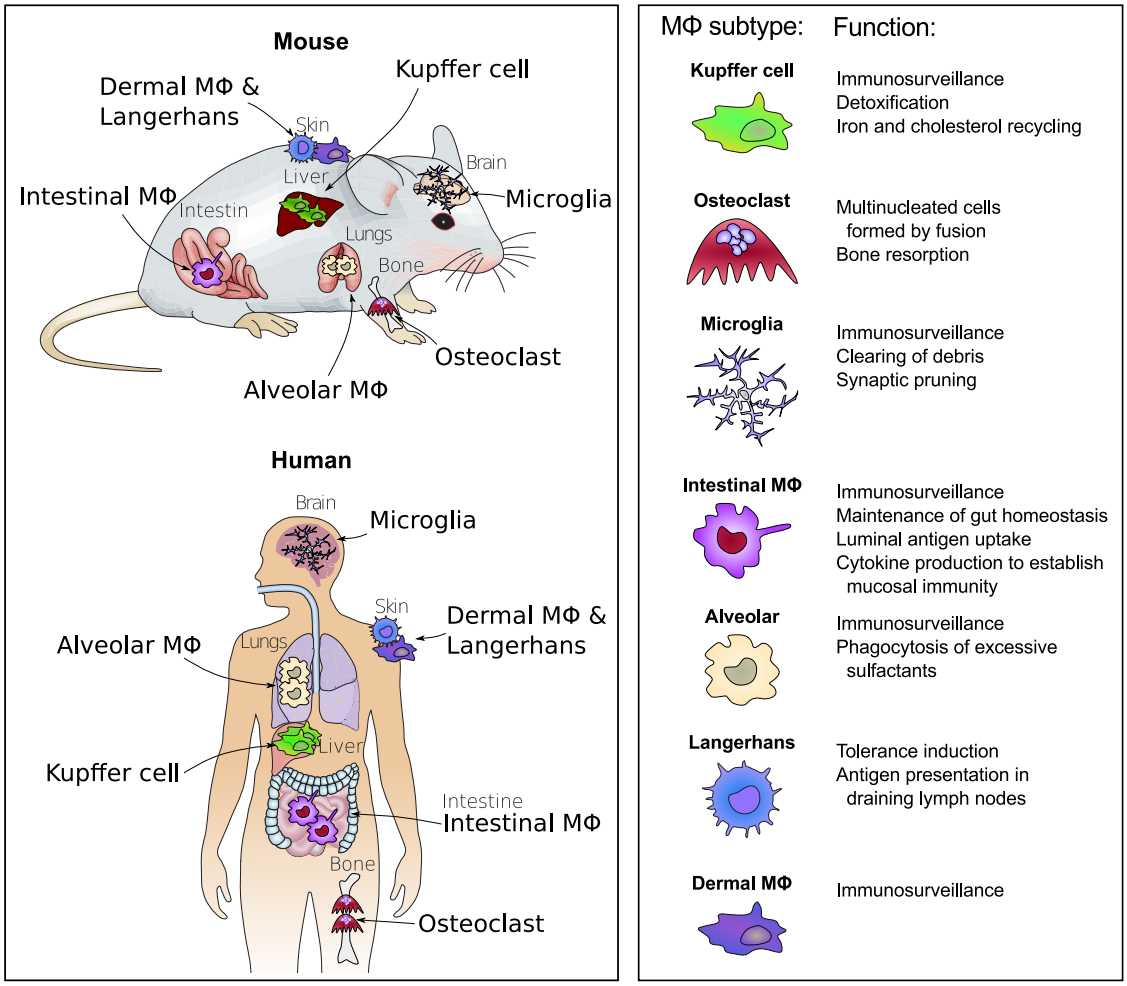

Figure 1.1: Mϕ heterogeneity in the human and mouse. Non-extensive distinct locations and functions of various tissue Mϕs in the mouse and human. Adapted from (Davies et al., 2013a)

summarised in figure 1.1. This tissue specialisation of Mϕs can be important and irreversible, for example osteoclasts fuse to form multinucleate cells that reabsorb bone (Pollard, 2009) and support the bone marrow (BM) hematopoietic stem cell (HSC) niche (Chow et al., 2011). Tissue-resident Mϕ specialisation also results in tissue-specific phenotypic markers, making macrophage phenotype very diverse, reviewed in (Davies et al., 2013a). Although Mϕs are highly plastic cells, once adapted to a tissue they cannot adapt efficiently to another tissue (Van de laar et al., 2016). In addition to tissue specialisation, Mϕs can also be polarised in response to local local inflammatory signals, the major subtypes described are M1 and M2 polarization (Sica and Mantovani, 2012; Murray et al.,

2014). Macrophage polarization, in contrast to tissue specialization is a fully reversible process. The environmental plasticity is also accompanied by multiple developmental origins of each Mϕ subtype. Mϕs are immune cells derived from hematopoiesis, but hematopoiesis is not a single event and it is this varied ontogeny that is the focus of this thesis.

1.2 Mammalian hematopoietic development

Hematopoiesis, the development of blood, has been studied extensively over the past decades using many different model systems including zebrafish, *Xenopus*, chick, mouse, rat, and human (Ciau-Uitz et al., 2014; Jaffredo et al., 2010). In general, hematopoiesis is similar in all vertebrates but there are many subtle differences between organisms (Ciau-Uitz et al., 2014). In this introduction I will focus on mammalian hematopoiesis (Mouse and Human) as these are the most relevant to my subject. The tools available in mouse have allowed for much more in depth studies; the knowledge derived from which can then be applied to human hematopoiesis.

1.2.1 Mouse hematopoietic development

1.2.1.1 *In vivo* studies of mouse hematopoietic development

During mouse embryonic development three spatially and temporally distinct waves of hematopoietic progenitors have been described, these progenitors then migrate to various organs where they proliferate and generate multiple mature hematopoietic cells (figure 1.2).

A first wave, generating primitive progenitors, occurs between E7.0 and E7.5 days post coitum in the blood islands of the yolk sac (YS), producing large, nucleated primitive erythrocytes, megakaryocytes and Mϕs (Palis et al., 1999). The cells giving rise to the first blood cells are thought to be fated to this lineage already at the epiblast stage (E6.5) (Padrón-barthe et al., 2014). The primary purpose of this wave is to provide tissue oxygenation through the formation of red blood cells (Orkin and Zon, 2008), which are the first cells to appear in blood islands of the extra-embryonic YS early in development (Palis et al., 1999). Primitive megakaryocytes

have been reported to be smaller than adult megakaryocytes and to rapidly mature and give rise to platelets to prevent hemorrhage in the developing blood vessels until definitive hematopoiesis is established (Xu M et al., 2001; Tober et al., 2007). Primitive Mϕs colonise the brain by E9.5 and the remaining embryonic tissues by E10.5 (Ginhoux et al., 2010; Hoeffel et al., 2012). The role and maintenance of primitive Mϕs will be further expanded on in detail later.

From E8.25, a second wave of hematopoietic cells emerge in the YS producing erythro-myeloid progenitors (EMPs) (Palis et al., 1999, 2001), via endothelial to hematopoietic transition (EHT) (Chen et al., 2009), that are capable of monocyte, Mϕ, granulocyte, megakaryocyte and erythrocyte differentiation. While they do not have any lymphoid potential and lack long-term repopulating potential (McGrath et al., 2015a), analysis of EMP-derived erythrocytes led to their classification as "definitive" progenitors (England et al., 2011). This second wave of hematopoietic progenitors has also been termed “transient definitive” because of the inability of EMPs to persist upon transplantation into an immunocompromised mouse. EMPs rapidly migrate to the fetal liver (FL) where they expand, mature and differentiate into multiple lineages including fetal monocytes and Mϕs (Palis and Yoder, 2001). The number of EMPs expand rapidly in the YS and migrate into the FL where they mature and reside until E16.5 (Gomez Perdiguero et al., 2015). In addition to EMPs, a small number of lymphoid progenitors capable of B- and T-cell differentiation have been detected around E9.0 in the YS and embryo proper, before HSC emergence (Yoshimoto et al., 2010, 2012; Böiers et al., 2013; Kobayashi et al., 2014). Lymphoid progenitors have limited Mϕ potential and therefore their contribution to tissue-resident Mϕs is thought to be limited. The impact of these early lymphoid progenitors on the adult hematopoietic system is still poorly understood (reviewed in (Lin et al., 2014)).

The third wave, from E10.5, consists of HSCs, that arise from the endothelium of the aorto-gonado-mesonephros (AGM) region of the embryo through EHT (reviewed in (Godin and Cumano, 2002; Moore, 2009)). HSCs first colonise the FL before migrating to the BM and spleen at birth, where they maintain and self-renew

through adult life and give rise to all blood lineages in the adult organism (Cumano and Godin, 2007). HSCs are distinguished from other hematopoietic progenitors by their long-term repopulating capacity of all blood lineages (Gekas et al., 2005).

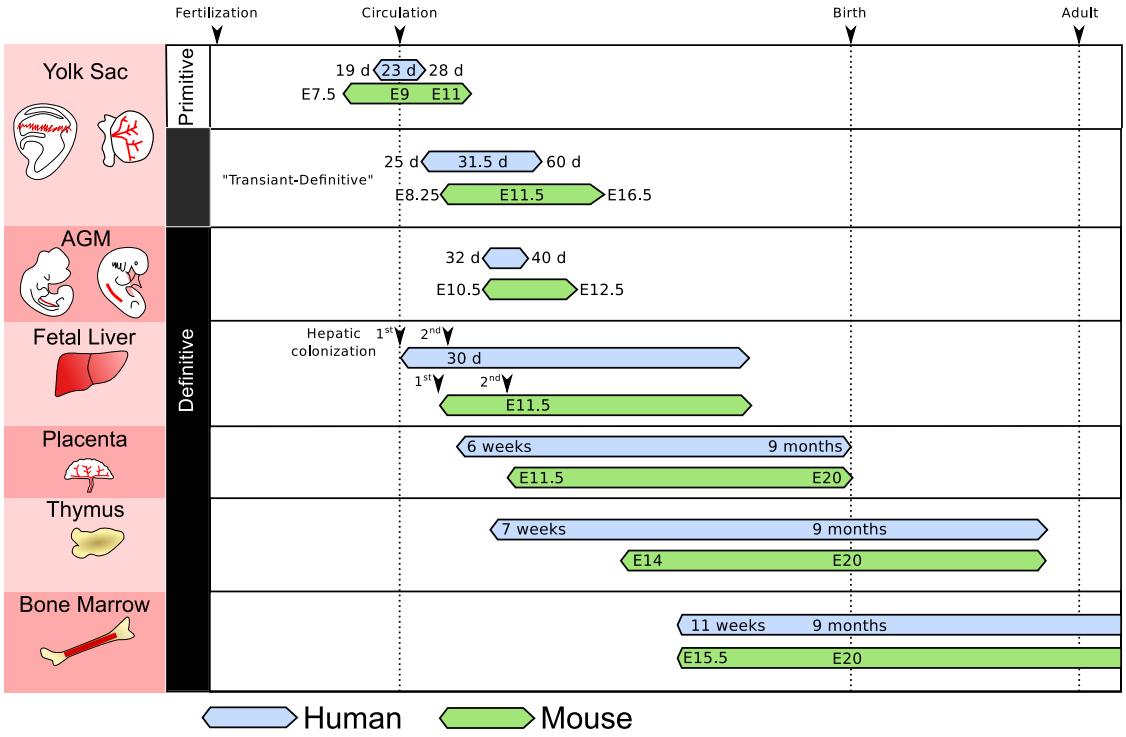

Figure 1.2: Mouse and Human hematopoietic development. Relative spacial and temporal emergence of the three hematopoietic waves in human (blue) and mouse (green) followed by secondary hematopoietic organ colonization. This figure has been modified and adapted from (Rowe et al., 2016).

1.2.1.2 Primitive precursors, EMPs and HSCs

The term EMP was originally used to distinguish primitive YS precursors from YS "transient-definitive" erythro/myeloid progenitors and AGM-derived HSCs (reviewed in (Frame et al., 2013)). In the publications of Ginhoux et al. (2010) and Kierdorf et al. (2013) microglia are described as being derived from EMPs. However, in both articles, due to the lack of clonal analysis of the cells, the progenitors described could relate to both primitive monopotent progenitors and EMPs. Recently, Hoffel et al. described “early" colony stimulating factor 1 receptor (CSF1R) positive EMPs as another progenitor cell arising at E7.25 in the mouse YS (Hoeffel et al., 2015).

Due to the use of CSFR1 promoter for lineage tracing, which marks both Mϕs and EMPs, in the absence of clonal study, it is likely that the "early" CSFR1$^+$ EMPs and the "late" Myb$^+$ EMPs described by Hoffel et al. are a combination of Myb$^-$ primitive monopotent Mϕ progenitors and Myb$^+$ EMPs, both labelled by the CSF1R promoter (reviewed in (McGrath et al., 2015a)). In my thesis for clarity I will use the nomenclature of "primitive progenitors" for the first wave, "EMP" for the second wave and "HSC" for the third wave.

1.2.1.3 Transcription factors MYB, RUNX1 and PU.1

Several transcription factors have been extensively used for the study of lineage potential in the mouse, including Myb, Runx1 and Spi1 (also called Pu.1).

Myb is a member of the MYB transcriptional factor family which are a group of transcription factors found in vertebrates, arthropods and plants. They are sequence specific transactivators that regulate cell proliferation, apoptosis and differentiation throughout development. In vertebrates the MYB family consists of three genes, A-myb (MYBL2), B-myb (MYBL1) and C-myb (Myb). Myb proteins where first discovered by a study of the avian myeloblastosis virus (AMV), a retrovirus causing erythroid and myeloid leukemia in chickens (Moscovici, 1975). The Myb proto-oncogene was first described as the cellular homologue of the viral v-myb gene of the AMV (Moscovici, 1975; M et al., 1979). It has since then been shown to play a major role in hematopoietic differentiation in chicken, zebrafish, mouse and human (reviewed in (Soza-ried et al., 2010)). Myb$^{-/-}$ mice were first reported to die in utero by day 15 of development due to severe anemia (Mucenski et al., 1991). While Myb$^{-/-}$ mice had normal primitive erythrocytes and Mϕs they lacked FL hematopoiesis. Subsequent studies showed that a functional Myb is required for HSC maintenance and self-renewal (Sumner et al., 2000; Lieu and Reddy, 2009; Schulz et al., 2012).

Runx1/AML1 encodes the DNA-binding subunit of the Runt domain transcription factor (Ito, 1999), Runx1$^{-/-}$ mice die in utero around E12.5 from central nervous system necrosis and hemorrhaging as well as lack of definitive hematopoiesis (Wang et al., 1996). Primitive erythrocytes are the only blood cells that still arise in Runx1

null embryos (Okada et al., 1998; Okuda et al., 1996; Wang et al., 1996), but their development is affected by the loss of Runx1 as they display a delayed maturation (Yokomizo et al., 2008). Runx1 has later been shown to be essential for HSC generation and maintenance, and play a crucial role in EHT (Chen et al., 2009).

Spi1 gene encodes for a transcription factor of the E26 transformation-specific (ETS)-domain family of DNA-binding proteins (Moreau-Gachelin et al., 1990), it was originally identified as the "spleen focus-forming virus (SFFV) provirus integration site-1" (Spi-1) as the Spi1 locus is a high frequency integration site of SFFV (Moreau-Gachelin et al., 1989, 1988). $Spi1^{-/-}$ mice die in utero by E17.5 due to anemia and show a marked lack of myeloid cells, T and B cells (Scott et al., 1994; McKercher et al., 1996). Primitive erythropoiesis, while still detected in $Spi1^{-/-}$ embryos is also affected as erythroid progenitors lose their self-renewal capacity and undergo proliferation arrest, premature differentiation, and apoptosis (Back et al., 2004).

1.2.1.4 Mouse embryonic stem cells (mESC) differentiation

After the derivation of mESC in 1981 and their adaptation to culture (Evans and Kaufman, 1981; Martin, 1981) in 1985 Doetschman et al. described formation of blood island like structures from mESCs using an embryoid body (EB) differentiation model (Doetschman et al., 1985). Subsequent studies showed that *in vitro* mESC differentiation closely resembles early hematopoietic development with a first wave of primitive erythropoiesis followed by myeloid progenitors and definitive erythrocytes (Keller et al., 1993; Wiles and Keller, 1991; Lindenbaum and Grosveld, 1990). During *in vitro* mESC differentiation, as *in vivo*, all blood cells are derived from mesodermal progenitors expressing the T box transcription factor Brachyury (Fehling, 2003). Mesodermal cells then give rise to blast colony-forming cells (BL-CFC) which gives rise to both endothelial and hematopoietic lineages (Choi et al., 1998; Nishikawa et al., 1998). Blood cells are then generated from subpopulations of hemogenic endothelium through EHT (Eilken et al., 2009; Lancrin et al., 2009). Generation of hematopoietic progenitors with *in vivo* engrafting proprieties and the ability to give rise to lymphoid lineages was reported in the mid-1990s (Gutierrez-Ramos and

Palacios, 1992; Potocnik et al., 1997; Müller and Dzierzak, 1993; Nisitani et al., 1994) but these cells were not capable of long-term engraftment and serial transplantation. Since then, with the use of Hoxb4 (Kyba et al., 2002), Cdx4 (Wang et al., 2005b) and Lhx2 (Kitajima et al., 2011) over-expression during mESCs differentiation, long-term repopulating hematopoietic progenitors have been generated, but the generation of long-term multilineage engrafting HSCs without forced gene expression has not been achieved yet in the mESC model (reviewed in (Garcia-Alegria et al., 2016)).

1.2.2 Human hematopoietic development

1.2.2.1 *In vivo*

The knowledge acquired through the rare studies on human embryos have shown that human hematopoietic development closely resembles that of other mammals (figure 1.2). The human YS blood islands start to be detectable after 16 days of development (Luckett, 1978) and the presence of mostly erythrocytes as well as some primitive Mϕs and megakaryocytes have been described in some rare histological studies in the YS after 19 days of development (Bloom and Bartelmez, 1940; Fukuda, 1973). This first wave fits the description of the mouse primitive wave of hematopoiesis which generates mainly primitive erythrocytes and some megakaryocytes and Mϕs. The first blood cells within the embryo vessels, indicating the onset of blood circulation, have been reported at 21 days of development (Tavian et al., 1999). Clonal colony-forming unit–granulocyte-erythrocyte-monocyte-megakaryocyte (CFU-GEMM), early burst forming unit-erythroid (BFU-E), or late colony-forming unit–erythrocyte (CFU-E) and colony-forming unit–granulocyte-macrophage (CFU-GM) progenitor appear in the human YS at 31.5 days of development (Migliaccio et al., 1986). Two subsequent studies confirmed these observations and reported the presence of clonogenic CFU-E, CFU-GM and CFU-GEMM as early as day 25 and 27 the YS (Dommergues et al., 1992; Huyhn et al., 1995). The generation of these clonogenic CFU-E, CFU-GM and CFU-GEMM are in close temporal relation with the first hepatic colonization occurring as early as day 23 and precedes the second hepatic colonization (Tavian et al., 1999) and the generation of the first true

multilineage HSC in the AGM which occurs at around 32 days of development (Ivanovs et al., 2011). This wave likely represents the second wave of "transiant-definitive" erythromyeloid progenitors observed in the mouse YS. YS hematopoietic progenitors were still detected up to 60 days of development, after which there is no hematopoietic activity in the YS (Dommergues et al., 1992; Huyhn et al., 1995). After YS and AGM hematopoietic waves, the FL becomes the main hematopoietic organ during fetal life (Tavian and Péault, 2005) which is supplanted by the long bone before birth (Charbord et al., 1996).

1.2.2.2 Human *in vitro* hPSC hematopoietic development

Human embryonic stem cells (hESCs) isolated and adapted to *in vitro* culture in 1998 by Thomson (1998) and more recently inducted human induced pluripotent stem cells (hiPSC) by Takahashi et al. (2007) and Yu et al. (2007) have allowed an alternative way of studying early human development *in vitro*. Soon after their discovery, hESC were directed to differentiate into all three germ layers *in vitro* by EB formation (Reubinoff et al., 2000; Itskovitz-Eldor et al., 2000; Thomson, 1998). By application of the knowledge acquired in the mouse and mouse ES cells, many protocols have been developed for the differentiation of various hematopoietic cells. Most of the strategies used for human pluripotent stem cell (hPSC) hematopoietic differentiation can be broadly separated into two categories: differentiation methods based on the co-culture of hPSC with various somatic cell lines (feeders) and feeder-free methods often based on the formation of an EB.

1.2.2.2.1 hPSC as a tool for studying development

hPSC have proven to be a invaluable model system for studying early hematopoietic development as they closely recapitulate early embryogenesis, giving an alternative for studying human early hematopoietic development and one that is genetically tractable. Many studies have characterised the sequential specification of hPSCs to mesoderm, hemogenic endothelium (HE) and hematopoietic precursors using co-culture and EB-based methods.

Using a *MIXL1*-GFP reporter hESC line (*MIXL1* is known to be expressed in primitive streak and early mesoderm (Pereira et al., 2012)), Davis et al. have identified a primitive streak (PS)-like cell that arises in EB culture at day 3 (Davis et al., 2008). The expression of *MIXL1* was induced by bone morphogenetic protein 4 (BMP4) or Activin A stimulation but not basic fibroblast growth factor (bFGF). These cells expressed some level of platelet-derived growth factor receptor-α (PDGFRα) and progressively lost expression of the E-Cadherin (CD324) stem cell marker. The expression of CD34, marking the beginning of hemato-endothelial differentiation was detected on day 8 in EB culture. Using an hPSC-OP9 co-culture method Vodyanik et al. showed that primitive mesoderm (PM) is induced in culture after 3 days, with first an up-regulation of transcription factors involved in induction of mesoderm (T, MIXL1, EOMES), followed by the up-regulation of lateral plate/extraembryonic mesoderm genes (FOXF1, HAND1, GATA2) (Vodyanik et al., 2010). These PM cells express APLIN receptor (APLNR) and PDGFRα (CD140a) and lack endothelial CD31, VE-cadherin, endothelial/mesenchymal CD73, CD105 and hematopoietic CD43, CD45 markers and were capable of producing bFGF-dependent BL-CFU in serum-free medium. In a later study using the same differentiation method Choi et al. have shown that after 4 days some PM cells differentiate into hematovascular mesoderm precursors, which still possess mesodermal characteristics but are committed to endothelium (Choi et al., 2012). This intermediate state is marked by the gradual loss of expression of PDGFRα and down regulation of PS genes MIXL1, EOMES, T, and MESP1 and upregulation of endothelial marker VEGFR2 (KRD) and hemato-endothelial genes LMO2, TAL1, CBFB, GATA2 and FLI1.

After endothelial specification, hematopoietic cells originate from a $CD31^+$ $CD34^+$ KDR^+ VE-$cadherin^+$ $CD45^-$ endothelial precursor capable of generating primitive and definitive hematopoietic cells (Wang et al., 2004; Kennedy et al., 2007; Wang et al., 2005a). Choi et al. further identified three different early endothelial subsets all of which express the classic endothelial markers VE-cadherin, CD34 and CD31 but can be separated based on their expression of CD117 (c-kit) and the

endothelial marker CD73 (5'-ectonucleotidase) (Choi et al., 2012). Non-hemogenic endothelial progenitors, which have lost the hemogenic capacity, express high levels of CD117 and CD73. Hemogenic endothelial progenitors which are capable of generating blood and endothelial cells upon co-culture with OP9 cells, express intermediate levels of CD117 but lack expression of CD73. Finally, angiogenic hematopoietic progenitors that possess primary hematopoietic characteristics but are capable of generating endothelial cells expressing low levels of CD117 and lack the expression of CD73 (Choi et al., 2012).

Using a dual-reporting transgenic hESC-line for the CD41a hematopoietic marker (expressed in definitive hematopoietic precursors in the mouse (Mikkola et al., 2003)) and VE-cadherin vascular marker, Rafii et al. studied the phenotypic progression of cells through EHT by live confocal microscopy (Rafii et al., 2013). By limiting dilution and live microscopy they show that a single VE-cadherin$^+$ CD31$^+$ CD43$^-$ CD73$^-$ HE cell can round up, detach itself and start to express CD41a and CD43, indicating the occurrence of HET. Interestingly two distinct waves of hematopoietic progenitors with differential CD41a expression were observed, first at day 12 a wave of CD41a-GFP^{bright} CD41a$^+$ CD43$^+$ cells, biased towards megakaryocyte linage were detected, then after day 15 a wave of CD41a-GFP^{dim} CD41a^{neg}CD43$^+$ cells biased towards multipotent myeloid progenitors arose. Furthermore this temporal switch in lineage potential coincided with a globin switch in CD71$^+$ erythroid cells from ϵ-globin (embryonic) and γ-globin (fetal) expressed in erythrocytes derived at day 11 to 15 to β-globin (adult) expressed at low level in erythrocytes derived at day 18 onwards. These results show that hPSC culture can recapitulate the first waves of hematopoiesis observed *in vivo*, and that culture time can play a major role in the linage potential of the derived cells.

1.2.2.2.2 hPSC hematopoiesis - primitive versus definitive

In the past 18 years, differentiation of hPSCs has rapidly evolved, and many different studies have now described methods for deriving essentially all myeloid

and lymphoid blood lineages (summarised in table 1.1 and 1.2). That being said, the generation of definitive hematopoietic cells such as B and T lymphocytes as well as generation of large enough quantities of clinically relevant mature cells remain challenging. In addition, although much progress has been made, generation of long-term repopulating HSCs (LT-HSC) has not been achieved yet (reviewed in (Vo and Daley, 2015; Ackermann et al., 2015)).

Early work into hematopoiesis using hESC systems suggested that the differentiation process of hESCs is more similar to YS and FL hematopoiesis than BM-derived HSC hematopoiesis. Lu et al. showed that $CD34^+$ $CD38^-$ hematopoietic cells generated from hESCs were transcriptionally different to HSCs and had a higher proliferative capacity (Lu et al., 2004). Consistent with this result, other protocols described around the same time were unable to generate mature adult enucleated erythrocytes expressing high level of adult globin (Vodyanik et al., 2005; Olivier et al., 2006; Chang et al., 2006).

While early protocols had been strongly biased towards primitive hematopoiesis, many groups have now described methods for generating mature hematopoietic lineages such as T lymphocytes (Timmermans et al., 2009; Kennedy et al., 2012; Uenishi et al., 2014; Sturgeon et al., 2014), B lymphocytes (Zambidis et al., 2008; French et al., 2015) and adult globin expressing enucleated erythrocytes (Olivier et al., 2016). While most mature erythrocytes can be generated in feeder-free condition (Olivier et al., 2016), lymphoid lineages still require complex stepwise protocols including different types of modified feeder cells (OP9-DL1 and OP9-DL4). The type of globin expressed by erythrocytes and the lymphoid potential have been two of the major ways of distinguishing primitive hematopoiesis from definitive hematopoiesis in the context of hPSC differentation. For monocyte and Mϕ differentation it is more difficult to assess their ontogeny without looking at the lineage potential of their progenitors. Of note, lymphoid potential has often been used as a readout for definitive AGM-like hematopoiesis in hPSC models as it was believed that lymphoid potential was restricted to HSCs. But lymphoid potential

has been shown to emerge before HSCs in the mouse, undermining the concept that lymphoid potential predicts the existence of an HSC (reviewed in Lin et al. (2014)).

Table 1.1: Different protocols described for the generation of mature myloid cells from human PSCs. This table was adapted from (Ackermann et al., 2015).

Cell type	PSC source	EB	FCS	Feeder cells	Cytokines	Reference
Erythrocyte	hESC	Yes	Yes	No	bFGF, VEGF, EPO, SCF, nFlt3-L, IL-3, IL-6, G-CSF, TPO	Chang et al. (2006)
	hESC	No	Yes	S17 and FH-B-hTERT	Clonogenic assay: SCF, GM-CSF, IL-3, EPO	Qiu et al. (2005)
	hESC	No	Yes	mFL stroma cells	Clonogenic assay: SCF, IL-3, IL-6, TPO, G-CSF, EPO	Ma et al. (2008)
	hESC, hiPSC	No	Yes	OP9, MS5	TPO, IL-3, IL-6, Flt3-L, SCF, EPO	Dias et al. (2011)
	hESC	No	Yes	FH-B-hTERT, MS5	IL-3, BMP4, Flt3-L, SCF, EPO, IGF-1	Olivier et al. (2006)
	hPSCs	Yes	No	No	BMP4, VEGF, Wnt3A, Activin A, FGFα, SCF, IGF2, TPO, Flt3L, IL3, IL11, EPO, small molecule inhibitors	Olivier et al. (2016)
Mk/platelets	hESC	Yes	No	No	BMP4, VEGF, bFGF, SCF, TPO, IL-3	Pick et al. (2013)
	hESC	Yes	Yes	OP9	BMP4, VEGF, IL-3, Flt3-L, TPO, SCF, EPO	Vanhee et al. (2015)
	hESC, hiPSC	No	No	No	BMP4, VEGF, bFGF, TPO, SCF, Flt3-L, IL-3, IL-6, IL-9	Feng et al. (2014)
	hESC	No	No	OP9, C3H	BMP4, VEGF, IL-6, IL-9, IL-11, bFGF, TPO, SCF	Lu et al. (2011)
Granulocyte	hESC	Yes	Yes	No	IGF-II, VEGF, SCF, Flt3-L, TPO, G-CSF	Saeki et al. (2009)
	hESC	No	Yes	OP9	BMP4, SCF, Flt3-L, IL-6, TPO, G-CSF	Yokoyama et al. (2009)
	hESC, hiPSC	Yes	No	No	BMP4, VEGF, SCF, TPO, Flt3-L, IL-3, G-CSF	Niwa et al. (2011)
	hiPSC	Yes	No	No	IL-3, G-CSF or GM-CSF	Lachmann et al. (2015)
	hESC, hiPSC	No	Yes	OP9	GM-CSF, G-CSF, IL-3, IL-5	Choi et al. (2009)
Mϕ	hESC, hiPSCs	Yes	No	No	IL-3, M-CSF	Karlsson et al. (2008) van Wilgenburg et al. (2013)
	hESC, hiPSC	Yes	No	No	IL-3, M-CSF, or GM-CSF	Lachmann et al. (2015)
	hESC, hiPSC	No	Yes	OP9	GM-CSF, M-CSF, IL-1β	Choi et al. (2009)
DC	hESC	Yes	hAS	No	SCF, Flt3-L, GM-CSF, IL-3, TPO, IL-4, TNF-α	Su et al. (2008)
	hESC	Yes	No	No	BMP4, GM-CSF, IL4	Tseng et al. (2009)
	hESC, hiPSC	No	Yes	OP9	GM-CSF, IL-4, TNF-α	Choi et al. (2009)
	hiPSC	No	Yes	OP9	GM-CSF, M-SCF, IL-4, TNF-α	Senju et al. (2011)

Table 1.2: Different protocols described for the generation of mature lymphoid cells from human PSCs. This table was adapted from Ackermann et al. (2015).

Cell type	PSC source	EB	FCS	Feeder cells	Cytokines	Reference
NK cells	hESSC, hiPSC	Yes	Yes	OP9-DL4	BMP4, bFGF, Activin A, VEGF, IGF-1, IL-6, IL-11, SCF, IL-3, EPO, TPO, IL-13, Flt3-L, IL-15	Sturgeon et al. (2014)
	hESC, hiPSC	Yes	hAS	OP9-DL1	BMP-4, VEGF, SCF, IL-3, Il-6, TPO, EPO, IL-7, Flt3-L, IL-15	Ferrell et al. (2015)
	hESC	No	Yes	S17, AFT024	IL-15, IL-3, IL-7, SCF, Flt3-L	Woll et al. (2005)
T cells	hESC	Yes	Yes	OP9-DL4	BMP-4, bFGF, Activin A, VEGF, IL-6, IGF-1, IL-11, SCF, EPO, TPO, Flt3-L, IL-7, IL-15	Kennedy et al. (2012)
	hESC, hiPSC	Yes	Yes	OP9-DL4	BMP4, bFGF, Activin A, VEGF, IGF-1, IL-6, IL-11, SCF, IL-3, EPO, TPO, IL-3, Flt3-L, IL-7	Sturgeon et al. (2014)
	hESC, hiPSC	No	Yes	OP9-DL1, OP9-DL4	BMP-4, bFGF, VEGF, TPO, SCF, IL-6, IL-3, IL-7, Flt3-L	Uenishi et al. (2014)
	hESC	No	Yes	OP9, OP9-DL1	Flt3-L, IL-7, SCF	Timmermans et al. (2009)
B cells	hESC	Yes	Yes	OP9	BMP4, VEGF, FGF1, bFGF, SCF, Flt3-L, TPO, GM-CSF, IL-2, IL-4, IL-15, G-CSF, IL-3, IL-6, IL-7	Zambidis et al. (2008)
	hiPSC	No	Yes	OP9, MS5	IL-7, IL-3, SCF, Flt3-L	French et al. (2015)

bFGF: Basic fibroblast growth factor, BMP4: Bone morphogenetic protein 4, EPO: Erythropoietin, Flt3-L: Fms-related tyrosine kinase 3 ligand, TNF-α: Tumor necrosis factor α, FGF1: Fibroblast growth factor 1, G-CSF: Granulocyte-colony stimulating factor, GM-CSF: Granulocyte-macrophage colony-stimulating factor, IGF-1: Insulin-like growth factor-1, IL: Interleukin, M-CSF: Macrophage colony-stimulating factor, Mk: Megakaryocyte, NK cell: Natural killer cell, SCF: Stem cell factor, TPO: Thrombopoietin, VEGF: Vascular endothelial growth factor, Wnt3A: Wnt Family Member 3A

1.3 Tissue-resident Mϕ ontogeny in the mouse

1.3.1 Early concepts of Mϕ ontogeny - The unified mononuclear phagocytic system

Historically, the unified mononuclear phagocytic system (MPS) theory held that all tissue-resident Mϕs are maintained by a constant supply of BM-derived blood monocytes (van Furth and Cohn, 1968; van Furth et al., 1972). However, more recent evidence has shown that, while dermal (Tamoutounour et al., 2013), gut (Bain et al., 2014) and a fraction of cardiac Mϕs (Epelman et al., 2014), are of blood monocyte origin, most tissue-resident Mϕs such as microglia, Langerhans cells (LC), Kupffer cells and splenic Mϕs self-maintain locally throughout adult life, independently of HSCs (Ginhoux et al., 2010; Schulz et al., 2012; Hashimoto et al., 2013; Yona et al., 2013; Epelman et al., 2014). Furthermore, it has now been established in the mouse that the three waves of hematopoietic progenitors produced in the developing embryo contribute differently to distinct populations of adult tissue-resident Mϕs (figure 1.3).

1.3.2 Contribution of YS primitive Mϕs to tissue-resident Mϕ populations

The very first Mϕs generated in the embryo arise from the primitive wave of monopotent Mϕ progenitors (Palis et al., 1999; Bertrand et al., 2005) and are found in the YS blood islands at E9.0 (Bertrand et al., 2005; Kierdorf et al., 2013). These Mϕs then colonise, through blood circulation, the brain by E9.5 and the remaining embryonic tissues by E10.5 (Ginhoux et al., 2010; Hoeffel et al., 2012). Although the first Mϕs are detected after the start of EMP generation it is unlikely that EMPs have already developed into mature Mϕs by E9.0. Interestingly, these Mϕs, although found in the blood of the developing embryo (Hoeffel et al., 2015), have been described as not undergoing a monocytic stage, but rather to differentiate directly from monopotent progenitor into Mϕs (Takahashi et al., 1989; McGrath et al., 2015a). The concept of monocyte and Mϕ in embryonic mouse development will be detailed later in the nomenclature section 1.3.5.2.

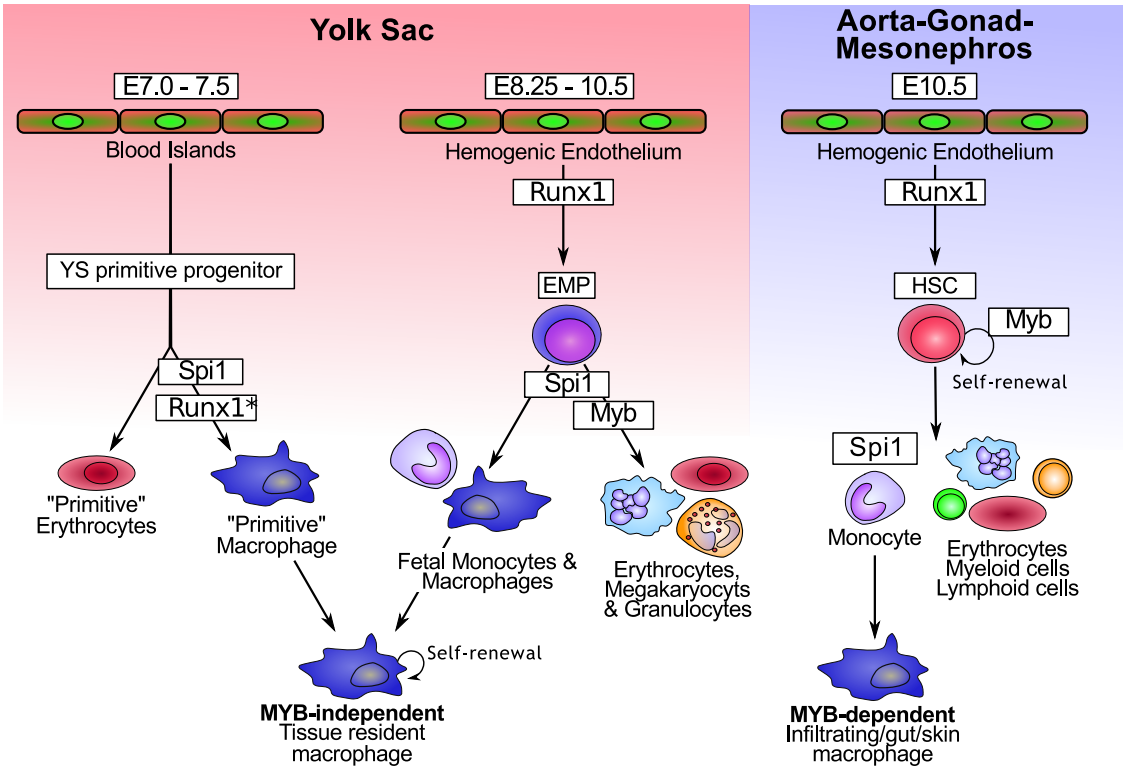

Figure 1.3: Myeloid development and maintenance in the mouse embryo and adult mouse. Three independent waves of myelopoiesis occur in the mouse embryo. A first wave of Myb-independent primitive Mϕs and erythrocytes is generated at E7.0-E7.5. (*) While Runx1 is required for Mϕ and EMP generation, it is dispensable for primitive erythrocyte differentiation (Wang et al., 1996), but they are affected by the loss of Runx1 (Yokomizo et al., 2008). A second wave of hematopoiesis occurs at E8.25 generating Runx1-dependent EMPs. These EMPs are likely capable of some Myb-independent monocyte and Mϕ production but require Myb for erythroid, megakaryocyte and granulocyte production. A third wave of hematopoiesis is generated at E10.5 in the AGM generating the future definitive multilineage HSCs. This third wave is dependent on both Runx1 and Myb for its generation and maintenance.

In line with the unified MPS theory, the wave of primitive Mϕs was initially considered transient and not contributing significantly to the adult Mϕ population. However, with the advances in mouse fate-mapping, BM chimeras, parabiosis and gene knock-out (KO) studies this vision shifted to a much more complex system. Ginhoux et al. in 2010 was the first to show using a tamoxifen-inducible $Runx1^{Mer-Cre-Mer}$ fate mapping model, developed by Samokhvalov et al. (2007), that microglia derive from YS-derived Mϕs. By inducing tamoxifen at E7.0-E7.5 they were able to show that microglia, as well as many other tissue-resident Mϕ

populations, derived from progenitors generated in the YS as early as E7.5. Labelled microglia persisted in the brain and were not substantially replaced by unlabelled monocyte-derived Mϕs. Later Schulz et al., using a Myb$^{-/-}$ mouse model were able to show that most YS-derived F4/80^{High} tissue-resident Mϕs developed in a Myb-independent fashion (Schulz et al., 2012). Myb, as mentioned earlier is required for HSC-derived hematopoiesis, while being dispensable for YS hematopoiesis. In addition to showing that most tissue Mϕs in the early embryo were derived from Myb-independent YS-Mϕs, they showed by injecting Myb$^{+/+}$ BM cells into a recipient conditional Myb KO mouse, that most F4/80^{High} tissue-resident Mϕs are only marginally replaced by blood monocytes.

1.3.3 Contribution of EMP-derived monocytes and Mϕs to tissue-resident Mϕ populations

More recent lineage tracing approaches have confirmed the early YS-Mϕ origin of microglia (Kierdorf et al., 2013; Hoeffel et al., 2015; Sheng et al., 2015) but have proposed a different origin for most other tissue-resident Mϕs. Hoeffel et al. showed that adult LCs derive primarily from FL monocytes with a minor contribution of YS-Mϕs (Hoeffel et al., 2012). Guilliams et al. showed that long-lived alveolar Mϕs developed from FL monocytes before birth and were maintained independently from HSC-derived adult monocytes (Guilliams et al., 2013). FL monocytes have also been described as being involved in the generation of adult Mϕs in the heart (Epelman et al., 2014). Subsequent studies showed that most tissue-resident Mϕs, including LC and Kupffer cells, kidney and alveolar Mϕs derived from EMPs (Hoeffel et al., 2015). A similar study the same year observed a comparable result by fate mapping FL monocyte using a monocyte specific promoter (S100a4) which is not expressed in YS-Mϕs (Gomez Perdiguero et al., 2015).

1.3.4 Contribution of fetal HSCs to tissue-Resident Mϕ populations

While many reports have supported the YS-Mϕ and fetal monocyte origin of most tissue-resident Mϕs, Sheng et al. challenged this view by suggesting that other

than microglia and LCs, all other tissue-resident Mϕs were derived from fetal HSCs (Sheng et al., 2015). This alternate view probably derives from the subtle differences between different lineage tracing models, which is one of the challenges for the future in this field and has been reviewed extensively (McGrath et al., 2015a; Perdiguero and Geissmann, 2015; Ginhoux and Guilliams, 2016).

1.3.5 Nomenclature of macrophage development

1.3.5.1 MYB-independent and MYB-dependent hematopoiesis

Since the publication of Schulz et al. the terms "Myb-independent" and "Myb-dependent" have been used to define a category of embryonic Mϕs. While Myb is required for HSC generation and proliferation (Sumner et al., 2000; Lieu and Reddy, 2009; Schulz et al., 2012) the requirement of Myb for EMPs and fetal monocyte generation has not been formally demonstrated. Initial studies of Schulz et al. have reported a large decrease in c-kit+ EMPs in the FL of $Myb^{-/-}$ mice leading to the early conclusion that Myb-independent Mϕs-derived mainly from primitive YS-progenitors. That being said, while the FL of $Myb^{-/-}$ animals have largely reduced number of kit+ EMPs, some are still detected, raising the possibility of a Myb-independent EMP subpopulation (Schulz et al., 2012). In addition, a recent study of Perdiguero et al. reported $CD11b^{high}F4/80^{low}$ fetal monocytes in the FL of E14.5 $Myb^{-/-}$ mice (Gomez Perdiguero et al., 2015). As an added complication, the short life span of $Myb^{-/-}$ mice, which die in utero at E15 (Mucenski et al., 1991) makes long-term study of FL hematopoiesis difficult. Taken together, observations in the mouse would suggest that although primitive Mϕs are Myb-independent, at least a subset of EMP-derived fetal monocytes and Mϕs are independent of Myb.

1.3.5.2 Monocytes and Mϕs

In the late 1980s, Naito et al first documented the in situ production of two different types of Mϕs at E8 to E8.5 in the mouse YS, one which was qualified as "primitive" and another as "definitive" (Naito et al., 1989). "Primitive" Mϕs expressed the terminal differentiation marker F4/80 and apparently bypassed the pro-monocyte

and monocyte stage of differentiation (Naito et al., 1989; Takahashi et al., 1989). "Definitive" Mϕs, detected at the same stage, were considered undergoing monocytic differentiation as they displayed Myeloperoxidase (MPO) activity, which is typically associated with monocytes. At E10 these "definitive" Mϕs reached maturation and expressed F4/80. The first wave of mature F4/80$^+$ "primitive" Mϕs described by Naito et al. was later found out to be a transient wave of mature CD45$^+$F4/80$^+$c-kit$^-$ maternal Mϕs detected at E7.5 - E8 (Bertrand et al., 2005; Kierdorf et al., 2013). The wave described as "definitive" by Naito et al. was most likely the first wave of immature YS-derived Mϕs, which are detected at E9 (Bertrand et al., 2005; Kierdorf et al., 2013) and found in the brain by E9.5 (Ginhoux et al., 2010; Hoeffel et al., 2012). Therefore the very first concept of "primitive" and "definitive" Mϕ described in 1989 was not the same as what is now described as primitive and definitive Mϕs.

What Naito et al. described as "definitive" Mϕs undergoing monocytic differentiation are most likely YS Mϕs-derived from monopotent precursors that are currently still not considered to undergoe monocyte differentiation. Monocytes by their current definition have not been detected in the mouse embryo before E12.5, after the establishment of these early Mϕs (Schulz et al., 2012).

In addition to the morphology, which is often used, most recent papers have defined YS-Mϕs and fetal monocytes by their expression of specific phenotypic markers. YS-Mϕs are defined as CD45$^+$ Cx3cr1$^+$ CD11b^{low} F4/80^{high} Ly6C$^-$ while fetal monocytes are defined as CD45$^+$ Cx3cr1$^+$ CD11b^{high} F4/80^{low} Ly6C$^+$ (Schulz et al., 2012; Gomez Perdiguero et al., 2015; Hoeffel et al., 2015). Upon tissue migration and Mϕ differentiation, fetal monocytes down-regulate Ly6C and up-regulate Cx3cr1 and CD64 and differentiate into tissue-resident CD45$^+$ Cx3cr1$^+$ CD11b^{high} F4/80^{low} Ly6C$^-$ CD64 $^+$ Mϕs (Schulz et al., 2012; Hoeffel et al., 2015).

Interestingly F4/80^{high}CD11b^{low} YS-Mϕs are not restricted to tissues, as they are found in the blood until E16.5 (Hoeffel et al., 2015). Furthermore, in circulation-deficient embryos, YS-Mϕs fail to colonise embryonic tissue, and are detected only in the YS (Ginhoux et al., 2010; Hashimoto et al., 2013).

1.3.6 Maintenance of tissue-resident Mϕ populations in disease and homeostasis

While in the developing embryo Mϕs are almost exclusively from YS-Mϕs or EMPs, their maintenance under homeostasis and pathological conditions is dependent on the balance between resident Mϕ proliferation and blood monocyte recruitment. Initially it was believed that mature Mϕs were unable to proliferate, however there is now strong evidence to show that Mϕs and monocytes can indeed self-renew. As will be detailed in this section, with age the balance between local proliferation and monocyte recruitment is altered, independently of pathology. The research done on the impact on Mϕ self-renewal and monocyte recruitment during pathological conditions is a nascent field but seems to be largely dependent on the organ/tissue and the type of pathology under study (reviewed in (Belhareth, 2015)).

1.3.6.1 Mϕ proliferation

Overall, various growth factors and cytokines such as M-CSF, IL-34, GM-CSF and IL-4 have been shown to stimulate Mϕ proliferation and self-renewal in a context and tissue-specific manner. M-CSF induces Mϕ proliferation *in vivo* and *in vitro*, both at steady state and during inflammation (Jenkins et al., 2013a; Hume and MacDonald, 2012; Davies et al., 2013b). In addition, study of uterine Mϕ and DC dynamics during mouse pregnancy under physiological conditions showed both a local proliferation of resident Mϕ, controlled by M-CSF, and recruitment of BM-monocytes driven by CCR2 (Tagliani et al., 2011). IL-34, an alternative ligand of the M-CSFR produced by neurons and keratinocytes, is required for LC development (Wang et al., 2014) and for microglia maintenance and proliferation in the brain (Greter et al., 2012). GM-CSF plays a major role in alveolar Mϕ maintenance (Shibata et al., 2001) and recovery after depletion (Hashimoto et al., 2013), as well as promoting peritoneal Mϕ proliferation *in vivo* (Eroğlu et al., 2002). While IL-4 does not play a role in M-CSF-dependent homeostatic proliferation of Mϕs (Hashimoto et al., 2013; Jenkins et al., 2013b; Davies et al., 2013b) the administration of IL-4 induced Mϕ proliferation in the mouse liver, spleen and

BM (Milner et al., 2010; Jenkins et al., 2011). In addition, IL-4 mediates local proliferation of pleural Mϕs during nematode infection (Jenkins et al., 2011). IL-4 likely acts in coordination with other cytokines in the tissue, as it is not sufficient to induce proliferation of Mϕs *in vitro* (Milner et al., 2010; Jenkins et al., 2011, 2013b).

1.3.6.2 Homeostatic control of proliferation and monocyte recruitment

1.3.6.2.1 Intestinal, Dermal Mϕs and LCs

Brain et al., using a functional and phenotypic approach showed that, after birth embryonic-derived Mϕs (F4/80^{high} CD11b^{low}) in the colon were rapidly replaced by BM-derived Mϕs (F4/80^{low} CD11b^{high}) (Bain et al., 2013) and that local tissue-resident Mϕs do display self-renewal but not enough to maintain the Mϕ population. A subsequent study, using a parabiosis approach confirmed the need for a constant CCR2-dependent recruitment of Ly6C^{high} BM-derived monocytes to maintain the intestinal Mϕ population (Bain et al., 2014). In the same study, administration of broad-spectrum antibiotics reduced the number of recruited BM-derived Mϕs but had little impact on tissue-resident Mϕs of embryonic origin indicating that the microbiota played a role in the maintenance of the intestinal macrophage population. It has been proposed that the frequent exposure to microorganisms within in the intestine causes a low level inflammation which induces recruitment of BM-monocytes resembling classical inflammation, this state was termed "primed homeostasis" (Zigmond and Jung, 2013). Thus, for the gut, embryonic Mϕs are present at birth but they are quickly replaced by BM-monocytes that replenish this pool throughout life.

Skin, another tissue with high microbial exposure, provides a very interesting model as it contains two major Mϕ populations, dermal Mϕs and epidermal LCs. Dermal Mϕs, as for intestinal Mϕs, are mainly derived from BM-derived monocytes and are distinct from dermal-dendritic cells, also of BM-derived monocyte origin (Tamoutounour et al., 2013). In contrast, LC, which are of embryonic origin (section 1.3.2), display a burst of proliferation just after birth (Chorro et al., 2009), and are

subsequently maintained in adulthood through low-level proliferation, independent of BM-derived monocytes (Merad et al., 2002; Chorro et al., 2009). After tissue irradiation, LCs replenish the tissues by proliferation. Interestingly, in this case not all LCs are equally proliferative, suggesting the possibility of "LC progenitors" within the skin (Ghigo et al., 2013).

1.3.6.2.2 Microglia

Microglia, potentially due to their seclusion behind the blood brain barrier, almost exclusively derive from YS-primitive progenitors, with very little input from EMP- or HSC-derived monocytes (section 1.3.2, 1.3.3 and 1.3.4). At birth, microglia expand rapidly in the brain by *in situ* proliferation (Ginhoux et al., 2010), after which they self-maintain by proliferation in response to injury or neurodegenerative conditions throughout adult life (Ajami et al., 2007). The maintenance of adult microglia under these homeostatic or challenging conditions is independent of BM-derived monocytes (Ajami et al., 2007; Ginhoux et al., 2010). Infiltration of BM-derived monocytes into the brain can occur only under conditions where the blood-brain barrier has been disrupted (Mildner et al., 2007). Ajami et al. have shown that in both multiple sclerosis and experimental autoimmune encephalomyelitis mouse model, BM-Mϕ influx occurs during inflammatory condition, but the BM-monocyte-derived Mϕs do not contribute to the microglial pool after remission and are progressively replaced by proliferation of microglia (Ajami et al., 2011).

1.3.6.2.3 Alveolar and Cardiac Mϕs and Kupffer cells

Mϕs in the lung, liver and heart all derive from EMP-derived fetal monocytes and their maintenance in the adult is less binary than the previous Mϕ populations described. Cardiac Mϕs are of embryonic origin but under steady state condition they are gradually replaced by BM-monocyte-derived Mϕs with age (Molawi et al., 2014). Interestingly, this gradual replacement of embryonic-derived Mϕs is reflected in a change in surface marker expression of cardiac Mϕs from a majority of CX3CR1^{+}

MHCII$^-$ to a majority of CX3CR1$^-$ MHCII$^+$ Mϕs. While BM-monocytes can differentiate into both subpopulations they are biased towards the CX3CR1$^-$ MHCII$^+$ Mϕ subpopulation. In line with the progressive replacement of cardiac Mϕs with age, their repopulation after depletion is aided by BM-monocytes, resulting in a mixed pool of Mϕs of various ontogenies within the heart (Epelman et al., 2014).

Alveolar Mϕs are maintained with minimal contribution of BM-monocytes during steady-state (Guilliams et al., 2013), however recruited Mϕs can repopulate the alveolar niche after lethal irradiation (Epelman et al., 2014). In addition, YS-Mϕs, fetal monocytes and BM-monocytes are all capable of colonizing the alveolar niche and differentiate into almost identical long-lived alveolar Mϕs (Van de laar et al., 2016). Similarly, Kupffer cells which are of embryonic origin and self-renew at the steady state can be replaced by BM-monocytes after specific diphtheria toxin receptor depletion (Scott et al., 2016).

1.3.7 How different are these Mϕ populations?

One major question which remains to be answered is to what degree ontogeny impacts function. A complicating factor in answering this question has been the high plasticity and diversity of Mϕs, and their capacity to specialise upon exposure to tissue-specific stimuli, making it hard to distinguish environmental and ontogenic impact.

Many studies have investigated the phenotypic and functional differences of tissue-resident Mϕs of embryonic origin and that of tissue-resident Mϕs derived from BM-monocytes and identified very few differences. In the heart and dermis, the MHCII$^+$ CX3CR1$^-$ and MHCII$^-$ CX3CR1$^+$ subpopulations (Tamoutounour et al., 2013; Epelman et al., 2014; Pinto et al., 2014) derive preferentially from embryonic Mϕs or BM-monocytes, respectively (1.3.6.2.3), but although biased, both subpopulations can be of mixed origin. Using a chimeric mouse model, Gibbings et al. showed that within the same mouse, alveolar Mϕs of host origin (embryonic-derived) and of donor origin (BM-derived) demonstrated that of the 30 000 genes only about 0.1% were linked to developmental origin and overall functional analyses were similar

(Gibbings et al., 2015). Scott et al. recently showed that BM-monocytes could differentiate into self-renewing Kupffer cells closely resembling embryonic-derived resident Kupffer cells in a diphtheria toxin-mediated depletion mouse model (Scott et al., 2016). In the case of alveolar Mϕs, a recent study showed that YS-Mϕs, fetal monocytes and BM-monocytes can all colonise an empty alveolar niche and generate alveolar Mϕs of similar function (Van de laar et al., 2016).

In contrast, a study of brain repopulation by BM-monocytes after genotoxic irradiation Bruttger et al. showed that BM-derived microglia differentially expressed more than 2000 genes compared to resident microglia (Bruttger et al., 2015). While this might be due to a larger difference between BM-monocyte-derived Mϕs and microglia it can very well also be due to genotoxic irradiation having a very strong impact on the brain homeostasis and thus the Mϕ microenvironment. In summary, although differences have been observed between embryonic- and BM-derived Mϕs it is hard to assess how much of the differences are due to microenvironment as Mϕs are very responsive to tissue damage and environmental signals.

Due to the plasticity of Mϕs it has been hard to assess whether their ontogeny has any impact on their function. However, several aspects of Mϕ biology that appears to be tightly linked to ontogeny is resistance to genotoxic stress, longevity and self-renewal. Using ionizing radiation depletion of LCs, Price et al. (2015) showed that LCs resisted depletion and apoptosis at high irradiation dose and rapidly repaired DNA damage after exposure. As stated previously, Mϕs deriving from all three developmental waves can repopulate an empty alveolar niche, in the same study Van de laar et al. (2016) also showed that in a competition study, fetal monocytes (which are the precursors of alveolar Mϕs) had a selective advantage compared to YS-Mϕs and BM-monocytes in colonizing the alveolar niche due to their higher proliferative capacity. In addition they showed that *in vitro*, fetal monocytes could be easily induced into proliferation by GM-CSF treatment while BM-monocytes had low levels of proliferation even though they had the same GM-CSF receptor density. Furthermore, as discussed previously, in many tissues recruited BM-monocytes fail to persist in the tissues after inflammation (Ajami

et al., 2007; Hashimoto et al., 2013; Zigmond et al., 2014). However, BM-monocyte-derived Mϕ can self-renewal under the right conditions (Van de laar et al., 2016; Scott et al., 2016). Infiltrating Mϕ proliferation, often liked to inflammation, also plays a critical role in certain diseases such as atherosclerosis, obesity and cancer (reviewed in (Gentek and Sieweke, 2014)).

1.4 Tissue-resident Mϕ ontogeny in the human

1.4.1 *In vivo* Mϕ ontogeny

Our knowledge of human embryonic myeloid development and the ontogeny of tissue-resident Mϕs is much more limited due to the limited availability of human embryos at such an early developmental stage (Ivanovs et al., 2011). Although little is still known regarding the ontogeny of human adult tissue-resident Mϕs *in vivo*, the different myeloid subpopulations of the skin have been extensively studied in regards to their maintenance. After HSC transplantation, dermal CD1a$^+$ and CD14$^+$ DC are rapidly replaced by donor-derived monocytes (complete replacement after 40 days), while CD1a$^-$ CD14$^+$ FXIIIa$^+$ dermal Mϕs were replaced at a much slower rate (median of 46% replacement after 100 days) (Haniffa et al., 2009). A subsequent study by the same group demonstrated that the CD14$^+$ DCs described in Haniffa et al. (2009) were in fact monocyte-derived Mϕs (and not DCs) with a high turnover rate (half-life of <6 days) (McGovern et al., 2014). These observations are consistent with studies in the mouse showing progressive replacement of dermal DCs and Mϕs by BM-derived monocytes (see section 1.3.6.2.1). Epidermal LCs on the other hand, in a study of human hand allograft, were still of donor origin 10 years postgraft (Kanitakis et al., 2011). In addition, donor-derived LCs undergoing mitosis were detected 8 years postgraft, indicative of their self-renewal capacity. Consistent with transplantation studies, patients harbouring mutations of GATA-2 or IRF8, resulting in a BM-monocyte deficiency, have normal numbers of CD1a^{High} langerin$^+$ LCs, reduced numbers of CD45$^+$ HLA-DR$^+$ dermal Mϕs and absence of CD1a$^+$ and CD14$^+$ DCs/Mϕs (Bigley et al., 2011; Hambleton et al., 2011). Overall this ties in with the observation in the mouse showing that dermal Mϕs

and DCs were replenished by BM-derived monocytes while LCs self-renew locally independently of BM-derived monocytes (1.3.6.2.1).

1.4.2 hPSC Mϕ protocols

Many different methods have described monocyte, Mϕ, DC and granulocyte differentation from hPSCs. As for most other lineages, these protocols can be broadly separated into co-culture methods and EB-based methods. Initial methods describing the generation of hESC-derived DCs and monocytes/Mϕs used co-culture with stromal feeder cells and complex cytokine cocktails in combination with purification steps (Anderson et al., 2006; Slukvin et al., 2006). These protocols allowed for the differentiation of Mϕs from sorted $CD34^+$ hematopoietic progenitors, a labor-intensive and expensive process. Our laboratory then described an EB-based method, involving spontaneous EB formation from hESC followed by direct differentiation to monocytes/Mϕs using a cocktail of IL-3 and M-CSF in FCS containing media (Karlsson et al., 2008). In contrast to most feeder based protocols, the new method allowed for the continuous generation of of homogenous monocyte/Mϕs (>90% $CD14^+$), without any prior selection or sorting step. This method can yield over $1x10^7$ monocytes/Mϕs from a 6-well plate of differentiated cultures once a week for 1–3 weeks, after which yields drastically decrease. Shortly after this development, many other groups described Mϕ differentiation methods, some with EB intermediates and some based on co-culture with stromal cells for the generation of monocyte/Mϕ from hESC or hiPSCs (Choi et al., 2009; Subramanian et al., 2009; Kambal et al., 2011; Choi et al., 2011; Senju et al., 2011). Subsequently, our laboratory published an improved protocol, based on the initial Karlsson et al. (2008) protocol, which is a fully chemically defined serum- and feeder-free EB-based method for hiPSC and hESC monocyte/Mϕ differentiation (van Wilgenburg et al., 2013). The removal of fetal calf serum (FCS) allowed for sustained generation of a large number of homogenous hPSC-derived monocytes/Mϕs for a period up to a year. Recently a very similar method, different mainly by its basal media

and EB formation technique has described generation of both monocyte/Mϕ cells and granulocytes (Lachmann et al., 2015).

1.4.3 Nomenclature - hPSC-derived Monocytes and Mϕs

Although in the mouse the morphological and phenotypic distinction between YS-Mϕs, monocytes and infiltrating Mϕs has been well described, this is not the case for humans. The first issue is that the two main mouse markers used for distinguishing these populations, EMR1, the human homologue of F4/80, is an eosinophil-specific marker (Hamann et al., 2007) and a Ly6C human ortholog is absent in humans (Lee et al., 2013) making the usage of the same panel of markers impossible in humans. This lack of markers, combined with the lack of monocyte/Mϕ data on early human embryos makes defining the difference between a YS-Mϕ, a fetal monocyte and an adult BM-derived monocyte in humans very challenging.

In the previous articles published by our lab the mononuclear phagocytic cells produced from hiPSCs/hESs have been described as monocytes mainly due to their initial non-adherent stage. Although it is true that in adults, monocytes are found in the blood and are, therefore, rounded non-adherent cells whereas Mϕs are found in the tissues as adherent cells, murine YS-Mϕs seed the tissues through the blood, like monocytes. Due to this lack of clarity regarding monocytes and Mϕs in human, I will for my thesis refer to the mononuclear phagocytic cells generated from our hiPSC differentiation method as iPS-Mo/Mϕ.

1.4.4 Pluripotent stem cell-derived Mϕ ontogeny

While many methods have been described for the generation of mature monocytes and Mϕs little is still known of the ontogeny of hiPSC-derived monocytes and Mϕs. As the core phenotypic and functional markers of Mϕs are common between all three hematopoietic waves it is difficult to classify mature hPSC-derived-Mϕs using classical Mϕ markers.

The discoveries in the mouse, at the start of my DPhil, showing that most tissue-resident Mϕs derive from a different developmental origin than adult monocytes-derived Mϕs shed light on our lack of knowledge of human iPS-Mo/Mϕ ontogeny. In light of these findings I set out to unravel the ontogeny of human iPS-Mo/Mϕs. Based on our understanding of *in vitro* hPSC hematopoietic differentiation (subsection 1.2.2.2) my first hypothesis was that iPS-Mo/Mϕs produced during the first weeks of hiPSC differentiation derived from either primitive or EMP origin. As iPS-Mo/Mϕ production can be sustained for several months in our model system, my second hypothesis was that iPS-Mo/Mϕs produced later during iPSC differentiation could derive from either primitive/EMP origin or HSC origin due to a lineage switch happening later in differentiation. Klimchenko *et al.* had shown that hES-derived Mo/Mϕs closely resemble, both transcriptionally and functionally, FL-derived Mo/Mϕs from first-trimester fetuses (Klimchenko et al., 2011). In my thesis I therefore used a similar transcriptional approach, with two main aims: detect a potential lineage switch by studying the transcriptional signature of iPS-Mo/Mϕs over time and transcriptionally classify iPS-Mo/Mϕs by comparing their transcriptional signature with that of primary human fetal microglia and adult blood monocytes (Chapter 3). Based on the mouse findings of Schulz et al. (2012) showing that most tissue-resident Mϕs derive in a Myb-independent fashion I also set out to investigated the transcription factor requirement of hiPSC myelopoiesis, which became the main focus of my thesis (Chapter 4).

The fundamental studies of Mϕ development will be critical for generating suitable *in vitro* tissue-resident Mϕ models for the study of genetic, developmental, immunological and pathogenic diseases. In addition this model allows the investigation of fundamental human myelopoiesis, which is an essential step towards potential means to secure a reproducible source of human leukocytes for personalized therapies.

2

General Materials and Methods

Contents

2.1 Ethics Statements for use of Adult Blood and Stem Cell Lines 31
2.2 hESC/hiPSC culture 32
2.3 iPS-Mo/Mϕ differentiation 32
2.3.1 EB formation 32
2.3.2 iPS-Mo/Mϕ differentiation (iPS-Mo/Mϕ Factories) . . . 33
2.4 Cell count and viability 34
2.5 Cell proliferation assay 34
2.6 Eosin and Methylene-Blue staining 34
2.7 Flow cytometry staining and antibodies 34
2.8 Lentiviral production 35
2.9 EB diameter measurement 35

2.1 Ethics Statements for use of Adult Blood and Stem Cell Lines

The human ES cell line HUES-2 (passages 16–38) was obtained from the HUES Facility, University of Harvard (Cowan et al., 2004). Ethical approval for work on all hESC lines was reviewed and approved by the UK Stem Cell Bank Steering Committee (Medical Research Council, London UK, 20.10.2005).

2.2 hESC/hiPSC culture

The derivation of the NHDF-1 and OX1-19 line has been published previously (van Wilgenburg et al., 2013), hiPSC AH016-03 is being published elsewhere (ref pending). Briefly, the three lines were derived from dermal fibroblasts of a healthy 44 year old female donor for NHDF-1, a 36 year old male donor for OX1-19 and healthy 80 year old male donor recruited by the Oxford Parkinson's Disease Centre for AH016-03. All three lines were reprogrammed using retroviral reprogramming vectors under standardised protocols in the James Martin Stem Cell Facility, Sir William Dunn School of Pathology. The single-nucleotide polymorphism (SNP) datasets and the Illumina HT12v4 transcriptome array results have been deposited in Gene Expression Omnibus (GEO) under accession numbers GSM2055806 (AH016-03) and Superseries GSE45472 (OX1-19 and NDHF-1).

In the current study, hiPSCs were cultured in feeder-free conditions. Culture dishes were coated with hESC-qualified matrigel (Scientific Laboratory Supplies 354277) a minimum of 1h before passage. Cells were passaged using TrypLE Express (Gibco by Life Technologies) and resuspended in mTeSR^{TM}1 (Stemcell^{TM} technologies) media containing 10 μmol/L Rho-kinase inhibitor Y-27632 (Abcam) and plated at a density of 5x10^5 cells per well of a 6 well plate. Media was changed daily and cells were passaged every 4 to 6 days at near-confluence. The number of passages was kept to a minimum to reduce the likelihood of genetic change and cells were frozen in SNP-Quality-Controlled batches, from which cells would be thawed for each experiment, to ensure consistency.

2.3 iPS-Mo/Mϕ differentiation

2.3.1 EB formation

Spin-EBs were formed using a 96-well ultra-low adherence plate (Costar 7007). hiPSCs were washed with Phosphate-Buffered Saline (PBS) and harvested by incubating the cells for 5 min at 37°C with 1 mL of warm TrypLE Express (Gibco by Life Technologies). Cells were counted, washed with PBS and resuspended at

a final cell concentration of 10^5 cells/mL in EB media: mTeSR^{TM}1 (Stemcell^{TM} technologies), 50 ng/mL BMP-4 (GIBCO® - PHC9534), 20 ng/mL SCF (Miltenyi Biotec Ltd), 50 ng/mL VEGF (GIBCO® - PHC9394). 100 μL of cell suspension supplemented with 10 μmol/L Y-27632 was added per well and the 96-well plate was centrifuged at 100g for 3 min. EBs were fed at day 2 and 3 by aspirating 50 μL medium and adding 50 μL of fresh EB medium.

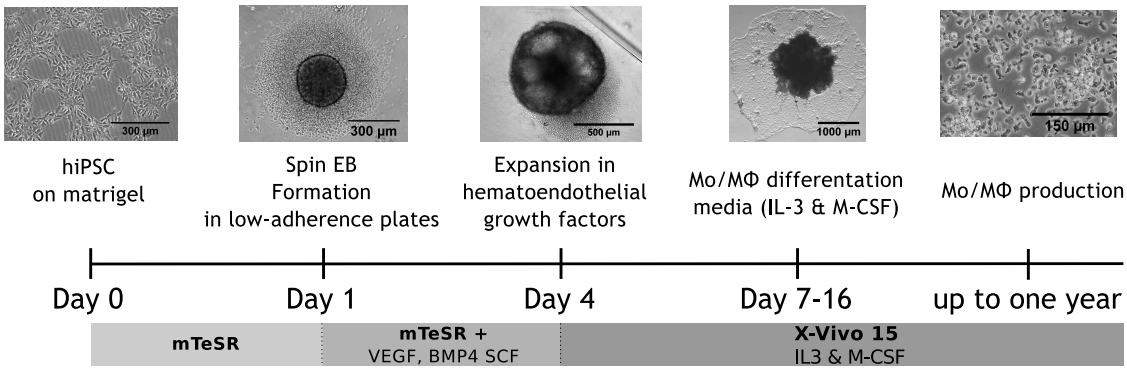

Figure 2.1: iPS-Mo/Mϕ stepwise differentiation. Spin-EBs are first generated from hPSCs on matrigel in mTeSR^{TM}1 supplemented with 50 ng/mL BMP-4, 20 ng/mL SCF and 50 ng/mL VEGF. After 4 days of growth EBs are plated in iPS-Mo/Mϕ differentiation media (Factory media). After 1 to 2 weeks iPS-Mo/Mϕs migrate out of the EBs and can be harvested in suspension.

2.3.2 iPS-Mo/Mϕ differentiation (iPS-Mo/Mϕ Factories)

The stepwise differentiation process of iPS-Mo/Mϕs, resulting in the generation of "factories" from which iPS-Mo/Mϕ can be harvested in the supernatant, is shown in figure 2.1. After 4 days of EB differentiation, EBs were transferred into a 6 well tissue culture plate (8 EBs/well) (Corning® Costar® 6 well flat bottom plate) and resuspended in factory differentiation media. Factory media, consisting of X-VIVO^{TM}-15 (Lonza), 100 ng/mL M-CSF (Invitrogen), 25 ng/mL IL-3 (R&D), 2 mM glutamax (Invitrogen), 100 U/mL penicillin and 100 mg/μL streptomycin (Invitrogen), and 0.055 mM β-mercaptoethanol (Invitrogen). Two thirds of the media was changed every 5 days. After the first production of hiPSC-derived iPS-Mo/Mϕs, non-adherent iPS-Mo/Mϕs were harvested in the supernatant every week for staining and counting.

2.4 Cell count and viability

For quantification of released iPS-Mo/Mϕs, cells were counted using the NC-3000 Viability and Cell Count Assays (chemometec). Solution 13 (1 μL), containing acridine orange (AO) and DAPI (4',6-diamidino-2-phenylindole) (chemometec) and 19 μL of cell suspension were mixed and from this 9 μL was loaded onto a chamber of an A8-slide (chemometec). For iPS-Mo/Mϕ quantification the number of total viable cells was normalised to the percentages of $CD14^+$ cells obtained by flow cytometry.

2.5 Cell proliferation assay

iPS-Mo/Mϕs were harvested, counted and $1x10^5$ cells were transferred into a well of a 12 well plate. iPS-Mo/Mϕs were pulsed with 10 μM EdU (5-ethynyl-2'-deoxyuridine) for 2 hours, after which they were harvested and stained according to the Click-iT^{TM} Plus EdU Flow Cytometry Assay Kit (ThermoFisher) manufacturer's protocol. Cells were analysed by flow cytometry on a FACSCalibur^{TM} (BD) instrument.

2.6 Eosin and Methylene-Blue staining

Cells ($5x10^4$) were centrifuged at 400g for 4 min onto a glass slide using a Cytospin 3 (Shandon). Slides were air dried briefly and stained using an eosin and methylene-Blue staining kit (HemoGurr®) as specified by manufacturers protocol. Images were acquired using an EVOS inverted microscope (Invitrogen).

2.7 Flow cytometry staining and antibodies

Harvested iPS-Mo/Mϕs or a single-cell suspension obtained from EB dissociation were pelleted at 400g for 5 min and washed once with PBS before being resuspended in 100 μL of FACS buffer (PBS + 10 μg/mL human serum IgG + 1% fetal bovine serum (FBS)). iPS-Mo/Mϕs were stained in FACS buffer + antibody (dilution 1:100) for 45 min at 4°C. Cells were then washed using PBS and resuspended in 2% Formaldehyde before being analysed using a FACSCalibur^{TM} Flow Cytometer (BD).

The following antibodies have been used in this study: α-CD14-APC antibody (MEM-15; Immunotools), IgG1-APC isotype (PPV-06 - Immunotools), α-CD34-APC (4H11; eBioscience), Mouse IgG1κ-APC isotype (P3.6.2.8.1; eBioscience), α-CD45-FITC (MEM-28; ImmunoTools), Mouse IgG1-FITC isotype (PPV-06; ImmunoTools), α-CD14-APC antibody (MEM-15; Immunotools), IgG1-APC isotype (PPV-06 - Immunotools), α-CD16-APC (LNK16; Immunotools), Mouse IgG1-APC isotype (PPV-06; ImmunoTools), α-CD11b-APC (ICRF44; BioLegend) and Mouse IgG1-APC Isotype (MOPC-21; BioLegend).

2.8 Lentiviral production

For lentiviral production the vector plasmids pCSRQ (Schaller et al., 2011), pSIN-RFP and pSIN-GFP (van Wilgenburg et al., 2013) were used. A 70% confluent 10 cm dish of human embryonic kidney (HEK) 293T cells was co-transfected with 5 μg of vector of interest, 8 μg of pCMVdR8.91 and 3 μg of vesicular stomatitis virus (VSV)-G envelope encoding plasmid using polyethylenimine (PEI) transfection. Briefly, the three plasmids were mixed in 2.5 mL of OptiMeM (Gibco®) after which, while vortexing, a solution of PEI (2.5 mL OptiMeM + 82 μL of 10 μM PEI) was added in a dropwise manner. PEI transfection solution was incubated for 15 min at room temperature (RT) after which it was added in a dropwise manner to the cells. Cells were incubated for 4h after which media was changed to DMEM + 10% FCS. Supernatant was harvested 48h post transfection, passed through a 45 μm filter and stored at -80°C.

2.9 EB diameter measurement

EBs were imaged 24h after formation on an EVOS inverted microscope (Invitrogen) and EB diameter was calculated using imageJ. Briefly, a straight line was drawn through the center of the EB and line length was calculated using the following macro:

```
macro "Measure Line... [m]"
{
      if (selectionType!=5)
          exit("Straight line selection required");

      name_out=getTitle();
      getLine(x1, y1, x2, y2, lineWidth);
      getPixelSize(unit, width, height, depth);
      x1*=width; y1*=height; x2*=width; y2*=height;
      length = sqrt((x2-x1)*(x2-x1)+(y2-y1)*(y2-y1));
      row = nResults();
      setResult("Label", row, name_out);
      setResult("Diameter", row, length);
      updateResults();
 }
```

3

Transcriptional & functional characterization of iPS-Mo/Mϕs over time

Contents

3.1 Introduction 38
3.2 Materials and methods 41
3.2.1 Transcriptome sample preparation 41
3.2.2 Transcriptome analysis 41
3.2.2.1 Data import, log2 transformation and normalization 42
3.2.2.2 Generating a ranked gene list 43
3.2.2.3 Pre-ranked Gene Ontogeny (GO) GSEA 44
3.2.2.4 GSEA result filtering and heatmap generation 44
3.2.2.5 Study of individual genes within a gene set . . 45
3.2.2.6 Metadata analysis 48
3.3 Results 51
3.3.1 Monocyte production, proliferation and morphology over time 51
3.3.2 Transcriptomic data analysis 56
3.3.2.1 Initial QC of data 56
3.3.2.2 Differential transcript expression study using RP approach 56
3.3.2.3 Closer look at the individual genes in a gene set 60
3.3.3 iPS-Mo/Mϕs are more similar to fetal microglia than adult blood monocytes 69
3.3.3.1 Comparative MDS vs blood monocytes and fetal microglia 69
3.3.3.2 iPS-Mo/Mϕ have higher proliferation gene expression than fetal microglia and blood monocytes 70

3.3.3.3 H1 iPS-Mo/Mϕ have lower adaptative immune gene enrichment than fetal microglia or blood monocytes 72
3.3.3.4 H5 iPS-Mo/Mϕ are very similar to fetal microglia 73
3.4 Discussion 76

3.1 Introduction

The generation of iPS-Mo/Mϕ from hESC/hiPSCs through EB formation offers a simple system for the study of human Mϕ and monocyte biology (Karlsson et al., 2008; van Wilgenburg et al., 2013). The protocol has become a routine method in our and other laboratories for the generation of iPS-Mo/Mϕs which can be used in many downstream applications (Van Wilgenburg et al., 2014; Flynn et al., 2015; Hale et al., 2015; Alasoo et al., 2015; van Wilgenburg et al., 2016; Blohmke et al., 2016). Each iPS-Mo/Mϕ factory, can generate a phenotypically and morphologically homogenous population of iPS-Mo/Mϕs over a period of up to a year (van Wilgenburg et al., 2013). However, no detailed comparison between cells produced at the beginning and those later had been done to evaluate the stability of the cells over time. Anecdotal evidence of early harvest cells being less adherent, less reactive and more proliferative suggested a difference that I aimed to investigate

Several reasonable hypotheses could explain a difference between early and late harvest iPS-Mo/Mϕs. First, early harvest cells might not be fully differentiated and closer to a precursor or immature Mϕ state and, therefore, behave slightly differently in experiments. Second, as the factories (M&M: 2.3) can produce iPS-Mo/Mϕs for up to a year it would not necessarily be surprising if over time there is a switch from a primitive YS-like Mϕ precursor origin to an EMP or HSC-like origin. Lineage switch over time in the same PSC differentiation culture between primitive hematopoietic progenitors and definitive hematopoietic progenitors generated from two different types of HE has been observed in several human PSC differentiation models (Choi et al., 2012; Rafii et al., 2013; Ditadi et al., 2015). Such a switch might be detectable as YS-Mϕs and Fetal monocytes can be distinguished from adult

monocytes by their higher proliferative potential in tissues, and lower expression of genes related to pathogen recognition and immune activation (Hoeffel et al., 2015; Van de laar et al., 2016).

To better understand on a global scale how iPS-Mo/Mϕs produced in early harvests compare to iPS-Mo/Mϕs produced several months later we decided to take a transcriptomic approach. The goal of this transcriptome is threefold, first it should allow us to better understand if and how different "early" iPS-Mo/Mϕs are compared to "late" iPS-Mo/Mϕs and therefore eliminate as much unwanted technical variability in our experiment which might be due to the time of harvest rather than the experimental conditions. Secondly, understanding how the transcriptomic signatures change over time might give us an insight into the possibility of a lineage switch over time. Lastly, it would allow for some meta-analysis to better classify the iPS-Mo/Mϕs with reference to the known different Mϕ subtypes.

For this purpose I performed a timecourse experiment in which "factories" from three different hiPSC lines were generated and iPS-Mo/Mϕs were harvested at different time points over a period of three months. The experimental design is summarised in figure 3.1. For my experimental setup I selected three control hiPSC lines, NHDF-1, AH016-3 and OX1-19, which are derived from 3 different donors reprogrammed (Yamanaka retroviruses) and have been previously quality-controlled and used extensively in our lab and are known to be capable of iPS-Mo/Mϕ differentiation. Initially I acquired some basic data regarding the size of the cells, their morphology, surface marker expression prior to analysing their transcriptome.

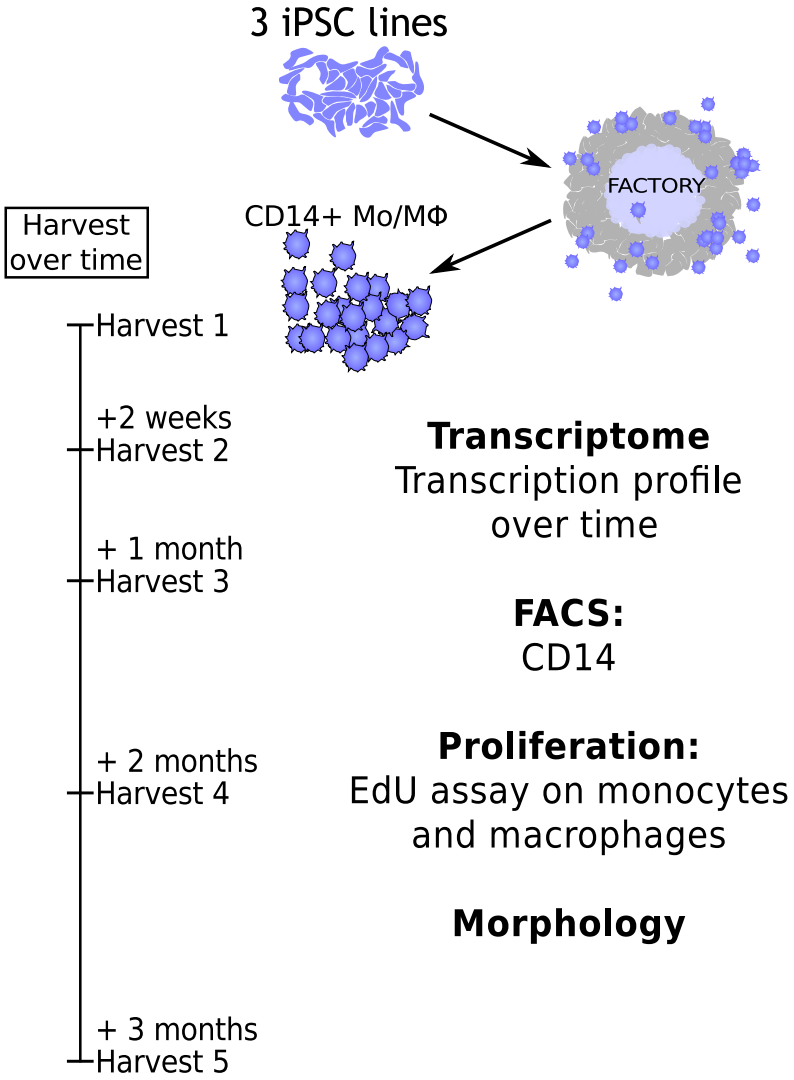

Figure 3.1: Experimental design. EB-derived factories of the three hiPSC lines AH016-03, NHDF-1 and OX1-19 were generated. Two weeks after the start of iPS-Mo/Mϕ production "harvest 1" iPS-Mo/Mϕs were collected. Subsequent harvests were collected at the indicated time points from the same factories. After that factories were maintained and iPS-Mo/Mϕs were harvested every two weeks to a month from the same factories. At each harvest, a sample was frozen for RNA extraction and transcriptome array and the remaining cells were used for antibody staining, EdU proliferation assay and imaging.

3.2 Materials and methods

3.2.1 Transcriptome sample preparation

For each harvest, 2x10^6 freshly harvested iPS-Mo/Mϕs were lysed using RLT buffer (QIAGEN) supplemented with 10 μL β-ME, homogenised using a QIAShredder column (QIAGEN) and immediately stored at -80°C for future RNA extraction. PBMCs from 3 healthy adult donors were isolated from blood by density gradient centrifugation with Ficol-Paque PLUS (17-1440-03, GE Healthcare) and monocytes were sorted using CD14 MACS beads (130-050-201, Miltenyi). CD14 sorted blood monocytes were lysed as described for iPS-Mo/Mϕs. RNA extraction was performed using the RNAeasy extraction kit (QIAGEN) as specificity by manufactures protocol. Human fetal microglia were isolated as described in (Durafourt et al., 2013) and RNA of fetal microglia was kindly provided by Dr Craig S Moore. 500 ng of RNA, at a concentration of 100 ng/μL was provided to the high-throughput genomics group at the Wellcome Trust Centre for Human Genetics (WTHG) for transcriptome analysis. Samples were run on a HumanHT-12 v4 BeadChip array (Illumina).

3.2.2 Transcriptome analysis

Data obtained from high-throughput genomics group at the Wellcome Trust Centre for Human Genetics were analysed using R. The code used for the analyses is detailed in this section, for clarity, only the code for the calculation of differential expression between harvest 1 and harvest 5 is shown here. The same code can be applied for all other differential expression analysis used in this chapter, by changing the variable to the right samples.

The provided data are:

12 bulk BeadChip HTv4 iPS-Mo/Mϕ samples from three donors (NHDF-1, OX1-19, AH016-03) over four harvest time points (H1 = 2 weeks, H2 = 4 weeks, H3 = 6 weeks, H5 = 10 weeks). The fourth harvest is omitted due to chip size. No technical replicates were made as this was an exploratory experiment. The RAW bead array data were converted to gene expression data using Genome Studio and

stored in csv format: "SampleGeneProfile.csv". Control probes were generated using Genome studio as well and stored in "ControlGeneProfile.csv".

3.2.2.1 Data import, log2 transformation and normalization

The gene expression data ("SampleGeneProfile.csv") were imported and the p-values were removed as using a ranked product (RP) approach does not rely on the p-value of expression but on the ranking of the genes. Data were then log2 transformed, which is better supported by the Linear Models for Microarray and RNA-Seq data (LIMMA) package for downstream analyses.

```
# read in data (this assumes that you are in the correct working
    directory)
exprs <- read.csv( "SampleGeneProfile.csv", check.names=F, as.is=T )

# clean up row and column names (also remove p-values)
row.names( exprs ) <- paste( exprs$ILMN_GENE )
exprs <- as.matrix( exprs[, grepl( ".AVG_Signal", colnames( exprs ) )
    ] )
colnames( exprs ) <- gsub( ".AVG_Signal", "", colnames( exprs ) )
colnames( exprs ) <- gsub( " ", "_", colnames( exprs ) )

# log scale

exprs <-  log2( exprs + 1 )
```

After importing the data and log2 scaling the expression values the LIMMA bioconductor package was used for quantile normalization of the data. Quantile normalization is one of the most commonly used method for analysing microarray data and works by transforming the empirical distribution of gene expressions so that they have a common distribution of intensities and can therefore be compared (Bolstad et al., 2003).

```
# Importing the LIMMA package
library( "limma" )

# quantile normalization
exprs <- normalizeBetweenArrays( exprs, "quantile" )
```

3.2.2.2 Generating a ranked gene list

R code for the RP approach (appendix A.2) based on the work of Heskes et al. for assessing the differential gene expression (Heskes et al., 2014) was provided by Quin Wills (Oxford Wellcome Trust Centre for Human Genetics). The RP approach is particularly useful for small datasets with limited technical repeats and for meta-data analyses. In the following example code the differential expression between Harvest 1 and H5 iPS-Mo/Mϕs is calculated. The list of differentially expressed genes is then sorted by the most significantly up-regulated to most significantly down regulated genes in H1 compared to H5. The sorted list is then directly saved as a pre-ranked gene list for Gene Set Enrichment Analysis (GSEA) (see section 3.2.2.3, below).

```
# load in the rankprod.R script: this also requires the 'qvalue'
    bioconductor package
library( "qvalue" )
source( "rankprod.R" )

# Harvest 1 and 5 differential expression
diffExprs <- exprs[, grepl( "H1_", colnames( exprs ) )] - exprs[,
    grepl( "H5_", colnames( exprs ) )]
diffExprs <- getRP( diffExprs )

# Apply a -1 multiplier to the Max logP of down-regulated genes
# This uses the fold change delta value generated by the ranked
    product algorithm

ranked_list <- (diffExprs[2] * (diffExprs[1] / abs(diffExprs[1])))

# After applying this multiplier:
# Highly expressed genes in H1 compared to H5 are positive
# Highly expressed genes in H5 compared to H1 are negative

# Sorting the gene list from largest to smallest max_logP
ranked_list.frame <- data.frame(ranked_list)  # order function
    required a data.frame
ranked_list.frame <- ranked_list.frame[order(-ranked_list.frame$max_
    logP), , drop = FALSE]

# Convert the rownames to a proper column of the data.frame
ranked_list.frame <- cbind(Row.Names = rownames(ranked_list.frame),
    ranked_list.frame)

# Remove the original rownames
rownames(ranked_list.frame) <- NULL

#Export csv format, directly with the .rnk extension used by GSEA
```

```
write.table(ranked_list.frame, file="Rank_product_test.rnk", sep="\t",
    row.names=F)
```

3.2.2.3 Pre-ranked Gene Ontogeny (GO) GSEA

The ranked gene list was used for pre-ranked GSEA using the GO biological process (BP) MSigDB database (c5.bp.v5.1.symbols.gmt) with 1000 permutations using GENE SYMBOL.chip as chip platform. Parameters used were "weighted" enrichment statistics, excluding sets smaller than 15 and larger than 500. Advanced fields were used as default (Collapsing mode for probe sets => 1 gene: Max Probe, Normalization method: meandiv, Omit features with no symbol match: true, Make detailed gene set report: true).

3.2.2.4 GSEA result filtering and heatmap generation

After GSEA, the full report files (`gsea_report_for_na_neg.xls` and `gsea_report_for_na_pos.xls`) were used to generate a list of pathways with a false discovery rate (FDR) q-value < 0.05. This list of significantly enriched pathways containing the pathway name and the associated enrichment score (ES) were used to generate a heatmap of pathways according to their ES.

```
# Read GSEA pathway/ES file
GSEA_ranked <- read.csv( "H1vsH5_GO_BP_Sorted_FDR_Ranked_ES.csv",
    check.names=F, row.names = 1, as.is = T)

# Heatmap generation required a matrix
GSEA_ranked.matrix <- data.matrix(GSEA_ranked)
# Create break value for centering the colors of the heatmap on 1 and
    using the same color distribution for each sample

break.arg <- c(-0.9, -0.8, -0.7, -0.6, -0.5, -0.4, -0.3, -0.2, -0.1,
    0, 0.1, 0.2, 0.3, 0.4, 0.5, 0.6, 0.7, 0.8, 0.9)

# Generate heatmap
heatmap.2(GSEA_ranked.matrix,
          main = "title",   # Title of the heatmap
          #col=colors,    # Colours to use (red-yellow by default)
          breaks=break.arg, # Using the break argument for deciding
              where to change color
          trace = "none",   # No distribution trace
```

```
          Rowv = F,      # No row clustering
          Colv = F,      # No column clustering
          margins = c(12,20),
          cexRow = 0.5,   # Size of font
          key=T,       # If you want to change the color labelling
          key.xlab=NA,
          key.ylab=NA)
```

3.2.2.5 Study of individual genes within a gene set

For the study of the individual genes the expression data were imported into R and quantile normalised as in 3.2.2.2.

```
# read in data (this assumes that you are in the correct working
    directory)
exprs <- read.csv( "SampleGeneProfile.csv", check.names=F, as.is=T )

# Clean up row and column names (also remove p-values)
row.names( exprs ) <- paste( exprs$ILMN_GENE )
exprs <- as.matrix( exprs[, grepl( ".AVG_Signal", colnames( exprs ) )
    ] )
colnames( exprs ) <- gsub( ".AVG_Signal", "", colnames( exprs ) )
colnames( exprs ) <- gsub( " ", "_", colnames( exprs ) )

# Quantil normalise expression data using LIMMA
library( "limma" )
exprs <- normalizeBetweenArrays( exprs, "quantile" )
```

For the calculation of the background gene expression level the expression data of the negative control probes present on the chip (ControlGeneProfile.csv) were used.

```

# read in data control gene data (this assumes that you are in the
    correct working directory)
ctrl.exprs <- read.csv( "ControlGeneProfile.csv", check.names=F, as.is
    =T )

# Clean up row and column names (also remove p-values)
row.names(ctrl.exprs) <- paste( ctrl.exprs$TargetID )
ctrl.exprs <- as.matrix( ctrl.exprs[, grepl( ".AVG_Signal", colnames(
    ctrl.exprs) ) ] )

# Extract negative gene mean row
Negative.probs <- ctrl.exprs["NEGATIVE",]

```

```
# Calculate mean intensity of negative gene controls
Negative.mean <- mean(Negative.probs)
```

For the generation of a plot of gene expression and a heatmap of fold change the specific genes and their expression values were extracted from the global gene expression array. Here as an example the `"CELL_CYCLE_PROCESS.csv"` is used, which can be generated from the `"CELL_CYCLE_PROCESS.xls"` output from the GSEA saved as a csv file.

```
# Read the output file of a gene set of GSEA
GSEA_list <- read.csv( "CELL_CYCLE_PROCESS.csv", check.names=T, as.is=
    T)

# Filter all non enriched genes of the geneset
GSEA_list <- GSEA_list[!GSEA_list$CORE.ENRICHMENT == "No", ]

# Create a list of Gene symbols
gene_list <- GSEA_list$GENE.SYMBOL

# Remove all "null" genes
gene_list <- gene_list[gene_list != "null"]

# Extract expression value of each gene, using the previously imported
    and normalised imported expression data
GO_Gene_List <- exprs[c(gene_list), ]
```

After extracting the gene expression information a bar plot of expression level of the genes can be generated. In the following example I am going to generate it for H1, but it could be done for any harvest.

```
# Import several required libraries
library(gplots)   # for plotting
library(Hmisc)    # for adding the error bars
library(ggplot2)  # plotting

# Extract expression of only H1 genes
H1_expression = GO_Gene_List[, grepl("H1", colnames(GO_Gene_List))]

#re-order into Harvests
GO_Gene_List <- GO_Gene_List[,c(1,5,9,2,6,10,3,7,11,4,8,12)]

# Calculate row mean
```

```
RowM <- rowMeans(H1_expression[, -ncol(H1_expression)])

# Calculate row standard deviation
SD = apply(H1_expression ,1, sd, na.rm = TRUE)

# Calculate upper limit of error bar
upper <- RowM + SD

# Calculate lower limit of error bar
lower <- RowM - SD

# Calculate upper limit of error bar for graphing (so that the error
    bar does not go out of the y axis)
yupper <- max(upper)

# Generate bar-plot, save coordinates of bars in bp (for correct
    placement of errorbars)
bp = barplot(RowM,
        main = "H1 average expression of MITOSIS", e
               col = NULL,
               legend = rownames(RowM),
               ylab = "Average expression",
               #cex.names = 0.5,     # change font size
               xlab=NULL,
               xlim = NULL,
               #ylim = c(0, yupper),  # Use the max y limit calculated
                   earlier for upper limit
               xpd = F,
               #log="y"        # un-comment if log plot
               )

# Add previously calculated error bars
errbar(bp[,1], RowM, upper, lower, add=T)

# Add background expression level line (calculated earlier)
abline(h=Negative.mean, col = "red")
```

After the bar plot a fold change heatmap of the same genes was generated.

```
# Normalise the values to H1
# AH016-03:
GO_Gene_List[, grepl("AH016", colnames(GO_Gene_List))] <- GO_Gene_List
    [, grepl("AH016", colnames(GO_Gene_List))]/GO_Gene_List[,1]
# OX1-19:
GO_Gene_List[, grepl("OX1", colnames(GO_Gene_List))] <- GO_Gene_List[,
     grepl("OX1", colnames(GO_Gene_List))]/GO_Gene_List[,2]
# NHDF1:
GO_Gene_List[, grepl("NHDF_1", colnames(GO_Gene_List))] <- GO_Gene_
    List[, grepl("NHDF_1", colnames(GO_Gene_List))]/GO_Gene_List[,3]

# Log2 scaling of the expression values (better for fold change)
```

```
GO_Gene_List <-  log2( GO_Gene_List )

# Convert into a matrix for heatmap
GO_Gene_List.matrix <- data.matrix(GO_Gene_List)

# Generate heatmap

par(cex.main=0.7) # Font size

heatmap.2(GO_Gene_List.matrix,
      main = "MITOSIS",   # Title
          col = redgreen,      # Colours
          trace = "none",      # No trace
          Rowv = F,        # No row clustering
          Colv = F,        # No column clustering
          margins = c(12,20), # Margin
          key=T ,        # Change colour labels
          cexRow = 0.5,      # Font size
          key.title= "Log2 gene expression fold change",  # Colour
              label
          key.xlab=NA,       # No x axis label for colour
          key.ylab=NA,       # No x axis label for colour
          tracecol=NA,       # No trace for colour
          density="density")
```

3.2.2.6 Metadata analysis

To place the iPS-Mo/Mϕs cells more accurately into the in-vivo monocyte/Mϕ populations the transcriptomes were compared to datasets generated by Dr W. Hänseler, a post doctoral researcher in our laboratory, that included primary fetal microglia and adult blood monocytes. Initially, both datasets were imported into R and merged. After merging the data it was quantile-normalised across all samples.

```
# Read in my data (this assumes that you are in the correct working
    directory)
exprs_JB <- read.csv( "WH/SampleGeneProfile_Julian.csv", check.names=F
    , as.is=T )

# Read in WH data (this assumes that you are in the correct working
    directory)
exprs_WH <- read.csv( "WH/SampleGeneProfile_Walther_reduced.csv",
    check.names=F, as.is=T )

# Clean-up my data
row.names( exprs_JB ) <- paste( exprs_JB$ILMN_GENE )
exprs_JB <- as.matrix( exprs_JB[, grepl( ".AVG_Signal", colnames(
    exprs_JB ) ) ] )
```

```
colnames( exprs_JB ) <- gsub( ".AVG_Signal", "", colnames( exprs_JB ) )
colnames( exprs_JB ) <- gsub( " ", "_", colnames( exprs_JB ) )

# Clean-up WH data
row.names( exprs_WH ) <- paste( exprs_WH$ILMN_GENE )
exprs_WH <- as.matrix( exprs_WH[, grepl( ".AVG_Signal", colnames( exprs_WH ) ) ] )
colnames( exprs_WH ) <- gsub( ".AVG_Signal", "", colnames( exprs_WH ) )
colnames( exprs_WH ) <- gsub( " ", "_", colnames( exprs_WH ) )

# Merge the two datasets and remove any row which is only present in one sample.
exprs <- merge(exprs_JB, exprs_WH, by = "row.names", all = FALSE)

# Rename rows properly after merge
row.names( exprs) <- paste( exprs[,1] )

# Delete the row.names column as it is not needed any more
exprs <- exprs[,-1]

# Convert to a matrix
exprs <- as.matrix(exprs)

# log scale
exprs <-  log2( exprs + 1 )

library( "limma" )
exprs <- normalizeBetweenArrays( exprs, "quantile" )
```

After normalization of the data it is possible to do a multidimensional scaling (MDS) plot to visualise the clustering of the samples on two dimensions.

```
# samples and harvests, with colours for plotting
samples_JB <- rep( c( rgb( 0.7, 0.15, 0.15, 0.5 ),
                      rgb( 0.95, 0.85, 0.5, 0.5 ),
                      rgb( 0.05, 0.4, 0.55, 0.5 ) ), each=4 )

# Colors for WH data plotting
samples_WH <- rep( c( "#458B74",
                      "#8A2BE2"), each=3 )

# Merging the two color variables
samples <- c(samples_JB, samples_WH)

# Add a name for each sample based on the sample name
names(samples) <- sapply( colnames( exprs ), function( x ) strsplit( x , split="_" )[[1]][3] )

```

```
# MDS plotting
plotMDS(exprs,
       top = 2000,   # Number of top genes used for distance
           calculation
       pch = 19,     # Type of symbol to use for plotting
       col=samples)  # Colours to use (previously generated variable)

# Adding graph legends
legend_title <- (sapply( colnames( exprs ), function( x ) strsplit( x,
     split="_" )[[1]][2] ))
legend('topright', cex = 0.71, legend = c("iPSC-Mono-JB", "iPSC-Mono-
    JB", unique(legend_title)), pch = 19, col=unique(samples))
```

After MDS plot generation a RP approach as previously described in subsection 3.2.2.2 was performed. GSEA and heatmap generation were also done as previously described in subsection 3.2.2.4.

3.3 Results

3.3.1 Monocyte production, proliferation and morphology over time

To account for donor variability, three different control hiPSC lines were selected that have been used extensively in the laboratory and are of broadly different age and gender but derived in the same fashion (Table 3.1). For all three lines low passage, feeder-free hiPSCs were used for the generation of aggrewell EBs (figure 3.2). After 3 to 4 weeks, factories (M&M: 2.3) started producing iPS-Mo/Mϕs, NHDF-1 and OX1-19 started producing roughly a week before AH016-03, therefore all AH016-03 harvests have been shifted by one week so that all cells have been harvested about 10-14 days after the start of iPS-Mo/Mϕ production. For every harvest $2x10^6$ iPS-Mo/Mϕs were pelleted, lysed in QIAGEN RLT buffer supplemented with 10 μL β-ME and immediately stored at -80°C for future RNA extraction. Remaining iPS-Mo/Mϕs were used for the EdU proliferation assay (M&M: 2.5), CD14 FACS staining (M&M: 2.7) and Methylene blue and Eosin staining (M&M: 2.6).

Table 3.1: General information on the donors and reprogramming method used for the hiPSCs used for the transcriptome analysis

Name	Age	Gender	Reprogramming method	Cells reprogrammed
NHDF-1	44	F	Retroviral	Fibroblast
OX1-19	36	M	Retroviral	Fibroblast
AH016-03	80	M	Retroviral	Fibroblast

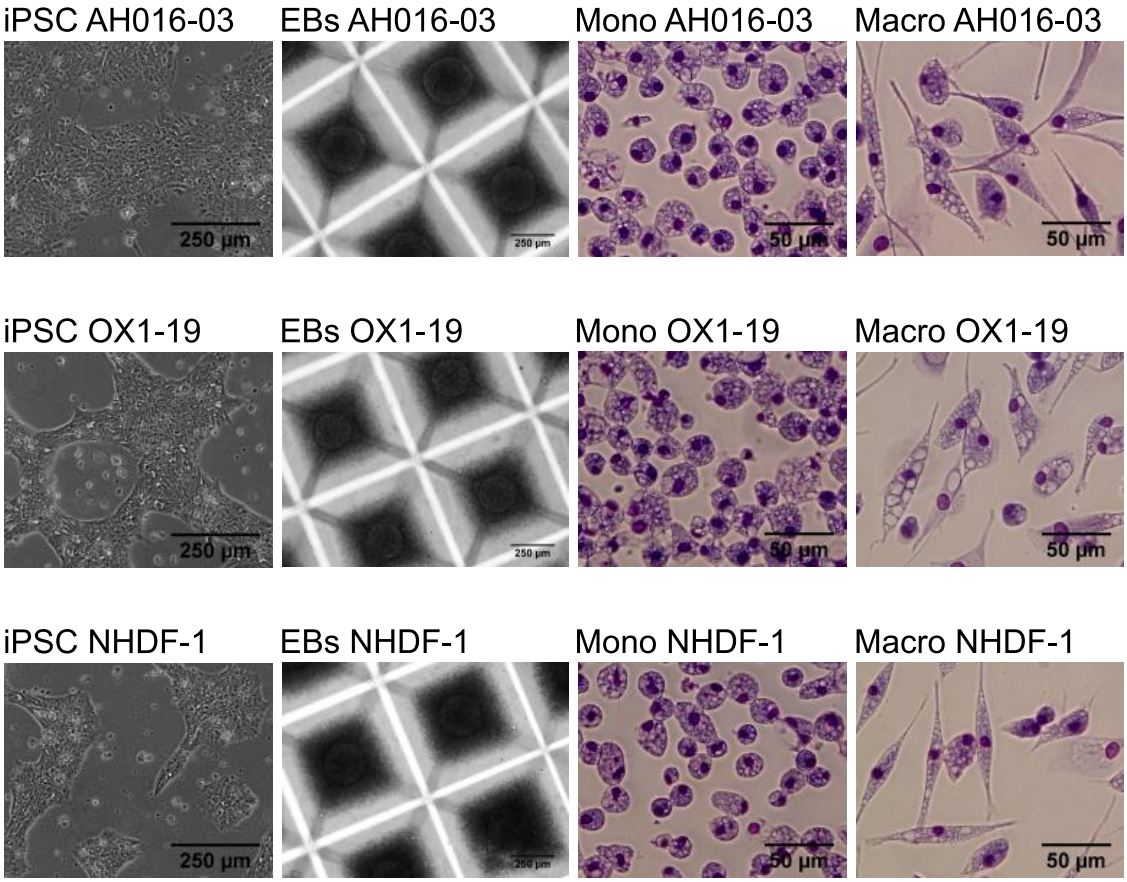

Figure 3.2: Image of the three hiPSCs lines used in this study and their differentiation. The hiPSC lines AH016-03, OX1-19 and NHDF-1 were differentiated using aggrewell^{TM} 800 EB formation. Shown are images of different stages of differentiation from stem cell (on the left) to Mϕ (on the right) taken on an EVOS inverted microscope. The iPS-Mo/Mϕ shown are from harvest 3 stained with eosin and methylene-blue directly cytospined after harvest (Monocyte) or after 7 days of differentiation with M-CSF (Macrophage).

All three hiPSC lines produced as expected over a period of three months as can be seen in figure 3.3A. Factory production did not decrease significantly over time and was not significantly different between the three lines. The cells produced were over 90-95% CD14$^+$ across all hiPSC lines used, as detected by antibody staining and flow cytometry (see figure 3.3E and F), irrespective of harvest time, indicating that the transcriptome signature comes from a high purity of CD14$^+$ iPS-Mo/Mϕ. Relative size as quantified by mean forward scatter height (FSC-H) of CD14$^+$ cells did not vary significantly over time (Figure 3.3B and C). In contrast, relative cell granularity as measured by side scatter height (SSC-H)

of $CD14^+$ cells increased progressively and significantly between harvest 1 and harvest 5, resulting in an overall 50 to 60% increase in SSC-H of iPS-Mo/Mϕs (Figure 3.3B and D), which may be linked to many biological processes such as phagocytosis, autophagy, cytokine secretion.

As tissue-resident Mϕ are capable of proliferation (reviewed in (Belhareth, 2015)) and proliferative capacity is higher in YS-Mϕs and fetal monocytes compared to adult blood monocytes (Van de laar et al., 2016), the iPS-Mo/Mϕs were assessed for proliferation using EdU pulse-labelling of freshly harvested iPS-Mo/Mϕ. In parallel HEK 293T were also pulse-labelled as positive control cells and iPS-Mo/Mϕs were treated with hydroxyurea (HU), which depletes all nucleotides and therefore blocks DNA replication, as negative controls. Only, harvest 1 $CD14^+$ cells displayed appreciable EdU^+ cells (3-4%) (Figure 3.4A). The gating strategy was set according to the HU and isotype controls and is shown in figure 3.4B. Although the EdU staining had lower intensity than would be expected, EdU^+ cells were absent in HU and isotype controls. As an additional control I did a small followup time-course experiment looking at the proliferation of iPS-Mo/Mϕs on a different set of OX1-19 factories, showing a nicer stain and similar trend (Appendix figure A.1). From these initial observations it would seem that early harvest iPS-Mo/Mϕ still possess some proliferative capacity which is then lost or very low in later harvests. While very few $CD14^+EdU^+$ iPS-Mo/Mϕs are detected in later harvests the very short pulse of EdU labelling precludes conclusions about potential of the cells to divide at a very slow rate.

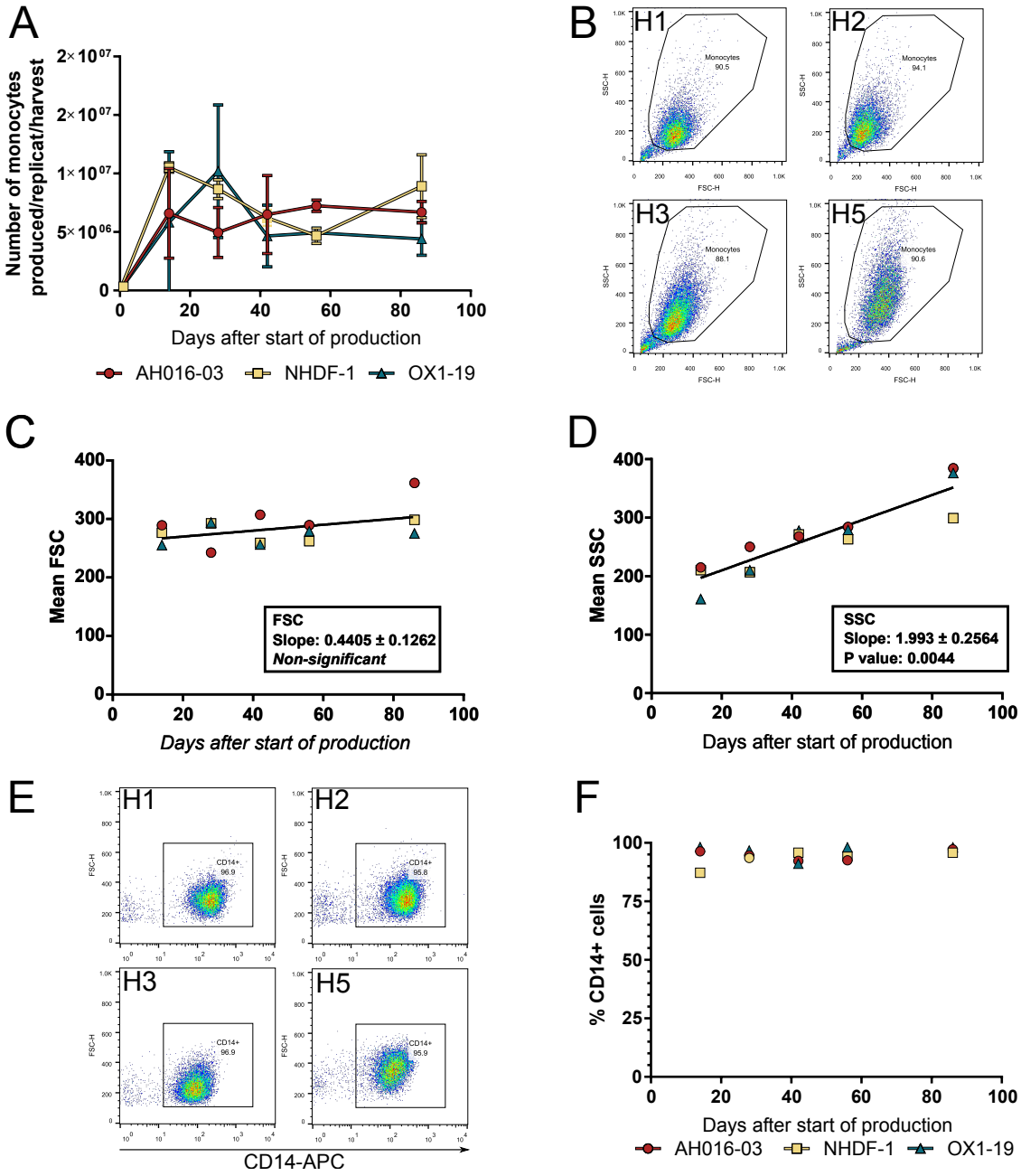

Figure 3.3: Basic experimental study of the iPS-Mo/Mϕ over time. A. Non-cumulative production of iPS-Mo/Mϕ produced per harvest over a period of 86 days after start of iPS-Mo/Mϕ production. Each time-point represents the mean number of CD14$^+$ cells harvested with standard deviation (n = 3 for each cell line). **B.** Representative flow cytometry gating strategy for FSC-H and SSC-H. **C.** Mean FSC-H of CD14$^+$ cells per harvest. Lineage regression analysis results in a non-significant deviation from zero. **D.** Mean SSC-H of CD14$^+$ cells per harvest. **E.** Representative flow cytometry gating strategy for CD14 expression. **F.** Average percentage of CD14$^+$ cells per harvest, for each line, calculated using FlowJo. Lineage regression analysis results in a significant deviation from zero and a slope of 1.94 ± 0.26, demonstrating an increase in cell granularity in later harvests.

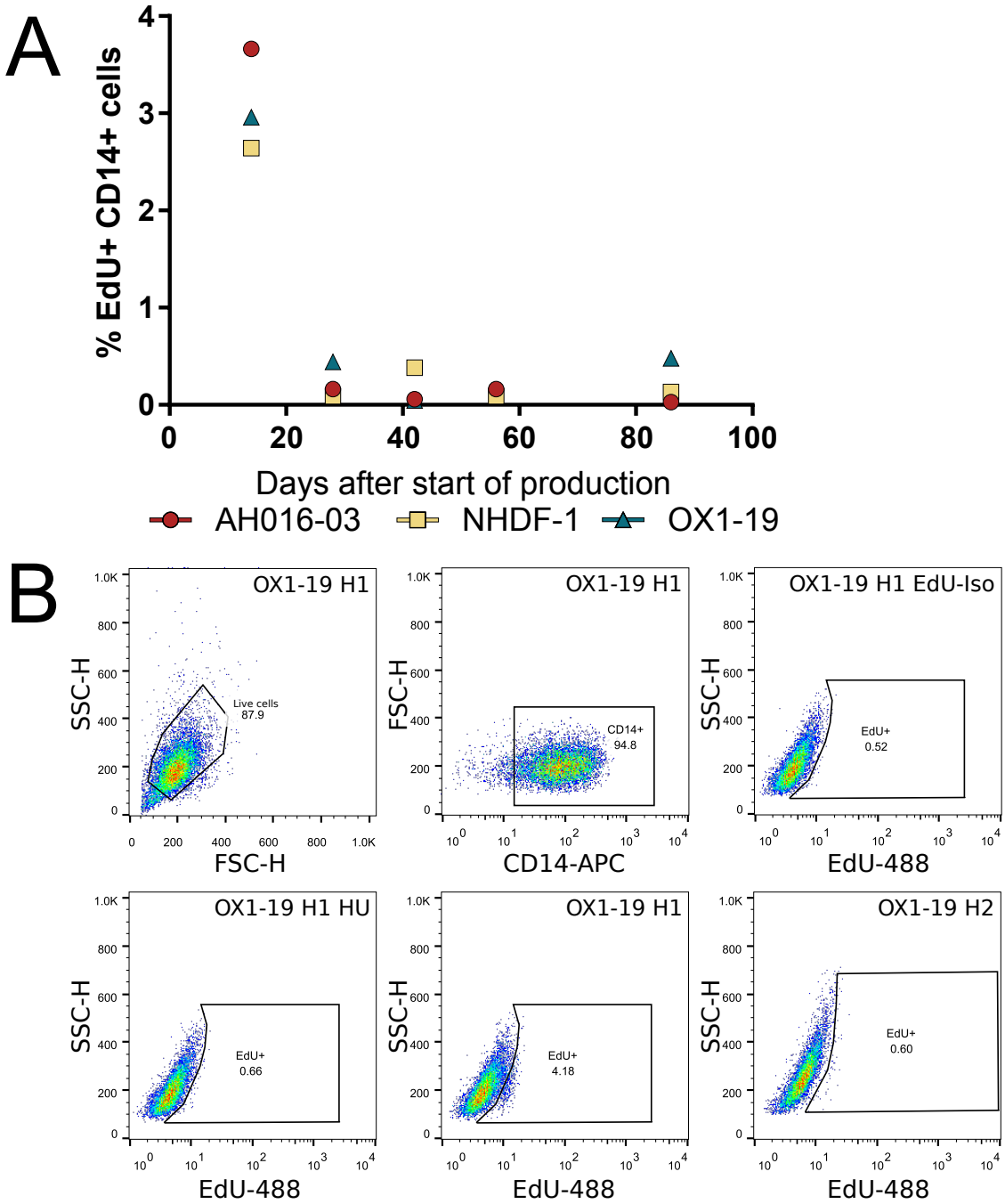

Figure 3.4: EdU staining of iPS-Mo/Mϕ over time. A. Freshly harvested iPS-Mo/Mϕs were pulsed for 2h with EdU and CD14^{+}EdU^{+} cells that had undergone DNA replication were detected by flow cytometry after Click-iT staining. **B.** Representative flow cytometry gating strategy for CD14 expression and EdU+ cells. HU: Hydroxyurea control. See also appendix figure A.1.

3.3.2 Transcriptomic data analysis

3.3.2.1 Initial QC of data

Samples were run on an illumina HTv12 v.4 beadchip array, which has a capacity of 12 samples. I therefore used only H1, H2, H3 and H5 of each cell line for a total of 12 samples. Samples gave good overall signal for the control probes for biotin indicating that the experimental steps were successful. For analysis of the RAW data I used GenomeStudio to read the bead intensity and generate an output file containing the expression data of each gene for each sample. A boxplot showing the global distribution of gene expression levels in each sample before normalization can be seen in figure 3.5A, the data was of acceptable quality as the signal distribution for each sample is similar across all 12 samples and no outlier samples were identified. Samples were normalised using quantile normalization, as described in the material and method section 3.2.2.1, (figure 3.5).

After normalization, an initial MDS plot was constructed to visualise the distribution of the samples (figure 3.6). MDS, like principal component analysis (PCA), is a dimension reduction technique frequently applied to microarray data. Here I used the 500 top most variable genes to generate a 2 dimensional plot of distances between samples. This should allow for clustering between biological samples (donor, cell line, cell type, treatment, etc.). On the MDS different cell lines (AH016-03, NHDF-1 and OX1-19) cluster while harvests are distributed in a similar pattern from right to left on dimension 1. This indicates that the main difference between the samples is due to the donor genetic background and that the harvest component accounts for less of the variability.

3.3.2.2 Differential transcript expression study using RP approach

The main objective of this experiment was to identify differentially expressed pathways and cellular functions with biological relevance between harvest. Many different methods for analysing microarray differential gene expression have been developed: significance analysis of microarrays (SAM), analysis of variance (ANOVA), empirical Bayes t-statistic, template matching, maxT, between group analysis

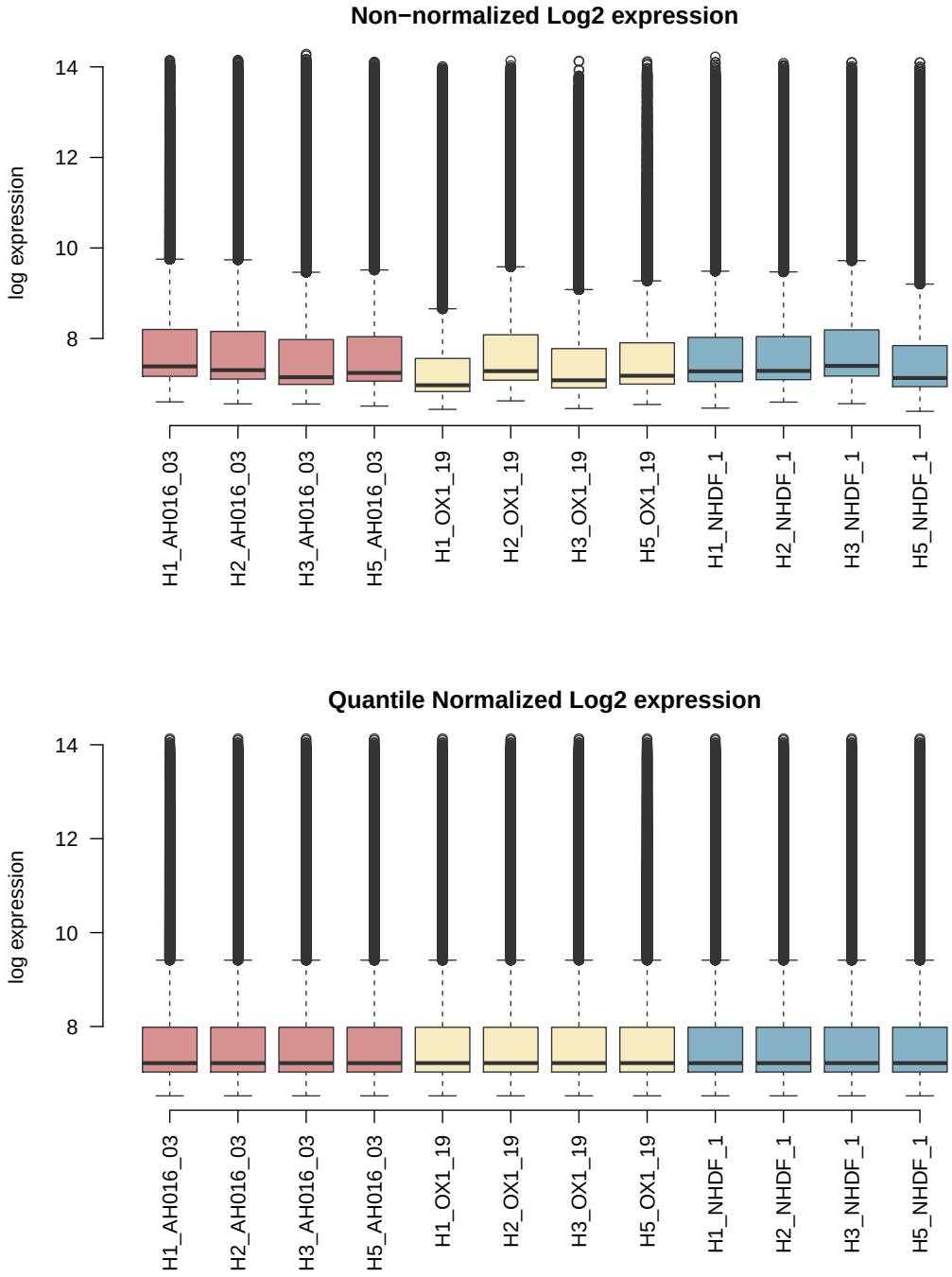

Figure 3.5: Normalization of expression data A. Shows a boxplot of the non-normalised log2 transformed intensity distribution of all genes in each sample. **B.** Shows the distribution of the log2 transformed intensities of all genes in each sample after quantile normalization.

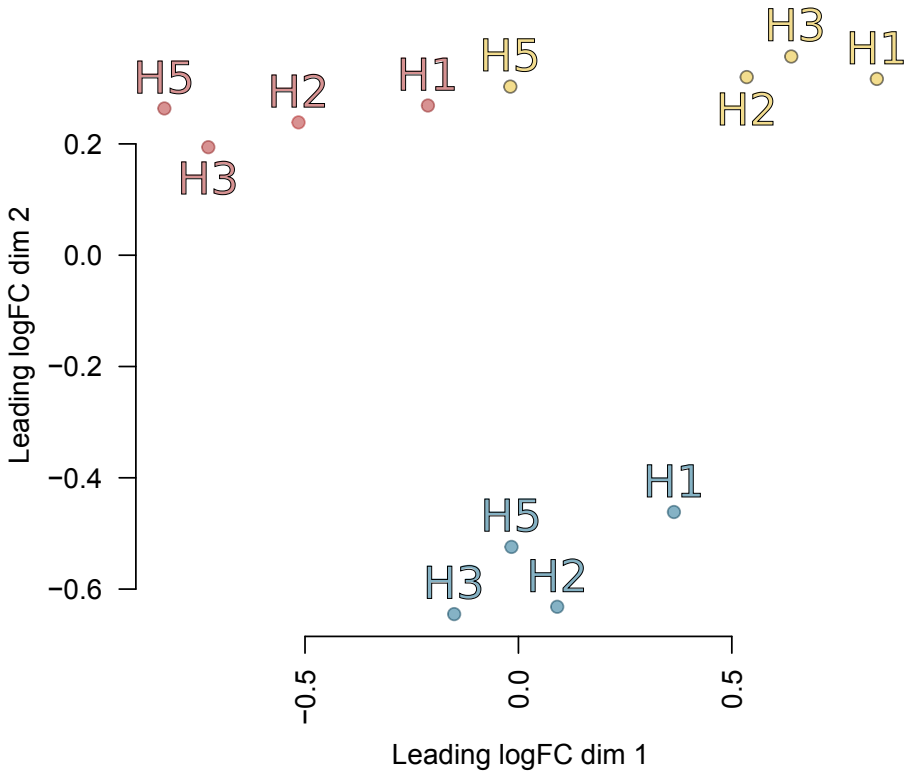

Figure 3.6: MDS plot MDS plot showing clustering of the 12 different iPS-Mo/Mϕ samples on 2 dimensions of distances between samples. Samples are labelled H1 to H5 for harvests 1-5 and AH016-03 (red), OX1-19 (yellow) and NHDF-1 (blue).

(BGA), Area under the receiver operating characteristic (ROC) curve, the Welch t-statistic, fold change and RPs (Jeffery et al., 2006). Each method has advantages and disadvantages depending on type of dataset analysed (number of replicas, noisiness, biological question) and simplicity of application (computational work load, statistical complexity). With the help of Dr Quin Wills (WTHG) a RPs approach for identifying differentially expressed genes between my harvests was selected (Breitling et al., 2004; Heskes et al., 2014). RP approach is a non-parametric approach for identifying differentially expressed genes that derived from biological reasoning rather than complex statistical modelling (Breitling et al., 2004). The reasoning behind RP is the following. If a gene is repeatedly at the top of a list ordered according to fold change difference between treated versus control (Harvest 1 versus Harvest 5 in our case) it is likely to be differentially expressed. This method is particularly relevant in small datasets with small number of replicas and

meta-analyses (Breitling et al., 2004; Heskes et al., 2014).

For this study I decided to focus on genes that are highly differentially expressed between harvest 1 iPS-Mo/Mϕ and later harvests (harvest 2, 3, 5). The RP approach generated a list of differentially expressed genes, ranked by significance (max log10 p-value of the RP statistics) of the differential expression. This list was sorted from most significantly up-regulated to most significantly down-regulated gene in harvest 1 compared to H2, H3 or H5.

The three ranked lists of differentially expressed genes (H1-H2, H1-H3 and H1-H5) were then used for GSEA (Subramanian et al., 2005). GSEA identifies the concentration of sets of genes towards the top (significantly up-regulated) or bottom (significantly down-regulated) of a ranked ordered gene list derived from an expression dataset. Gene sets are groups of genes that share common biological function, chromosomal location or regulation. I decided to use GO gene sets derived from The Gene Ontogeny Consortium project (Consortium, 2000) for my GSEA. GO belong to one of three ontogenies: molecular function (MF), cellular component (CC) and biological process (BP), the last of which was selected for this study. After GSEA of my three ranked gene lists against the GO BP gene set database I removed all enriched pathways with a FDR > 0.05, keeping only the significantly enriched pathways in H1 compared to H2, H3 and H5. A heatmap of the ES of all significantly positively or negatively enriched pathways can be seen in figure 3.7. Any gene set with a positive ES is enriched in H1 compared to H2, H3 or H5, while any gene set with a negative ES is enriched in H2, H3 or H5 compared to H1. From the heatmap it is clear that any gene set which is enriched in H1 compared to H2 is also enriched in H1 compared to H3 and H5. Any pathway which is significantly enriched in H2 compared to H1 is also enriched in H3 and H5 compared to H1.

From the results it is possible to conclude that H1 iPS-Mo/Mϕs are enriched for cell cycle genes compared to all other harvests. This result correlates very nicely with figure 3.3E showing greater number of EdU$^+$ cells in H1 iPS-Mo/Mϕ compared to subsequent harvests. While cell cycle genes are enriched in H1, immune response genes are enriched in later harvests. This would indicate that later harvests are

more immunologically responsive than early harvests. From these results it would seem that early harvest iPS-Mo/Mϕ are functionally distinct from later harvests, having greater proliferative potential and being immunologically immature.

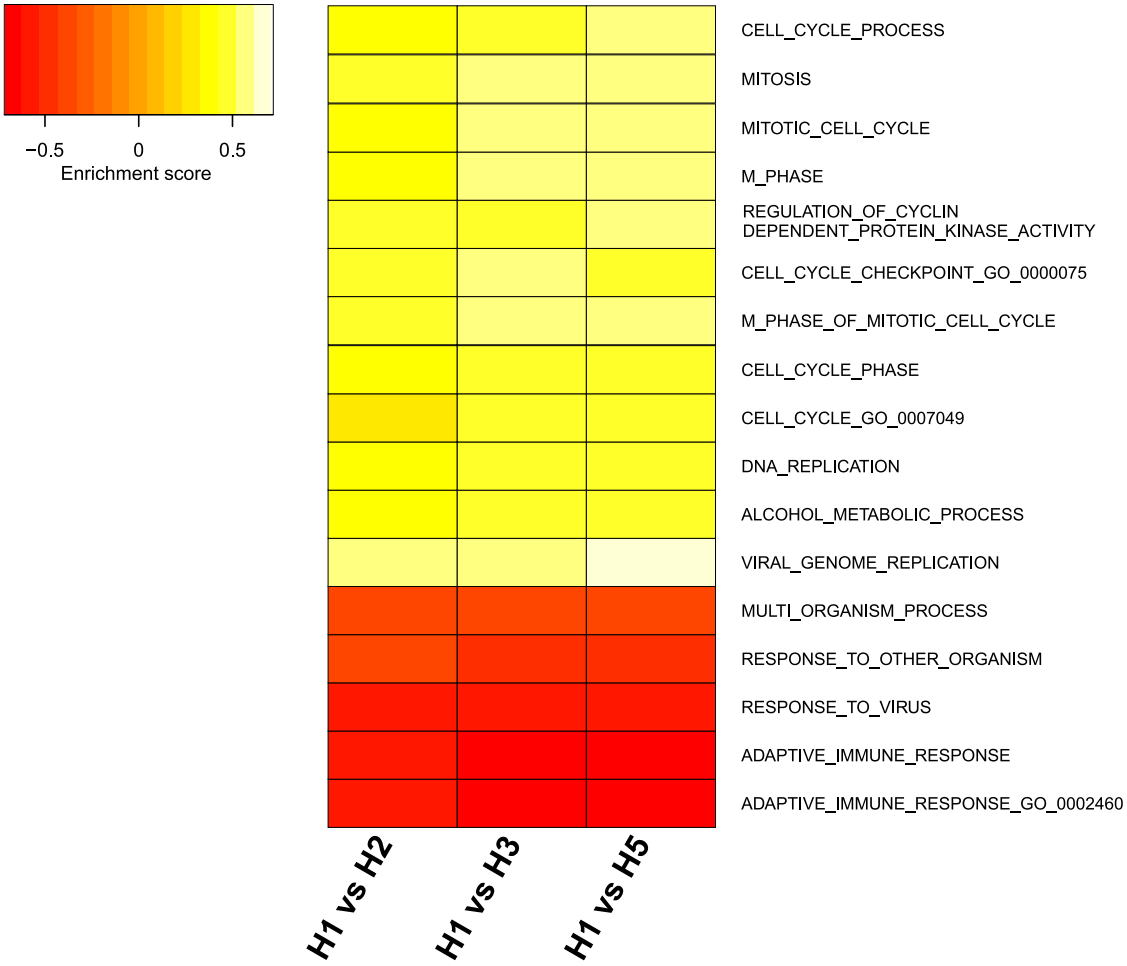

Figure 3.7: GSEA clustering of GO gene sets. Heatmap of the significantly enriched (FDR < 0.05) gene sets. Heatmap colouring was done according to ES. Positively enriched scores (yellow) represent gene sets higher expressed in H1 compared to later harvests while negative ESs (red) represent gene sets lower expressed in H1 compared to later harvests.

3.3.2.3 Closer look at the individual genes in a gene set

The GSEA results are based on differential expression but are not directly tied to the level of expression. However, by looking at expression level it is possible to have a better understanding if the genes are progressively up or down regulated over time or if the change happens immediately after H1. I selected four gene sets

that I believe represent the general signature observed: CELL CYCLE PROCESS, MITOSIS, RESPONSE TO VIRUS and ADAPTATIVE IMMUNE RESPONSE as well as one outlier (VIRAL GENOME REPLICATION) to look at the expression level of the individual genes. For each gene set, the average gene expression level, in H1, of each individual significantly (p-value < 0.05) enriched gene was plotted. In addition a heatmap of the log2 fold change in gene expression level compared to H1 for all three lines is shown underneath (figures 3.8, 3.9, 3.10, 3.11 and 3.12).

3.3.2.3.1 Cell cycle genes are progressively downregulated between H1 and H5

Most genes in the two cell cycle related GO gene sets (CELL CYCLE PROCESS and MITOSIS) are expressed above background levels and some are at high levels, such as RAN, RB1, BACT1 (Figure 3.8A and 3.9A). As expected many genes, such as RAN, are present in both CELL CYCLE PROCESS and MITOSIS, as a gene can be present in multiple GO gene sets. When looking at the heatmap of fold change across harvests of each individual gene it is clear that there is a global downregulation of most genes over the course of the harvests, as would be expected from the enrichment results. Of note, in H2 the expression of several genes are either unchanged (black) or upregulated (green) while in H5 almost all genes are downregulated (red) compared to H1. It would therefore seem that the overall downregulation of the cell cycle genes is not immediate but rather progressive, as the factories age.

3.3.2.3.2 Viral genome replication related genes are high early on and get downregulated over time

The only GO gene set not being directly related to cell cycle which was enriched in H1 compared to subsequent harvests is the "VIRAL GENOME REPLICATION" GO gene set. It is a relatively small gene set and 6 genes were significantly enriched, being CCL3, IL8, TOP2A, PPIA, DEK and SMARCB1. TOP2A, PPIA, DEK and

SMARCB1 are all involved in chromatin remodelling and transcription processes, TOP2A is a known LPS response gene (Sharif et al., 2007), while PPIA (encoding Cyclophilin A) and SMARCB1 can both play a role in human immunodeficiency virus-1 (HIV-1) replication (Luban et al., 1993; Yung et al., 2001). CCL3, also known as Macrophage inflammatory protein-1α (MIP-1α) is a member of the CC chemokine family and is a monocyte and lymphocyte chemoattractant. CCL3 also is involved in myeloid differentiation and regulates the proliferation of HSCs in the BM (Broxmeyer et al., 1989a; Cook, 1996). IL8 (also named CXCL8) is also a chemoattractant and previously known as neutrophil-activating protein (NAP-1) (Kownatzki et al., 1986). Interestingly, IL8 and CCL3 both are capable of HSC mobilisation to the peripheral blood after injection (Laterveer et al., 1996; Broxmeyer et al., 1989b). Expression of these two highly transcribed chemokines into the media might be related to the migration of the monocytes out of the EBs and could also induce migration of precursors into the media. The reduction in expression of these chemokines by iPS-Mo/Mϕs might be linked with the reduction in iPS-Mo/Mϕ production by factories with age. Therefore although they are classified under the category "VIRAL GENOME REPLICATION" these genes may well be linked with progenitor cell proliferation, regulation and differentiation as well as migration of the iPS-Mo/Mϕ out of the EBs. This being said as part of our laboratory works on HIV-1 it is important to consider differential expression of PPIA and SMARCB1 as they might influence HIV-1 infectibility of iPS-Mo/Mϕs.

3.3.2.3.3 Adaptative immune response genes get progressively upregulated

While early harvest iPS-Mo/Mϕs have an enrichment in proliferative genes, later harvests upregulate adaptive immune related genes such as interferon (IFNAR1), chemokines (CCL5, CCL8), interleukins (IL10, IL18), complement (C2) and TLRs (TLR7, TLR8) (3.11 and 3.12). This would indicate that later harvest iPS-Mo/Mϕs are more apt at dealing with viral or bacterial infection, which is a core property of

monocytes and Mϕs. This global up-regulation of immune response associated genes is worth knowing if one uses these cells in a model of innate or adaptative immunity.

3.3.2.3.4 Summary

Cell cycle genes are progressively down-regulated while immune related genes are progressively up-regulated in iPS-Mo/Mϕs. Immune genes include cytokines, chemokines and pattern recognition receptors involved in Mϕ function. The "response to virus" gene set is the only non cell cycle gene set which is progressively down-regulated and possibly linked to differentiation, progenitor proliferation and cell migration rather than viral response.

OX1-19 displayed a different pattern than AH016-03 and NHDF-1 iPS-Mo/Mϕs in all analysed gene sets. OX1-19 iPS-Mo/Mϕs display only a minor change in gene expression between H1 and H2/H3, while there is a major gene expression shift in H5. This "late maturation" signature can be due to a cell line specific bias or due to an an unknown bias in this differentiation. Due to the limited number of samples, I can not conclude on the reason for this difference in expression pattern. It would be interesting to investigate too which extent iPS-Mo/Mϕs derived from different donors behave differently over time.

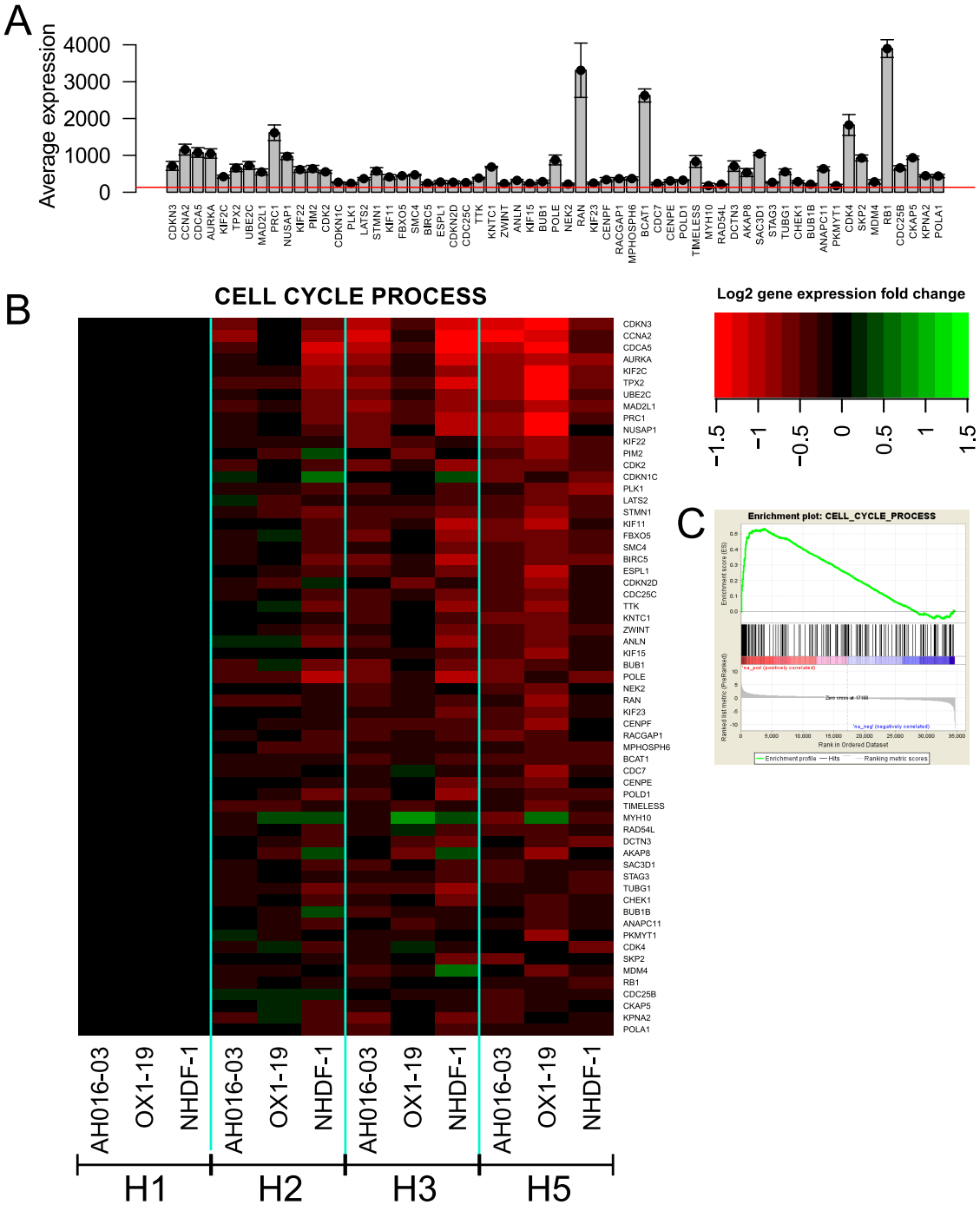

Figure 3.8: Analysis of the cell cycle process gene cluster expression. A. Average expression level of all "CELL CYCLE PROCESS" GO genes which are positively enriched H1 iPS-Mo/Mϕ compared to H5. For a gene to be considered as expressed it has to be above the red line, representing the average intensity of negative control probes. **B.** Heatmap of the log2 fold change in expression of the above genes in H2, H3 and H5 compared to H1. Red represents a reduction in expression, while green represents an increase in expression of the specific gene. **C.** Enrichment plot, provides a graphical view of the ES for the cell cycle process gene set.

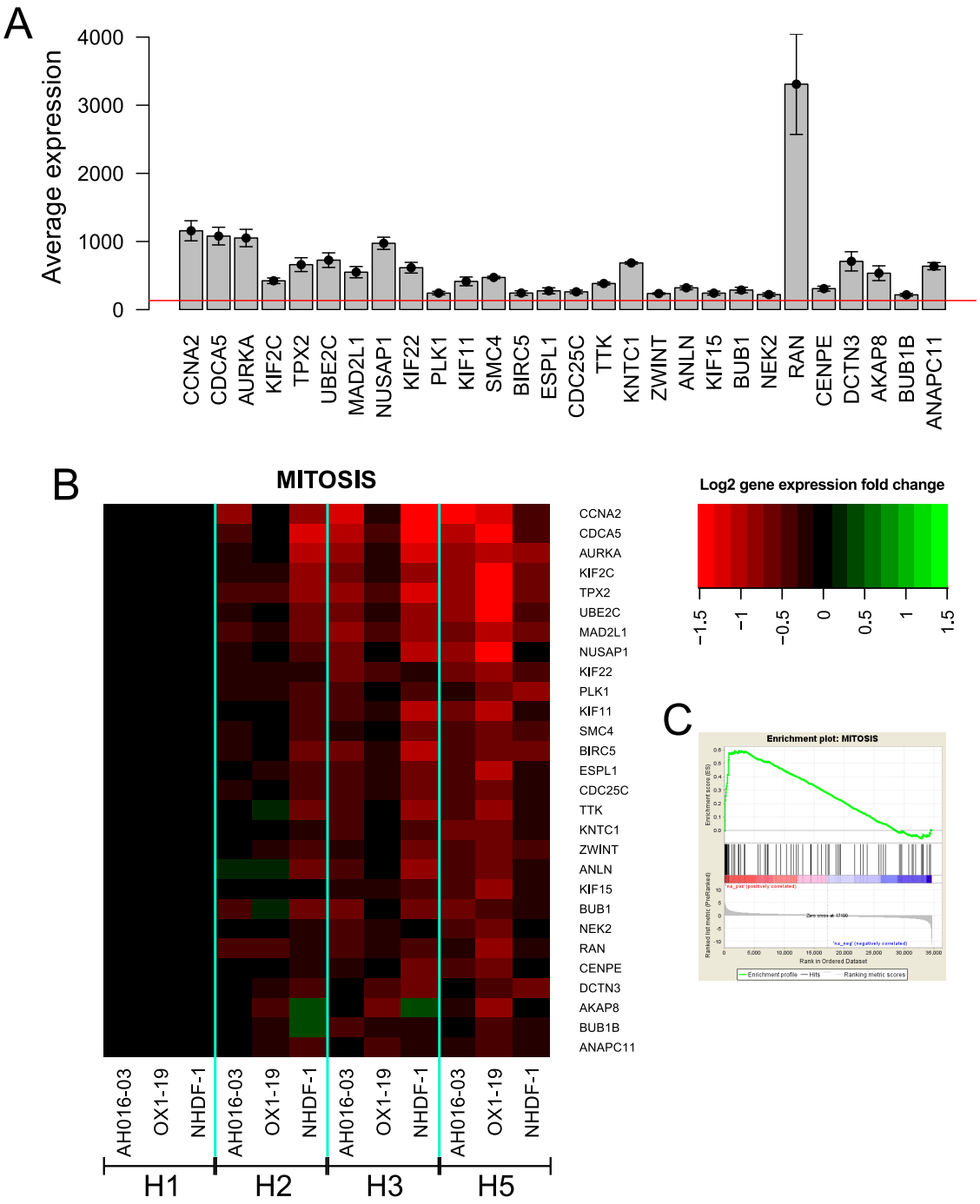

Figure 3.9: Analysis of the mitosis gene cluster expression. **A.** Average expression level of all "MITOSIS" GO genes which are positively enriched in H1 iPS-Mo/Mϕ compared to H5. For a gene to be considered as expressed it has to be above the red line, representing the average intensity of negative control probes. **B.** Heatmap of the log2 fold change in expression of the above genes in H2, H3 and H5 compared to H1. Red represents a reduction in expression, while green represents an increase in expression of the specific gene. **C.** Enrichment plot, provides a graphical view of the ES for the mitosis gene set.

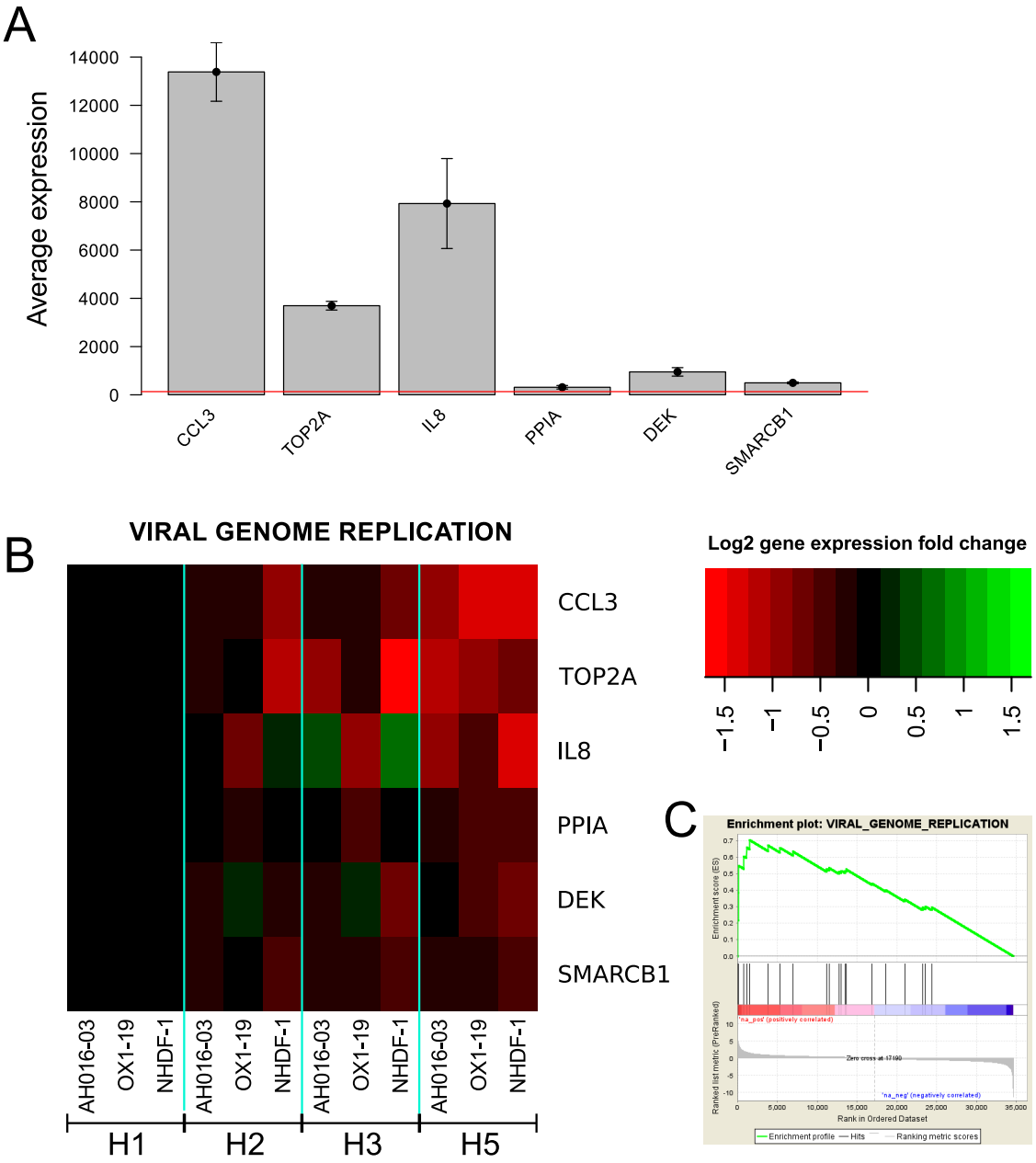

Figure 3.10: Analysis of the viral genome replication gene cluster expression. **A.** Average expression level of all "VIRAL GENOME REPLICATION" GO genes which are positively enriched in H1 iPS-Mo/Mϕ compared to H5. For a gene to be considered as expressed it has to be above the red line, representing the average intensity of negative control probes. **B.** Heatmap of the log2 fold change in expression of the above genes in H2, H3 and H5 compared to H1. Red represents a reduction in expression, while green represents an increase in expression of the specific gene. **C.** Enrichment plot, provides a graphical view of the ES for the viral genome replication gene set.

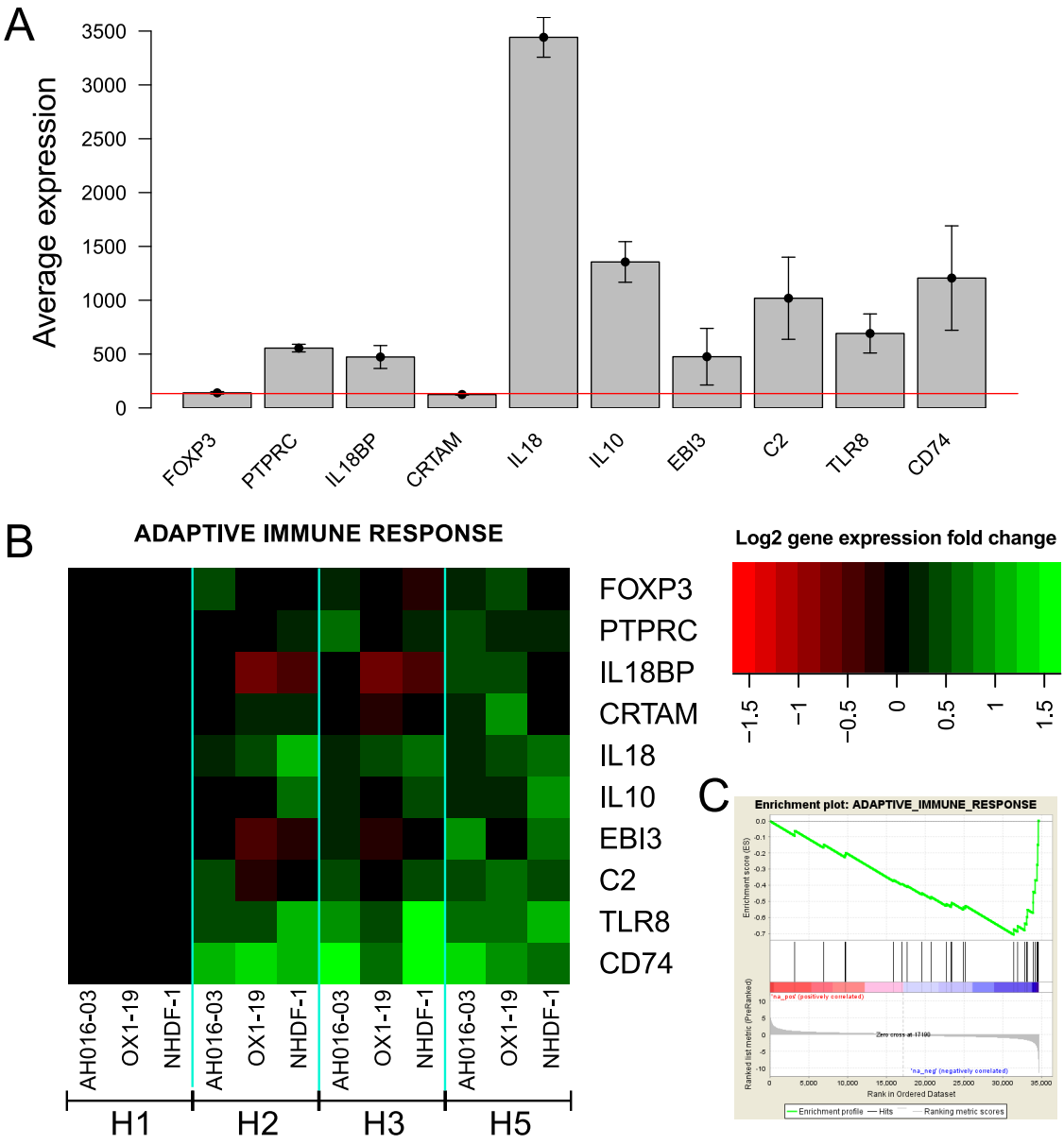

Figure 3.11: Analysis of the adaptive immune response gene cluster expression. A. Average expression level of all "ADAPTATIVE IMMUNE RESPONSE" GO genes which are positively enriched in H1 iPS-Mo/Mϕ compared to H5. For a gene to be considered as expressed it has to be above the red line, representing the average intensity of negative control probes. **B.** Heatmap of the log2 fold change in expression of the above genes in H2, H3 and H5 compared to H1. Red represents a reduction in expression, while green represents an increase in expression of the specific gene. **C.** Enrichment plot, provides a graphical view of the ES for the adaptive immune response gene set.

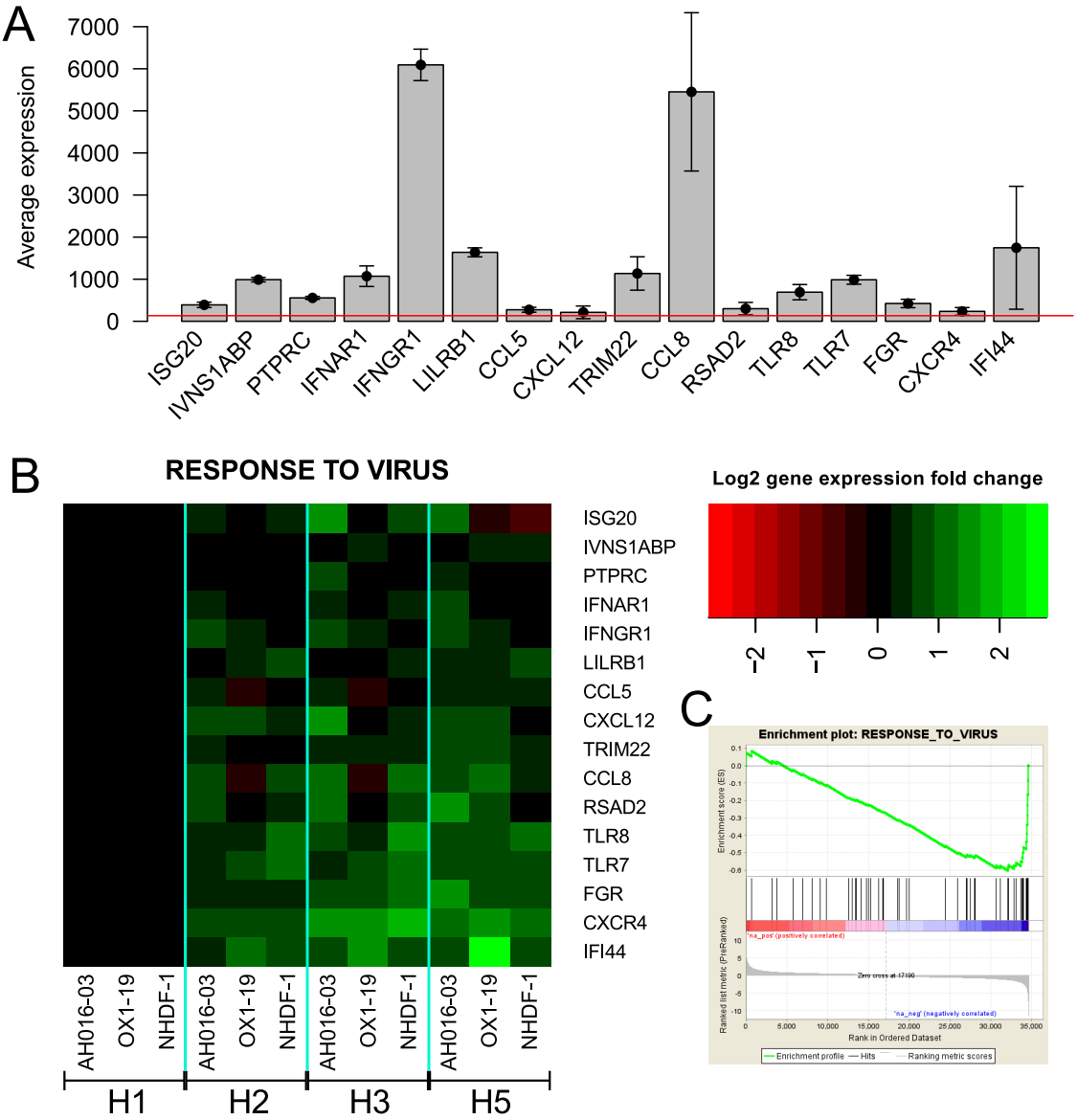

Figure 3.12: Analysis of the response to virus gene cluster expression. A. Average expression level of all "RESPONSE TO VIRUS" GO genes which are positively enriched in H1 iPS-Mo/Mϕ compared to H5. For a gene to be considered as expressed it has to be above the red line, representing the average intensity of negative control probes. **B.** Heatmap of the log2 fold change in expression of the above genes in H2, H3 and H5 compared to H1. Red represents a reduction in expression, while green represents an increase in expression of the specific gene. **C.** Enrichment plot, provides a graphical view of the ES for the response to virus gene set.

3.3.3 iPS-Mo/Mϕs are more similar to fetal microglia than adult blood monocytes

The second objective of this transcriptome was to perform a meta analysis to compare the transcriptome obtained from our iPS-Mo/Mϕs to existing datasets of human monocyte and Mϕ populations. Meta-data analyses can be very powerful but are skewed by technical effects due to the group and person processing the data (such as cell culture conditions, samples processing, BeadChip used, etc.) and these often dominate over biological effects and result in false positives. As my knowledge in usage of GEO databases and cross platform chip normalization was limited I decided to only use data produced by our lab to try and reduce the number of technical variables which could affect differential gene expression level. Dr Walther Hänseler, a post-doctoral researcher in the lab, studies microglial differentiation and has generated transcriptomic data from adult blood monocytes and also primary human fetal microglia using the same RNA extraction and Illumina beadchip array as were used for my study. The aim was to understand how similar iPS-Mo/Mϕs were from either primary adult blood monocytes or primary human microglia, which derive from two developmentally different origins.

3.3.3.1 Comparative MDS vs blood monocytes and fetal microglia

To get an initial overview of the clustering of the different cell groups and get an idea of divergence I used a MDS plot on inter-array quantile normalised expression values using the top 2000 most variable genes, as described previously (see section 3.3.2.1). In this MDS plot I also included control samples of undifferentiated hiPSCs that should be distinguished on this type of analysis. The MDS clearly highlights the separation between myeloid cells and hiPSCs (dim 1), but also demonstrates a distance between the various myeloid samples (dim 2). On dimension 2, the distance between iPS-Mo/Mϕ and blood monocytes was greater than the distance between iPS-Mo/Mϕs and fetal microglia indicating that iPS-Mo/Mϕs are transcriptionally closest to fetal microglia.

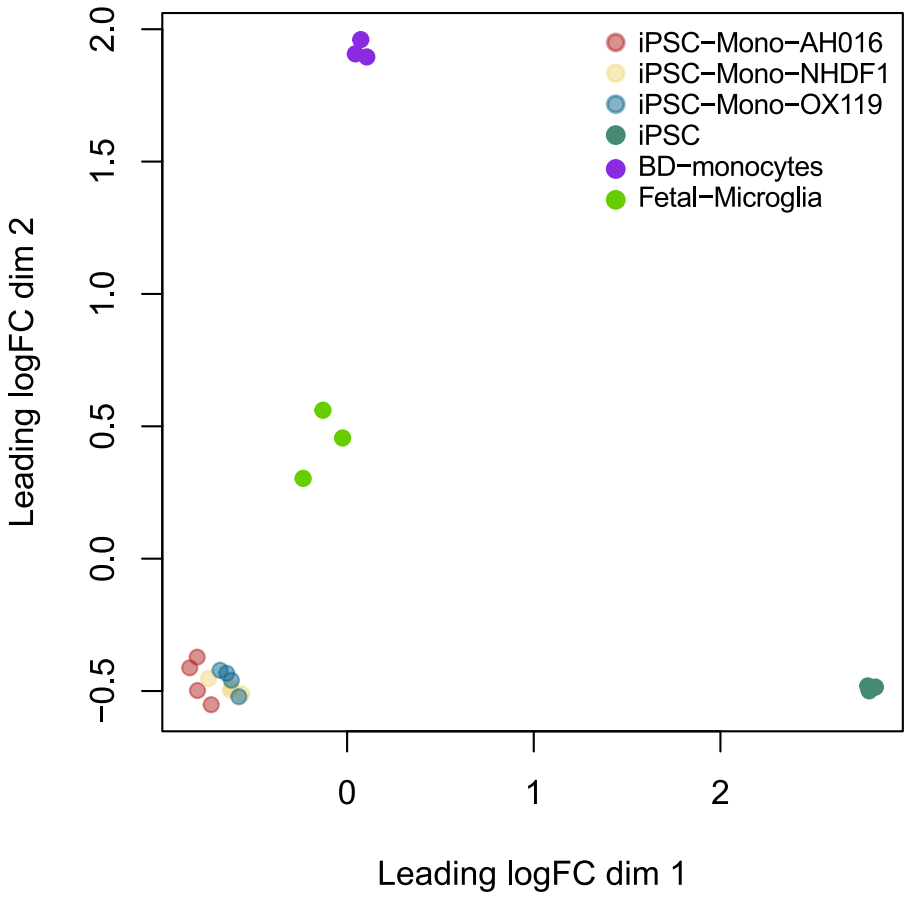

Figure 3.13: MDS plot of iPS-Mo/Mϕs, fetal microglia, blood monocytes and hiPSCs MDS plot showing clustering of the 12 different iPS-Mo/Mϕ, 3 fetal microglia, 3 adult blood monocyte and 3 undifferentiated hiPSC on 2 dimensions of distances between samples.

3.3.3.2 iPS-Mo/Mϕ have higher proliferation gene expression than fetal microglia and blood monocytes

To investigate more precisely the differences between the various myeloid cells I used the same RP approach as before. The RP approach is a robust method for meta-data analysis since it does not use distribution data, which often varies between samples generated on different chips. To limit the amount of data produced and to generate the clearest signal, I decided to use only H1 and H5 iPS-Mo/Mϕ for differential expression analysis with fetal microglia or blood monocytes. After differential expression analysis and GSEA against GO BP gene sets I first looked at which pathways were enriched in all four iPS-Mo/Mϕ samples compared to either microglia or blood monocytes. The GO gene sets which were significantly (FDR <

0.05) enriched were cell cycle GO BP gene sets as seen in figure 3.14. From this we can conclude that although H1 iPS-Mo/Mϕs have a higher cell cycle gene expression than H5, all iPS-Mo/Mϕs, independently of harvest have an enriched cell cycle gene signature compared to adult blood monocytes or fetal microglia. Although this signature is stronger in iPS-Mo/Mϕs the EdU results I obtained from later harvests showed very low to no proliferation of $CD14^+$ iPS-Mo/Mϕs (figure 3.3E). This result would suggest that either iPS-Mo/Mϕs have a low level ongoing proliferation even at later harvests or that they might have greater dormant proliferative capacity. This could either be due to an inherent property of hiPSC-derived cells being more prone to proliferation or due to the fact that the cells produced have been produced from precursor cells most likely one or two weeks before harvest and were not subsequently further differentiated, compared to fetal microglia which are already 2-3 months old and have been differentiated in situ within the tissue.

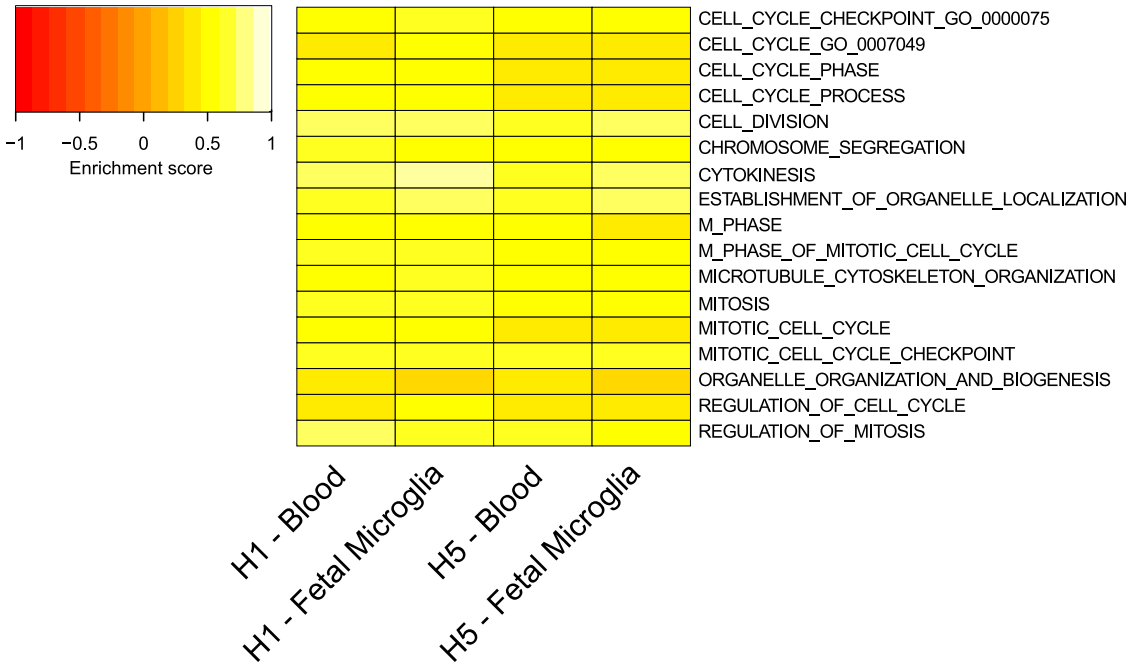

Figure 3.14: Cell cycle genes are enriched in iPS-Mo/Mϕs Heatmap of the significantly enriched (FDR < 0.05) gene sets in iPS-Mo/Mϕs compared to fetal microglia and blood-derived monocytes. Heatmap colouring was done according to ES. Positively enriched scores (yellow) represent gene sets higher expressed while negative ESs (red) represent gene sets lower expressed in iPS-Mo/Mϕs compared to fetal microglia or blood monocytes.

3.3.3.3 H1 iPS-Mo/Mϕ have lower adaptative immune gene enrichment than fetal microglia or blood monocytes

In addition to cell cycle gene sets, which were enriched in all tested iPS-Mo/Mϕ conditions, H1 iPS-Mo/Mϕs had many other significantly enriched gene sets compared to fetal microglia or blood monocytes (figure 3.15). GSEA results have been filtered to remove all cell cycle gene sets to increase readability and gene sets were manually subdivided into broad functional categories for further readability. The major category being enriched in iPS-Mo/Mϕs compared to fetal microglia and blood monocytes are genes involved in metabolism, biogenesis, transcription and translation (green). It is hard to estimate the origin of these differences, as they could be caused by many different factors such as cell culture conditions, media composition and also be linked to the previously detected cell cycle gene sets. The high metabolic signature in H1 iPS-Mo/Mϕs compared to blood monocytes is likely linked to *in vitro* culture conditions of iPS-Mo/Mϕs and fetal microglia, as blood monocytes have never been in culture. Metabolic changes could also be linked to altered metabolic processes between M1 (increased glycolysis) and M2 (increased oxidative phosphorylation) polarised Mϕs (reviewed in (Kelly and O'Neill, 2015)). In addition, iPSC derived and fetal cells are known to have a different metabolic signature compared to terminally differentiated cells (Panopoulos et al., 2012; Shyh-Chang et al., 2013; Hu et al., 2016), which could be another cause for this observed metabolic difference.

When looking at other gene sets, interestingly, fetal microglia only displayed a few immune related gene set differences, with enriched phagocytosis signature in iPS-Mo/Mϕs, and a higher adaptative immune response signature in fetal microglia. Several DNA damage and stress response gene sets were enriched in H1 iPS-Mo/Mϕs as well compared to fetal microglia.

Blood monocytes on the other hand displayed more differences with H1 iPS-Mo/Mϕs than fetal microglia, in agreement with the original MDS results (figure 3.13). They had lower levels of neuronal, cytoskeletal and stress response gene expression than H1 iPS-Mo/Mϕs while having a much stronger immune signature. The

immune signature result is not necessarily surprising given adult blood monocytes are fully matured cells, which developed in a potentially non-sterile environment with more adjuvants and antigens than iPS-Mo/Mϕs or fetal microglia. In addition my previous results showed that H1 iPS-Mo/Mϕs displayed a weaker immune signature than latter harvest iPS-Mo/Mϕs, therefore the immune differences might be less pronounced in later harvests.

While cytoskeletal genes could be related to cell cycle they can also be related to phagocytosis and motility. Blood monocytes in a non-adhered state in blood, and although iPS-Mo/Mϕs are released as non-adherent cells they morphologically resemble more to YS-Mϕs which can be found in the blood (See Chapter 4). The different morphology could be directly linked with different cytoskeletal gene expression pattern linked to cell motility, shape and adherence. iPS-Mo/Mϕs having an enriched neuronal signature compared to blood monocytes is quite surprising, but interestingly, this is not detected when comparing iPS-Mo/Mϕs to the fetal microglia population. This could be due to a more microglia-like phenotype of iPS-Mo/Mϕs, possibly related to a closer developmental origin (see Chapter 4), or due to some neuronal background differentiation happening in the EB culture.

3.3.3.4 H5 iPS-Mo/Mϕ are very similar to fetal microglia

When doing the same analysis as previously but this time looking at differences between H5 iPS-Mo/Mϕs compared to fetal microglia and blood monocytes, H5 iPS-Mo/Mϕs displayed mostly the same differences as H1 iPS-Mo/Mϕs with the exception of the immune gene sets (figure 3.16). H5 iPS-Mo/Mϕs displayed only a few immunological gene set difference with fetal microglia and blood monocytes, this result ties in with the previous results showing that H5 iPS-Mo/Mϕs had a stronger immune signature than H1 iPS-Mo/Mϕs. Furthermore except for the metabolism (and cell cycle) iPS-Mo/Mϕs show almost no difference with fetal microglia. When comparing H5 iPS-Mo/Mϕs to blood monocytes, cytoskeletal genes and neuronal genes are still detected as previously. Taken together these results show that H5 iPS-Mo/Mϕs are very close to fetal microglia. They display

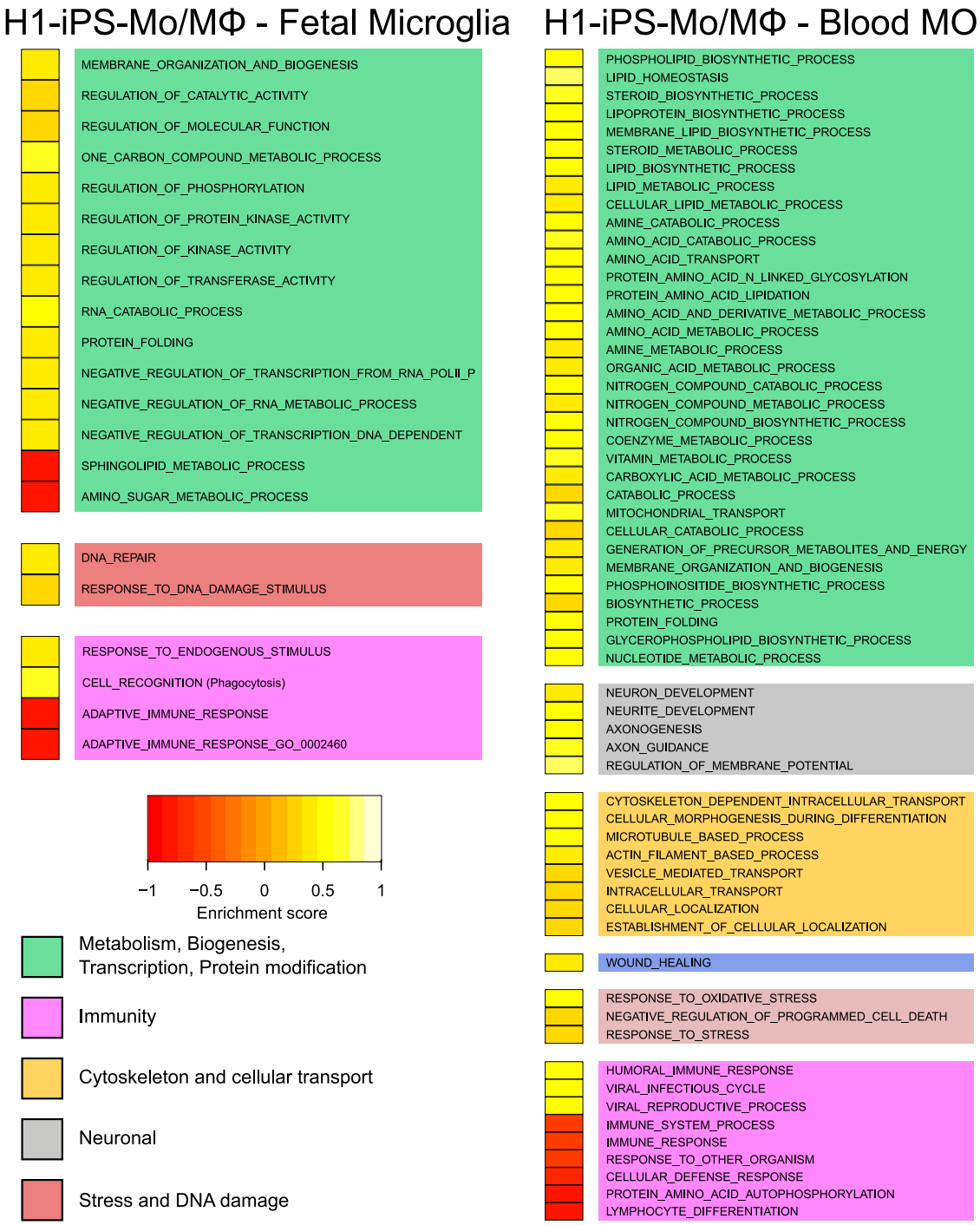

Figure 3.15: GSEA analysis of H1-iPS-Mo/Mϕs compared to fetal microglia or blood monocytes Heatmap of ESs of either GSEA of differentially expressed genes between H1-iPS-Mo/Mϕs and Fetal microglia or H1-iPS-Mo/Mϕs and blood monocytes. Gene sets have been clustered manually by overall biological function represented by coloured boxes.

a stronger cell cycle signature, although they are not strongly cycling (shown by the low level EdU staining - figure 3.3E) and have a very similar immunological signature. In comparison, using the same analysis conditions but comparing H5 iPS-Mo/Mϕs to undifferentiated hiPSCs over 220 gene sets were highlighted as significantly enriched, with strong enrichment of immune genes in iPS-Mo/Mϕs and strong enrichment of cell cycle and cell genes in hiPSCs (data not shown).

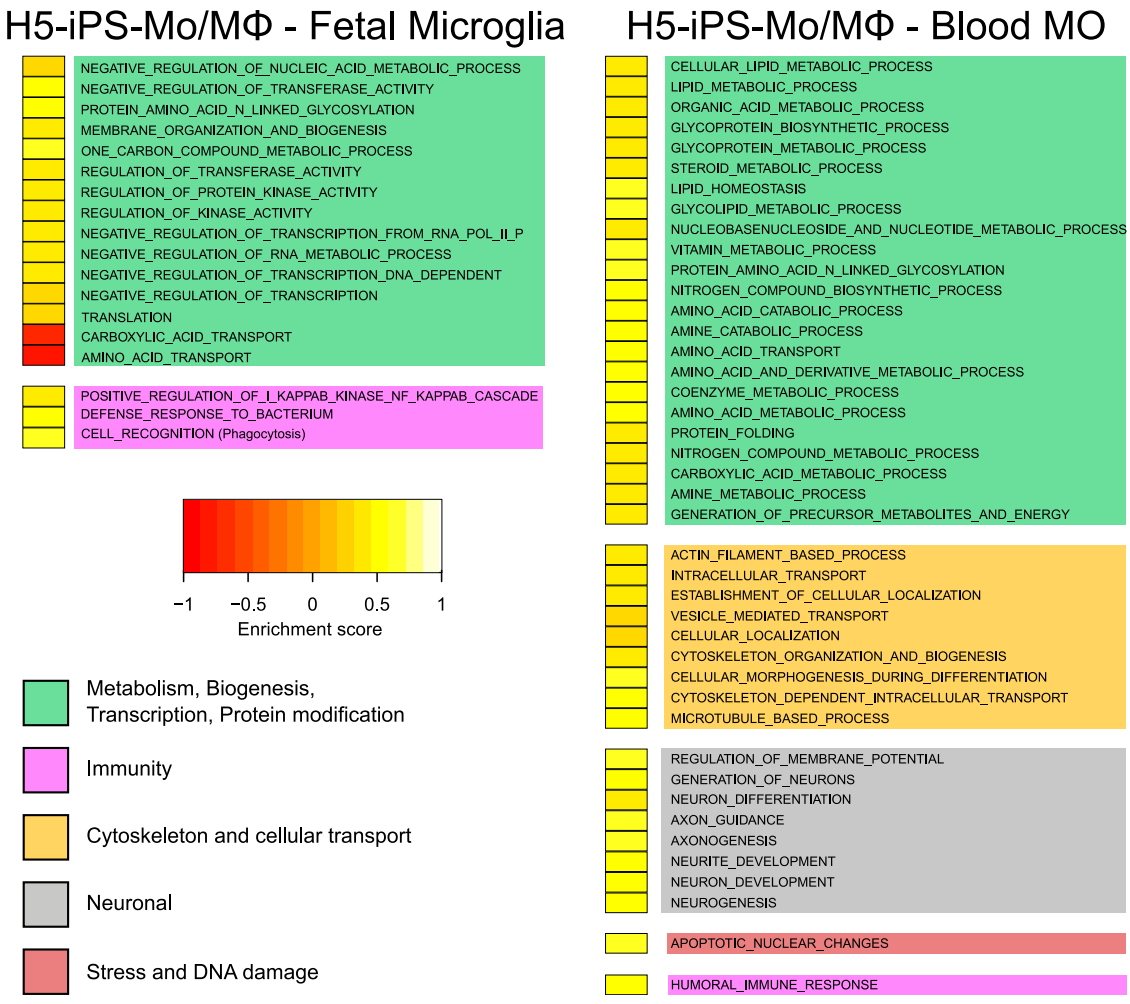

Figure 3.16: GSEA analysis of H5-iPS-Mo/Mϕs compared to fetal microglia or blood monocytes Heatmap of ESs of either GSEA of differentially expressed genes between H5-iPS-Mo/Mϕs and Fetal microglia or H5-iPS-Mo/Mϕs and blood monocytes. Gene sets have been clustered manually by overall biological function represented by colorred boxes.

3.4 Discussion

In this chapter I have used a transcriptomic approach to investigate the differences between iPS-Mo/Mϕs produced by young EBs/Factories soon after the start of differentiation compared to iPS-Mo/Mϕs produced by older EBs/factories. Understanding if and how "early" and "late" iPS-Mo/Mϕs are different can allow for a reduction in unwanted technical variability in our experiments, give us a new insight into the possibility of a lineage switch over time and allow us to better classify the iPS-Mo/Mϕs with reference to the known different Mϕ subtypes. For this I have done a time-course where I harvested iPS-Mo/Mϕs from young factories (H1) and after that every two to four weeks to see how the transcription profile of the cells develops over time. This analysis showed experimentally and transcriptionally that early harvests iPS-Mo/Mϕs possess some proliferative capacity which becomes less pronounced the more the factories age. This could be due to a less mature stage of H1-iPS-Mo/Mϕs, with the cells still displaying some progenitor like characteristics. This could also be an indication of a more YS like origin of iPS-Mo/Mϕs as it has been shown that most tissue-resident Mϕs, of YS-origin, self-renew (Hashimoto et al., 2013; Epelman et al., 2014) and that early in development primitive Mϕs and fetal monocytes have a high proliferative capacity (Van de laar et al., 2016). Experimentally this indicated that it is probably better to use the iPS-Mo/Mϕs only after the second harvest to get consistent experimental results as H1 iPS-Mo/Mϕs are the most different compared to later harvests (particularly if the technique requires a specific cell count which might be skewed by differential proliferation). It would therefore be important to optimising certain experiments according to harvest time.

With the exception of immune genes and a proliferative signature, the transcriptome from H1 and H2, H3 and H5 iPS-Mo/Mϕs are very similar and cluster together when compared to other cell types. In combination with their similar overall morphology over time this would imply that H1-iPS-Mo/Mϕs represent a more immature stage of differentiation. That being said, we cannot exclude the possibility of H1 and H5-iPS-Mo/Mϕs deriving from two different hematopoietic waves as the differences between YS-Mϕs, FL-monocytes and BM-derived monocytes

might be only very subtle. A recent study by Van de laar et al. (2016) has shown by transferring YS-Mϕs, FL-Monocytes or BM-Mϕs independently or together into an empty alveolar niche of neonate Csf2rb$^{-/-}$ mouse that although FL-monocytes had a selective advantage in colonizing an empty alveolar niche due to their higher proliferative capacity and GM-CSF responsiveness, when the three populations were transferred individually, all three populations colonised the niche and generated AMs that were transcriptionally almost identical, self-maintained, and durably prevented alveolar proteinosis.

In addition to the analysis of the iPS-Mo/Mϕ samples, meta-data analysis comparing my data to those of Dr Hänseler has shown that while H1 iPS-Mo/Mϕ display a weaker immune signature than either fetal microglia or blood monocytes, later harvest iPS-Mo/Mϕs are immunologically very similar. Although no strong proliferation was detected experimentally by EdU labelling all iPS-Mo/Mϕs displayed a stronger proliferation signature than fetal microglia or blood monocytes. Therefore although later harvests are almost non-proliferative they might be more prone to proliferation. Overall my results show that iPS-Mo/Mϕs are more similar to fetal microglia than adult blood monocytes and would imply a YS-like origin of the iPS-Mo/Mϕs.

4

hiPSC-derived monocyte & Mϕ ontogeny

Contents

4.1 Introduction 80
4.2 Materials and Methods 82
4.2.1 shRNA 82
4.2.1.1 shRNA design 82
4.2.1.2 Cloning of the shRNA vectors 83
4.2.1.3 p24 ELISA 83
4.2.1.4 Generation of shRNA-expressing cell lines . . . 85
4.2.2 CRISPR/Cas9 86
4.2.2.1 In-silico design 86
4.2.2.2 High resolution melt analysis (HRM) primer design 87
4.2.2.3 Vector construction 87
4.2.2.4 Gene editing and single-cell cloning 88
4.2.2.5 Clone screening, DNA extraction and HRM . . 89
4.2.2.6 Screening for WT contamination 91
4.2.2.7 DNA extraction and Illumina SNP array . . . 91
4.2.3 Molecular biology and functional assays 93
4.2.3.1 Phagocytosis assay 93
4.2.3.2 TNFα enzyme-linked immunosorbent assay (ELISA) 93
4.2.3.3 ROS assay 93
4.2.3.4 EB dissociation and colony forming assay . . . 94
4.2.3.5 Western bloting 94
4.2.3.6 RNA extraction, reverse transcription (RT) and quantitative Polymerase Chain Reaction (qPCR) 95
4.3 Results 96
4.3.1 Using shRNAs to knock-down MYB in hiPSCs 96
4.3.1.1 MYB shRNAs had limited KD efficiency in Jurkat and CCRF-CEM cell lines 96

4.3.1.2 MYB shRNAs had limited KD efficiency in hESC 98
4.3.1.3 Effect of MYB KD using shRNAs on iPS-Mo/Mϕ differentiation 100
4.3.2 Optimizing the CRISPR-Cas9 protocol to generate hiPSC KO 101
4.3.3 Exon 9 MYB KO 106
4.3.3.1 Structure of MYB and gRNA design 106
4.3.3.2 MYB$^{\Delta Ex9}$ hiPSC lines have un-modified iPS-Mo/Mϕ differentiation capacity 109
4.3.4 Generation of the RUNX1, SPI1 and MYB KO hiPSC lines 111
4.3.4.1 Why chose these genes and this location? . . . 111
4.3.4.2 Different generated KO clones 115
4.3.4.3 Quality control of the hiPSCs 115
4.3.4.4 iPS-Mo/Mϕ development is MYB independent but RUNX1 and SPI1 dependent 119
4.3.4.5 MYB$^{\Delta Ex6}$ iPS-Mo/Mϕs display no apparent phenotypic or functional defects 121
4.3.4.6 MYB KO results in increased number of hematopoietic progenitors within the EB 121
4.3.4.7 hiPSC-derived erythrocytes and granulocytes are dependent on MYB, RUNX1 and SPI1 . . 124
4.4 Discussion 124

4.1 Introduction

Adult murine Mϕs, in contrast to most other adult hematopoietic cells which renew from HSCs (Gekas et al., 2005), can derive from all three temporally and spatially distinct hematopoietic waves arising in the mouse embryo (McGrath et al., 2015b). Most tissue-resident Mϕs derive from Myb-independent YS progenitors generated before the emergence of HSCs (Schulz et al., 2012), after which they self-renew locally, independently of circulating monocytes and HSCs (Hashimoto et al., 2013; Epelman et al., 2014). In contrast, adult blood monocytes as well as infiltrating, gut and dermal Mϕ derive from Myb-dependent HSCs. These findings are derived from the mouse, in which a combination of anatomical location, embryonic day of development, phenotypic markers as well as gene KOs and lineage tracing has been used to precisely map the temporal and spacial emergence of the Mϕ subpopulations.

As described previously our laboratory has developed a feeder-free EB-based protocol for the generation of a homogeneous iPS-Mo/Mϕ population from hESC/hiPSC

(van Wilgenburg et al., 2013; Karlsson et al., 2008). These cells express classical mononuclear phagocyte markers ($CD14^{high}$, $CD16^{low}$, $CD163^{+}$), are morphologically similar to BD-Mo/Mϕ and display a Mϕ-like cytokine expression profile while resting or activated using classical (INFγ/LPS) or alternative activation (IL-4) (van Wilgenburg et al., 2013). In previous studies, iPS-Mo/Mϕ produced using this protocol have also been shown to display oxidative burst capacity (Flynn et al., 2015), high phagocytic capacity, and are infectible by HIV-1 (Van Wilgenburg et al., 2014), dengue virus (Cowley et al., 2012), influenza virus (van Wilgenburg et al., 2016), *Leishmania* and *Mycobacterium tuberculosis* (unpublished data). Interestingly, iPS-Mo/Mϕs produced using this protocol express low level of MHCII (van Wilgenburg et al., 2013), which is a phenotypic specificity enriched in fetal monocyte-derived dermal and cardiac Mϕs in the mouse (1.3.6.2.3).

While these are clearly Mϕ-like cells, the markers and functions they display are common to all Mϕs. Although functionally very similar, YS-Mϕ and FL-monocytes display higher proliferative capacity and longevity compared to adult blood monocyte-derived Mϕs, giving them a selective advantage in a tissue niche (Van de laar et al., 2016). The results from chapter 3 show that iPS-Mo/Mϕ derived using our protocol are highly proliferative in early harvests and maintain a high cell cycle gene expression profile even in later harvests suggesting a fetal origin of the iPS-Mo/Mϕs. Furthermore they displayed fewer differences in immunological signatures from fetal microglia compared with blood monocytes, further reinforcing this hypothesis. In regards to the developmental origin of human iPS-Mo/Mϕ two studies have tried to adress this scientific question. Klimchenko *et al.* have shown that hESC-derived monocytes/Mϕs closely resemble, both transcriptionally and functionally, FL-derived monocytes/Mϕs from first-trimester fetuses (Klimchenko et al., 2011). Whereas Vanhee *et al.* recently showed using a MYB-eGFP reporter human embryonic stem cell line that $CD14^{+}$ Mϕs were generated through a $CD34^{+}$ $CD43^{+}$ GFP^{-} hematopoietic precursor (Vanhee et al., 2015).

Although these observations are suggestive of a MYB-independent fetal-like ontogeny of human iPS-Mo/Mϕ another possibility could be the generation of

two temporal distinct waves of myelopoiesis occurring in our EB system, a first wave of MYB-independent highly proliferative iPS-Mo/Mϕ followed rapidly by a later wave of MYB-dependent less proliferative iPS-Mo/Mϕ. I therefore set out to investigate the transcription factor requirement of human hPSC myelopoiesis in order to map their identity onto human hematopoietic development. Due to the limited data on human embryos, the lack of definitive human phenotypic markers discriminating tissue resident Mϕ from fetal monocyte or adult blood monocytes, as well as the lack of anatomical location in an hiPSC system I decided to genetically define their ontogeny.

The main aim was to use the differential requirement of MYB, RUNX1 and SPI1 transcription factors for the three hematopoietic waves described in the mouse to characterise the ontogeny of the iPS-Mo/Mϕ generated in our lab. I first set out to use a knock-down (KD) strategy before the advent of clustered regularly interspaced short palindromic repeats (CRISPR)/Cas9 gene editing, after which I decided to use a gene KO approach, which seemed more appropriate for answering my experimental question, as the KD approach gave inconclusive results. Section 4.3.4 of this chapter has now been published in stem cell reports (Buchrieser et al., 2017).

4.2 Materials and Methods

4.2.1 shRNA

4.2.1.1 shRNA design

For the KD of MYB I used a published shRNA sequence, showing a strong KD of MYB in the MCF-7 (Michigan Cancer Foundation-7) cancer cell line (Drabsch et al., 2007). The shRNA used by Drabsch et al. is 27 nucleotide (nt) long which is more likely to be detected by PKR (Hannon and Rossi, 2004), I therefore designed a shortened, 21 nucleotide version of the same shRNA (figure 4.1). As a control for the 27 nt shRNA the scrambled control published by Drabsch et al. was used and for the 21 nt shRNA an already established 21 nt long scramble shRNA was used (van Wilgenburg et al., 2013) (figure 4.1). The different shRNAs will be referred to as as shMYB^{27nt}, shMYB^{21nt}, shCTRL^{27nt} and shCTRL^{21nt}.

Figure 4.1: Sequence and hairpin loop structure of the two MYB shRNAs used in this chapter. shMYB^{27nt} is a published shRNA targeting MYB (Drabsch et al., 2007) while shMYB^{21nt} has been shortened by 6 nucleotides (labelled by a red box) to reduce potential detection by DNA sensors and off-target effects.

4.2.1.2 Cloning of the shRNA vectors

Oligonucleotides (table 4.1) were resuspended at a 100 μM and top and bottom oligonucleotides of each shRNA were mixed at a 1:1 ratio and annealed (95°C for 30 sec, 72°C for 2 min, 37°C for 2 min, 25°C for 2 min). 1 μg of pCSRQ backbone (Nup358) was digested using XbaI. Annealed oligonucleotides at a concentration of 0.5 μM were ligated with the linearised pCSRQ backbone using T4 DNA ligase for 3h at RT. One Shot Stbl3 Chemically Competent *E. coli* (Invitrogen) were transformed with the ligated plasmids. Briefly, competent bacteria were thawed on ice, 2 μL of ligation mix was added to 50 μL of competent bacteria and incubated on ice for 30 min. Bacteria were heat shocked for 45 sec at 42°C, incubated on ice for 2 min after which 300 μL of S.O.C. medium was added and bacteria were incubated for 40 min at 37°C while shaking. Transformed bacteria were plated on Lysogeny broth (LB)-Agar containing 100 μg/mL Ampicillin (Sigma) and incubated at 37°C over night. Colonies were picked, amplified and sequenced for the presence of the correct ligated plasmid using the `EcoRI_U6_F` primer (5'- GCTAGAATTCGGGCAGGAAGAGGGC -3'). Correct colonies were grown overnight in 50 mL LB containing 100 μg/mL ampicillin and plasmid DNA was isolated using a PureLink® HiPure Plasmid Filter Midiprep Kit (Thermo Fisher Scientific).

4.2.1.3 p24 ELISA

Viral samples were inactivated for 1h at 56°C in a final concentration of 0.5% Empigen BB^{TM} (Sigma 45165) in a heat resistant 96-well plate and stored at

Table 4.1: shRNA oligonucleotides.

Code	Name	Sequence - 5' to 3'
JB-1	Top shRNA MYB (27 nt)	GATCCGAACCTCTTAGAATTTGCAGAAACACTTTCATGAGA-AGTGTTTCTGCAAATTCTAAGAGGTTCTTTTTTTCTAGAG
JB-2	Bottom shRNA MYB (27 nt)	AATTCTCTAGAAAAAAAGAACCTCTTAGAATTTGCAGAAAC-ACTTCTCATGAAAGTGTTTCTGCAAATTCTAAGAGGTTCG
JB-3	Top shRNA CTRL (27 nt)	GATCCATAAGAATGTCCATCAGTTACGCCATATTCATGAGATA-TGGCGTAACTGATGGACATTCTTATTTTTTTTCTAGAG
JB-4	Bottom shRNA CTRL (27 nt)	AATTCTCTAGAAAAAAAATAAGAATGTCCATCAGTTACGCC-ATATCTCATGAATATGGCGTAACTGATGGACATTCTTATG
JB-5	Top shRNA MYB (21 nt)	GATCCGTTAGAATTTGCAGAAACACTTTCATGAGAAGTGT-TTCTGCAAATTCTAACTTTTTTTCTAGAG
JB-6	Bottom shRNA MYB (21 nt)	AATTCTCTAGAAAAAAAGTTAGAATTTGCAGAAACACTT-CTCATGAAAGTGTTTCTGCAAATTCTAACG

-80°C. Grenier ELISA plates were coated overnight with 100 μL/well of 10 μg/mL α-HIV-1-p24 antibody (D7320 - Aalto). Samples were thawed at 37°C and the ELISA plate was washed 3x in 200 μL of wash buffer (Tris-buffered saline (TBS) (50 mM Tris-Cl, pH 7.5, 150 mM NaCl) + 0.05% Tween) followed by 30 min at room temperature with 200 μL blocking buffer (TBS + 2% BSA). HIV-1 p24 antigen standards (Aalto - BC1071-BIOT) were prepared in triplicate by generating a serial dilution series with a dilution factor of 1/2 using 100 μg/mL for the highest concentration. The ELISA plate was washed 3x in 200 μL of wash buffer and 100 μL of sample and standard, in triplicate, were transferred into the plate. Plates were incubated for 2h at 37°C with gentle agitation (75 rpm). The ELISA plate was washed 6x in 200 μL of wash buffer, following which 100 μL/well of 1:1000 diluted stock of biotinylated α-HIV-1-p24 antibody (Aalto BC1071-BIOT) in TMT/SS buffer (TBS, 2% BSA, 20% FCS) was added and the plate was incubated at room temperature for 2h. ELISA plate was washed 6x in 200 μL of wash buffer and 100 μL/well of 0.1 μg/mL of streptavidin-HRP (Serotec STAR5B) in TMT/SS buffer was added. After incubation at room temperature for 1h the ELISA plate was washed 6x in 200 μL of wash buffer and 100 μL/well of 1-step Utlra TBM-ELISA (Pierce, 34028) was added after which the reaction was stopped with 100 μL/well of 0.5M H_2SO_4. The optical density of each well was measured at 450 nm and 570 nm (SpectraMax® M3) and the 570 nm readings were subtracted from the 450 nm

reading to obtain an accurate read based on the volume in each well. Unknowns were interpolated from the fit from the standard curve.

4.2.1.4 Generation of shRNA-expressing cell lines

All four shRNA constructs were cloned in the vector pCSRQ lentiviral vector (figure 4.2A) which was derived by subcloning the shRNA expression cassette from pSIREN RetroQ into pCSGW (Schaller et al., 2011). VSVg pseudotyped shRNA-expressing lentiviral vectors were generated by co-transfection of the shRNA-containing pCSRQ plasmid and the required helper plasmids HEK 293T cells (M&M: 2.8). As the generated lentiviral vectors contained no tractable marker, an additional lentiviral vector expressing GFP under the control of EF1α promoter (LV-EF1a-GFP-IRES-Puromycin^R - (van Wilgenburg et al., 2013)) was generated and viral titres were quantified using p24 ELISA (figure 4.2D). The GFP vector was used to generate an infection standard curve in HUES-2 hESCs (figure 4.2E). These results were used in combination with the p24 ELISA results to extrapolate an approximate concentration of shRNA-expressing pCSRQ lentiviral vector needed to obtain 10% lentiviral transduction of hESC. I aimed for 10% as this results in 99.5% of the transfected cells having only a single integrant, according to Poisson distribution (Ellis and Delbrück, 1939). By having mainly single integrants I aimed to obtain consistent shRNA expression level across the four different shRNA constructs. HUES-2 hESCs, Jurkat and CCRF-CEM cells were transduced using the four different shRNA-expressing lentiviruses and selected with puromycin. After 48h of selection 80-90% of cell death was observed indicating that most surviving cells should only have a single lentiviral integrant. Jurkat and CCRF-CEM cells were chosen as a control as they are known to express MYB constitutively (Lin et al., 2008).

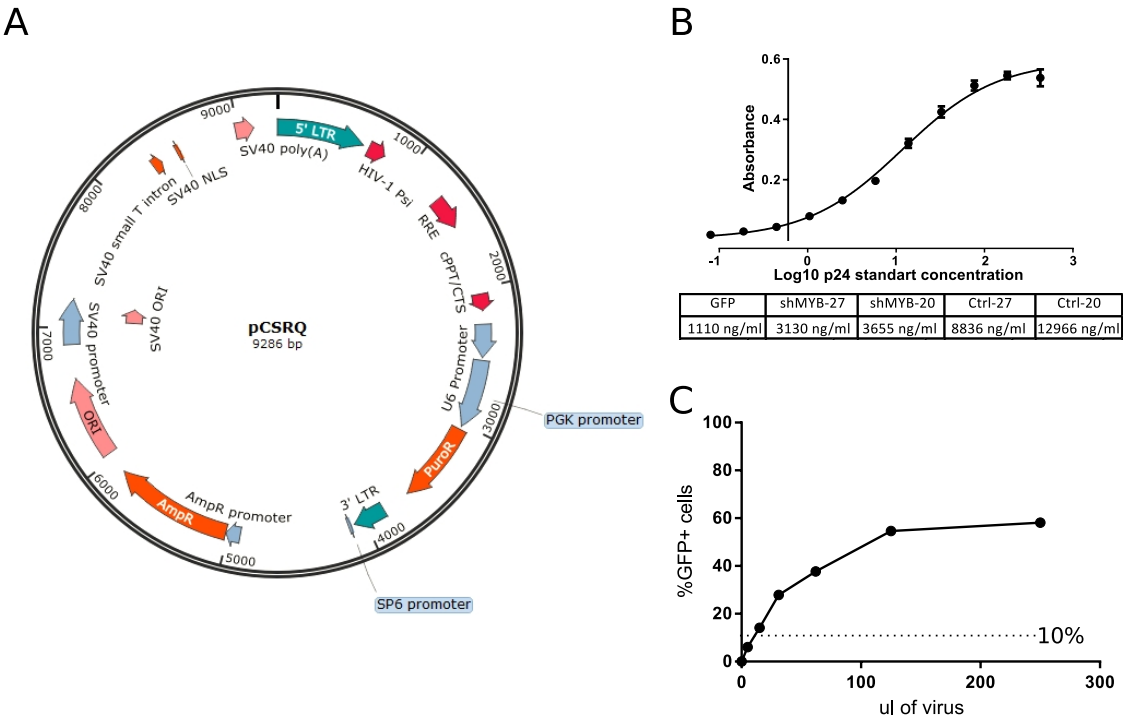

Figure 4.2: A. Full plasmid map of the lentiviral vectors. **B.** p24 ELISA standard curve and the extrapolated concentration of virus generated. **C.** Infection titration curve using the GFP virus as a control.

4.2.2 CRISPR/Cas9

4.2.2.1 In-silico design

CRISPR KO target site was chosen according to the following criteria. Firstly, the first or last exons were excluded, as an out-of-frame mutation in the first exon can lead to the usage of an alternative start site and an out-of-frame deletion in the last exon will not induce nonsense-mediated mRNA decay (NMD) of the selected; target transcript. Second, only exons conserved between all isoforms of the protein were selected, if the exon targeted is only present in a specific splice variant of the protein the induced frameshift will be spliced out in all other variants which will still be viable and expressed. Third, a large enough exon was chosen as any the deletion generated by the CRISPR/Cas9 cleavage spanning across the exon-intron boundary would result in a loss of a splice site and a possible loss of the exon from the protein. Lastly, it is best to target an exon before the active site or DNA-binding domain of the protein in case NMD is not 100% efficient, in

which case the protein translated would still be nonfunctional. The guide RNA (gRNA) locations were detected using the http://crispr.mit.edu/ website to find all possible gRNAs for each exon of interest. For dual gRNA targeting, the offset of the two gRNAs should not be greater than 10 bp, nor should the two gRNA targets overlap, as either would result in loss of cutting efficiency.

4.2.2.2 High resolution melt analysis (HRM) primer design

HRM primers were designed using the PrimerExpress software, using the TaqMan quantification default settings. The amplification region should be of 150-200 bp and if possible leave at least 70 bp between the first CRISPR cut site and the forward binding primer. This is not necessary but allows for sequencing of the HRM PCR product. Primers were designed with a minimum offset of 30-40 bp from the Cas9 cutting site. If they are close, the primer-binding site can be destroyed by the deletion generated by the CRISPR/Cas9 cut, resulting in no PCR amplification during HRM analysis. A schematic representation of the target choice and primer design of MYB can be found in figure 4.3.

4.2.2.3 Vector construction

The CRISPR-Cas9 vectors used in this study were based on the dual Cas9- and gRNA-, puromycin-resistance gene-expressing, pSpCas9n(BB)-2A-Puro (pX462) vector Cong et al. (2013) (gift from Feng Zhang (Addgene plasmid #48141)). Cloning was performed as previously described Cong et al. (2013) using oligonucleotides JB-73 (5'- CACCGGCTTGTGGCCACTGCTGGC -3') and JB-74 (5'- AAACGCCAGCAGTGGCCACAAGCC -3') with pX462 to create pX462-gMYBt; oligonucleotides JB-75 (5'- CACCGCAGAAGAACAGTCATTTGA -3') and JB-76 (5'- AAACTCAAATGACTGTTCTTCTGC -3') with pX462 to create pX462-gMYBb; oligonucleotides JB-81 (5'- CACCGCAGTGACCAGAGTGCCATC -3') and JB-82 (5'- AAACGATGGCACTCTGGTCACTGC -3') with pX462 to create pX462-gRUNX1t; oligonucleotides JB-83 (5'- CACCGGGCAATGATGAAAAC-TACT -3') and JB-84 (5'- AAACAGTAGTTTTCATCATTGCCC -3') with pX462

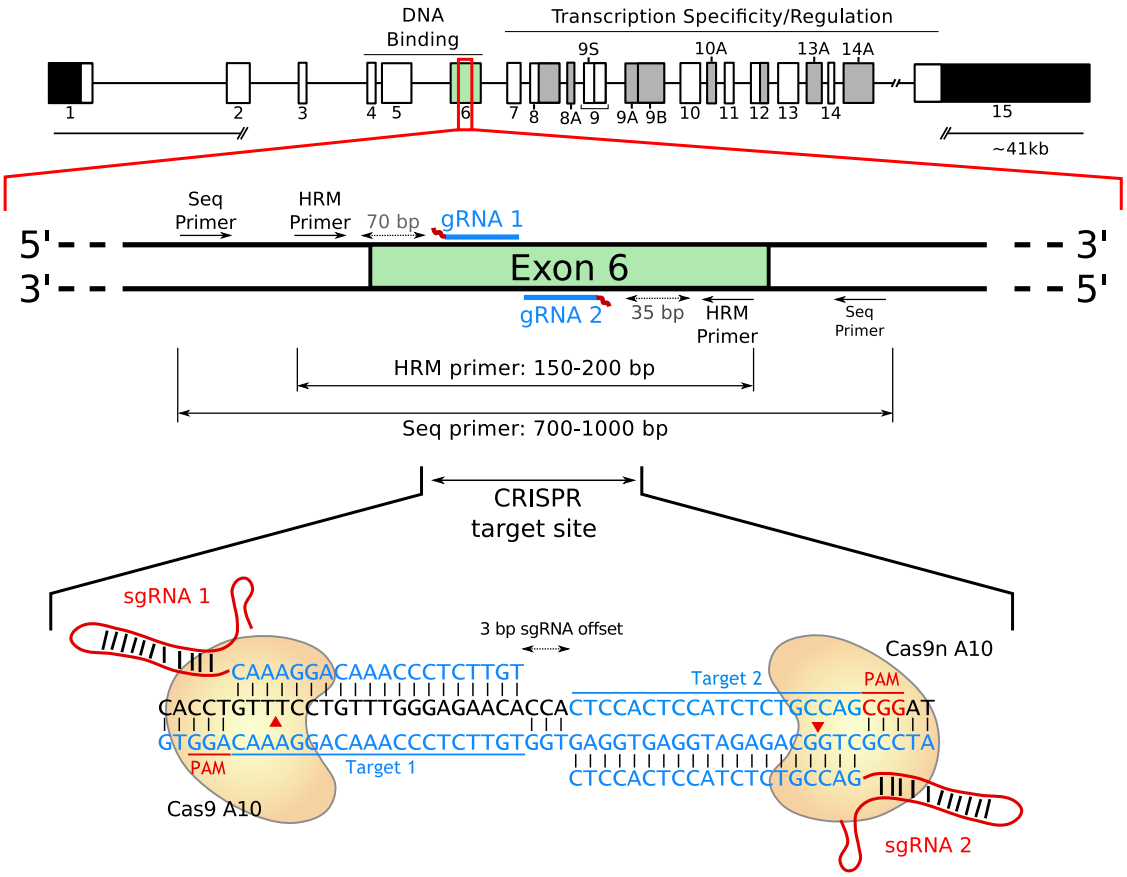

Figure 4.3: Schematic representation of the choice of the gRNA target location and primer design. The choice of the target site for CRISPR-Cas9 KO is crucial for success. In this example I have represented the Human MYB genomic structure which contains many alternatively spliced exons (represented in grey), a DNA binding site and a regulatory domain. After the choice of target location two different sets of primers need to be designed, a set of HRM primers for screening and a set of sequencing primers for analysis of the pre-screened clones.

to create pX462-gRUNX1b; oligonucleotides JB-101 (5'- CACCGCTGCGGGGGCT-GCACGCTC -3') and JB-102 (5'- AAACGAGCGTGCAGCCCCCGCAGC -3') with pX462 to create pX462-gSPI1t; and oligonucleotides JB-103 (5'- CACCGCAGCAGCTC-TACCGCCACA -3') and JB-104 (5'- AAACTGTGGCGGTAGAGCTGCTGC -3') with pX462 to create pX462-gSPI1b.

4.2.2.4 Gene editing and single-cell cloning

Schematic representation of the CRISPR-Cas9 based KO strategy in hiPSCs is shown in Figure 4.4. $2x10^6$ feeder-free hiPSCs were transfected with two pX462 Cas9-

gRNA-puromycin expressing plasmids in a single-cell suspension by electroporation (Neon® transfection system, Invitrogen), using a 100 μL tip with 10 μg DNA (5 μg top strand pX462-gRNA and 5 μg bottom strand pX462-gRNA). After one pulse of electroporation at 1000 V and 40 ms pulse width, 1x10^6 transfected cells were plated onto a matrigel-coated 12 well plate in mTeSR^{TM}1 supplemented with 10 μmol/L Y-27632 without penicillin/streptomycin. After 48h, cells were puromycin selected (0.4 μg/mL; MP Biomedicals) for 48h. Surviving cells were plated at 10^4 per 10cm dish on mitotically-inactivated mouse embryonic fibroblast feeder cells (MEF; outbred Swiss mice established and maintained at the Department of Pathology, Oxford Gardner (1982); Chia et al. (2005)) on gelatin-coated tissue culture plates in hESC medium (KO-DMEM, 2 mmol/L L-Glutamine, 100 mmol/L non-essential amino acids, 20% serum replacement, and 8 ng/mL basic fibroblastic growth factor (FGF2)), supplemented with 10 μmol/L Y-27632 on the day of the plating. After 7 days of expansion, individual single-cell colonies were picked manually onto a matrigel coated 96 well plate in mTeSR^{TM}1.

4.2.2.5 Clone screening, DNA extraction and HRM

After picking, hiPSCs clones were expanded and split into two 96 well plates. One plate was used for DNA extraction using over night lysis at 55°C in lysis buffer (10mM tris pH 7.5, 10mM Ethylenediaminetetraacetic acid (EDTA), 10mM NaCl, 0.25% triton X100, 1mg/mL proteinase K) after which DNA was precipitated for 2h using a -80°C precipitation solution (75mM NaCl in 100% EtOH), washed in EtOH three times, air dried and re-suspended in distilled water. Pre-screening of targeted clones was performed using HRM on a StepOnePlus^{TM} Real-Time PCR System (ThermoFisher). HRM is a PCR based method for detecting mutations and polymorphisms in a piece of double stranded DNA and allows for pre-screening of clones and removal of all wild type (WT) unmodified clones before sequencing (figure 4.5). For HRM, AmpliTaq® Gold DNA Polymerase (ThermoFisher) was used with LCGreen Plus+ (BioChem) melting dye. The following primers were

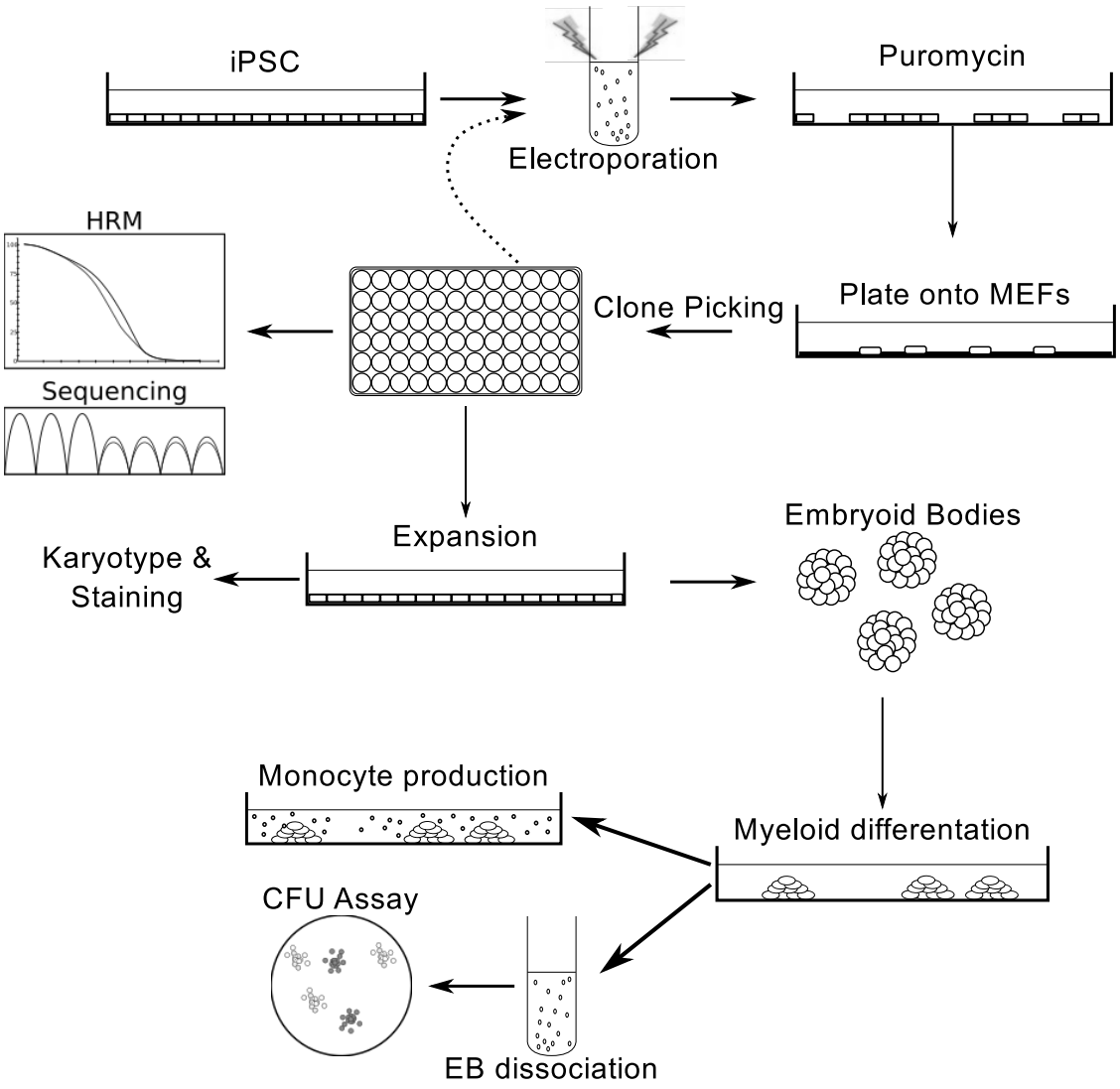

Figure 4.4: Schematic representation of the CRISPR-Cas9 based KO strategy in iPSCs. hiPSCs generated from a healthy donor were cultured under feeder-free conditions, electroporated with two pX462 plasmids for Cas9-gRNA-puromycin expression. Transfected cells were selected by transient puromycin treatment after which they were plated at low density onto mouse embryonic fibroblast feeder cells. After 7 days of expansion, individual single cell colonies were picked into a 96 well plate directly in feeder-free conditions and clones were expanded. hiPSC clones were pre-screened for insertions or deletions in the targeted region using HRM (Supplementary Fig. 2a) and sequenced to determine the exact sequence of each clone. Clones harbouring a single out-of-frame or a double out-of-frame deletion in the gene of interest were expanded, stained for pluripotency markers, karyotyped, assessed for monocyte differentiation potential and hematopoietic colony formation capacity.

used: JB-71 (5'- ACAGGAAGGTTATCTGCAGGAGTCT -3') + JB-72 (5'- AGTG-GCAGGGAGTTGAGCTGTA -3') for MYB, JB-79 (5'- ATCACTACACAAAT-

GCCCTAAAAGTG -3') + JB-80 (5'- TTAAATCTTGCAACCTGGTTCTTCA -3') for RUNX1 and JB-99 (5'- CAGACCATTACTGGGACTTCCA -3') + JB-100 (5'- GGGTATCGAGGACGTGCATCT -3') for SPI1. Genetically modified clones detected by HRM were sequenced and analysed for insertions and/or deletions. The first round of transfection produced several single out-of-frame deletion MYB clones but did not result in any double out-of-frame KO clones, we therefore used a single out-of-frame KO clone, clone D6, for re-targeting. Clone D6 was expanded and transfected with the two pX462 Cas9-gRNA-puromycin expressing plasmids targeting MYB and processed as previously. After a second round of targeting, several out-of frame KOs were generated and 3 clones (Clone B5, C5 and E6) were used in this study.

4.2.2.6 Screening for WT contamination

Single cell clones were checked for presence of WT DNA by standard PCR using WT specific primers, forward primers were designed to span the deletion and/or insertion present in the KO clones hindering binding of the primers and amplification of KO sequence but allowing the amplifying WT sequence. $MYB^{\Delta Ex6}$ clones were tested using forward primer JB-107 (5'- TGGCCACAAGCTTCCAGAAG -3') and reverse primer JB-64 (5'- ACCATACCTACACCCTATCTACTTCAAAG -3'). $RUNX1^{\Delta Ex5}$ clone was tested using forward primer JB-110 (5'- GGCTGGCAATGATGAAACCT -3') and reverse primer JB-78 (5'- GATAGCCCACAGATCATACGTCAA -3'), the forward primer was designed with an extra mismatch to increase specificity as one allele of the $RUNX1^{\Delta Ex5}$ clone is a short 2 bp insertion. $SPI1^{\Delta Ex3}$ clone was tested, forward primer JB-108 (5'- GAGCTCCAGAGCGTGCAGCC -3') and reverse primer JB-92 (5'- CAGGAGGGCCCACAACAA -3').

4.2.2.7 DNA extraction and Illumina SNP array

For SNP analysis, $2x10^6$ feeder-free hiPSCs were pelleted and their DNA was extracted using the DNeasy Blood & Tissue Kit (QIAGEN) following manufacturers protocol. All optional steps were performed, including the RNase A incubation to obtain RNA free DNA. DNA was normalised to 100 ng/μL. SNP analysis was

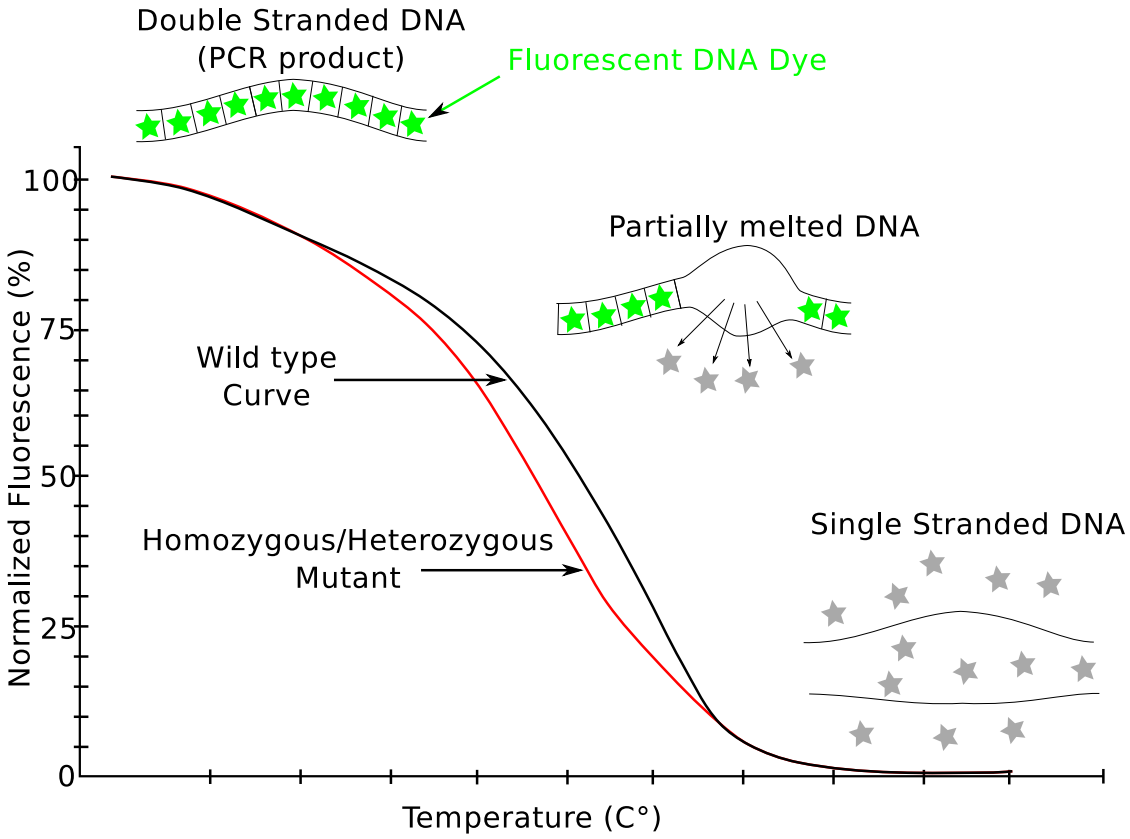

Figure 4.5: Schematic representation of HRM analysis. HRM of nucleic acid collects information of fluorescence as a function of temperature in a mixture that contains a fluorescent double-strand DNA binding dye and a PCR product. Mutations in PCR products result in destabilisation of the dsDNA and therefore different melting temperatures which are detected by changes in the shape of the melting curve compared to a reference sample. In this schematic example WT is represented in black and the shifted mutant allele in red.

performed by the high-throughput genomics group at the Wellcome Trust Centre for Human Genetics on an OmniExpress24 chip covering 700,000 markers. The SNP datasets and the Illumina HT12v4 transcriptome array results of the parental cell line have been deposited in Gene Expression Omnibus under accession number GEO: GSM2055806. The SNP datasets of the genetically modified lines have been deposited in GEO: GSE93285. Results were analysed using KaryoStudio (Illumina).

4.2.3 Molecular biology and functional assays

4.2.3.1 Phagocytosis assay

Harvested iPS-Mo/Mϕs were differentiated to Mϕs for 7 days in Mϕ differentiation media (X-VIVO^{TM}-15 (Lonza), supplemented with 100 ng/mL M-CSF (Invitrogen), 2 mM glutamax (Invitrogen), 100 U/mL penicillin and 100 mg/μL streptomycin (Invitrogen), and 0.055 mM β-mercaptoethanol (Invitrogen)). On the day of the analysis negative control wells were pre-treated with 10 μM cytochalasin D (MP Biomedical) for 1h. After pre-treatment all wells were fed with media containing 2 particles per cell of 488nm-Zymosan (Z-23373, Thermo Fisher). Mϕs were lifted using PBS supplemented with Lidocaine for 30 min at 37°C. Unphagocytosed membrane-bound zymosan was quenched using 250 μg/mL TrypanBlue (Gibco) for 5 min and the cells were fixed in 2% formaldehyde. Results were acquired on a FACSCalibur^{TM} flow cytometer (BD).

4.2.3.2 TNFα enzyme-linked immunosorbent assay (ELISA)

Harvested iPS-Mo/Mϕs were differentiated for 7 days in Mϕ differentiation media (4.2.3.1). Positive control wells were activated with lipopolysaccharide (LPS) at 100 ng/mL for 24h. Cleared cell culture supernatants were diluted 1:5 and probed using the TNFα ELISA Ready set go (88-7346-86, eBiosciene) according to the manufacturer's instructions.

4.2.3.3 ROS assay

Harvested iPS-Mo/Mϕs (1x10^5) were plated onto 96 well black clear bottom assay plate (Corning 3603) Mϕ differentiation media (4.2.3.1) 24 hours prior to analysis. On the day of the assay, cell viability was assessed using the luminol compatible CellTiter-Fluor^{TM} assay (Promega). Briefly, media was replaced with 100 μL of viability assay solution (0.1 μL GF-AFC Substrate, 20 μL Assay buffer, 80 μL of 0.5% bovine serum albumin (BSA) Hanks' balanced salt solution (HBSS) with calcium and magnesium). Cells were incubated for 15 min at 37°C and total cell viability was quantified at Ex438-400 nm/Em 505nm on a PHERAstar FS

(BMG Labtech) platereader. After viability quantification, the PHERAstar FS was programmed to inject 100 μL of 2x luminol solution (200 μg/mL luminol in 0.5% BSA HBSS) with or without 400 ng/mL phorbol 12-myristate 13-acetate (PMA) (200 ng/mL final concentration). Individual wells were then monitored for light released at 1 sec intervals for 300 sec.

4.2.3.4 EB dissociation and colony forming assay

EBs (24 per condition) were harvested using a 100 μm cell strainer, washed in PBS, and resuspended in 500 μL of Accumax^{TM} Solution (Sigma). EBs were incubated for 5 min at 37°C, mechanical dissociation was started by carefully pipetting up and down using a 200 μL pipette for 1 min, after which the EBs were incubated an extra 5 min at 37°C and mechanical dissociation was repeated for an additional minute. Cell suspension was filtered using a 70 μm cell strainer before being centrifuged for 5 min at 400g. A colony forming cell assay was performed according to manufacturers protocol using a cell concentration of 3x10^5 cells/mL resulting in a final plating concentration of 3x10^4 cells per 35mm dish of MethoCult^{TM}H4344 complete media (STEMCELL technologies) containing SCF, IL-3, EPO and GM-CSF. Colonies were scored by morphology 14 days after plating.

4.2.3.5 Western bloting

Cells were harvested, washed once with PBS and pelleted at 400g for 5 min. The supernatant was removed and the cell pellets placed on ice. Cells were lysed in 50 μL of cold RIPA buffer (50 mM Tris-HCL, 150 mM Sodium Chloride, 1% NP-40, 0.5% Sodium deoxychlorate, 0.1% sodium dodecyl sulfate, pH 8.0) per 1x10^6 cells. Lysates were vortexed at full speed for a couple of seconds and placed back on ice and shaken for 30 min. Lysates were then centrifuged at 17000g for 15 min at 4°C and clarified supernatant was collected in a fresh eppendorf tube. Protein was quantified using Pierce® BCA protein assay kit (Thermo Fisher Scientific) and 50 μg of protein was denatured in NuPAGE® LDS Sample Buffer by heating to 95°C for 4 min. Proteins were loading in Novex® 12% Tris-Glycine Mini Gels (Life technologies), run for 1h at 150V in NuPAGE® MES SDS Running Buffer (life technologies) and

transferred onto methanol activated Low-Fluorescence PVDF Transfer Membrane (Thermo Scientific) for 1h at 110V using a tris-glycine buffer (192 mM Glycine, 25 mM Tris, 20% Methanol). The membrane was blocked for 3h in blocking solution (PBS, 0.05% Tween 20 and 5% milk) and stained over night with the primary α-MYB (H-141 – Santa Cruz) at 1:100 for hiPSC lysate and 1:1000 for Jurkat and CCRF-CEM cells. The control antibody αGAPDH (clone 2275-PC-100, R&D Systems) was added at 1:5000. The membrane was washed 3 times for 5 min with PBS + 0.05% tween and stained with a LI-COR secondary antibody GoatαRabbit IgG IRDye® 680RD (LI-COR) and GoatαMouse IgG IRDye® 800RD (LI-COR) for 1 to 3h at RT at 1:5000. Blot was scanned using a LI-COR Odyssey® scanner.

4.2.3.6 RNA extraction, reverse transcription (RT) and quantitative Polymerase Chain Reaction (qPCR)

RNA extraction was performed using the RNeasy® kit (Qiagen) according to manufacturer's protocol. Potential DNA contamination was removed by adding a step of Ambion® TURBO DNA-*free*® according to manufacturer's protocol (Life technologies). Reverse transcription was performed using the RetroScript® (Ambion) kit using random decamers. qPCR was performed using Power SYBR Green (Life technologies). The following primers were used for MYB: Forward 5'- GCCAATTATCTCCCGAATCGA -3' and reverse 5'- ACCAACGTTTCGGACCGTA -3'. The amplification product is of 155 base pairs and crosses intron-exon boundary to eliminate any signal for residual DNA contamination. Actinβ control reverse and forward primers were purchased from Eurogentech.

4.3 Results

4.3.1 Using shRNAs to knock-down MYB in hiPSCs

In the mouse haploinsufficiency of Myb is sufficient to significantly affect definitive hematopoiesis during *in vitro* differentiation of mESCs, while not reducing number of primitive erythrocytes and Mϕ produced (Jieping et al., 2007). I therefore started with an shRNA KD approach, as a strong KD of MYB should strongly reduce definitive hematopoiesis without affecting primitive hematopoiesis. Therefore if MYB KD does not affect iPS-Mo/Mϕ differentiation while affecting other lineages this would be a strong indication of MYB-independent iPS-Mo/Mϕ ontogeny. For MYB KD and scramble control shRNAs I used two different length variants of the same published shRNAs (shRNA material and method section 4.2.1) (Drabsch et al., 2007). I will refer to the four different shRNAs as shMYB^{27nt}, shMYB^{21nt}, shCTRL^{27nt} and shCTRL^{21nt}.

4.3.1.1 MYB shRNAs had limited KD efficiency in Jurkat and CCRF-CEM cell lines

As the expression of MYB in hESC and hiPSCs is not well defined I first used Jurkat and CCRF-CEM cells, which are known to express high levels of MYB, for optimizing MYB western blot and RT-qPCR. After protocol optimization Jurkat and CCRF-CEM cells transduced with shMYB^{27nt}, shMYB^{21nt}, shCTRL^{27nt} and shCTRL^{21nt} were used for initial assessment of the efficiency of MYB KD. Jurkat and CCRF-CEM cells were cultured under constant puromycin selection before being analysed for MYB mRNA and protein levels. shMYB^{21nt} and shMYB^{27nt} reduced MYB mRNA levels by 50% in Jurkat cells while only reducing MYB mRNA levels by 15% and 40% in CCRF-CEM$^{shMYB\text{-}21}$ and CCRF-CEM$^{shMYB\text{-}27}$ respectively (Figure 4.6A). In contrast, western blot quantification of MYB protein showed a higher KD of MYB in CCRF-CEM cells compared to Jurkat with a 32% and 64% KD in CCRF-CEM$^{shMYB\text{-}21}$ and CCRF-CEM$^{shMYB\text{-}27}$ cells while no major MYB protein KD was detected in Jurkat$^{shMYB\text{-}21}$ or Jurkat$^{shMYB\text{-}27}$ cell lines (Figure 4.6B and C). Together, these results show that although the shRNAs had an effect

on MYB expression, this effect was weak and variable between CCRF-CEM and Jurkat cell lines. As Jurkat and CCRF-CEM cells are cancer cell lines known to express high levels of MYB, shRNA expression might not be sufficient for proper KD, therefore I decided to directly test the efficiency of the shRNAs in hESCs. The hESC line HUES-2 was selected as candidate cell line for the KD as it was widely used in the laboratory at the time and was known for robust Mo/Mϕ production.

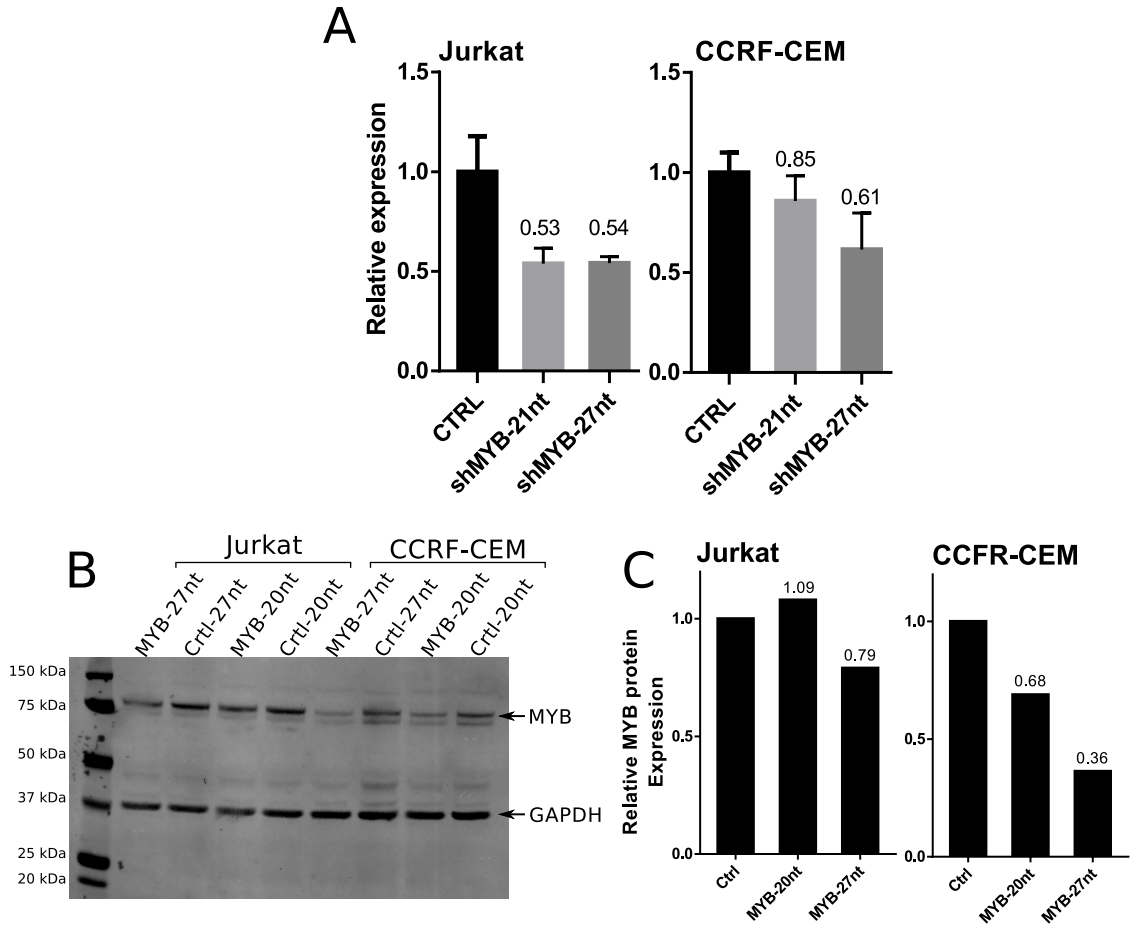

Figure 4.6: MYB shRNAs had limited KD efficiency in Jurkat and CCRF-CEM cell lines. A. Relative expression of MYB mRNA in Jurkat and CCRF-CEM cells. Each sample has been internally normalised to β-actin mRNA levels, relative quantity is expressed compared to the respective scramble shRNA control. **B.** Western blot of Jurkat and CCRF-CEM cells expressing different shRNA constructs, stained with α-MYB and α-GAPDH antibodies. **C.** Densitometry quantification of MYB intensity using imageJ. Each sample has has been internally normalised to GAPDH and then normalised to the respective control.

4.3.1.2 MYB shRNAs had limited KD efficiency in hESC

While Myb protein can be detected in mESCs (Jieping et al., 2007) the expression level of MYB in hESC/hiPSCs is not well documented. Therefore, I initially did a small time-course study of MYB expression levels during hiPSC differentiation. For this I used the OX1-19 hiPSC line and collected samples at three different time-points. A sample of undifferentiated feeder-free hiPSCs, a sample of whole EBs after 7 days of differentiation and a sample of iPS-Mo/Mϕ. MYB mRNA level was highest in undifferentiated hiPSCs, five-times lower in whole EBs and close to background levels in iPS-Mo/Mϕ (figure 4.7A). As the mRNA level was highest in undifferentiated hiPSCs I decided to quantify the MYB KD directly in HUES-2 hESCs rather than EBs.

The MYB mRNA KD was stronger in the hESC line HUES-2 than in Jurkat or CCRF-CEM cells, 70% and 62% for HUES-2$^{\text{shMYB-27}}$ and HUES-2$^{\text{shMYB-21}}$ respectively (figure 4.7B). This might be due to the overall expression level of MYB being substantially lower (196-fold for Jurkat and 351-fold for CCRF-CEM) in HUES-2 than in Jurkat or CCRF-CEM cells as indicated by the ΔCt difference between MYB and actin when comparing HUES-2 and Jurkat/CCRF-CEM cells (figure 4.7C). In contrast to mRNA which was present at a detectable level by RT-qPCR, the protein level of MYB could not be confirmed satisfactorily. Initial western blots using the same conditions as for Jurkat and CCRF-CEM cells had very low apparent MYB signal while a strong GAPDH control signal was detected. After optimisation of the protocol, increasing antibody concentration several fold and increasing staining time, several bands could be detected by western blot, including one at 75 kDa, the predicted size of MYB (figure 4.7D). Visual inspection and quantification of the blot by densitometry showed no major KD of the 75 kDa band (figure 4.7D). This failure could either be due to inefficient KD of MYB by the shRNA or due to the band being a non-specific band detected after increase of antibody and staining time. As MYB protein might not be expressed at all at the stem cell level or only at a very low level it is difficult to draw any conclusions on the specificity of the band without a KO line as a negative control.

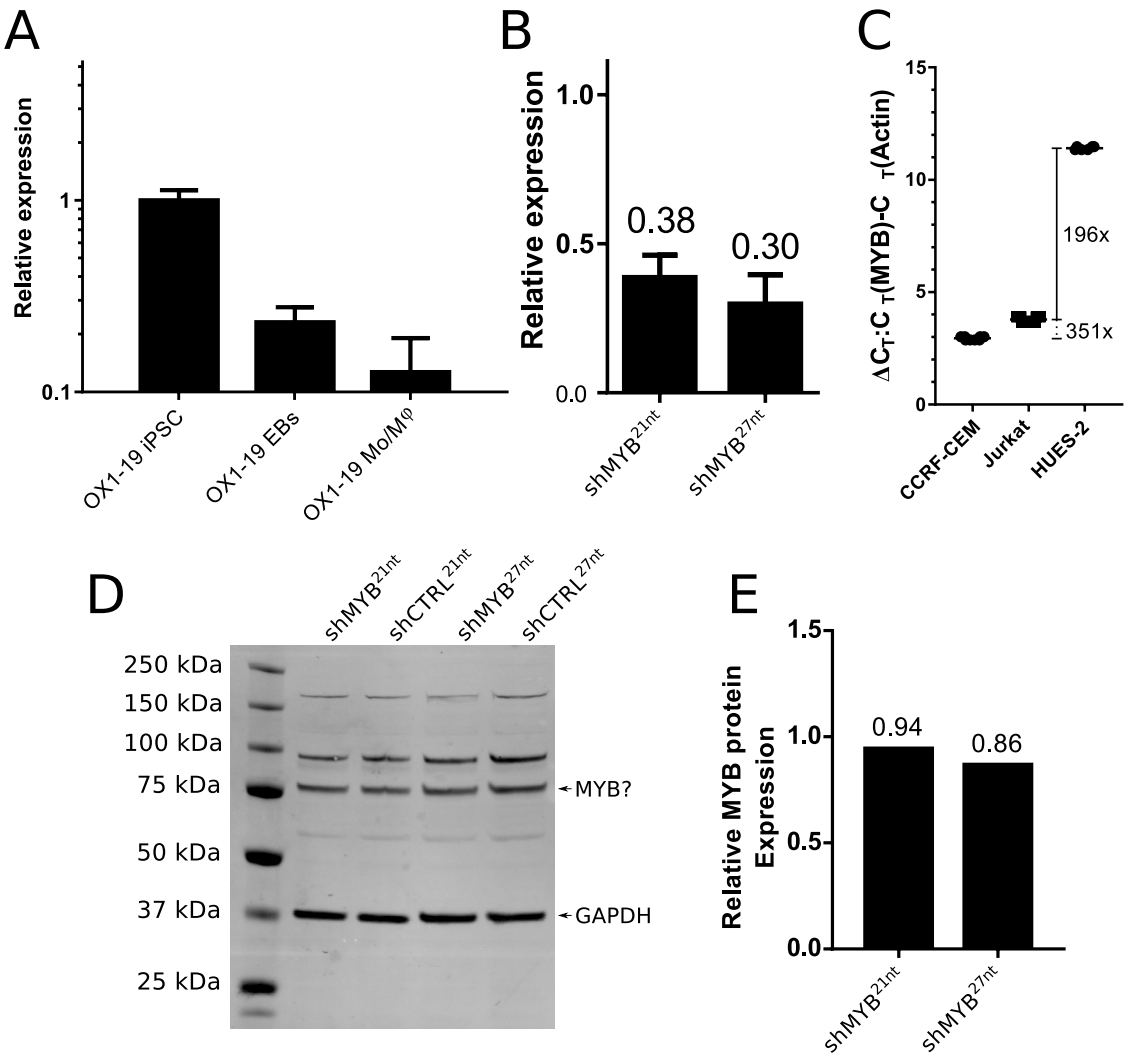

Figure 4.7: MYB shRNAs had limited KD efficiency in hESC. A. Relative expression of MYB mRNA in OX1-19 hiPSCs compared to OX1-19 day 7 EBs and OX1-19 iPS-Mo/Mϕ. Each sample has been run in technical triplicate and internally normalised to 18S mRNA. **B.** Relative expression of MYB mRNA between HUES-2$^{\text{CTRL-21}}$, HUES-2$^{\text{CTRL-27}}$ and HUES-2$^{\text{shMYB-21}}$ and HUES-2$^{\text{shMYB-27}}$. Each sample has been run in technical triplicate and internally normalised to actin mRNA. **C.** ΔCt value of MYB mRNA compared to actin in Jurkat, CCRF-CEM and HUES-2 hESCs. **D.** Western blot of HUES-2 hESCs stably expressing either shMYB$^{21\text{nt}}$, shMYB$^{27\text{nt}}$, shCTRL$^{21\text{nt}}$ or shCTRL$^{27\text{nt}}$ and stained for MYB and GAPDH. GAPDH band is strongly detected at 37 kDa. Two additional bands can be detected at 75 kDa and 90 kDa after staining for MYB. **E.** Densitometry quantification of the relative quantity of MYB normalised to GAPDH. Quantification have been done using ImageJ.

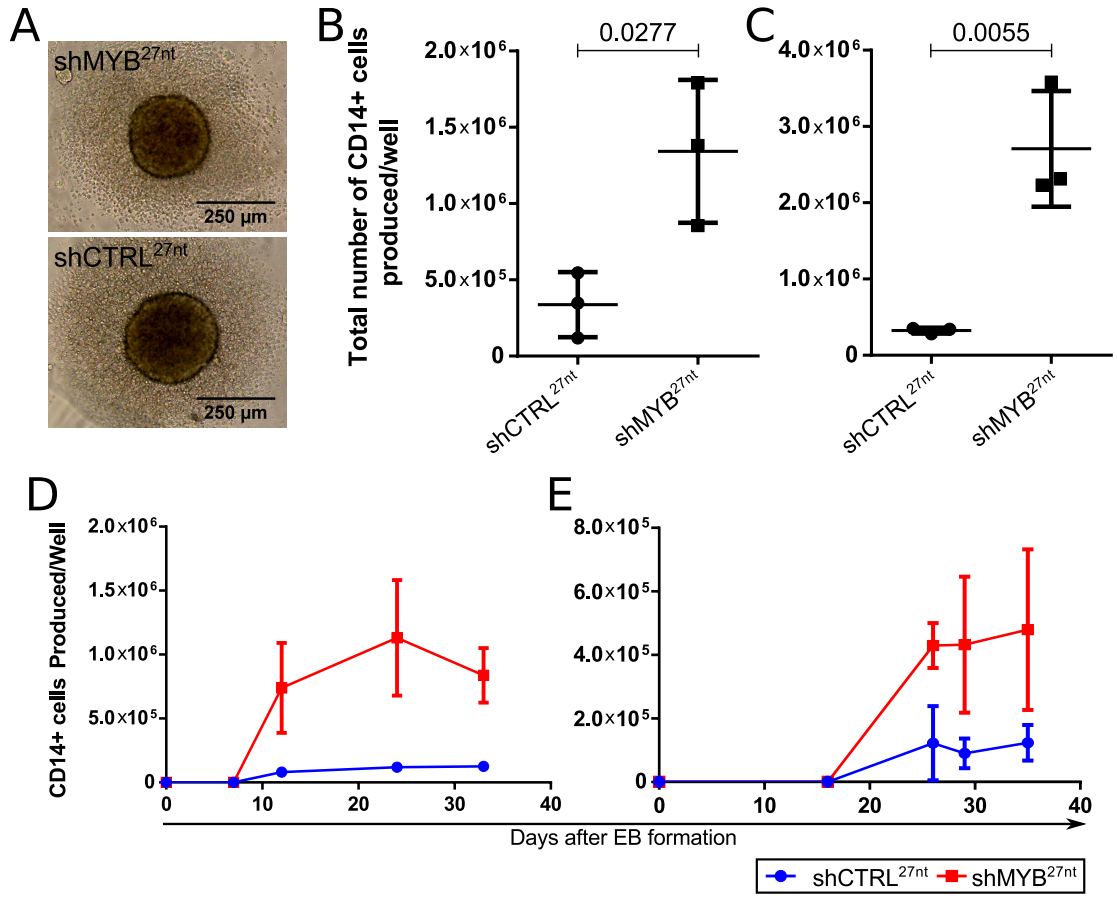

Figure 4.8: HUES-2$^{\text{shMYB-27}}$ were capable of hES-Mo/Mϕ differentiation while shCTRL^{27nt} had defective differentiation. A. Representative image of HUES-2$^{\text{shMYB-27}}$ and HUES-2$^{\text{CTRL-27}}$ EBs one day after formation. **B and C.** Total number of CD14+ hES-Mo/Mϕ generated per well of a 6 well containing 8 EBs (3 wells per replicate), over a period of one month. **C.** Non-cumulative representation of the hES-Mo/Mϕ production over time from experiments B and C.

4.3.1.3 Effect of MYB KD using shRNAs on iPS-Mo/Mϕ differentiation

Although overall the KD results were unconvincing I observed a consistent reduction of MYB mRNA in all three cell lines tested, highest in HUES-2 cells using the published shMYB^{27nt} (70% KD of mRNA levels in HUES-2) and consistently stronger than the shortened shMYB^{21nt} version I designed. I therefore decided to get some preliminary results to asses the impact of shMYB^{27nt} on hES-Mo/Mϕ differentiation from hESCs. shMYB^{27nt} and shCTRL^{27nt} transduced HUES-2 hESC had normal undifferentiated morphology and were both capable of forming healthy EBs of similar

size under puromycin selection (Figure 4.8A). Although both HUES-2$^{\text{shMYB-27}}$ and HUES-2$^{\text{CTRL-27}}$ were capable of EB formation, HUES-2$^{\text{CTRL-27}}$ produced significantly lower numbers of hES-Mo/Mϕ over a period of one month compared to HUES-2$^{\text{shMYB-27}}$ as seen in figure 4.8B and C. This reduction in production was not due to a late onset of production as HUES-2$^{\text{CTRL-27}}$ started producing at the same time as HUES-2$^{\text{shMYB-27}}$ and continuously produced hES-Mo/Mϕ but at a much lower level, as seen in figure 4.8D and E. The number of hES-Mo/Mϕs produced by HUES-2$^{\text{shMYB-27}}$ was in the expected range of hES-Mo/Mϕ production observed using this protocol, while HUES-2$^{\text{CTRL-27}}$ produced significantly fewer iPS-Mo/Mϕ than expected. Since HUES-2$^{\text{CTRL-27}}$ were unable to produce hES-Mo/Mϕ properly it is likely that shCTRL$^{\text{27nt}}$ is having a deleterious effect on hESC differentiation which makes it is very difficult to asses the impact of shMYB$^{\text{27nt}}$ on hES-Mo/Mϕ differentiation. In contrast to shCTRL$^{\text{27nt}}$, HUES-2$^{\text{shMYB-27}}$ produced quantities of hES-Mo/Mϕ in the normal range (van Wilgenburg et al., 2013) which leads to the conclusion that either shMYB$^{\text{27nt}}$ had a negligible effect on MYB levels and therefore did not significantly impact differentiation, or that hES-Mo/Mϕ do not require MYB and hence were unaffected by the KD of MYB.

4.3.2 Optimizing the CRISPR-Cas9 protocol to generate hiPSC KO

Most murine results regarding MYB requirements have been generated using complete Myb KO rather than KD. With the advent of the CRISPR/Cas9 technology and in light of the inconclusive shRNA results, a KO approach seemed more appropriate for answering my experimental question. I therefore set out to generate a complete KO of MYB in hiPSCs using CRISPR/Cas9 given its recent development the KO protocol required optimization and as this was an important part of achieving the end goal of my project I will, in this section, cover the different improvements and pitfalls of gene KO in hiPSCs.

At the time I started the KO of MYB in hiPSCs the paper describing double nicking CRISPR-Cas9 KO strategy (Ran et al., 2013) had just been published

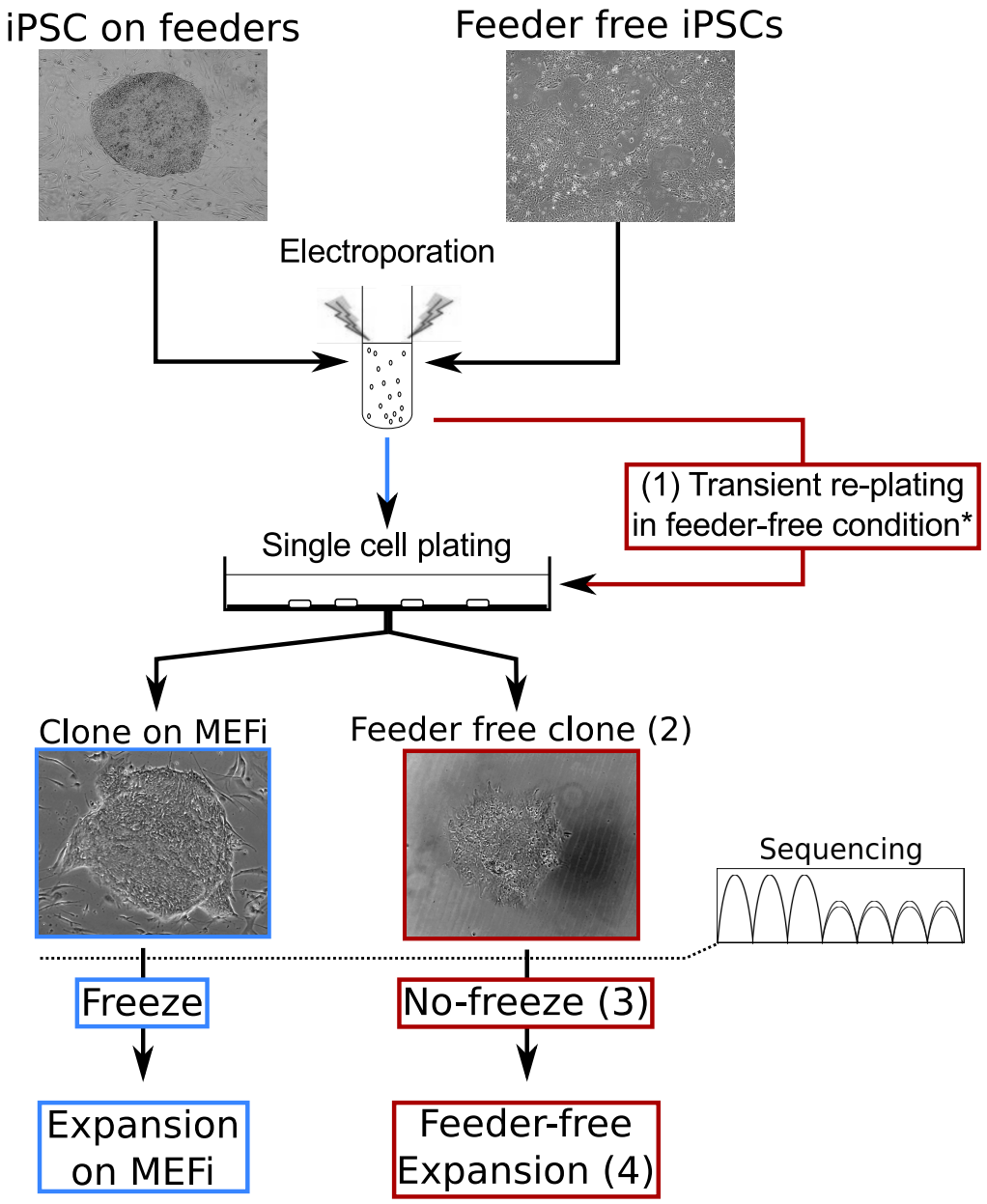

Figure 4.9: Schematic representation of the optimization of the CRISPR KO protocol in hiPSCs and hESCs. Original protocol is labelled in blue while optimised protocol is labelled red. Four changes had a significant impact on the protocol efficiency: (1) Transiant re-plating in feeder-free condition of the transfected hiPSCs after electroporation. (*) When we switched to the X462 puromycin selectable plasmid, this transient re-plating allowed for puromycin selection. (2) picking single cell colonies directly into feeder-free condition, (3) eliminating the freezing step by increasing screening and sequencing speed and (4) expansion in feeder-free condition.

and our experience in the lab regarding this approach was limited. Dr. R Flynn and Dr. M.D. Moore had setup a base protocol for the use of double-nicking

CRISPR KO in hiPSCs. I started using the initial protocol and participated in improving it to its current version (as described in 4.2.2). Over the course of my DPhil I have attempted several KOs which lead to several key improvements to the protocol which are summarised in figure 4.9.

My first two KO attempts resulted in low viability of the hiPSCs after electroporation of the cells 4.9 (1*), followed by high differentiation of the hiPSCs after single cell plating (table 4.2). After single cell plating and clone picking all hiPSC clones had differentiated or died. This was likely due to the very high stress induced by electroporation followed immediately by single cell plating, which is a strong cell death driving factor in hiPSCs (Watanabe et al., 2007). To improve survival we decided to add an additional step to the protocol and re-plate the cells at high density in feeder-free conditions for 2 to 3 days, as shown in figure 4.9 (1). This allowed cells to recover better from the stress induced by electroporation and resulted in less differentiation.

My third KO attempt resulted in limited differentiation after single cell plating, which allowed me to pick 96 clones onto MEF feeder cells. Of 96 picked clones over half differentiated after picking and the 40 undifferentiated clones were analysed using HRM. Only a single clone showed a shift in the melt curve and the sequencing result showed it was a clone possessing a single in-frame deletion . This very low frequency of targeted clones can be explained by the lack of selection for gRNA-CRISPR/Cas9 transfected cells. These results coincided with the generating of the new pX462 vector by the Feng Zhang lab (Cong et al., 2013), which contains a puromycin resistance gene allowing for transient selection of transfected clones.

For my fourth attempt I cloned my gRNAs into pX462 and included an additional 2 day puromycin selection step 24h after electroporation of the cells 4.9 (1*). Puromycin selection at 0.4 μg/mL for 2 days was enough to obtain 100% death of non-transfected control cells. hiPSCs were then plated onto MEFs at low density for single cell clone expansion as previously. This resulted in a high number of undifferentiated colonies, of which I picked 96 onto MEF feeders. As previously observed, about 50% of the 96 clones differentiated after picking. The 50 remaining clones were

passaged into two plates, one which was frozen and one which was analysed using HRM. This time, out of the 50 undifferentiated clones 18 showed a significant HRM shift, of which several were single allele out-of-frame deletions and one was shown to be a double-out-of-frame KO by sequencing. After thawing the targeted clone onto feeders they were strongly differentiated and in an unrecoverable state.

For all subsequent KO attempts I made two additional changes which allowed me to get low differentiation and full recovery of all hiPSC clones after picking and analysis. The first change I made was to pick the hiPSC colonies directly into feeder-free conditions (Figure 4.9 (3)). This first step eliminated almost all differentiation after clone picking I had observed previously. In addition to the change in picking method I optimised the clone analysis step and brought the time needed for complete analysis of the clones down to four days, which allowed me to avoid the 96 well freezing step (Figure 4.9 (4)) which had caused the loss of my previous clones. In addition to these changes, I tested several hESC and hiPSC lines which showed variable recovery after transfection and single cell plating. AH016-03 displayed the least differentiation and the best survival rate among the iPSC lines I tested. These changes altogether resulted in the final protocol I used for all subsequent gene KOs.

Table 4.2: Key points changed over the course of the CRISPR/Cas9 KO protocol optimization.

Experiment	17.01.2014	19.02.2014	10.04.2014	13.05.2014	03.10.204	03.02.2015	03.02.2015	03.02.2015	29.04.2015
hiPSC line	OX1-19 on MEFs	OX1-43 mTeSR	OX1-43 on MEFs	OX1-19 mTeSR	AH016-3 mTeSR	AH016-3 mTeSR	AH016-3 mTeSR	AH016-3 mTeSR	AH016-3 MYB-/+
gRNA	MYB Ex9	MYB Ex9	MYB Ex9	MYB Ex9	MYB Ex9	MYB Ex6	RUNX1	SPI1	MYB Ex6
Plasmid	pX335	pX335	pX335	pX462	pX462	pX462	pX462	pX462	pX462
Clones picked	N/A	52	96	96	140	160	160	160	48
Picked onto:	N/A	MEF	MEF	MEF	Matrigel	Matrigel	Matrigel	Matrigel	Matrigel
Recovered clones	N/A	0	40	∼50	∼130	160	160	160	48
Freezing clones?	N/A	N/A	Yes	Yes	No	No	No	No	No
HRM Hits	N/A	N/A	1	18	29	17/160	4/96	10/96	25
KO clones	N/A	N/A	0	1	2	0	1	1	5/10

4.3.3 Exon 9 MYB KO

4.3.3.1 Structure of MYB and gRNA design

4.3.3.1.1 Genomic structure of MYB

MYB is a complex gene which spans 41 kb, has 15 exons of which 6 can be alternatively spliced as well as two alternative start sites (figure 4.10). Exon 4, 5 and 6 which code for the highly conserved DNA binding domain are present in all isoforms of MYB while most of the downstream exons, which are involved with the target gene specificity of MYB (Lei et al., 2004; Quintana et al., 2011), can be alternatively spliced. Exon 7, 8 and 9 possess splice variants which cause the addition of the alternative exons 9A or 9B to the gene (O'Rourke and Ness, 2008). In addition exon 9 possesses a cryptic splice site resulting in a shorter form of the exon named 9S (O'Rourke and Ness, 2008). Exon 6, 9 and 14 were the only exons where all parameters for in silico design where present (as described in 4.2.2) and I decided to initially target exon 9 for KO.

4.3.3.1.2 Generating MYB Exon 9 KO hiPSCs

After optimization of the protocol I first generated two exon 9 KO clones from AH016-03 hiPSC line (table 4.2) one clone being a homozygous double out-of-frame deletion (clone E12) and one being a heterozygous double out-of-frame deletion (Clone F5). The AH016-03 iPSC line was chosen as it had high survival and low differentiation rate after transfection and single cell plating. Melt curves of the two clones compared to WT can be seen in figure 4.10B and the sequences can be seen figure 4.10C. I will refer to these two clones as hiPSC AH016-03 $MYB^{\Delta Ex9}$ E12 and F5. In addition to the two KO clones I selected two WT control clones, H7 and A10, which had undergone CRISPR/Cas9 transfection, selection and single cell cloning but had not been mutated. All expanded clones displayed undifferentiated stem cell like morphology (Figure 4.11B) and expressed the pluripotency markers Tra-1-60 and Nanog (Figure 4.11A).

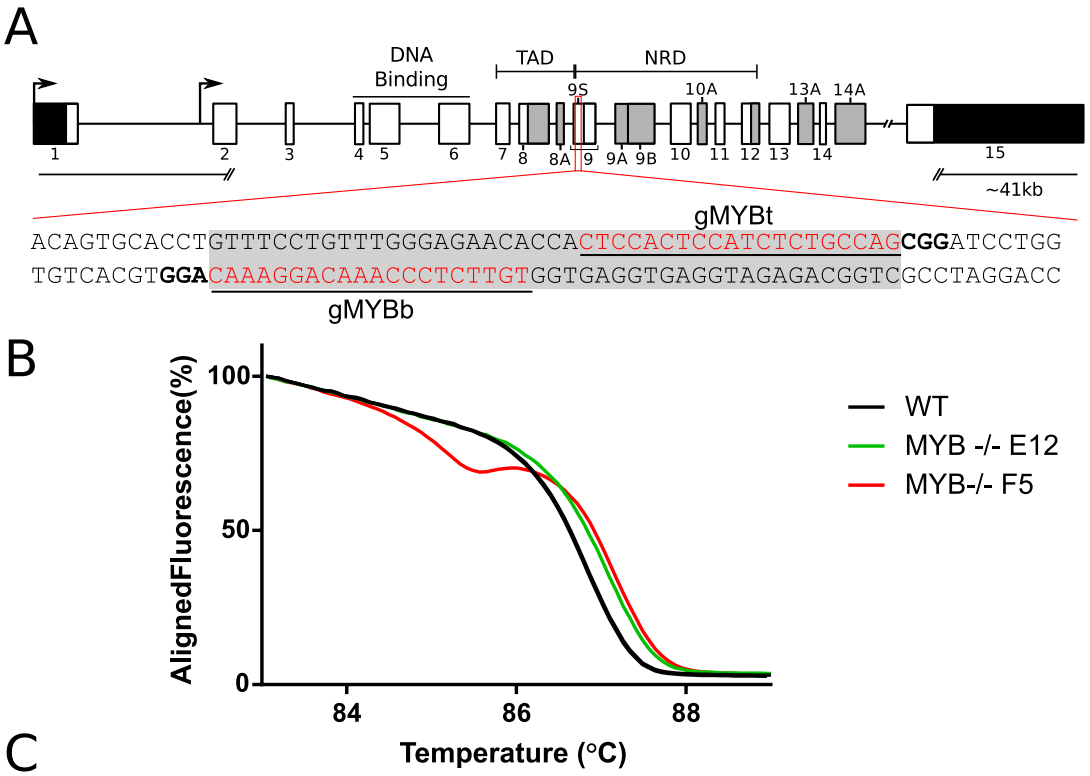

Figure 4.10: Genomic structure of MYB and CRISPR/Cas9 targeting of exon 9. **A.** Human MYB genomic structure showing conserved exons in white, alternatively spliced exons in grey and non-coding region in black. Functional domains are highlighted, showing the highly conserved DNA binding domain of MYB and the variable transactivation domain (TAD) and negative regulatory domain (NRD) of MYB. A sequence view of the two gRNA target sites is shown in red underneath with the PAM site in bold. **B.** HRM analysis of the two double KO clones E12 and F5, several WT control melt curves are represented in black and the melt curve of the targeted clones is represented in red and green. **C.** Sequence of the two MYB KO clones E12 and F5. Grey area represents the CRISPR/Cas9 target area.

The CRISPR/Cas9 based KO approach I used here relies on the generation of a frame shift by insertion or deletion formation resulting in premature termination codon (PTC) formation. Given the previous difficulty in observing KD of MYB by western blot I pursued qRT-PCR to observe the effect of the gene edit on MYB mRNA. Although introducing a frame shift does not itself result in an impact on

mRNA expression as is seen with RNAi KD, any mRNA containing stop codons prior to the final exon should be degraded by NMD (Brogna and Wen, 2009). Therefore, the effect of the MYB gene edit should be detectable by qRT-PCR. As can be seen in figure 4.11C the MYB mRNA expression was reduced by 56% and 45% in MYB$^{\Delta Ex9}$ E12 and F5 clones compared to WT. Although the reduction is not dramatic, the efficiency of NMD is cell type and donor dependent (Nguyen et al., 2014; Zetoune et al., 2008; Linde et al., 2007), and any residual mRNA should only express non-functional protein.

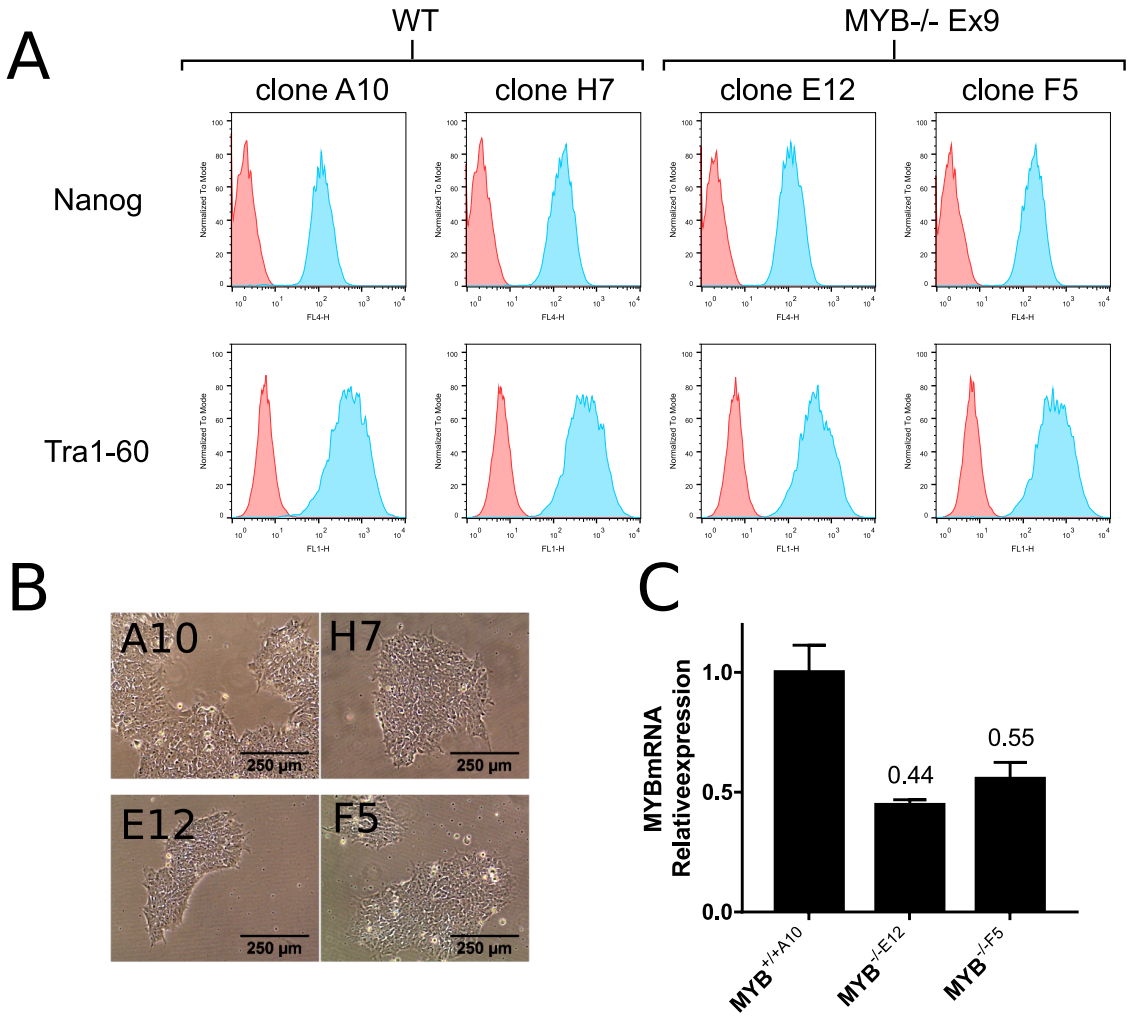

Figure 4.11: **A.** hiPSCs lines were stained for TRA-1-60 (1.5 μg/mL; α-TRA-1-60-AlexaFluor®488; Biolegend) and NANOG (0.3 μg/mL; α-NANOG-AlexaFluor®647; Cell Signalling Technologies), flow cytometry analysis are shown as histograms, antibody staining (blue) and isotype (red). **B.** Image of the four AHO16-03 clones. **C.** RT-qPCR of MYB mRNA relative expression normalised to AH016-03$^{+/+}$ clone A10.

4.3.3.2 MYB$^{\Delta Ex9}$ hiPSC lines have un-modified iPS-Mo/Mϕ differentiation capacity

To investigate the capacity of MYB$^{\Delta Ex9}$ hiPSCs clones to undergo myelopoiesis I differentiated the hiPSCs to iPS-Mo/Mϕ using our EB-based differentiation protocol. All four hiPSC lines were capable of forming healthy EBs, which were comparable in size across all four clones (Figure 4.12A and B). Over a period of 50 days WT and MYB$^{\Delta Ex9}$ hiPSCs both produced an average of 4-5x10^6 iPS-Mo/Mϕs per well containing 8 EBs, suggesting that exon 9 KO of MYB had no effect on iPS-Mo/Mϕ commitment (figure 4.12C). When plotted as a non-cumulative production of iPS-Mo/Mϕs over time both WT and MYB$^{\Delta Ex9}$ showed a very similar kinetic of production in both repeats (Figure 4.12D and E) so the results were not due to wild type cell contamination (data not shown). All iPS-Mo/Mϕ produced were sequenced and still harboured the same deletion in MYB exon 9 as seen in figure 4.10C (data not shown). The MYB$^{\Delta Ex9}$ iPS-Mo/Mϕs showed no major difference in morphology (Figure 4.12E) or CD14/CD16 expression levels when compared to MYB$^{+/+}$ control iPS-Mo/Mϕs (Figure 4.12F).

These results strongly imply that MYB is not required for iPS-Mo/Mϕ differentiation using this protocol, however there are number of issues with the exon 9 approach that made me reconsider the validity of these results. The limited reduction in mRNA for MYB should not have been an issue if the gene is targeted in a location which results in any protein that does get translated being non-functional. In hindsight, I realised that by targeting exon 9 rather than exon 6 the remaining protein could still be functional. Exon 4, 5 and 6 code for the highly conserved DNA binding domain while exon 7, 8 and the first part of exon 9 code for the transactivation domain (TAD) while most of exon 9 and downstream exons code for the negative regulatory domain (NRD) of MYB. Modifications of the NRD of MYB are known to be involved in cancer (Ramsay and Gonda, 2008). Therefore if NMD is not fully efficient there remains the possibility of some truncated highly active MYB protein being translated. Furthermore at the time I designed my gRNAs I was unaware of the rare possibility of exon 8, 9 or 10 skipping which is present

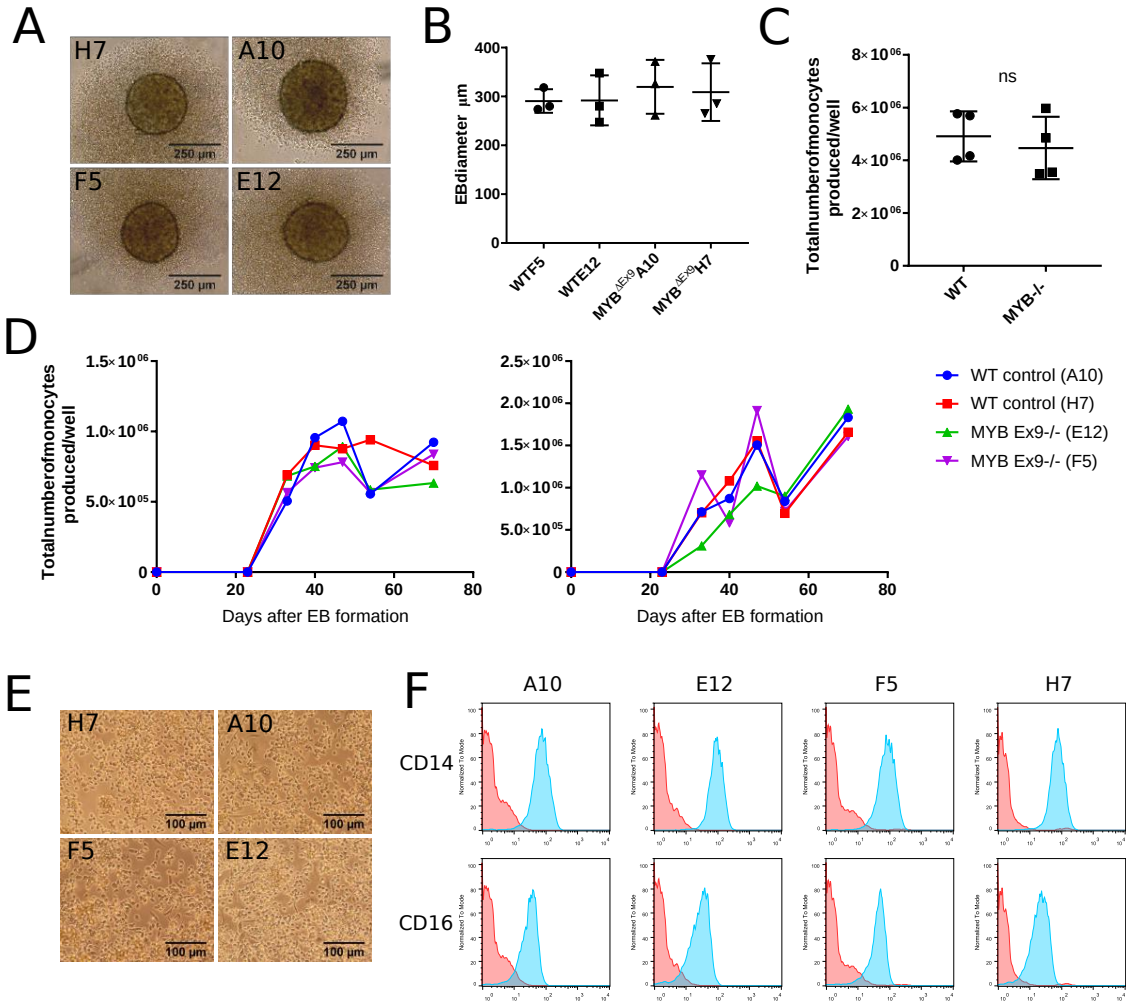

Figure 4.12: MYB$^{\Delta Ex9}$ hiPSC lines have un-modified iPS-Mo/Mϕ differentiation capacity. A. Representative image of 1 day old EBs formed by WT and MYB$^{\Delta Ex9}$ hiPSC clones. **B.** Quantification of the EB size, each data point represents the mean diameter in μm calculated from 16 individual EBs (M&M: 2.9). Experiment done in triplicate. **C.** Total number of iPS-Mo/Mϕs produced per well of a 6 well containing 8 EBs, 2 clones run in technical duplicate. **D.** Non-cumulative production of the same factories over the same period of time. Each data point reprents the pooled cell count from three wells. **E.** Brightfield image of the iPS-Mo/Mϕs produced by the four different clones. **F.** CD14 and CD16 staining of the iPS-Mo/Mϕs, isotype is represented in red and antibody staining in blue.

at very low frequency, 0.45%, 0.26% and 0.09% respectively, in CD34^{+} progenitor cells (O'Rourke and Ness, 2008). If exon 9 is skipped this would result in a normal ΔExon 9 isoform of MYB as the frameshift would be spliced out.

Although the AH016-03$^{\Delta Ex9}$ clones are most likely true KOs, taken together the lack of phenotype and the possibility of some residual highly active MYB in

the AH016-03$^{\Delta Ex9}$ lead to the necessity of a redesign of the experimental approach. In light of my results I therefore set out to generate new MYB KO hiPSCs, this time targeting exon 6. In addition I decided to generate two additional gene KO lines targeting RUNX1 and SPI1 which are involved in hematopoiesis, as positive controls. This should allow for much more precise analysis of the hematopoietic pathway used by hiPSCs.

4.3.4 Generation of the RUNX1, SPI1 and MYB KO hiPSC lines

4.3.4.1 Why chose these genes and this location?

My previous results using shRNA and CRISPR/Cas9 have been limited by the fact that I could not be 100% sure if I had a proper KD/KO and by the fact that I did not have enough controls. Furthermore, from work in the mouse it was becoming clear that MYB alone, although sufficient for knocking-out HSC definitive hematopoiesis, is not sufficient for entirely defining from which YS wave iPS-Mo/Mϕ are derived. I therefore chose to KO two additional genes, RUNX1 which is involved in the endothelial to hemogenic transition and SPI1 which is involved in all myeloid lineage differentiation. While SPI1 is required for all myeloid lineages RUNX1 is dispensable for primitive erythrocyte generation (although the erythrocytes show some abnormal phenotypes in the absence of RUNX1). If combined with the analysis of other lineages such as erythrocytes and granulocytes it should be possible to correctly and accurately define the ontogeny of the iPSC-Monocyte and iPSC-Mϕ generated by hiPSCs *in vitro*.

4.3.4.1.1 Targeting location

For all genes I designed gRNAs against exons which were present in all isoforms of the protein and upstream of the transactivation or DNA binding site of the protein. This is particularly important as all three genes are only upregulated in a subset of cells during differentiation making the quantification of the KO complicated at the stem cell level, as shown previously with MYB.

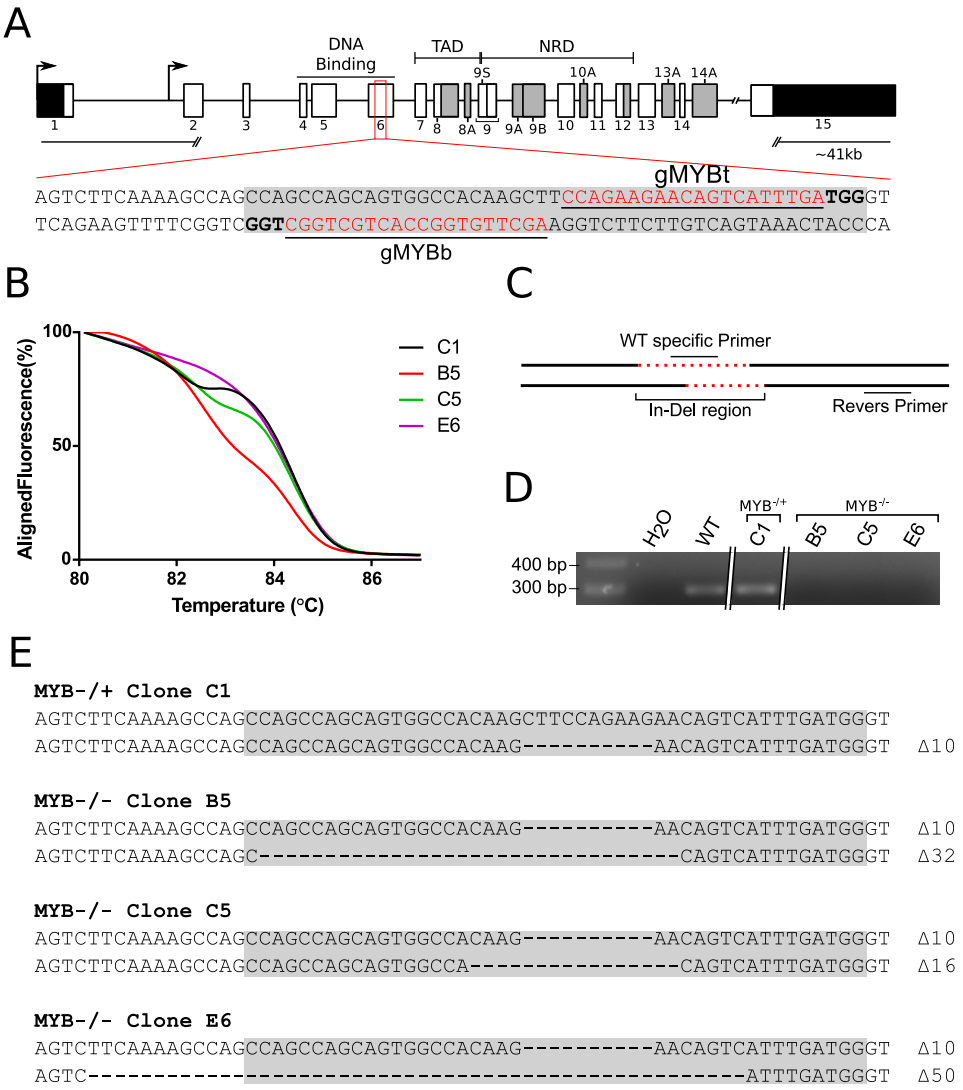

Figure 4.13: Genomic structure of MYB and CRISPR/Cas9 targeting of exon 6. A. Exon structure, splice variants, major functional domains and CRISPR-Cas9 target site of the MYB gene. TAD = Trans Activation Domain, NRD = Negative Regulatory Domain. Exons are represented by boxes, black regions represent none coding regions and white represent coding regions and grey regions can be alternatively spliced. An enhanced view of the target sequence is shown, with the exon 6 CRISPR-Cas9 targeting site in red and PAM sites in bold. **B.** HRM curve showing the aligned melt curve of the MYB$^{\Delta Ex6}$ clones B5, C5 and E6 compared to the single allele KO clone C1. **C.** Schematic representation of WT specific primer design, forward primers were designed to span the deletion and/or insertion present in the KO clones hindering binding of the primers and amplification of KO sequence but allowing the amplifying WT sequence. **D.** PCR of MYB$^{\Delta Ex6}$ clones B5, C5 and E6 compared to WT using a WT specific primer unable to amplify the KO sequence. **E.** Sequence of the B5, C5 and E6 double out-of frame MYB$^{\Delta Ex6}$ clones, and the single C1 MYB$^{-/+\ Ex6}$ clone. Grey boxes represents the CRISPR-Cas9 target region.

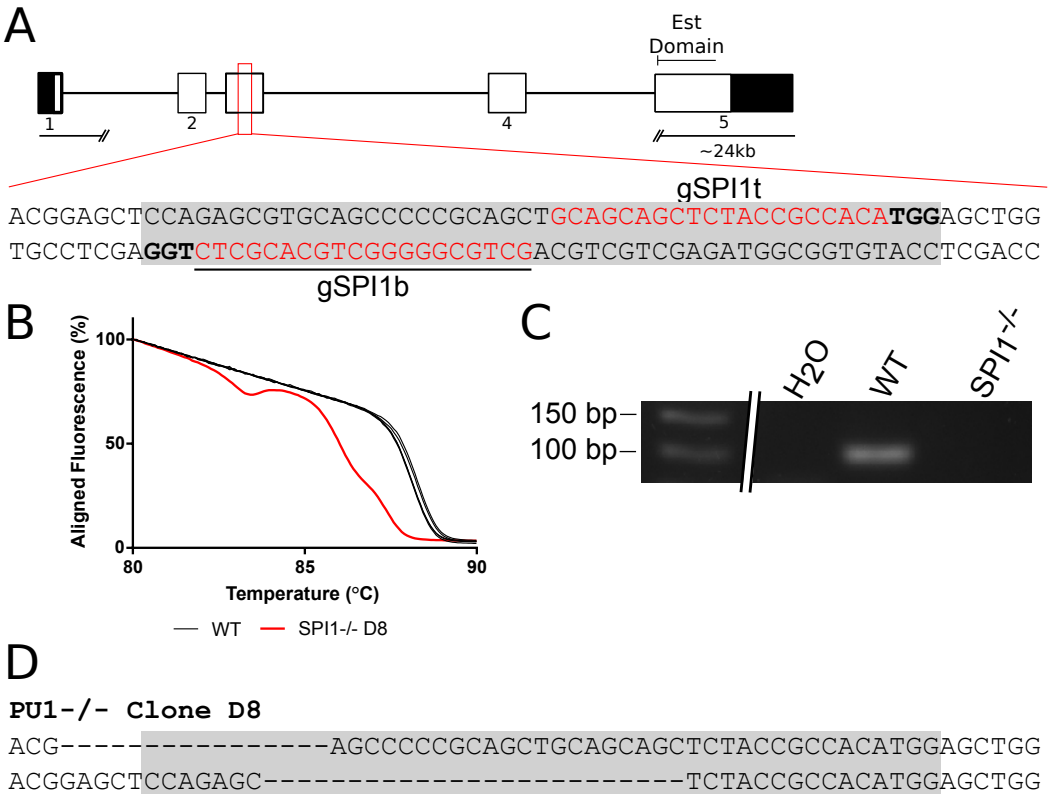

Figure 4.14: Genomic structure of SPI1 and CRISPR/Cas9 targeting. A. Exon structure, splice variants, major functional domains and CRISPR-Cas9 target site of the SPI1 gene. Exons are represented by boxes, black regions represent none coding regions and white represent coding regions. An enhanced view of the target sequence is shown, with the CRISPR-Cas9 targeting site in red and PAM sites in bold. **B.** HRM curve showing the aligned melt curve of the SPI1$^{\Delta Ex3}$ clone D8 compared to WT cells. **C.** PCR of SPI1$^{\Delta Ex3}$ clone D8 compared to WT using a WT specific primer unable to amplify the KO sequence. **D.** Sequence of the D8 double out-of frame SPI1 KO clone, grey box represents the CRISPR-Cas9 target region.

MYB was targeted in exon 6, which codes for part of the highly conserved DNA binding domain and is located before the transactivation and negative regulatory domain of the protein (figure 4.13). The SPI1 gene only possesses two isoforms produced by alternative splicing which differ by a single amino-acid in exon 2 and the functional domain is present in the last exon, therefore any disruption before the last exon should result in non-sense mediated decay and the theoretical truncated protein encoded by residual mRNA should be non-functional (figure 4.14). The RUNX1 locus on the other hand has a very complex exon and splicing structure, spanning 260 kb and encoding for 3 major isoforms, RUNX1a, RUNX1b and RUNX1c. For RUNX1

I targeted the highly conserved runt domain before the transactivation domain in exon 5 which should result in KO of all three RUNX1 isoforms (figure 4.15).

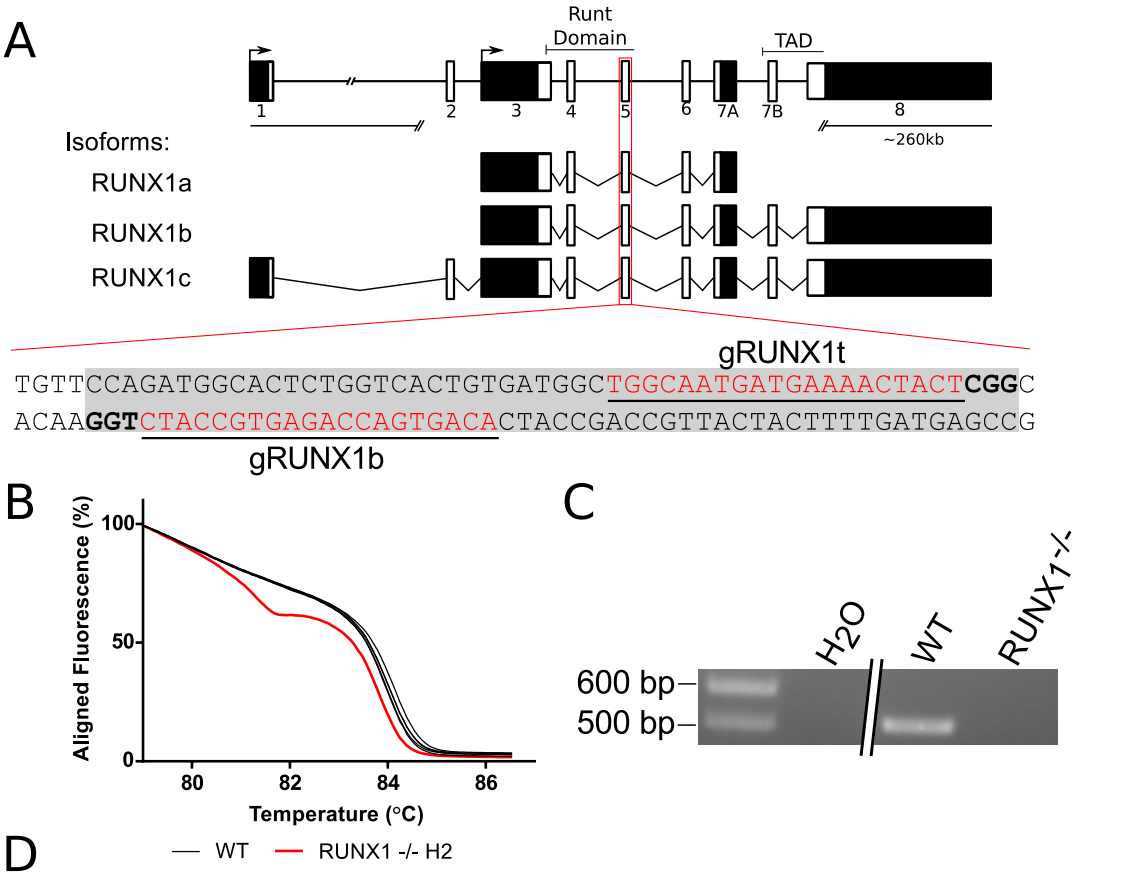

Figure 4.15: Genomic structure of RUNX1 and CRISPR/Cas9 targeting. A. Exon structure, splice variants, major functional domains and CRISPR-Cas9 target site of the RUNX1 gene. All three major isoforms of RUNX1 (RUNX1a, b and c) are shown underneath, isoform representation has been adapted from (Osato, 2014). Exons are represented by boxes, black regions represent none coding regions and white represent coding regions. The two arrows indicate the location of the two alternative start sites. An enhanced view of the target sequence is shown, with the CRISPR-Cas9 targeting site in red and PAM sites in bold. **B.** HRM curve showing the aligned melt curve of the RUNX1$^{\Delta Ex5}$ clone H2 compared to WT cells. **C.** PCR of RUNX1$^{\Delta Ex5}$ clone H2 compared to WT using a WT specific primer unable to amplify the KO sequence. The forward primer was designed with an extra mismatch to increase specificity as one allele of the RUNX1$^{\Delta Ex5}$ clone is a short 2 bp insertion. **D.** Sequence of the H2 double out-of frame RUNX1$^{\Delta Ex5}$ clone, grey box represents the CRISPR-Cas9 target region.

4.3.4.2 Different generated KO clones

I established KO hiPSC lines of MYB, RUNX1 and SPI1 in order to study their requirement in the *in vitro* differentiation of iPS-Mo/Mϕs and Mϕs from hiPSCs. For this purpose I used the same optimised dual gRNA-targeting strategy as described in section 4.3.2. The knowledge gained from my previous KO experiments allowed me to obtain highly viable clones, out of 160 picked clones per gene KO all 160 clones were maintained without differentiation and analysed by HRM and sequenced. Although stem cell differentiation was very low and the number of recovered clones was close to 100% the CRISPR efficiency was lower than the exon 9 dual gRNA CRISPR/Cas9 experiment. Out of the 160 clones I manages to get 1 double KO clone for SPI1 and RUNX1 but did not manage to obtain a double MYB KO (only single allele KO). This reduction in efficiency is most likely directly linked to the cutting efficiency of the specific gRNA/CRISPR/Cas9 pairs. I therefore chose to re-target one of the single allele deleted clone in which the CRISPR target site was only present on the WT allele, using the same methodology. This greatly increased specificity as only one allele was targetable and out of 48 clones picked, 30 had a shift in the melt curve, of which I sequenced 10 and obtained 5 double KO clones of which I used 3 for my downstream experiments. One single allele KO clone which was picked from the unmodified clones that went through two rounds of transfection was used as single allele KO control. The different KO clone HRM curves and sequences can be seen in figure 4.13 for MYB, figure 4.14 for SPI1 and figure 4.15 for RUNX1. After clone expansion, presence of WT cells in the single-cell clone KO hiPSC lines was excluded by PCR using WT specific primers, as shown in figure 4.13C and D for MYB, figure 4.14C for SPI1 and figure 4.15C for RUNX1.

4.3.4.3 Quality control of the hiPSCs

Single cell clone KO hiPSC lines showed normal undifferentiated morphology, expressed pluripotency markers Tra-1-60 and Nanog (Figure 4.16) and were analysed for genome integrity using SNP array (Figure 4.16 and 4.17). No major karyotypic abnormalities were detected and the different KO clones displayed the same SNP

profile. One minor amplification accounting for <10% of Chromosome 20, which was not present in the parent line but was present in all KO clones as well as in the WT control clone was detected. This amplification affects several genes which promote survival and pluripotency, such as, anti-apoptotic gene BCL2-like 1 (BCL2L1), the pluripotency-associated gene inhibitor of DNA binding 1 (ID1) and DNA methyltransferase 3B (DNMT3B). Chromosome 20 amplifications are commonly observed in hESC and hiPSC lines (14.5%) (Lund et al., 2012). This amplification should not affect the downstream results as none of the genes of interest are directly affected and the amplification is present on both the gene KO lines as well as the control line.

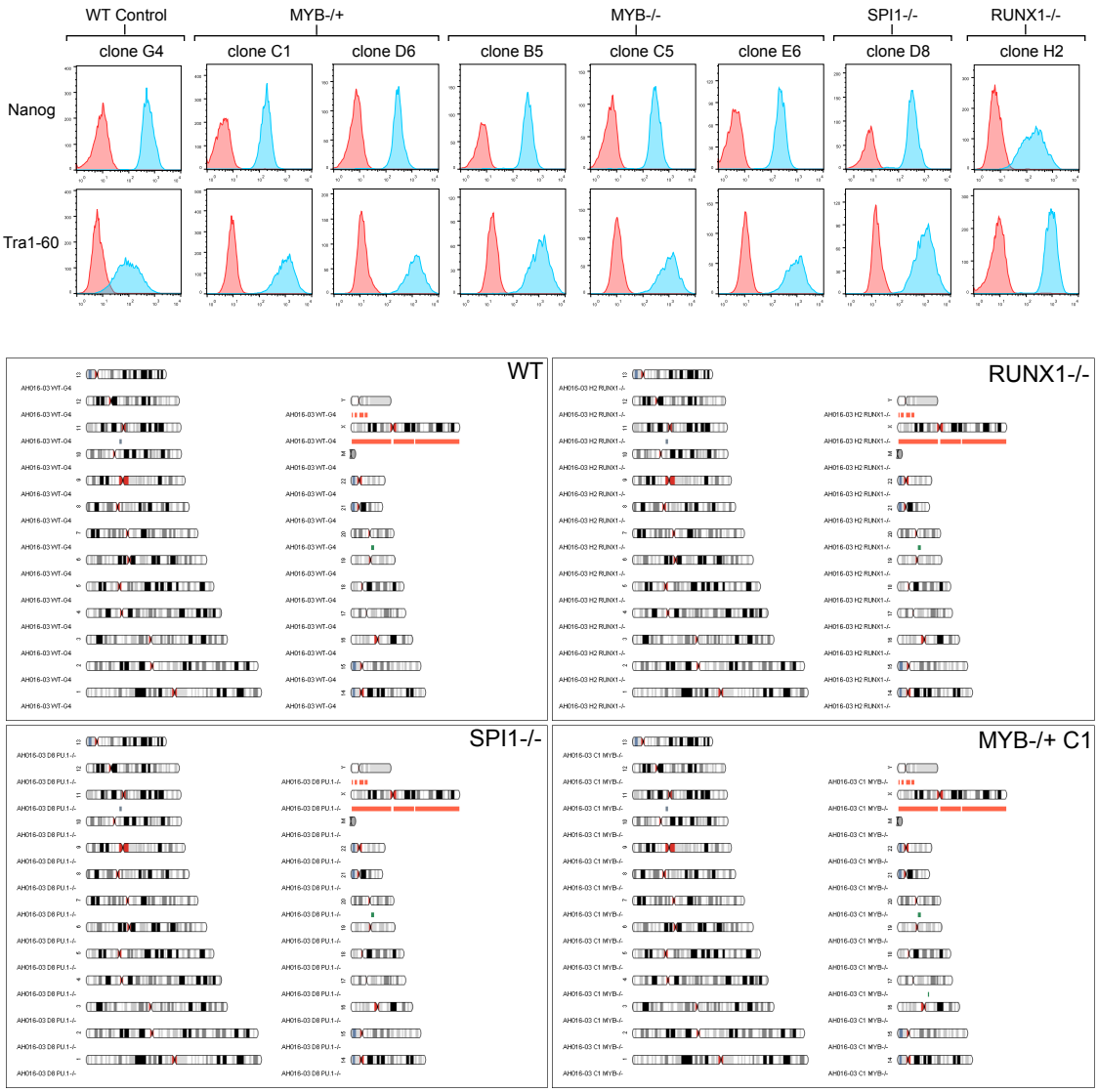

Figure 4.16: Gene-KO hiPSC lines maintained pluripotency and karyotype. **A.** hiPSCs lines were stained for TRA-1-60 (1.5 mg/mL; α-TRA-1-60-AlexaFluor®488; Biolegend) and NANOG (0.3 mg/mL; α-NANOG-AlexaFluor®647; Cell Signaling Technologies), flow cytometry analysis are shown as histograms, antibody staining (blue) and isotype (red). **B.** DNA extracted from the hiPSCs was karyotyped using a SNP array (Illumina OmniExpress24 chip covering 700,000 markers) and analysed using KaryoStudio (Illumina) to detect copy number variations across the genome. Red indicates a single copy of the SNPs (demonstrated by the single X copy in this male patient's DNA); gray indicates loss of heterozygosity; and green indicates duplications of a stretch of DNA (one amplification on ch20 was present on all hiPSC clones).

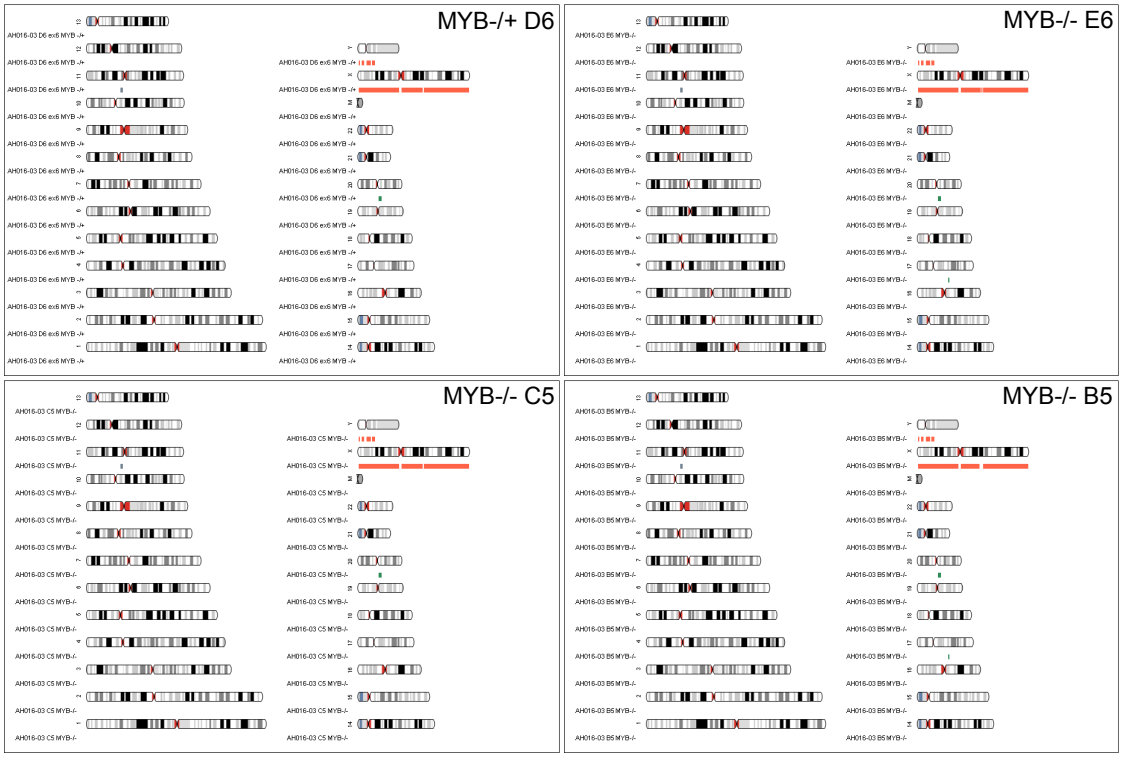

Figure 4.17: Gene-KO hiPSC lines maintained pluripotency and karyotype. (continued) DNA extracted from the hiPSCs was karyotyped using a SNP array (Illumina OmniExpress24 chip covering 700,000 markers) and analysed using KaryoStudio (Illumina) to detect copy number variations across the genome. Red indicates a single copy of the SNPs (demonstrated by the single X copy in this male patient's DNA); gray indicates loss of heterozygosity; and green indicates duplications of a stretch of DNA (one amplification on ch20 was present on all hiPSC clones).

4.3.4.4 iPS-Mo/Mϕ development is MYB independent but RUNX1 and SPI1 dependent

To investigate the capacity of $MYB^{\Delta Ex6}$, $MYB^{-/+\ Ex6}$, $SPI1^{\Delta Ex3}$ and $RUNX1^{\Delta Ex5}$ hiPSCs to undergo myelopoiesis I differentiated the hiPSCs to iPS-Mo/Mϕs using our EB differentiation protocol. Over a period of 30 days WT and $MYB^{-/+\ Ex6}$ hiPSCs produced an average of $3x10^6$ iPS-Mo/Mϕs per well containing 8 EBs, suggesting MYB-haploinsufficiency had no effect on iPS-Mo/Mϕ commitment (figure 4.18A). Interestingly $MYB^{\Delta Ex6}$ hiPSCs were capable of myeloid differentiation and produced two-fold more $CD14^+$ cells than WT and $MYB^{-/+\ Ex6}$ (figure 4.18A). This result confirms my previous results that, using this protocol, hiPSC-derived iPS-Mo/Mϕs can develop independently of the transcription factor MYB. Furthermore the increased production of iPS-Mo/Mϕs observed in $MYB^{\Delta Ex6}$ hiPSC suggest an increased proliferation or commitment of either the hematopoietic progenitors or the iPS-Mo/Mϕs. When plotted as a non-cumulative production of $CD14^+$ cells over time it is apparent that $MYB^{\Delta Ex6}$ hiPSCs produce significantly more iPS-Mo/Mϕs than the WT control or $MYB^{-/+\ Ex6}$ hiPSCs during the first weeks of production (figure 4.18B). In contrast, $SPI1^{\Delta Ex3}$ and $RUNX1^{\Delta Ex5}$ hiPSCs were unable to produce any $CD14^+$ iPS-Mo/Mϕs (figure 4.18A), although the EBs increased in size as expected and were comparable in their morphology when compared to WT or $MYB^{\Delta Ex6}$ EBs (figure 4.18C and D).

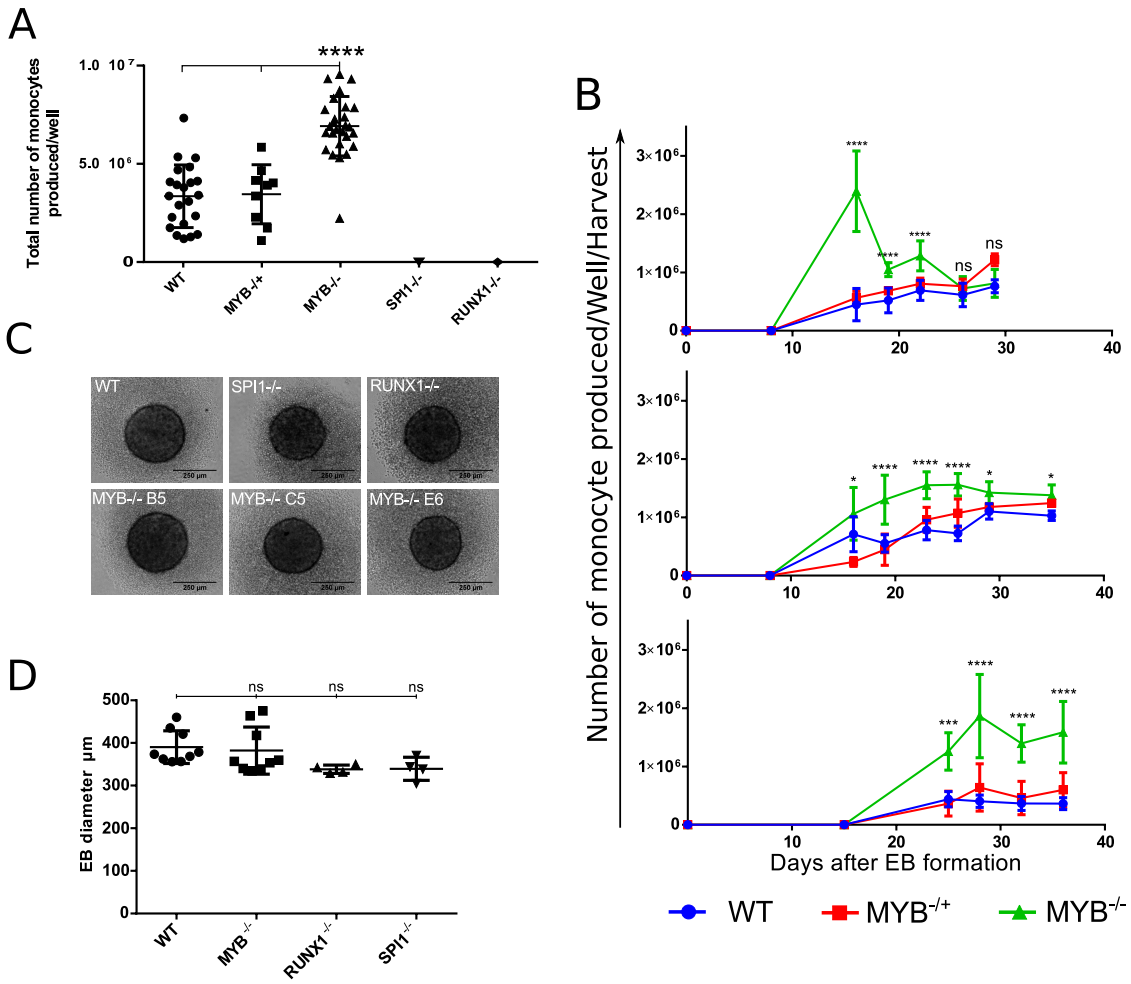

Figure 4.18: iPS-Mo/Mϕ production capacity of WT, MYB$^{-/+\ Ex6}$, MYB$^{\Delta Ex6}$, RUNX$^{\Delta Ex5}$ and SPI1$^{\Delta Ex3}$ hiPSCs. A. Total number of iPS-Mo/Mϕs produced by well (each well contained exactly 8 EBs) over a period of 30 days, 3 biological replicates, number of total wells: WT n=22 (from 3 independent clones), MYB$^{\Delta Ex6}$ n=27 (from 3 clones), MYB$^{-/+\ Ex6}$ n=9 (from 1 clone), SPI1$^{\Delta Ex3}$ n=9 (from 1 clone), and RUNX1$^{\Delta Ex5}$ n=9 (from 1 clone). Statistical comparison were performed using an unpaired t-test, ****=P<0.0001 **B.** Non-cumulative production of iPS-Mo/Mϕs per well over a period of 30 days. Each timepoint represents the mean number of iPS-Mo/Mϕs harvested per well of MYB$^{\Delta Ex6}$ (n=9), WT (n=6) and MYB$^{-/+\ Ex6}$ (n=3) hiPSCs. Statistical comparison were done using a 2 way-ANOVA, ns=non-significant, *=P<0.05, **=P<0.01, ***=P<0.001, ****=P<0.0001 **C.** Representative image of WT, MYB$^{\Delta Ex6}$, MYB$^{-/+\ Ex6}$, RUNX1$^{\Delta Ex5}$ and SPI1$^{\Delta Ex3}$ EBs after 1 days of differentiation. **D.** Mean diameter with standard deviation of WT, MYB$^{\Delta Ex6}$, RUNX1$^{\Delta Ex5}$ and SPI1$^{\Delta Ex3}$ EBs , each data point represents one biological replica (n=16). Diameter was calculated using ImageJ (M&M: 2.9) and statistical comparison were performed using a non-parametric one way ANOVA comparing the mean of each column with the mean of the WT control column.

4.3.4.5 MYB$^{\Delta Ex6}$ iPS-Mo/Mϕs display no apparent phenotypic or functional defects

As MYB is a major player in hematopoietic differentiation and hematopoietic cell function I checked to see if deletion of MYB affected the phenotype or function of the iPS-Mo/Mϕ generated. MYB$^{\Delta Ex6}$ and WT iPS-Mo/Mϕ showed no difference in morphology (eosin and methylene-blue staining), phenotype (classical mononuclear phagocyte markers CD45, CD11b, CD14 and CD16), reactive oxygen species (ROS) production, TNF-α release after LPS stimulation and phagocytosis (Zymozan uptake) (Figure 4.19 A, B, C, D, E and F). Interestingly, when compared to the mouse, the morphology of YS-Mϕs and fetal monocytes observed by Hoeffel et al. (2015), the non-adherent iPS-Mo/Mϕs on the day of harvest (4.19 A) resemble more to YS-Mϕs (which can be found in the blood during early development) than fetal monocytes.

4.3.4.6 MYB KO results in increased number of hematopoietic progenitors within the EB

YS Mϕs and fetal monocytes have a high-proliferative capacity compared to BM-derived monocytes (Van de laar et al., 2016), thus I set out to identify whether the increase in iPS-Mo/Mϕ from the MYB$^{\Delta Ex6}$ hiPSC lines was due to the proliferation of the iPS-Mo/Mϕ during the first week of production (a time-point at which we have observed the maximum rate of cell division - chapter 3). To detect the rate of iPS-Mo/Mϕ division, I pulsed the iPS-Mo/Mϕs with EdU for 2 hours (Figure 4.19G). No significant difference was observed in iPS-Mo/Mϕ undergoing S phase (CD14$^+$ EdU$^+$) between MYB$^{\Delta Ex6}$ and WT, suggesting that the increased iPS-Mo/Mϕ production is most likely due to an event upstream of the iPS-Mo/Mϕ differentiation stage.

To investigate whether MYB$^{\Delta Ex6}$ EBs generated more hematopoietic progenitors, I enzymatically dissociated EBs at various time points into single cells and stained for the expression of the pan-hematopoietic marker CD45 and the endothelial/hematopoietic marker CD34. Hemogenic and non-hemogenic endothelial cells are labelled CD34$^+$ CD45$^-$, hematopoietic progenitor cells are labeled CD34$^+$ CD45$^+$, while committed hematopoietic cells are labelled CD34$^-$ CD45$^+$ (figure 4.20A).

While the percentage of total $CD34^+$ cells was similar between WT and $MYB^{\Delta Ex6}$ on day 9 and 11, the percentage of $CD34^+$ $CD45^+$ cells was highest in $MYB^{\Delta Ex6}$ on day 11 (0.5% in WT compared to 5% in $MYB^{\Delta Ex6}$), which would suggest that $MYB^{\Delta Ex6}$ hiPSCs undergo hematopoietic commitment earlier than WT hiPSCs. Day 14 WT EBs show a major hematopoietic commitment with 27.2% $CD45^+$ $CD34^-$ but only 1.01% $CD34^+$ $CD45^+$ cells indicating that the hematopoietic progenitor pool is small within the EBs. $MYB^{\Delta Ex6}$ EBs on the other hand, display two distinct hematopoietic sub-populations at day 14, 4.47% $CD34^+$ $CD45^+$ and 8.49% $CD45^+$ $CD34^-$, indicating that a larger hematopoietic progenitor cell pool is maintained within the $MYB^{\Delta Ex6}$ EBs. The total number of cells per EB was similar between $MYB^{\Delta Ex6}$ and WT, as would be expected from previous observations (figure 4.18C).

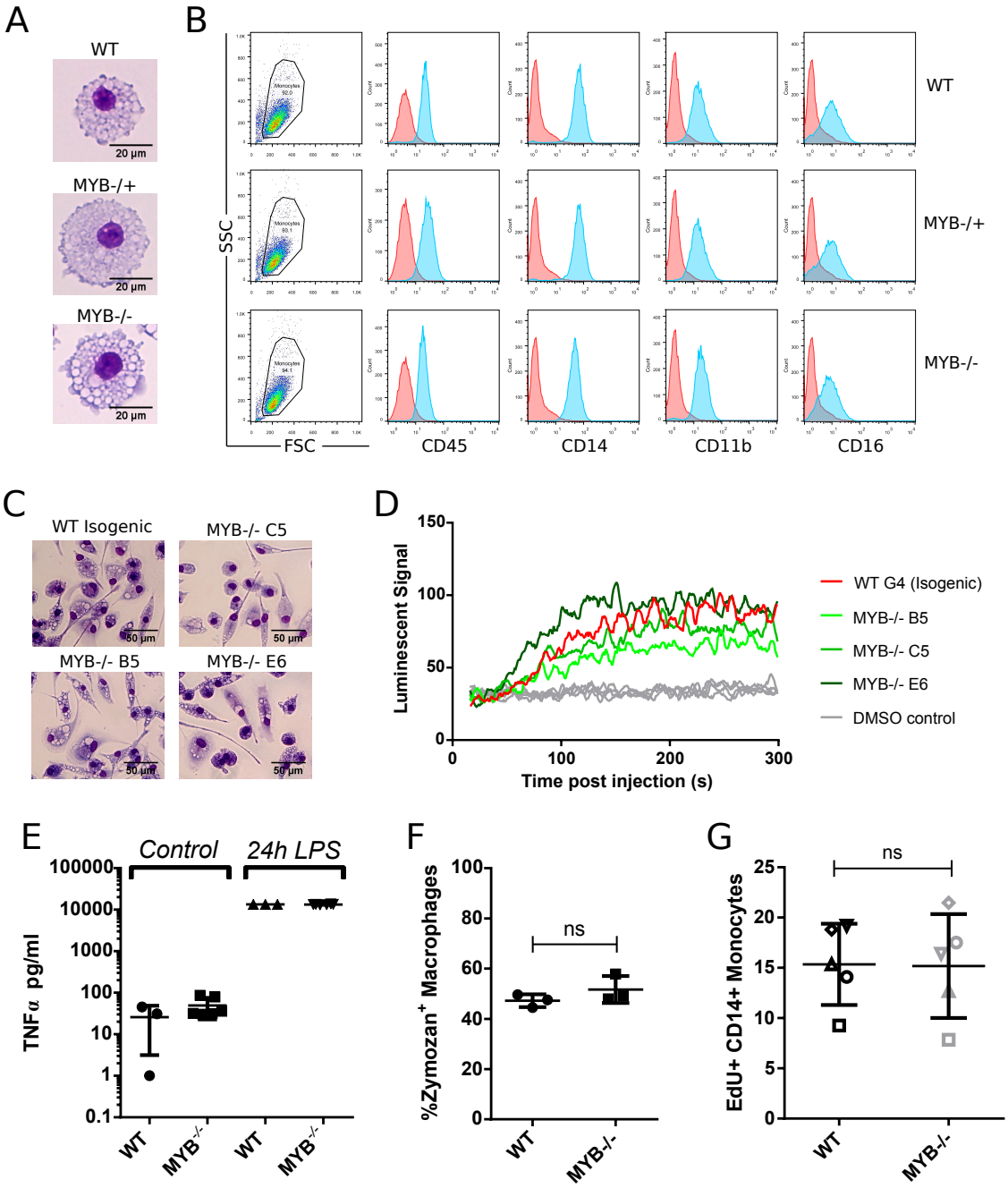

Figure 4.19: MYB$^{\Delta Ex6}$ iPS-Mo/Mϕs display no apparent phenotypic or functional differences compared to WT controls. A. Representative images of eosin and methylene-blue stain of cytospun WT, MYB$^{-/+\ Ex6}$ and MYB$^{\Delta Ex6}$ iPS-Mo/Mϕs on the day of harvest (M&M: 2.6). **B.** Flow cytometry staining of iPS-Mo/Mϕs for common myeloid cell surface makers, showing live cell gate on the left and histogram plots on the right, antibody staining (blue) and isotype (red). **C.** Representative images of eosin and methylene-blue stain of WT, MYB$^{-/+\ Ex6}$ and MYB$^{\Delta Ex6}$ Mϕs differentiated for 7 days in M-CSF (M&M: 2.6). **D.** iPS-Mo/Mϕs from WT and MYB$^{\Delta Ex6}$ hiPSCs were treated with luminol reagent in the presence or absence of PMA stimulation. Individual wells were monitored for light released at 1 sec intervals for 300 sec in triplicate using a PHERAstar FS (BMG Labtech). The mean of three wells were normalised to the average

of the 5 sec before luminol addition and are plotted with smoothing for clarity (average of four neighbouring data points). **E.** ELISA measuring the TNFα released by one week differentiated Mϕs after 24h LPS stimulation compared to untreated treated controls **F.** Phagocytosis assay measuring the fluorescent labelled zymozan uptake by one week differentiated WT and MYB$^{\Delta Ex6}$ Mϕs. Cells were analysed by flow cytometry and the percentage of AlexaFluor-488-Zymozan^{+} Mϕs was plotted **G.** First harvest iPS-Mo/Mϕs were pulsed with EdU and CD14^{+} EdU^{+} cells that had undergone DNA replication were detected by flow cytometry after Click-iT staining (M&M: 2.5). Five independent experiments are shown, where MYB$^{\Delta Ex6}$ represents the pooled results obtained for three different MYB$^{\Delta Ex6}$ hiPSC clones.

4.3.4.7 hiPSC-derived erythrocytes and granulocytes are dependent on MYB, RUNX1 and SPI1

To investigate the progenitor potential of MYB$^{\Delta Ex6}$, RUNX1$^{\Delta Ex5}$ and SPI1$^{\Delta Ex3}$ hiPSCs, EBs were differentiated for 14 days as for iPS-Mo/Mϕ differentiation, followed by enzymatic dissociation into single cells. Single cell suspensions were plated into MethoCult^{TM} H4434, which supports the growth of erythroid progenitors (CFU-E and BFU-E), granulocyte-Mϕ progenitors (CFU-GM, CFU-G and CFU-M) and multi-potential granulocyte, erythroid, Mϕ and megakaryocyte progenitors (CFU-GEMM). After 14 days of expansion, colonies were scored according to morphology. WT hiPSCs generate CFU-E, CFU-GM and CFU-M colonies, whereas MYB$^{\Delta Ex6}$ hiPSCs on the other hand generated only CFU-M colonies (figure 4.20B and C). RUNX1$^{\Delta Ex5}$ hiPSC were unable to generate any hematopoietic colonies, indicating the likely absence of primitive erythrocyte progenitors in day 14 EBs, as in the mouse primitive erythrocytes are detected in Runx1$^{-/-}$ embryos (Okada et al., 1998; Okuda et al., 1996; Wang et al., 1996). As expected, SPI1$^{\Delta Ex3}$ hiPSCs were also unable to generate any hematopoietic colonies, (data not shown).

4.4 Discussion

In this chapter I have used both shRNA KD and CRISPR/Cas9 KO approaches targeting key transcription factors in hiPSCs that are known to be involved in murine myeloid development. I used a feeder-free EB differentiation model to

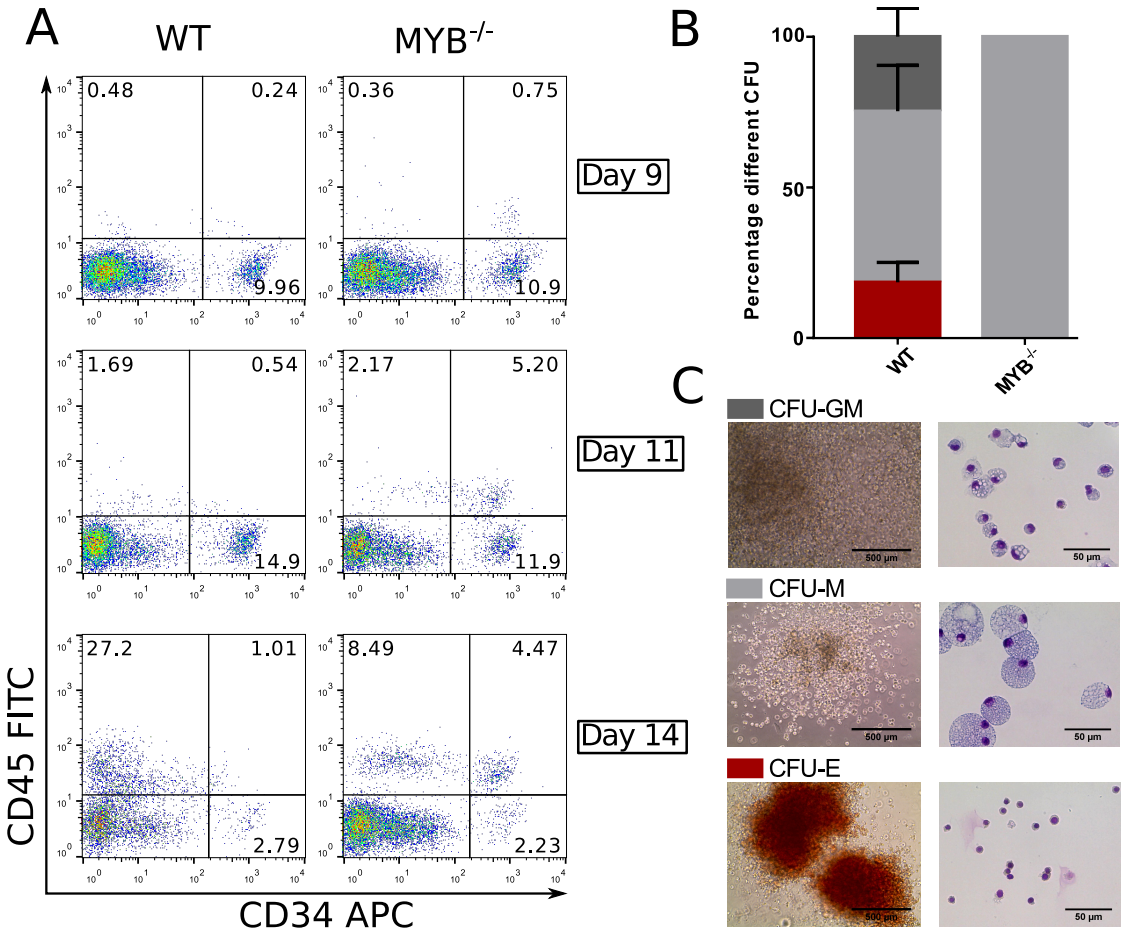

Figure 4.20: Study of the progenitor cells within the hiPSC-derived EBs. A. Day 9, 11 and 14 EBs of WT and MYB$^{\Delta Ex6}$ hiPSCs were enzymatically dissociated, stained for expression of CD34 and CD45, and analysed by flow cytometry. Hemogenic and non-hemogenic-endothelial cells are CD34^{+} CD45^{-}, hematopoietic progenitor cells are CD34^{+} CD45^{+} and differentiated hematopoietic cells are CD34^{-} CD45^{+}. **B.** Dissociated day 14 EBs were plated into H4434 MethoCult^{TM}, after 14 days colonies were scored. The percentage of each type of colony is displayed as mean with standard deviation (WT n=5, MYB$^{\Delta Ex6}$ n=3 for each KO clone). Presence of erythroid (CFU-E), granulocyte-Mϕ (CFU-GM) and Mϕ progenitors (CFU-M) can be detected in WT hiPSC differentiation whereas MYB$^{\Delta Ex6}$ hiPSCs display only CFU-M potential. **C.** Image of the different colony types. The images on the left show a bright-field image of representative CFU-E, CFU-M and CFU-GM WT colonies in methylcellulose media at day 14, while the images on the right show the cytospined and eosin and methylene-blue stained cells present within the three different types of colonies.

understand the developmental ontology and transcription factor requirement of *in vitro* generated iPS-Mo/Mϕ and thus map human iPSC myelopoiesis onto mouse hematopoietic development. My results show that, using this protocol, iPS-Mo/Mϕ are independent of the transcription factor MYB, which is required for HSC-

dependent hematopoiesis in the mouse (Schulz et al., 2012), while being dependent on the transcription factor RUNX1, which is required for EHT (Chen et al., 2009), as well as SPI1, which is required for myeloid differentiation and plays a major role in many monocyte and Mϕ functions (Zakrzewska et al., 2010; Anderson et al., 1998). The hematopoietic progenitors within the EBs are capable of Mϕ, granulocyte and erythrocyte potential, but in the absence of MYB only Mϕ colonies are detected by colony-forming assay in semi-solid media, suggesting that both CFU-E and CFU-GM are generated in a MYB-dependent fashion from EMPs. While at the moment I started this project, most reports excluded possibility of Myb-independent EMP hematopoiesis this vision changed, therefore my results do not exclude EMP origin of the Mϕ colonies, as in MYB$^{-/-}$ mice, although significantly reduced in number, some Kit+ hematopoietic progenitors are detected in the FL (Schulz et al., 2012) and a more recent study showed that CD11b^{high} F4/80^{low} fetal monocytes are present at E14.5 within Myb$^{-/-}$ mouse embryos (Gomez Perdiguero et al., 2015). Furthermore, loss of erythrocyte colony potential in the MYB KO hiPSCs would indicate the absence of RUNX1- and MYB-independent monopotent primitive erythrocyte precursors within the EBs using this protocol. Taken together, my results suggest that iPS-Mo/Mϕs can derive independently of MYB from EMPs and/or primitive unilineage Mϕ progenitors.

While we cannot exclude the possibility that some MYB-dependent HPC/HSCs are generated during normal WT hiPSC differentiation, we would expect a reduction in iPS-Mo/Mϕ production if the majority of the iPS-Mo/Mϕs were derived from MYB-dependent progenitors. In contrast, we observed an increase in production of iPS-Mo/Mϕ in the MYB$^{\Delta Ex6}$ hiPSCs, without any major change in phenotype or function of the cells. Furthermore, using a similar EB-based hESC differentiation protocol Vanhee et al. observed that multipotent HPCs expressing high levels of MYB were not generated in their cultures and that Mϕs were generated from precursors not expressing detectable MYB (Vanhee et al., 2015). Combined with my data, this strongly suggests that in WT hiPSC differentiation most, if not all, iPS-Mo/Mϕ are produced in a MYB-independent fashion, and the contribution of

MYB-dependent multilineage HPC/HSCs-derived hematopoiesis in our EB-based monocyte differentiation protocol is negligible, if not absent.

In addition to the increased iPS-Mo/Mϕ production, I observed an increased number of CD34$^+$ CD45$^+$ hematopoietic progenitor cells within MYB$^{\Delta Ex6}$ EBs. A similar, but not identical phenotype has been observed in Myb$^{-/-}$ mESC differentiation by Clarke *et al.* (Clarke et al., 2000). First, they observed that Myb$^{-/-}$ mESCs were capable of Mϕ and primitive erythrocyte colony formation but the kinetics of formation was different between the control line and the Myb$^{-/-}$ mESCs. The number of CFU-E was lower in Myb$^{-/-}$ while the generation of CFU-M was increased at day 7 when compared to the WT control. Secondly, no BFU-E were generated by Myb$^{-/-}$ mESCs, indicating a block of definitive erythrocyte production. Thirdly, they observed a higher number of CD34$^+$ Sca-1$^+$ hematopoietic progenitor cells within the Myb$^{-/-}$ EBs, but these progenitors were unable to progress further in differentiation. The increase in progenitors in both Myb$^{-/-}$ hiPSCs and mESC could be due to an increased hematopoietic commitment, progenitor proliferation or an accumulation of committed erythrocyte/granulocyte progenitors which cannot progress further through differentiation due to the lack of MYB. The elevated number of Mϕs for both hiPSCs and mESCs, would imply that in normal conditions the presence of MYB directly or indirectly reduces iPS-Mo/Mϕ differentiation. This could be explained by the presence of erythrocyte progenitors present within the EBs which do not progress further through differentiation in the high concentration of MCSF and IL3 present in our iPS-Mo/Mϕ differentiation conditions but in absence of MYB they are unable to commit to erythrocyte lineage and instead progress down the Mϕ lineage. It will be interesting to understand the precise mechanism of action underlying this increase in precursor cells and iPS-Mo/Mϕ for MYB$^{\Delta Ex6}$ hiPSCs. With the mounting data suggesting that tissue resident Mϕs and BM monocyte-derived Mϕs can play different roles in diseases such as cancer (Lahmar et al., 2015) and parasite infection (Rückerl and Allen, 2014), having access to authentic embryonic-derived monocytes and Mϕs *in vitro* will be of considerable scientific value. Patient-derived tissue-resident Mϕs are very difficult to obtain, are inherently

genetically variable and notoriously difficult to genetically modify, making their study laborious and unreliable. On the other hand, hiPSC can be generated from a patient with a specific genetic background and can be modified by multiple mechanisms such as lentiviral transduction or CRISPR-Cas9 gene-editing. The demonstration that MYB-independent monocytes/Mϕs can be generated in our differentiation protocol lays the foundation for their use in the development of reliable protocols for generating the tissue-specific sub-types of Mϕs for the *in vitro* study of their role in pathology and homeostasis. Moreover, hiPSC differentiation is a potential source of tissue-resident Mϕs for cell therapy, as has recently been shown in the mouse with the use of mESC-derived $Myb^{-/-}$ alveolar-like Mϕs as a cell source for treating a mouse model of adenosine deaminase deficiency ($ADA^{-/-}$) (Litvack et al., 2016).

5

Investigating the differentiation bottleneck

Contents

5.1 Introduction 129
5.2 Materials and methods 133
5.2.1 Copy number variation (CNV) digital droplet PCR (ddPCR) 133
5.3 Results 134
5.3.1 RFP-GFP statistical model 134
5.3.1.1 Poisson distribution and assumptions 134
5.3.1.2 A dual reporter system to quantify the bottleneck 136
5.3.1.3 GFP/RFP model confirms GeCKO library results 138
5.3.1.4 Clonal RFP-GFP experiment 141
5.3.2 Using RUNX1$^{\Delta Ex5}$ hiPSCs to investigate the differentiation bottleneck 144
5.3.2.1 Proof of concept 144
5.3.2.2 Effect of MYB$^{\Delta Ex6}$ on the differentiation bottleneck 146
5.4 Discussion 148

5.1 Introduction

During iPS-Mo/Mϕs differentiation of hESC/hiPSCs, each EB is generated from 10^4 cells and can produce 2x10^4 to 10^5 iPS-Mo/Mϕs per week, over the course of several months (as shown in chapter 3, 4 and (van Wilgenburg et al., 2013)). From

these 10^4 starting hPSCs it is safe to assume that not all will undergo hematopoietic differentiation, the remaining cells will differentiate into various other cell types within the EB. Therefore, during the differentiation process there is likely to be a bottleneck where only a fraction of the starting cells will be at the origin of all iPS-Mo/Mϕs generated by a particular EB. This chapter will be focused on studying this bottleneck and developing a method for estimating the average number of hESC/hiPSC that go through this differentiation bottleneck in our model system in order to study the mechanisms that control hematopoiesis.

This project stems from a result obtained by Dr MD Moore in our lab, which I will present here. Dr Moore generated a genome-scale CRISPR KO (GeCKO) lentiviral library, which he transduced at a low Multiplicity of infection (MOI) into hiPSCs, such that most cells receive only one copy of gRNA, knocking out one gene per cell (Sanjana et al., 2014; Shalem et al., 2014). This library is designed to target 18,080 genes with 64,751 unique gRNAs allowing for positive and negative KO screening. Each gRNA is barcoded, one can therefore using next-generation high throughput deep sequencing (NGS) of the gRNA sequences present in the genomic DNA of the starting cell population, apply selection with a specific phenotype (cell death, HIV-1 infectibility, cell proliferation, etc.) and upon selection, cells can be sequenced again for presence of gRNAs. Using this method it is possible to identify genes which are positively or negatively enriched after selection.

The generation of the GeCKO library is schematically represented in figure 5.1A. The main objective of Dr Moore's experiment was to identify novel HIV-1 restriction factors in Mϕs using the GeCKO screen. As monocytes and Mϕs are notoriously difficult to transduce, the stem cell iPS-Mo/Mϕ differentiation system seemed like the most appropriate as it allowed for the generation of a large pool of hiPSCs transduced with the full lentiviral GeCKO library and use these stem cells for the generation of iPS-Mo/Mϕs. These iPS-Mo/Mϕs harbouring the GeCKO library could then be used for positive HIV-1 infection screening to find genes involved in HIV-1 restriction. This approach is limited by the assumption that during hiPSC differentiation to iPS-Mo/Mϕ only a minor proportion of gRNA diversity is lost, which relies on

the differentiation process being highly efficient (for each starting hiPSC a large proportion have to undergo hematopoietic and iPS-Mo/Mϕ differentiation).
The starting hiPSC population was sequenced using NGS and close to 49,000 unique gRNAs were represented. For iPS-Mo/Mϕ differentiation 900 EBs ($\sim$9x10^6 hiPSCs) were generated, which produced over 6x10^7 iPS-Mo/Mϕ per week. The NGS result analysis of the generated iPS-Mo/Mϕs showed that from the 49 000 starting gRNAs present in the undifferentated hiPSCs only 536$\pm$100 were represented in the iPS-Mo/Mϕ population (figure 5.1A). This shows that, from the 9x10^6 hiPSCs used to generate the EBs only about 500 were at the origin of all iPS-Mo/Mϕs. This result implies that from the 10^4 hiPSCs which form an EB only about 0.5 hiPSCs will become iPS-Mo/Mϕ progenitors resulting in a 20 000 fold loss in the heterogeneity during differentiation (figure 5.1B). EBs used for the generation of these iPS-Mo/Mϕ had similar gRNA diversity than the undifferentiated iPSCs, suggesting that the bottleneck occurs during hematopoietic specification. This also showed that with the current differentiation protocol it is not possible to apply the GeCKO approach to iPS-Mo/Mϕs by differentiation of transduced hiPSCs unless the number of EBs are increased to an unreasonable amount (>200 EBs/gRNA).
The severity of the bottleneck observed in the GeCKO result, although disappointing for genome wide screening of iPS-Mo/Mϕs, opens up several biological questions regarding the differentiation process of iPS-Mo/Mϕs: How many cells per EB go through the bottleneck? Can several cells pass through the bottleneck in a single EB? Is this fate decision event random or controlled by a feedback loop? Can the bottleneck be modulated?
Firstly I set out to design a simpler, faster and cheaper method than GeCKO or cellular barcoding for investigating the differentiation bottleneck. Once established, the first objective was to validate the method by replicating the results obtained by the GeCKO library. The second objective was to better understand if the fate decision event at the origin of the bottleneck is a random low frequency event or if it is highly controlled and can only happen once per EB (feedback loop inhibiting any further events occurring once it has occurred). The final objective was to apply

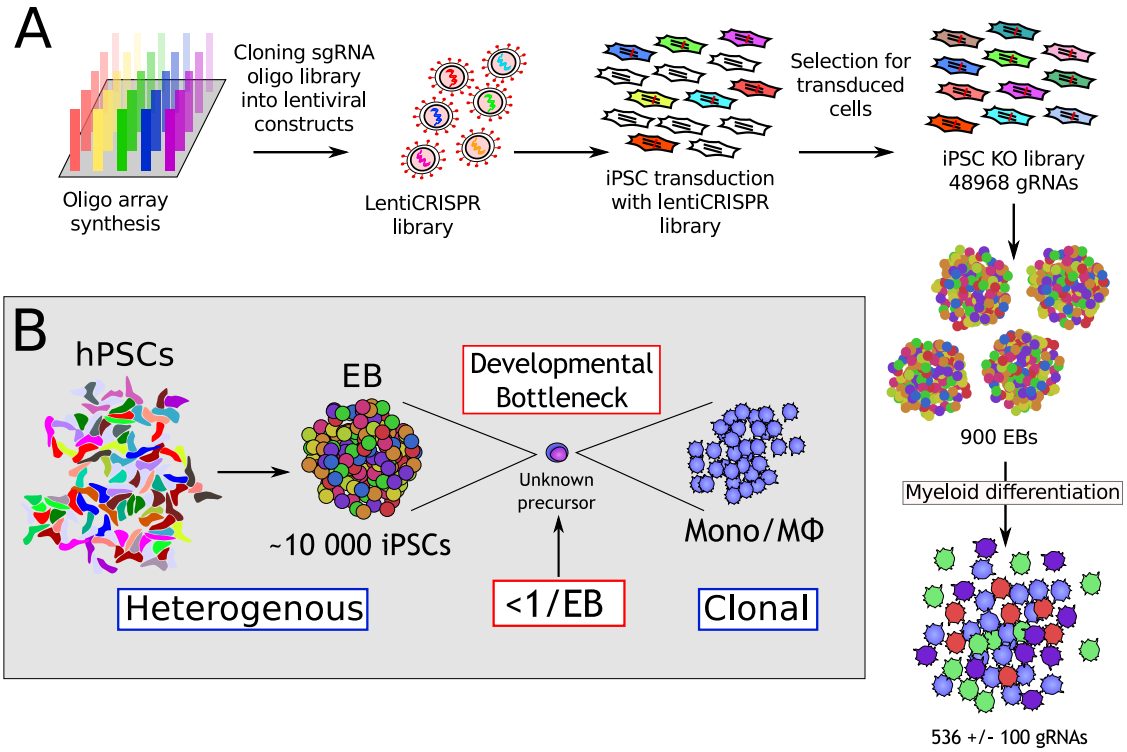

Figure 5.1: Hematopoietic differentiation bottleneck. A. Schematic representation, adapted from (Shalem et al., 2014), of the GeCKO hiPSC screening experiment of Dr MD Moore. After generation of the CRISPR/Cas9 expressing lentiviral library, hiPSCs were transduced at low MOI. Resulting polyclonal population was selected for transduced cells generating an hiPSC KO library. The starting hiPSC population was deep sequenced and close to 49 000 gRNAs were represented. After EB formation and differentiation, resulting iPS-Mo/Mϕ were deep sequenced and only about 500 gRNA were represented in the iPS-Mo/Mϕ population. **B.** Schematic representation of the bottleneck happening during iPS-Mo/Mϕ differentiation. In each EB composed of a heterogenous starting population of about 10 000 hiPSCs, on average, less than 1 hiPSC cell is at the origin of all iPS-Mo/Mϕs generated by that EB.

this method to investigating if this bottleneck can be modulated, for instance in the case of MYB$^{\Delta Ex6}$ hiPSCs, which produce increased numbers of iPS-Mo/Mϕs. Do MYB$^{\Delta Ex6}$ EBs have a higher hematopoietic commitment early in differentiation or does MYB KO result in more downstream proliferation of hematopoietic progenitors.

5.2 Materials and methods

5.2.1 Copy number variation (CNV) digital droplet PCR (ddPCR)

The AH016-03 hiPSC and HUES-2 hESC lines were transduced with a second generation, SIN-GFP or -RFP lentiviral vector (LV-EF1a-RFP-IRES-Puromycin^R and LV-EF1a-GFP-IRES-Puromycin^R) (van Wilgenburg et al., 2013) at a high MOI. Cells were kept under continuous puromycin selection (2 μg/mL: a concentration sufficient to kill untransduced cells). For single cell cloning AH016-03-RFP or -GFP single cell clones were picked as previously described in section 4.2.2.

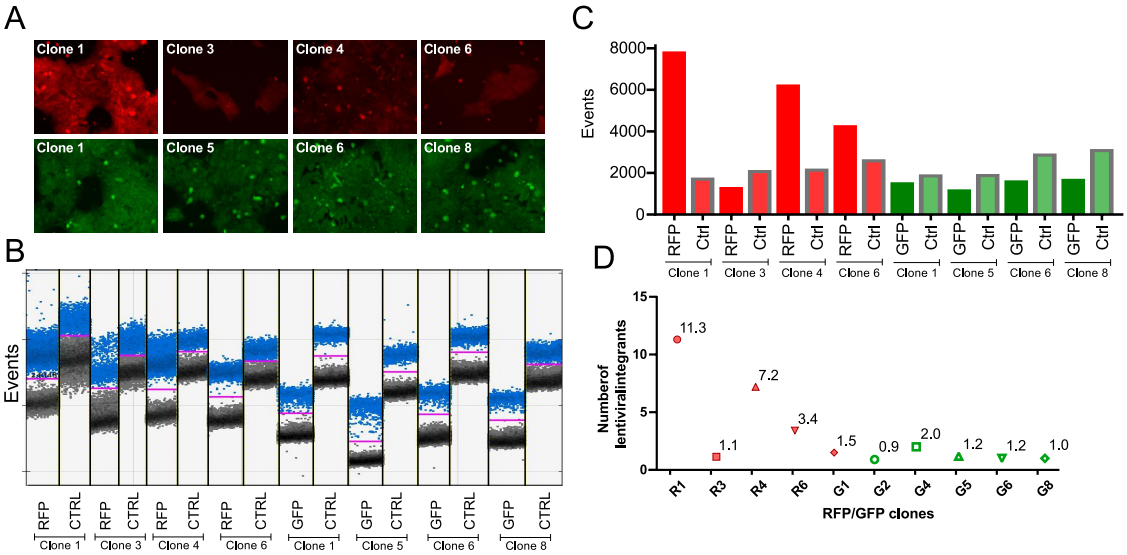

Figure 5.2: CNV analysis using ddPCR. A. Fluorescent images of the different hiPSC sub-clones. **B.** Raw ddPCR droplet counts, blue droplets contain a PCR reaction and grey droplets are negative. For each clone an RFP or GFP primer was used to quantify the number of lentiviral genomic copies compared to the MYB control, present in two copies. **C.** Total number of RFP and GFP events compared to MYB events for each clones. **D.** Number of lentiviral copies (as quantified by GFP or RFP copies integrated in the cells) after applying Poisson distribution and normalizing to endogenous MYB control.

The number of lentiviral integrants per clone was quantified using ddPCR using analysis of copy number variation (CNV) (Bio-Rad QX200) according to the manufacturer's protocol. In my case analysis of CNV involves determining the number of lentiviral copies compared to an invariant reference locus (MYB).

Briefly, 2 μL of EcoRI digested genomic DNA at 100 ng/μL was used with the EvaGreen Super Mix and 100 nM forward and reverse primers. The following RFP primers were used: JB-111 (5' - ATGCAGAAGAAAACACGCGG - 3') and JB-112 (5' - CCGGGCATCTTGAGGTTCTT - 3'). The following GFP primers were used: JB-114 (5' - CGCCGAGGTGAAGTTCGA - 3') and JB-115 (5' - CTTGATGCCGTTCTTCTGCTT - 3'). PCR primers for the MYB gene, were used as endogenous control: JB-71 (5' – ACAGGAAGGTTATCTGCAGGAGTCT – 3') and JB-72 (5' – AGTGGCAGGGAGTTGAGCTGTA - 3'). I tested four AH016-03 RFP and GFP clones, results can be seen in figure 5.2, for future experiments. For consistency I decided to use clone R3 and clone G8 which both had a single lentiviral integrant.

5.3 Results

5.3.1 RFP-GFP statistical model

5.3.1.1 Poisson distribution and assumptions

There are two general possible assumptions for the differentiation event at the origin of the bottleneck observed in our hiPSC model:

1. It is a controlled event with a defined number of events per EB. (For example a feedback loop blocking any further differentiation events occurring once one happened somewhere in the EB).

2. It is a random low frequency event.

If for both models we consider, for this example, that the average number of differentiation events per EB equals 1:
In case of assumption (1) this would mean that in a controlled ideal system 100% of the EBs produce iPS-Mo/Mϕs and in each individual EB only a single cell was at the origin of all derived iPS-Mo/Mϕs. And if we were to increase the efficiency of the differentiation system, it would still result with a maximum of 1 event per EB.

In case of assumption (2), some EBs would not produce, some EBs would have a single differentiation event happening and some EBs would have two or more differentiation events happening. The frequency of this type of distribution is described by the Poisson distribution (Siméon Denis Poisson, 1838) which would in this example predict that 37% of the EBs would not produce ($P_0 = 0.368$), the same percentage of EBs would have 1 event occurring ($P_1 = 0.368$) and 26% would have two or more events happening ($P_{\geq 2} = 0.264$). The Poisson distribution is described by the following equation:

$$P_k = \frac{\lambda^k}{k!} e^{-\lambda}$$

Where:

- P_k is the predicted fraction of EBs which will produce iPS-Mo/Mϕ
- λ is the size of the bottleneck (average number of differentiation events per EB)
- e is the base of the natural logarithm, approximately equal to 2.71828

This equation can be simplified to calculate the expected frequency of null EBs (unable to produce any iPS-Mo/Mϕs ($k = 0$)) for a given bottleneck (λ).

$$P_0 = e^{-\lambda}$$

In our case we do not know what the size of the bottleneck is, but if we plate EBs in individual wells we can count the number of EBs unable to produce iPS-Mo/Mϕs (frequency of null EBs (P_0)) in our culture. The frequency of nulls, can be used for calculating the average bottleneck (λ):

$$P_0 = e^{-\lambda} \iff \lambda = -ln(P_0)$$

This means that if the differentiation event occurring in the EBs follows the Poisson distribution it is possible to calculate the size of the bottleneck (average number of differentiation events occurring per EB) by using the frequency of non-producing EBs (P_0). This calculation relies on the assumption that the event distribution is

random, in our system we do not know if the differentiation event at the origin of the bottleneck is random or if it is controlled by a feedback loop blocking several differentiation events occurring per EB.
Once the bottleneck λ has been calculated it can be used to calculate the predicted frequency of EBs with a given number of events by replacing k in the base formula by the number of interest.
Number of EBs with a single event:

$$P_1 = \lambda e^{-\lambda}$$

Number of EBs with a two event:

$$P_2 = \frac{\lambda^2}{2!} e^{-\lambda}$$

Previously calculated frequencies can then be used to calculate the number of EBs with three or more events:

$$P_{\geq 3} = 1 - (P_0 + P_1 + P_2)$$

5.3.1.2 A dual reporter system to quantify the bottleneck

To calculate the bottleneck using the Poisson formula, all that is needed is the number of non-producing EBs, which can be obtained easily by plating EBs individually and monitoring their production. That being said, this assumes that we are in a situation where Poisson distribution applies, which we have not confirmed in our model system. By using a dual reporter system it is possible to estimate the number of single and double events occurring per EB and validate if the differentiation event follows Poisson distribution.
The experimental model idea is very simple, if we generate EBs using 50% GFP and 50% RFP expressing hiPSCs and plate each EB in an individual well we can quantify the number of EBs that: do not produce any iPS-Mo/Mϕs, produce only GFP iPS-Mo/Mϕs or RFP iPS-Mo/Mϕs and the ones that produce a mix of RFP and GFP iPS-Mo/Mϕs. Any EB with a single cell bottleneck will produce single coloured iPS-Mo/Mϕs, of the EBs with a two cell bottleneck $\frac{1}{3}$ will produce

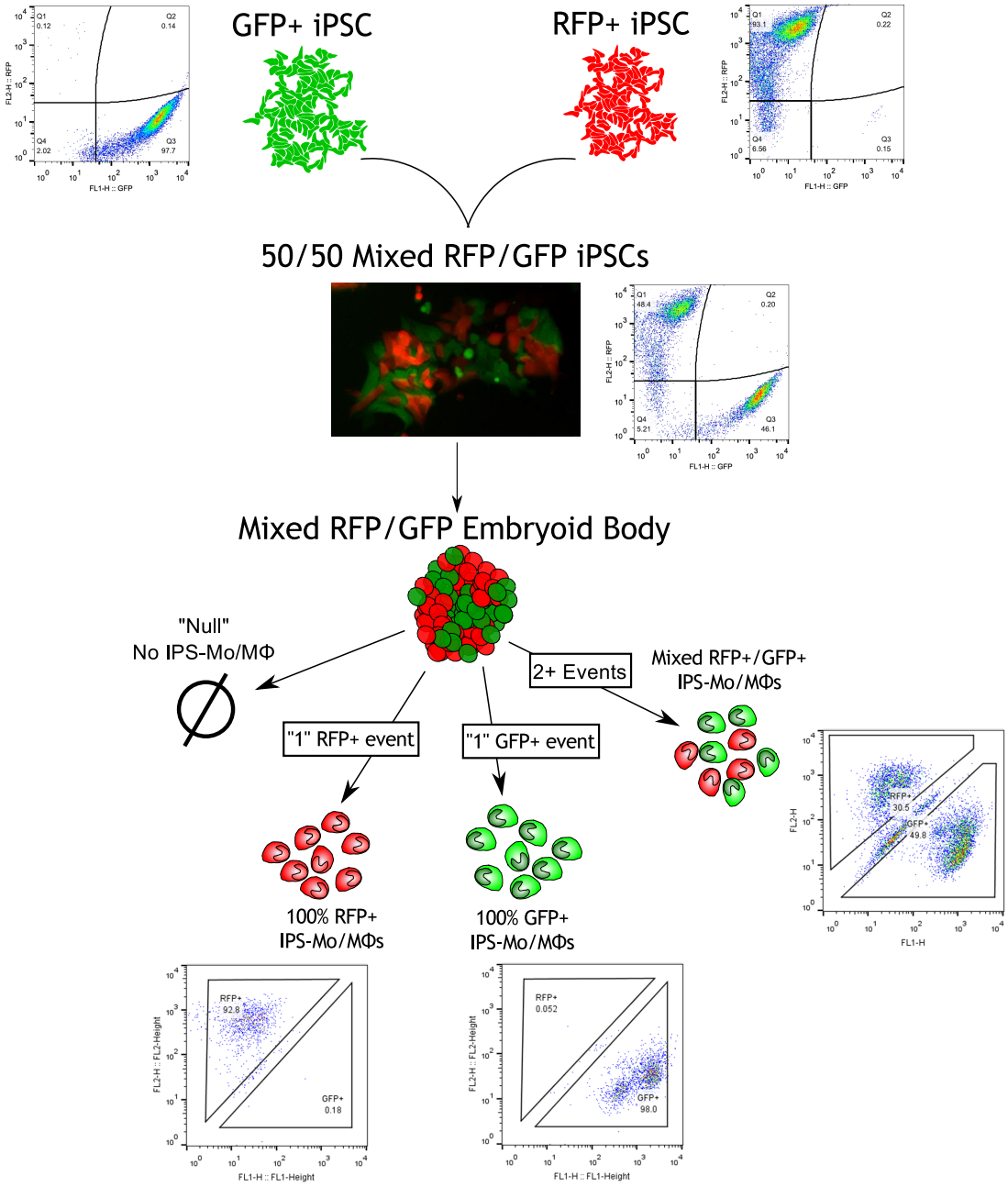

Figure 5.3: Schematic representation of the GFP/RFP statistical model. By generating EBs using 50% GFP expressing hiPSCs and 50% RFP expressing cells and plate each EB in an individual well it is possible to analyse the iPS-Mo/Mϕ production of each EB separately. Each EB has three possible outcomes, (1) it does not produce, (2) it produces iPS-Mo/Mϕs of a single colour or (3) it produces a mixture of GFP$^+$ and RFP$^+$ iPS-Mo/Mϕs. The frequency of EBs which do not produce will be used as the frequency of nulls (P_0), the frequency of single and double coloured EBs will be used to approximate the frequency of single events (P_1) and multiple events ($P_{\geq 2}$).

iPS-Mo/Mϕs of mixed colour and $\frac{2}{3}$ will produce iPS-Mo/Mϕs of single colour (composed of two GFP or two RFP cell). Using this information, it is therefore possible to estimate the average number of EBs with a single differentiation event and the number of EBs in which multiple events have occurred (figure 5.3). By comparing this estimated number with the one calculated using Poisson distribution we can estimate if the event follows the Poisson distribution.

5.3.1.3 GFP/RFP model confirms GeCKO library results

To test the results obtained using the GeCKO library, I generated mixed EBs using at first RFP and GFP expressing HUES-2 hESCs. Both HUES-2 RFP and HUES-2 GFP lines were generated using lentiviral transduction and used as a polyclonal population after puromycin selection. The HUES-2 hESC line was chosen at the time as it was widely used in the laboratory and was known for robust Mo/Mϕ production. For the purpose of this experiment I used a 96 well spin EB method where each well generated a single EB (Materials and methods 2.3.1). After 4 days of initial EB culture, each individual EB was transferred to a flat bottom 96 well plate in differentiation media allowing for study of hES-Mo/Mϕ production of each EB individually. Each spin EB was generated with a total of 10^4 cells, 5x10^3 GFP and 5x10^3 RFP. To check that the stem cells had similar viability and growth rate I plated part of the hESC mix used for the EB generation and grew them for several days. The hESCs showed a RFP and GFP mosaic under the microscope (figure 5.4A). To check that the cell counts were accurate, the initial mixture of hESCs used for EB generation was assayed by flow cytometry, 48% of the hESCs were RFP$^+$ and 46% were GFP$^+$ which shows that the initial counts were accurate (figure 5.4 B). Some of the hESCs displayed low level fluorescence, which is an issue we have encountered often in lentivirally transduced polyclonal hESC/hiPSC culture. This loss of fluorescence in a subpopulation of the cells can be due to the insertion of a mutation in RFP or GFP during reverse transcription of the lentiviral vector or silencing of the transgene by the hESC/hiPSCs. EBs started producing after two weeks and hES-Mo/Mϕ of each well were harvested individually and analysed by

flow cytometry. Out of 72 EBs, 43 (60%) produced hES-Mo/Mϕs, while 29 (40%) did not produce (figure 5.4C). Using the frequency of nulls (0.4) we can estimate that the average bottleneck is $\lambda = 0.91$ cells per EB (figure 5.4D). This result is higher than the result obtained from the GeCKO library (0.5 cells/EB) but still in a similar range. If the event is distributed according to Poisson distribution then we would expect out of 72 EBs: 26 EB with a bottleneck of a single cell ($P_1 = 0.37$), 12 EBs with a bottleneck of two cells ($P_1 = 0.17$) and 4 EBs with a bottleneck of three or more cells ($P_{\geq}3 = 0.06$). Any EB with a single cell bottleneck is single coloured, $\frac{1}{3}$ of the EBs with a two cell bottleneck will be of mixed colour and $\frac{2}{3}$ will be either composed of two GFP or two RFP cell and therefore single coloured. As the frequency of single coloured EBs with a bottleneck of three or more cells is low, I will consider all EBs with three or more events being double coloured. This results in a final approximation of 34 single coloured EBs ($P_{single-colour} = 0.48$) and 9 double coloured EBs ($P_{double-colour} = 0.12$).

From the flow cytometry results several observations can be made. Although the whole differentiation was done under constant puromycin selection, in addition to GFP and RFP cells, in many wells the hES-Mo/Mϕs produced were non-fluorescent (silenced). The presence of silenced cells complicated the quantification of single or double GFP/RFP producing EBs as we cannot know if the silenced cells are GFP or RFP transduced. As there is a severe bottleneck in differentiation it is more likely that the silencing occurs after the bottleneck, I therefore counted silenced cells as the same colour than the main, non-silenced hES-Mo/Mϕ population. For quantification of the number of single and double coloured cell population I set an arbitrary threshold: any well with more than 5% of GFP and RFP was counted as double coloured and silenced cells were considered as the same colour as the main population. Using these assumptions, 32 EBs produced single coloured hES-Mo/Mϕs and 11 produced double coloured hES-Mo/Mϕs (figure 5.4D). This is in line with the expected number calculated using Poisson distribution: 34 single coloured EBs and 9 double coloured EBs.

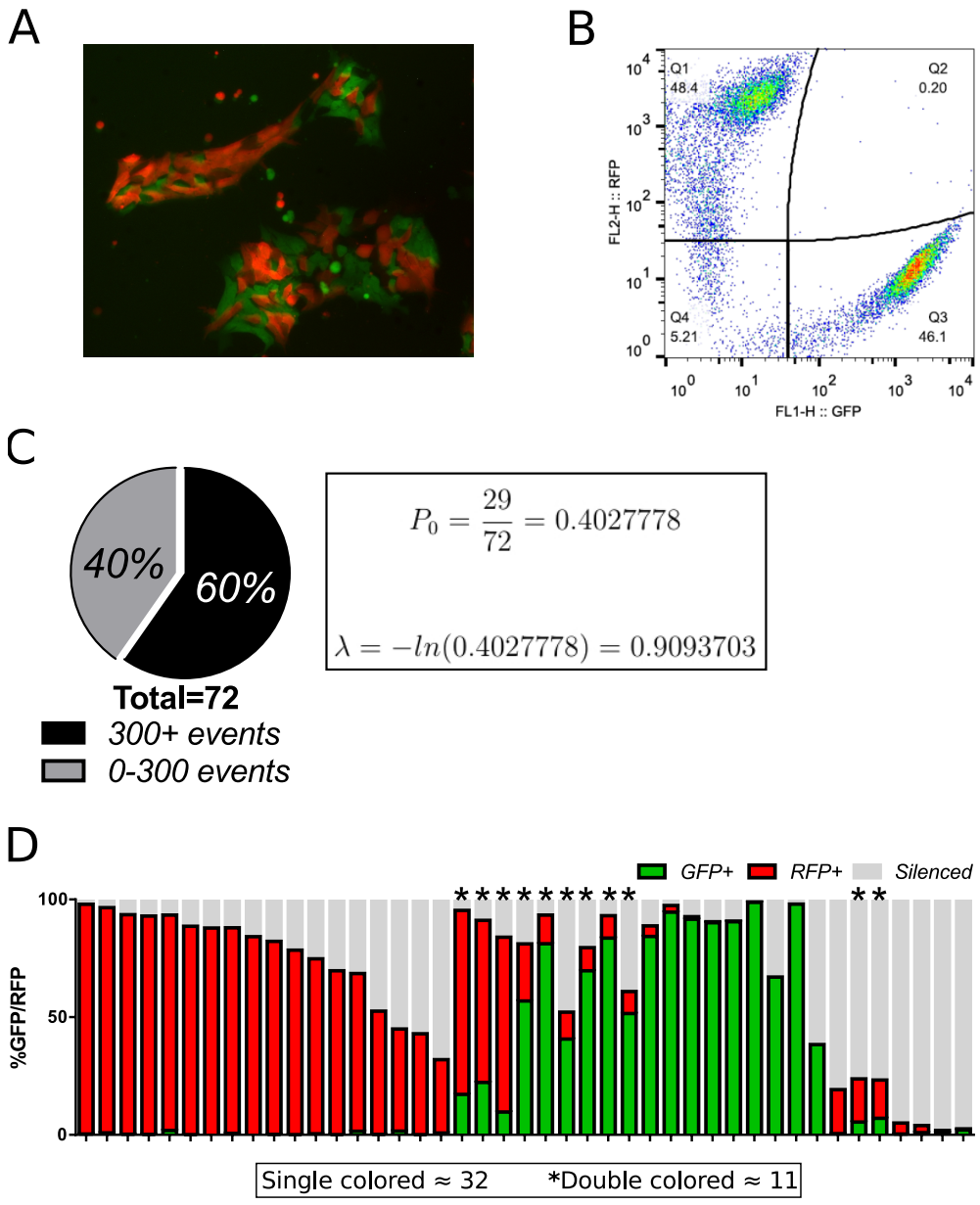

Figure 5.4: HUES-2 polyclonal GFP/RFP model. A. Fluorescent microscopy image of HUES-2 RFP and GFP hESC one day after plating the mixed cell suspension used for EB formation. **B.** Flow cytometry of the starting mix of cells used for EB formation showing a 50/50% split between RFP and GFP hESCs. **C.** Frequency of null EBs (less than 300 events detected by flow cytometry) and calculation of the bottleneck (λ) using Poisson distribution equation. **D.** Percentage of RFP, GFP and silenced cells produced by each individual producing EB (300+ events), quantified by flow cytometry.

This preliminary experiment, although having many issues, allowed me to gather some initial data regarding the hES-Mo/Mϕ differentiation system. First, the

results tie in with the results obtained from the GeCKO library, reinforcing the idea that there is a severe differentiation bottleneck occurring during hESC/hiPSC differentiation resulting in a loss of heterogeneity. Second, an EB can have two events occurring as some EBs produced both GFP and RFP hES-Mo/Mϕs. This would indicate that there is not a strict feedback system blocking several events occurring per EB. Thirdly, from the distribution results it would indicate that the fate decision event is a low frequency event broadly following Poisson distribution. However, these conclusions need further validation as silencing of the RFP and GFP constructs is a problem which greatly reduces reliability of the observations.

5.3.1.4 Clonal RFP-GFP experiment

5.3.1.4.1 AH016-03 subcloning

Silencing during iPS-Mo/Mϕ differentiation is a known problem with hiPSCs and one of the ways to reduce variability in silencing is using single cell clones which have a known number of lentiviral integrants. I therefore decided to sub-clone the AH016-03 RFP and GFP cell lines, as AH016-03 is the cell line I used for my other experiments and will be more comparable with my KO results in the future since it has the same genetic background. Single cell clones were generated as previously described for CRISPR/Cas9 KO single cell clone plating and picking (Chapter 4 - 4.2.2). Only uniformly coloured clones were kept, expanded and quantified for the number of lentiviral integrant using ddPCR; detailed explanation of the usage of ddPCR for CNV can be found in the materials and methods part of the chapter: 5.2.1.

5.3.1.4.2 AH01603 results

GFP and the RFP clones with a single integrant (AH016-03-RFP clone 3 and AH016-03-GFP clone 1) were used with the same experimental design as the mixed RFP and GFP experiment using polyclonal HUES-2 (subsection 5.3.1.3). As an additional control the same experiment was setup without puromycin selection, to

asses the impact of puromycin on the differentiation bottleneck, as the previous experiment was done under puromycin selection.

After differentiation and flow cytometric analysis the following results were obtained: out of 78 EBs, 39 produced in the puromycin condition and 38 produced in the no-puromycin condition (figure 5.5). Although the removal of puromycin during differentiation did not influence the overall number of producing EBs, and therefore did not change the bottleneck, it did significantly increase the quantity of silenced iPS-Mo/Mϕs. The average bottleneck per EB can be calculated by using the same equation as seen previously resulting in $\lambda = 0.69$ for the puromycin condition and $\lambda = 0.73$ for the no-puromycin condition, which is in the same range as the GeCKO and HUES-2 RFP and GFP results. If the event is distributed according to Poisson distribution, using the same approach as previously described (5.3.1.3), out of 78 EBs we expect: 33 single coloured EBs ($P_{single-colour} = 0.42$) and 6 double coloured EBs ($P_{double-colour} = 0.07$).

When looking at the distribution of EBs producing single RFP and GFP or double coloured iPS-Mo/Mϕs it is clear that in the presence of puromycin there is very little silencing when compared to the previous HUES-2 polyclonal results. With the exception of 6 EBs which produced over 40% silenced iPS-Mo/Mϕs, most other EBs produced mainly RFP, GFP or a mix of both, indicating that cloning of the cells improved the assay. Furthermore most silenced cells are likely RFP as AH016-03-RFP was more prone to silencing than AH016-03-GFP (data not shown). Quantification of the single and double coloured iPS-Mo/Mϕ producing EBs results in 28 EBs producing single coloured iPS-Mo/Mϕs, which is lower than the 33 predicted and 11 EBs producing double coloured iPS-Mo/Mϕs which is higher than the predicted 6. It is possible that I am overestimating the number of double coloured EBs by setting my threshold at 5% and therefore counting possible non-hematopoietic cells which have detached during harvesting of the non-adherent cells. While further investigation would be needed to verify if this increase in double coloured EBs is reproducible, overall, this result is broadly in the range of what would be expected from previous experiments.

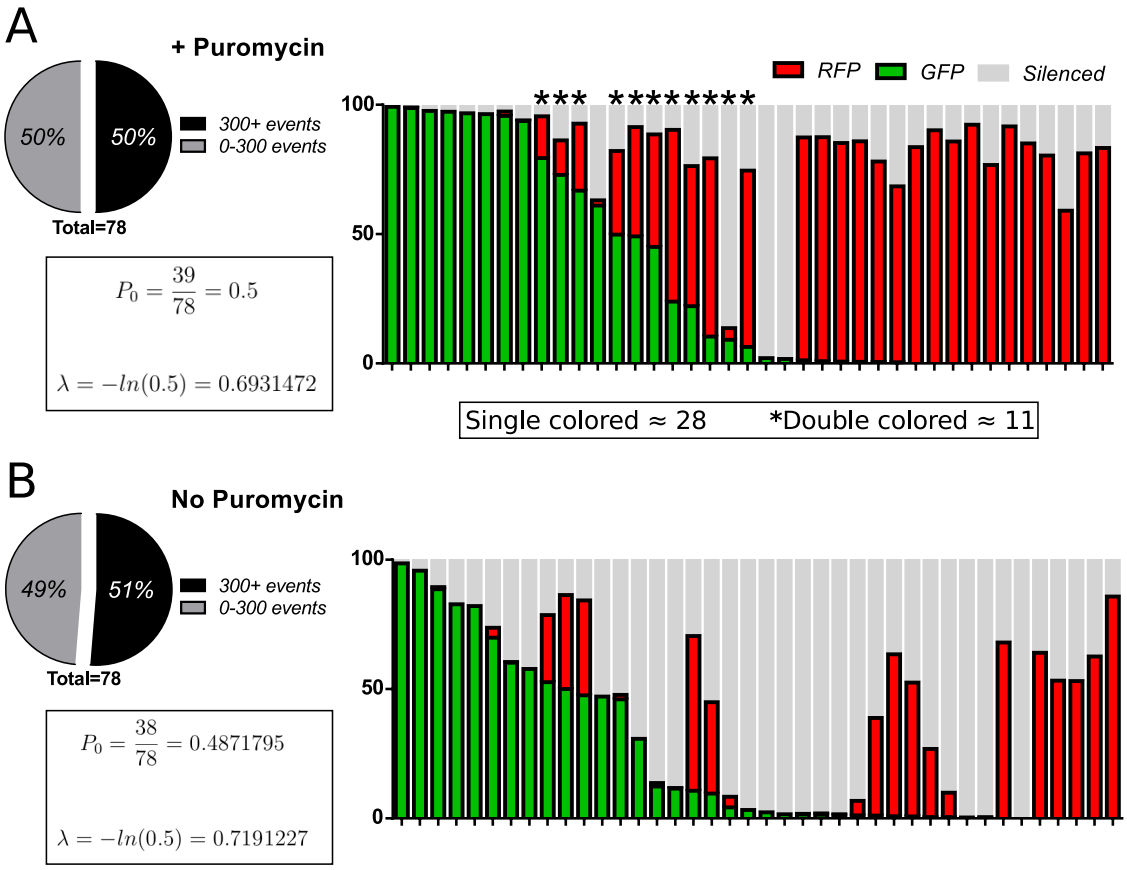

Figure 5.5: AH016-03 clonal GFP/RFP model A. Puromycin treated condition. **B.** Untreated condition. For both conditions, frequency of null EBs (less than 300 events detected by flow cytometry) and calculation of the bottleneck (λ) using Poisson distribution equation on the left. On the right is shown the percentage of RFP, GFP and silenced cells produced by each individual producing EB (300+ events), quantified by flow cytometry.

For these two experiments we can confirm that there is a strong bottleneck occurring during EB based iPS-Mo/Mϕ differentiation and that this bottleneck is in the range of 0.5 to 1 cell per EB of 10^4 cells. The differentiation event is a low frequency stochastic event which therefore likely follows the Poisson distribution.

The method developed here using RFP and GFP cells is quite powerful for assessing the bottleneck but has two major issues: silencing and the requirement for generation of RFP and GFP expressing cells in each cell line of interest. One of the objectives of this study was the quantification of the bottleneck of WT hiPSCs compared to MYB$^{\Delta Ex6}$ KO hiPSCs, as MYB$^{\Delta Ex6}$ hiPSCs produced twice as many iPS-Mo/Mϕs (Chapter 4 - 4.3.4.4).

5.3.2 Using RUNX1$^{\Delta Ex5}$ hiPSCs to investigate the differentiation bottleneck

MYB$^{\Delta Ex6}$ hiPSCs produced on average twice as many iPS-Mo/Mϕs compared to WT controls and had an increased number of CD34^{+} CD45^{+} progenitors within the EB (Chapter 4 - 4.3.4.4 and 4.3.4.6). Therefore finding out if there were more cells undergoing hematopoietic commitment within the MYB$^{\Delta Ex6}$ EBs would give us additional insight in the reasons for the increased MYB$^{\Delta Ex6}$ iPS-Mo/Mϕ production. If I were to use the same approach as previously, it would require the generation of single cell AH016-03 MYB$^{\Delta Ex6}$ GFP and RFP lines. This is a long process and would result in unreliable results as the cells would have undergone many extra passages, have random lentiviral integrants which could have integrated in important genes and would be more prone to karyotypic abnormalities due to the extra single cell cloning step. I therefore decided to use a different approach adapted from my previous results.

As my RFP and GFP results showed that the bottleneck event is likely distributed according to Poisson distribution, the number of non-producing EBs alone should be sufficient to calculate the bottleneck. The issue with using negatives as a readout is that if the differentiation is efficient or if the bottleneck is >1 there will be very few negatives and I will require many EBs to get a statistically significant result. I therefore decided to take advantage of my previously established RUNX1$^{\Delta Ex5}$ hiPSC line, which is unable to undergo hematopoietic differentiation.

5.3.2.1 Proof of concept

RUNX1$^{\Delta Ex5}$ hiPSCs are unable to produce iPS-Mo/Mϕs and it is known that RUNX1 is required for endothelial to hematopoietic transition (Chen et al., 2009). RUNX1$^{\Delta Ex5}$ hiPSCs should therefore be unable to generate any iPS-Mo/Mϕs even when mixed with WT or MYB$^{\Delta Ex6}$ hiPSCs. Mixing WT or MYB$^{\Delta Ex6}$ hiPSCs with RUNX1$^{\Delta Ex5}$ hiPSCs allowed me to vary the number of hiPSCs capable of hematopoietic differentiation while maintaining the same size of EB (figure 5.6A). This way it is possible to titrate down the number of WT or MYB$^{\Delta Ex6}$ input

hiPSCs within an EB and use Poisson distribution to calculate the mean number of cells undergoing the differentiation bottleneck within an EB without using any florescent markers. This also allows me to get a more precise result by increasing the number of nulls and see if the progression is linear between concentrations, which will be an additional indication if the event is stochastic or if it is promoted. (If there is a low number of cells capable of iPS-Mo/Mϕ differentiation, will they fill the empty niche at the same frequency.)

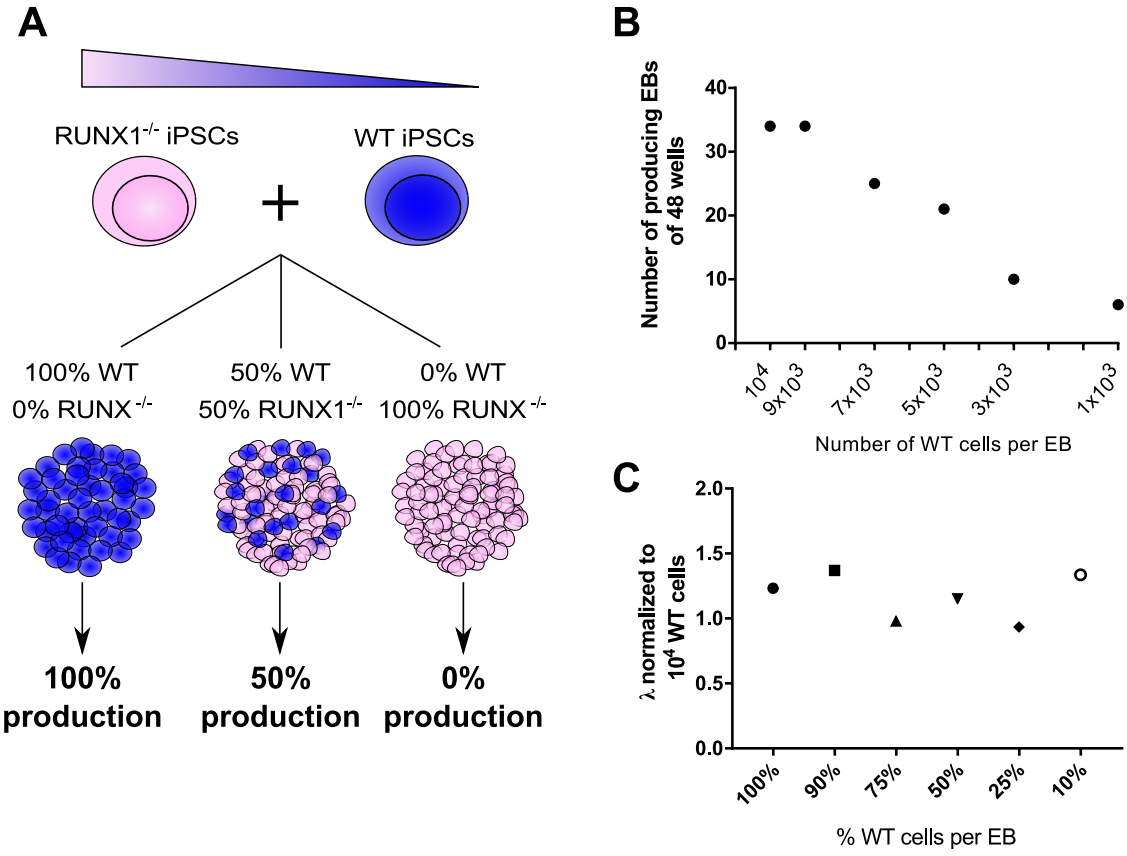

Figure 5.6: Using RUNX1$^{\Delta Ex5}$ hiPSCs to investigate the differentiation bottleneck. A. To vary the number of input hiPSCs in an EB and therefore modulate the number of null EBs in our system, while maintaining the EB size the same, I used RUNX1$^{\Delta Ex5}$ hiPSCs to generate EBs using the same number of total hiPSCs but varying numbers of WT hiPSCs. **B.** Number of EBs out of 48 total EBs capable of iPS-Mo/Mϕ production compared to the number of input WT hiPSCs per EB. **C.** Calculation of the normalised bottleneck (λ) for each condition. The frequency of nulls was used to calculate the λ for each condition and then multiplied by the dilution to normalise it to 10^4 cells per EB.

As a pilot experiment I generated EBs using varying amounts of WT AH016-03

WT and AH016-03 RUNX1$^{\Delta Ex5}$ as follows: 100% WT, 90%WT-10%RUNX1$^{\Delta Ex5}$, 70%WT-30%RUNX1$^{\Delta Ex5}$, 50%WT-50%RUNX1$^{\Delta Ex5}$, 30%WT-70%RUNX1$^{\Delta Ex5}$ and 10%WT-90%RUNX1$^{\Delta Ex5}$. For each condition I generated 48 EBs using a total of 10^4 input hiPSCs per EB and each EB was plated individually in a well of a 96 well plate. After the start of production I counted the number of EBs producing iPS-Mo/Mϕs and the number of nulls in each condition. As can be seen in figure 5.6B the reduction in number of EBs capable of producing iPS-Mo/Mϕs is almost linearly correlated with the drop in number of WT hiPSCs added to the EBs. This reinforces the hypothesis of the differentiation being a random low frequency event. From each condition one can calculate the average bottleneck per EB (λ) and then normalise it to the number of input cells (figure 5.6C). λ varies between 0.98 and 1.36 for all different EB composition conditions. By taking the average and standard deviation of each individually calculated λ we increase greatly the confidence of the result. In this example it would indicate that on average 1.16 ± 0.18 cells per EB passes the bottleneck.

This pilot experiment demonstrates the power of this method for accurately estimating the bottleneck happening during differentiation and has the advantage of not modifying the cells of interest.

5.3.2.2 Effect of MYB$^{\Delta Ex6}$ on the differentiation bottleneck

After validating the method I used the same experimental approach using either AH016-03 WT or MYB$^{\Delta Ex6}$ hiPSCs to investigate if the increase in iPS-Mo/Mϕ production observed in MYB$^{\Delta Ex6}$ hiPSCs is due to a change in the differentiation bottleneck. EBs were closely monitored on a daily basis to detect the start of iPS-Mo/Mϕ production, after start of production the number of EBs producing were scored every two days. This way I generated a time-course of the λ over time. The reason I decided to do a time-course was that AH016-03 MYB$^{\Delta Ex6}$ hiPSCs developed CD45$^+$ CD34$^+$ hematopoietic progenitors earlier than WT controls (Chapter 4 - 4.3.4.6) and therefore could start producing iPS-Mo/Mϕs earlier.

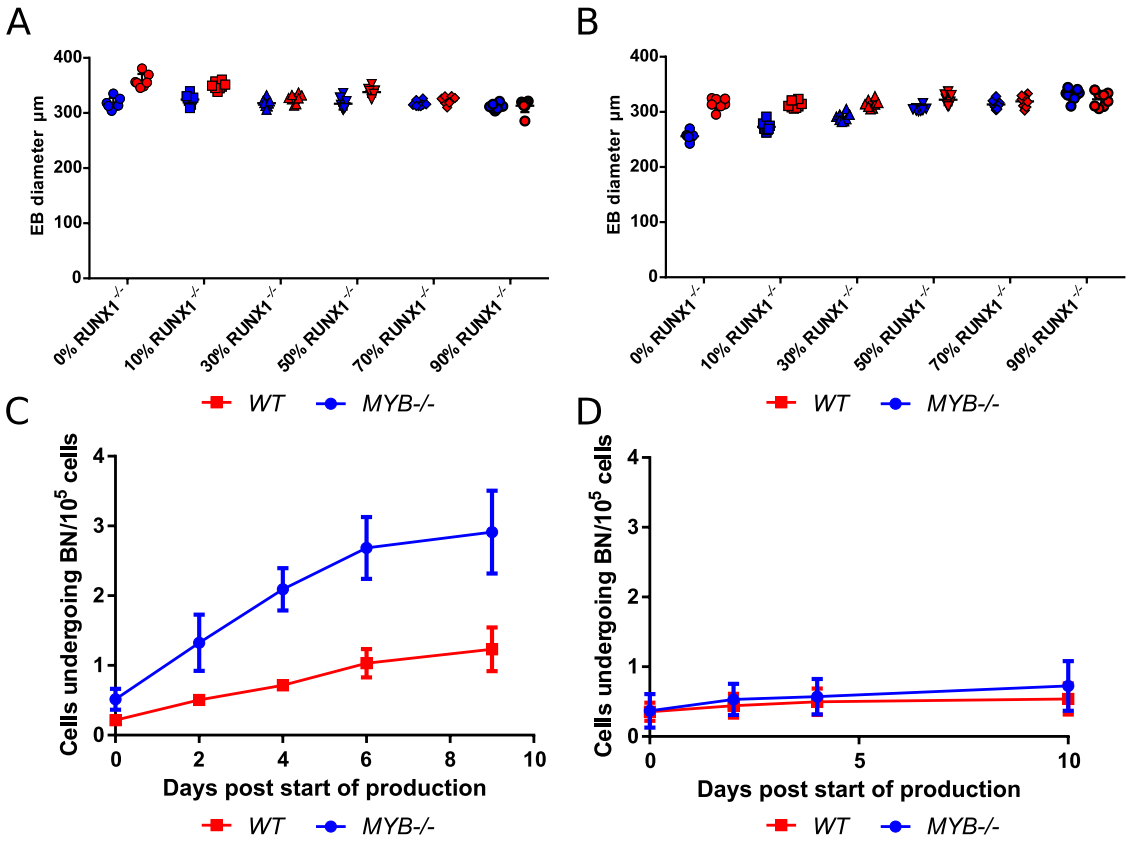

Figure 5.7: Investigating the role of MYB during cell fate decision in hiPSCs differentiation to Mϕ A and B. Quantification of the EB size of each condition, each data point represents the mean diameter in μm calculated from 8 individual EBs. Experiment A and B are two independent repeats. **C and D.** Mean bottleneck (λ) time-course. Each data point represents the mean $\lambda\pm$ SD normalised to 10^4 cells per EB. Each λ has been calculated from 48 individual EBs containing varying numbers of WT/MYB$^{\Delta Ex6}$ and RUNX1$^{\Delta Ex5}$ hiPSCs.

The experiment was run in duplicate and EB size was quantified one day after EB formation (figure 5.7 A and B). In the first experiment, although WT AH016-03 EBs were slightly larger the overall size of the EBs did not vary much with the varying cell composition of the EBs, while in the second experiment, 100% and 90% AH016-03 MYB$^{\Delta Ex6}$ EBs were quite small. When calculating the λ I obtained two very different results in the two replicate experiments (figure 5.7 C and D). Experiment number 1 (figure 5.7 C) shows a clear distinction between AH016-03 MYB$^{\Delta Ex6}$ and AH016-03 WT. AH016-03 MYB$^{\Delta Ex6}$ started producing earlier, and there was an increased hematopoietic commitment as shown by the $\lambda = 2.91 \pm 0.59$ compared to the $\lambda = 1.23 \pm 0.31$ of WT control cells. Experimentally

this resulted in 47/48 EBs producing in the AH016-03 MYB$^{\Delta Ex6}$ condition without addition of AH016-03 RUNX1$^{\Delta Ex5}$. Visually the MYB$^{\Delta Ex6}$ EBs produced vastly more iPS-Mo/Mϕs than the WT counterpart as the wells were rapidly covered with iPS-Mo/Mϕs. While this was a clear result, my second repeat of this experiment did not display any differences between AH016-03 WT and AH016-03 MYB$^{\Delta Ex6}$ and the overall bottleneck is lower, $\lambda = 0.72 \pm 0.33$ for MYB$^{\Delta Ex6}$ and $\lambda = 0.54 \pm 0.20$ for WT (figure 5.7 D). Due to technical and time issues I was not able to repeat this experiment additional times for this thesis. Although I cannot conclude which result is accurate it is worth noting that the first repeat showed a $\lambda = 2.91 \pm 0.59$ for AH016-03 MYB$^{\Delta Ex6}$ which is an about 3 to 6 fold higher than all previous results with WT lines. This shows that under certain conditions the bottleneck can be substantially increased. Investigating this further might uncover previously unappreciated roles for MYB in early human hematopoietic commitment.

5.4 Discussion

In this chapter I have developed two methods for quantifying a rare fate decision event occurring within the EBs leading to the generation of the progenitor of iPS-Mo/Mϕs. The first method, using RFP and GFP expressing hiPSCs, allowed me to show that the bottleneck occurring during iPS-Mo/Mϕ differentiation likely follows Poisson distribution, but this method was technically impracticable for usage with other cell lines. The second method using RUNX1$^{\Delta Ex5}$ allowed for a precise quantification of the bottleneck using a serial dilution of the hiPSCs while maintaining the total EB size. The use of RUNX1$^{\Delta Ex5}$ hiPSCs in the second method also showed that RUNX1$^{\Delta Ex5}$ hiPSCs were capable of supporting hematopoietic development of WT cells while not being able to contributing to the pool of hematopoietic cells. This could open possibilities of using RUNX1$^{\Delta Ex5}$ as feeder cells within the EB which I will detail in the final discussion of this thesis. Using both methods, my results showed that on average, in the WT hiPSCs tested, there is 0.5 to 1 cell per EB undergoing this fate decision and that this event seems to be a randomly distributed low frequency event. However the molecular mechanism

and the moment of fate decision remains unclear. While it is a low frequency event, I have shown that an EB can have two or more cells going through the bottleneck, which is in line with blood islands in the mouse YS being of polyclonal origin (Ueno and Weissman, 2006). In the mouse differentiation using a retrospective *in vivo* clonal analysis, Padron-Barthe et al. have shown hemapoietic lineages in the blood islands are fated as early as the epiblast stage (E6-E6.5) (Padrón-barthe et al., 2014). Mouse cells in the developing epiblast possess pluripotency at the clonal level until E5.5 (Rossant et al., 1978). This would suggest that the fate decision at the origin of the bottleneck could be made very early during hiPSC differentiation. By comparing $MYB^{\Delta Ex6}$ and WT hiPSCs I showed that the bottleneck can be modulated under certain conditions (reaching 2.9 cells/EB in one of the repeats). Although the results using the $MYB^{\Delta Ex6}$ line need to be reproduced, the fact that the bottleneck can reach a λ of 2.9 implies that the differentiation process is far from optimal and could potentially be improved in regards to quantity and polyclonality of iPS-Mo/Mϕs produced. This developmental bottleneck has important technical implications for future experiments which require a large pool of heterogenous iPS-Mo/Mϕs (like GeCKO) and also could have implications in experimental reproducibility and differentiation efficiency. It would therefore be important to understand the limiting factors imposing such a bottleneck to be able to manipulate it and further optimise the production of iPS-Mo/Mϕ. Modulating EB size would be an easy place to start, we already know that EBs of up to 50,000 cells can produce iPS-Mo/Mϕs but do not know if bigger EBs can sustain more progenitors. Investigating if the same restrictions apply in 2D feeder-free and feeder based hiPSC hematopoietic differentiation system would also help in understanding how hiPSC differentiation protocols differ. As a further study it would be interesting to investigate if such bottlenecks apply to the differentiation of other types of cells (neuronal, muscular, etc), as in this current study only the hematopoietic lineage has been studied.

An additional conclusion we can draw from these results is that in a time-frame of 2-4 weeks most hiPSCs derive from a single cell in each EB which would go against

several hematopoietic waves happening in a timely manner during the first weeks, unless the fate decision happens early in differentiation resulting in both waves originating from the same hiPSC. This would need to be properly investigated by doing a controlled time-course of longer periods and trace each EB individually.

6 Discussion

6.1 Summary of results

In this thesis I set out to investigate human mononuclear phagocyte ontogeny and development using a hPSC myeloid differentiation model of hematopoiesis, capable of iPS-Mo/Mϕ production over prolonged periods of time.

As time is a critical component of hematopoietic development and the type of cells produced and organ of production varies greatly over the course of embryonic and fetal life I first set out to investigate how time impacted the transcription profile and function of iPS-Mo/Mϕs.

Using a non-parametric transcriptomic approach I showed that iPS-Mo/Mϕs produced early in differentiation are more proliferative and less immunologically mature than iPS-Mo/Mϕs produced later in differentiation. As discussed earlier this ties in with *in vivo* mouse development where embryonic- and fetal-derived monocytes and Mϕs are more proliferative and displaying a different immunological signature than adult blood monocytes and infiltrating Mϕs.

Using datasets of other human myeloid subtypes I was able to show that the proliferative signature of early and late iPS-Mo/Mϕs was overall stronger than that of primary human blood monocytes and fetal microglia. That being said, only early iPS-Mo/Mϕs were truly proliferative as detected by DNA replication.

By pairwise comparison I was also able to show that early iPS-Mo/Mϕs had weaker immunologic signature than both fetal microglia and blood monocytes. This could be linked to them being more progenitor-like or representing immature Mϕs early in embryonic development, compared to fetal microglia which are already several months old and blood monocytes which derive from adult HSCs. Late iPS-Mo/Mϕs on the other hand were highly similar to fetal microglia. This suggests that iPS-Mo/Mϕ may represent a similar subpopulation of Mϕs as fetal microglia, which would imply a YS origin of iPS-Mo/Mϕs. hPSC development has often been shown to recapitulate early *in vivo* embryonic and fetal hematopoiesis rather than adult BM-hematopoiesis which could explain the iPS-Mo/Mϕs being transcriptionally closer to fetal microglia than adult blood monocytes.

To investigate if the highly similar transcriptional signature of iPS-Mo/Mϕ and fetal microglia was due to the iPS-Mo/Mϕs being of YS-origin, I set out to investigate the transcription factor requirement for their differentiation. Targeting of the MYB transcription factor has been successfully used in the mouse for investigating the ontogeny of tissue resident Mϕs, which are MYB-independent.

As the initial shRNA KD approach was inconclusive I used a CRISPR/Cas9 KO approach which lead to much clearer results. After optimization of the CRISPR/Cas9 protocol I generated three different genetic KOs targeting MYB, RUNX1 and SPI1, which are known to be differentially required during murine hematopoietic differentiation. My results showed that MYB was not required for iPS-Mo/Mϕ differentiation, while SPI1 and RUNX1 were required. MYB-independence has been linked to the first two waves of YS hematopoiesis and therefore iPS-Mo/Mϕs differentiate from a HSC-independent YS-like origin. This indicates that iPS-Mo/Mϕs are ontologically similar to most tissue-resident Mϕs and, therefore, are a good model for the development of tissue-specific Mϕ subtypes *in vitro*. This statement is strengthened by the results obtained in chapter 3, showing that iPS-Mo/Mϕs are transcriptionally similar to fetal microglia. In addition, MYB$^{\Delta Ex6}$ EBs were capable of iPS-Mo/Mϕ production for at least three months, indicating that the

change in transcriptome observed in chapter 3 is unlikely due to a MYB-independent to MYB-dependent switch during the first weeks of differentiation.

While MYB was not required for iPS-Mo/Mϕ generation it did have a positive impact on the number of iPS-Mo/Mϕs produced while having no apparent impact on iPS-Mo/Mϕ function, phenotype or proliferation. Since the increase of production was not linked with iPS-Mo/Mϕ proliferation it was hypothesised to be due to an event upstream of iPS-Mo/Mϕ generation. By flow cytometry I observed an increased number of hematopoietic progenitors within the MYB$^{\Delta Ex6}$ EBs indicating that MYB might impact progenitor differentiation or expansion.

When investigating the lineage potential of the hematopoietic progenitors within the EB at early timepoints in the different KO hiPSC lines I showed that WT EBs generated CFU-E, CFU-GM and CFU-M indicative of erythroid, granulocyte and Mϕ potential of the progenitors within the WT EBs. In contrast when MYB is knocked-out only Mϕ colonies are observed as would be expected if the Mϕs derived from EMPs, as previously discussed. I therefore hypothesised that most iPS-Mo/Mϕs derive from MYB-independent EMPs which lose their erythrocyte and granulocyte differentiation potential when MYB is knocked-out.

In the case of RUNX1 and SPI1 no colonies were observed, indicative of absence of viable progenitors capable of hematopoietic differentiation within the EBs. Primitive erythrocytes are detected in MYB, RUNX1 and SPI1 KO mice and therefore, if they were generated, should be detected in all KO hiPSC conditions. The absence of primitive erythrocyte progenitors is therefore a further indication of an EMP rather than primitive progenitor origin of iPS-Mo/Mϕs. That being said, without proper clonal analysis of the progenitors we cannot exclude the presence of MYB-independent monopotent primitive Mϕ progenitors in our model.

As mentioned previously, MYB KO EBs had elevated numbers of progenitors that give rise to an increased iPS-Mo/Mϕ production capability. However, how early in the differentiation process this occurs was unknown. Within an EB there are technically a finite number of cells fated to hematopoiesis; a number that determines the bottleneck inherent to the differentiation.

In my last chapter I have developed two methods for quantifying the differentiation bottleneck occurring during hiPSC differentiation to iPS-Mo/Mϕs, both for answering several biological questions, such as the increase in MYB$^{\Delta Ex6}$ iPS-Mo/Mϕ production, and improving our technical understanding of the EB differentiation method.

The first method, using RFP and GFP expressing hiPSCs, allowed me to show that the bottleneck occurring during iPS-Mo/Mϕ differentiation broadly follows the Poisson distribution, but this method was technically impracticable for usage with other cell lines. The second method using RUNX1$^{\Delta Ex5}$ allowed for a precise quantification of the bottleneck using a serial dilution of the hiPSCs while maintaining the total EB size. My results showed that on average, in the WT hiPSCs tested, there is 0.5 to 1 cell per EB undergoing this fate decision. However the molecular mechanism and the moment of fate decision remains unclear.

To further investigate the increase in iPS-Mo/Mϕ produced by MYB$^{\Delta Ex6}$ hiPSCs I applied the second method for comparing the bottleneck in WT with that of MYB KO cells and obtained some interesting but inconsistent preliminary results. While I could not conclude on the consistency of the increased bottleneck in MYB KO, I observed a three to 6 fold increase in the number of cells going through the bottleneck in one of the experiments. While this experiment needs to be repeated it showed that the bottleneck could be modulated under certain conditions and did result in much higher differentiation efficiency, as 98% of the EBs produced in that experiment. This technique will be a great tool both to answer biological questions and to improve technical aspects of the differentiation method (see below).

6.2 Implications and perspectives

The main aim of my thesis was to define the developmental origin of iPS-Mo/Mϕs using a transcriptional and knock-out approach. I showed that iPS-Mo/Mϕs derive from MYB-independent, RUNX1- and SPI1-dependent progenitors, tying them to the primitive or EMP wave of hematopoiesis. This has several implications

for their use as a model for *in vitro* studies and their use as a potential source of cells for cellular therapies.

Blood-monocyte-derived Mϕs have been extensively used as an *in vitro* model for studying Mϕ biology. However, with the recent advances in understanding Mϕ development, they may not be ideal for modeling tissue-resident Mϕs at the steady state as they derive from different developmental origins and are thought to be more representative of short-lived infiltrating Mϕs. On the other hand, hiPSC-derived Mϕs, as I have shown, derive from the same ontogeny as MYB-independent Mϕs making them a potentially more relevant model for the development of tissue-resident Mϕs subtypes with long-lived homeostatic functions. Given the importance of Mϕs in tissue homeostasis, housekeeping functions, immunomonitoring and pathological conditions, the generation of iPSC-derived tissue models containing relevant Mϕ populations will be critical for accurate disease modeling using hPSC.

There is currently a need for the development of representative tissue-derived models of Mϕs, particularly models of microglia, as primary human microglia are not easily accessible, and current methods used for their isolation may alter their characteristics and function (Smith et al., 2013). Several protocols have described the derivation of microglia-like cells from blood monocytes (Ohgidani et al., 2014; Etemad et al., 2012) but the phenotypic and transcriptomic signature of these cells is still quite distinct from primary microglia (Butovsky et al., 2014; Melief et al., 2012). Recently a method for deriving microglia from hiPSCs has been described (Muffat et al., 2016) but the yields of this protocol are relatively low (1 to 8x10^6 microglia cells from 2x10^6 hPSCs over the course of 8 weeks). Dr W. Hänseler in the lab has developed a neuronal co-culture based microglia differentiation protocol using iPS-Mo/Mϕs (unpublished data) in which he showed that only after a few days iPS-Mo/Mϕs take ramified microglia morphology, express common microglia markers, and displayed microglial functions as well as a microglial transcriptomic signature. This is an encouraging result indicating that in addition to their MYB-independence iPS-Mo/Mϕs are indeed more adapted for microglial differentiation than blood-derived Mϕs.

The cellular and non-cellular components of the hematopoietic system are extensively used in clinic with the routine use of plasma, platelets, red blood cells as well as HSCs. HSC transplantation has been the most widely used stem cell therapy and one of the most successfully clinical applications of stem cells (Daley, 2012). Since the derivation of human iPSCs there has been a major effort of using iPSCs for the generation of patient specific HSCs (reviewed in (Daniel et al., 2015)). While iPSC-derived HSCs are likely still far from clinical application, the potential of deriving any terminally differentiated hematopoietic cell from human iPSCs has great potential for regenerative medicine and cell therapy.

As MYB-independent tissue-resident Mϕs can be generated from hiPSC they have the potential to be used for clinical applications. There have been several Mϕ transplantation studies done in mouse. Rybalko et al. (2015) have shown that HSC derived M1 polarized Mϕs transplantation could accelerate myofiber repair and decreases fibrotic tissue deposition after tourniquet induced ischemia/reperfusion injury (Rybalko et al., 2015). In the same study non-polarized Mϕs negatively impacting myofiber repair, indicating that polarization of HSC-derived Mϕs prior to transplantation is critical for the outcome. Haga et al. (2014) have generated TAP deficient mES-derived Mϕs which displayed anticancer properties in allogeneic recipient mice, without detectable malignancy (Haga et al., 2014). More recently, Litvack et al. (2016) used mESC-derived Myb$^{-/-}$ alveolar-like Mϕs as a cell source for treating a mouse model of adenosine deaminase deficiency (ADA$^{-/-}$) and showed that these Mϕs remained in healthy airways for at least 4 weeks, are capable of neutrophil phagocytosis during acute lung injury, promote pulmonary tissue repair and promote survival of recipient ADA$^{-/-}$ mice without any pathological damage or teratoma formation (Litvack et al., 2016). These studies show that PSC-derived Mϕs have potential for cell therapy and beneficial effects on pathological conditions as well as tissue repair. Their use in tissue-regeneration also showed a lot of promise compared to blood-derived Mϕs, as they can be derived in an autologous manner, genetically modified, long-lived and are less immunoreactive. In the future iPS-Mo/Mϕs could serve as cells for treating Mϕ disfunction related pathologies

such as chronic granulomatous disease and Hurler syndrome as well as potential broader applications in cancer and tissue-repair. That being said there is still a large gap between the bench and the bed side.

Primitive hematopoiesis and EMPs are often described as a transient wave which does not persist long after HSC emergence (Jagannathan-Bogdan and Zon, 2013). In humans, studies have shown that after 60 days of development no hematopoietic progenitors are detected in the YS any more, also suggesting a transient wave of YS hematopoiesis (Dommergues et al., 1992; Huyhn et al., 1995). My results show production of MYB$^{\Delta Ex6}$ iPS-Mo/Mϕs for at least three months (after which I stopped the experiment) and WT iPS-Mo/Mϕs have been produced for up to one year (van Wilgenburg et al., 2013). As shown in chapter 3, the proliferation of iPS-Mo/Mϕs is minimal after the first weeks of differentiation indicating that iPS-Mo/Mϕ production is not driven by their own proliferation. This would lead to the hypothesis that MYB-independent precursors are maintained within the EBs for prolonged periods while constantly producing iPS-Mo/Mϕs, which suggests the presence of long-lived progenitors present in a form of stem cell niche, potentially capable of asymmetric division. This observation could indicate that MYB-independent hematopoiesis is maintained for longer than expected during human hematopoiesis. In addition, this differentiation model might provide an *in vitro* hematopoietic niche model which would be worth exploring. It is important to note that low rate iPS-Mo/Mϕs proliferation could also account for a large proportion, if not all iPS-Mo/Mϕs produced in later harvests and would need to be formally investigated first. Coupled with the results of the bottleneck (Chapter 5), showing that very few hiPSCs are fated to become iPS-Mo/Mϕs, the data would indicate that possibly only a few of these niches are created per EB. Investigating this early fate decision could teach us a lot about human hematopoietic specification and help improve the efficiency and potentially the type of hematopoietic progenitors produced. In the last months of my DPhil I have applied for a 6 months MRC extension which will allow me to do two follow-up projects, stemming from the results of my thesis.

First, the bottleneck experiment using RUNX1$^{\Delta Ex5}$ hiPSCs showed that it is possible to generate chimeric EBs with 10 to 20% non-producing hiPSCs, with only a limited alteration of the iPS-Mo/Mϕ production. It is known that cytokines and soluble messengers are key in hematopoietic progenitor differentiation and maintenance of the stem cell niche (Robb, 2007), but cell-cell interactions also play a critical role (Kirouac et al., 2009). While soluble factors can be added ectopically, cell-cell interactions are more complex to integrate into a differentiation model, particularly one based on an EB method. I hypothesis that expression of receptor ligands on RUNX1$^{\Delta Ex5}$ hiPSCs could induce beneficial signalling cascades in the neighbouring WT hiPSCs. The concept of transducing feeder cells with a receptor ligand is not new as it has been successfully used previously in non-EB based differentiation of lymphoid lineages using OP9 feeder cells transduced with the notch ligands DL1 and/or DL4 (Timmermans et al., 2009; Kennedy et al., 2012; Uenishi et al., 2014; Sturgeon et al., 2014; Ferrell et al., 2015). The notch signalling pathway acts via direct cell-to-cell contact and plays a central role in hematopoietic fate decision and in the maintenance of the HSC niche (Butko et al., 2015). For this purpose I have generated lentiviral constructs for inducible expression of DL-1 or DL-4, and have transduced RUNX1$^{\Delta Ex5}$ hiPSCs. The goal is to investigate if inducing notch signalling at a given point during differentiation in a subpopulations of the cells within the EB has an impact on hematopoietic commitment and lineage choice. This project relies on the assumption that RUNX1 knock-out does not affect the supportive role of the RUNX1$^{-/-}$ feeder iPSCs. While there is no evidence for RUNX1 playing such a role, it is worth keeping in mind, as other transcription factors such as HOXB4 can have both a autocrine and paracrine effect in mESC chimeric EB models (Jackson et al., 2012). Several initial readouts can be used such as colony forming potential and change in the bottleneck, but ultimately I am interested in improving hematopoietic commitment and potentially shifting the balance of differentiation from primitive to more definitive hematopoietic lineage. Second, with the advances in CRISPR/Cas9 technology new possibilities are available for investigating early hematopoietic fate decision. Identifying where

and when this fate decision occurs would be of great scientific value as it would allow us to study this fate decision and potentially modulate it in the future. In the mouse one of the earliest tractable marker indicative of hematopoietic commitment is the RUNX1+23 enhancer activity which marks the onset of EHT (Swiers et al., 2013). In collaboration with the group of Prof. Marella De Bruijn at the Weatherall Institute for Molecular Medicine (WIMM) I am generating a human mCherry-RUNX1+23 enhancer knock-in reporter hiPSC line. This reporter line should allow for the tracking of hemogenic endothelial commitment and EHT in hiPSCs. This has many applications, such as locating the emergence of HE within the EBs, tracking it's maintenance over time and quantifying the number of different locations in which hematopoietic cells are generated. This reporter line should give us new tools for isolating HE as well as studying the underlying mechanics of early EHT and in combination with the murine work of Prof. De Bruijn it will allow us to bridge the knowledge gap between mouse and human hematopoietic development and contribute ultimately to the necessary knowledge for the generation of HSCs *in vitro*. To conclude, I think it is vital to better understand how *in vivo* and *in vitro* hematopoiesis is regulated as this knowledge is necessary for the development of relevant models of pathology, drug discovery and ultimately the use of hiPSCs as a source of HSCs and mature hematopoietic cells for cell therapy and transplantation.

Appendices

A Appendix

Contents

A.1 EdU staining 163
A.2 Rank Product 164

A.1 EdU staining

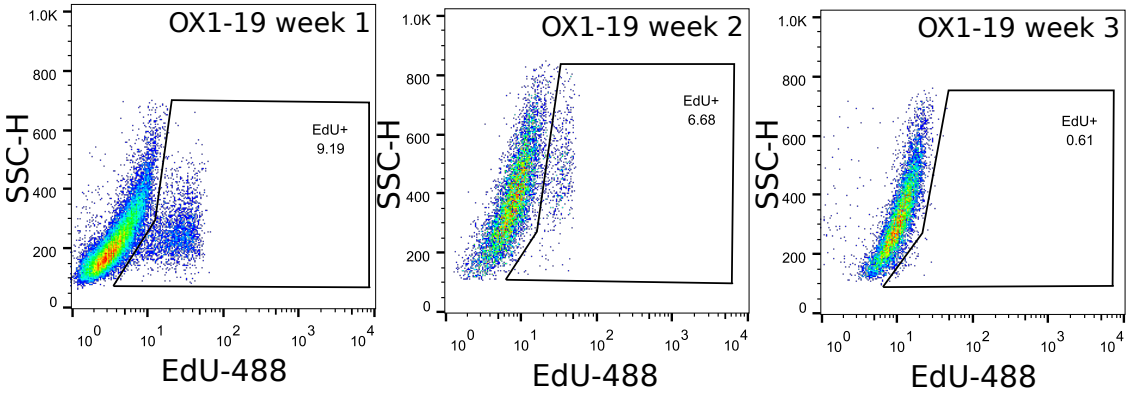

Figure A.1: Supplementary EdU staining of iPS-Mo/Mϕ over time. Freshly harvested OX1-19 iPS-Mo/Mϕs obtained from three different harvests (week 1, 2 and 3 after start of production) were pulsed for 2h with EdU and $CD14^{+}EdU^{+}$ cells that had undergone DNA replication were detected by flow cytometry after Click-iT staining.

A.2 Rank Product

The following R code (rankprod.R script) for the ranked product approach based on the work of Heskes et al. for assessing the differential gene expression (Heskes et al., 2014) was provided by Quin Wills (Oxford Wellcome Trust Centre for Human Genetics).

```
# Rank Product
###############

# My function below, with the core Breitling functions following

getRP <- function(rp,fdr=0.05) {

  require("qvalue")

  RP <- apply(rp,2,function(i) rank(-i)) # test for increased expression
  RP <- apply(RP,1,prod) # rank product
  RP <- rankprodbounds(RP,n=length(RP),k=ncol(rp),Delta="geometric")
  RP <- qvalue(RP,fdr.level=fdr)
  result <- data.frame(delta=apply(rp,1,mean),max_logP=NA,high_pvalue=RP$pvalues,high_qvalue=RP$qvalues,
                       high_significant=RP$significant,low_pvalue=NA,low_qvalue=NA,low_significant=NA)
  row.names(result) <- row.names(rp)

  RP <- apply(rp,2,function(i) rank(i)) # test for decreased expression
  RP <- apply(RP,1,prod)
  RP <- rankprodbounds(RP,n=length(RP),k=ncol(rp),Delta="geometric")
  RP <- qvalue(RP,fdr.level=fdr)
  result$low_pvalue <- RP$pvalues
  result$low_qvalue <- RP$qvalues
  result$low_significant <- RP$significant

  result$max_logP <- -log10(result$high_pvalue) # rank by maximum overall logP
  result$max_logP[result$low_pvalue<result$high_pvalue] <- -log10(result$low_pvalue)[result$low_pvalue<result$high_pvalue]
  result <- result[order(result$max_logP,decreasing=T),]
  result
}

# rankprodbounds
#
# Description
#
# This function computes bounds on the p-value for rank products.
#
# Usage
```

```
#
# rankprodbounds(rho,n,k,Delta = c('lower','upper','geometric'))
#
# Arguments
#
# rho     a vector of integers corresponding to the rank products for which one wishes to
#         compute the p-value.
# n       the number of molecules.
# k       the number of replicates.
# Delta   a character string indicating whether an upper bound ('upper'), lower bound
#         ('lower'), or geometric approximation ('geometric') should be computed.
#
# Value
#
# A vector of p-values, one for each rank product.
#
# Details
#
# The exact p-value is guaranteed to be in between the lower and the upper bound. The
# geometric mean of the two bounds can be used as an approximation. Each bound is a piecewise
# continuous function of the rank product. The different pieces each have an analytic form,
# the parameters of which can be computed recursively.
#
# Note
#
# This implementation closely follows the description in Heskes, Eisinga, Breitling:
# "A fast algorithm for determining bounds and accurate approximate p-values of the
# rank product statistic for replicate experiments", BMC Bioinformatics, referred to
# below to as HEB. More specifically, this R function corresponds to the recursive variant,
# sketched as pseudocode in the additional material of HEB.

rankprodbounds <- function(rho,n,k,Delta){

  # INPUT HANDLING

  if(any(rho > n^k)  any(rho < 1)) stop('rho out of bounds')

  if(is.numeric(Delta) == FALSE) {
    if(Delta == 'geometric') {
      temp1 <- rankprodbounds(rho,n,k,'upper')
      temp2 <- rankprodbounds(rho,n,k,'lower')
      pvalue <- sqrt(temp1*temp2)   # geometric mean of upper and lower bound
      return(pvalue)
    }
```

```
    else {
      Delta <- switch(Delta,
                      upper = 1,        # for computing upper bound
                      lower = 0)        # for computing lower bound
    }
  }


  # COMPUTE INTERVALS THAT CONTAIN THE RANK PRODUCTS

  logn <- log(n)
  allj <- ceiling(-(log(rho)/logn)+k)   # index specifying the
      interval that contains rho
  minj <- min(allj)                     # lowest interval index
  maxj <- max(allj)                     # highest interval index


  # INITIALIZE PARAMETERS

  param <- matrix(list(), nrow=k+1, ncol=maxj+1)
  for(i in 1:(k+1)){
    for(j in 1:(maxj+1)){
      param[[i,j]] <- list(a=c(),b=c(),c=c(),d=c(),e=c())
    }
  }

  # param is a matrix of lists; each element of param is a list with
      values for the parameters
  # a through e, which correspond to the parameters alpha through
      epsilon in HEB;
  # specifially, param[[i+1,j+1]]$a corresponds to alpha_{i,j} in HEB,
       etc, where the offset
  # of 1 is introduced to be able to represent, for example, alpha_
      {0,0};
  # a, b, and c can be vectors (with possibly different lengths for
      different i and j),
  # d and e are scalars


  # COMPUTE PARAMETERS

  for(j in minj:maxj){
    param <- updateparam(param,n,k,j,Delta)
  }

  # call to the function updateparam which recursively computes all
      parameters that are needed
  # to calculate the p-value for a rank product rho that lies in the
      interval with index j


  # COMPUTE RANK PRODUCTS GIVEN PARAMETERS

  k1 <- 1+k
  G <- rep(0,length(rho))    # G is a vector of the same length as rho,
```

```
  # for each rho bounding the number of rank products
  for(j in minj:maxj) {
    j1 <- 1+j
    iii <- which(allj == j)          # indices of all rank products
        that fall in interval j:
    # bounds for these rank products can be computed with
    # the same set of parameters
    thisrho <- rho[iii]
    thisparam <- param[[k1,j1]]
    thisG <- thisparam$e
    if(j != 0) {
      nrho <- length(thisrho)
      nterms <- length(thisparam$a)
      thisG <- thisG + thisparam$d*thisrho
      d1 <- matrix(thisparam$c) %*% thisrho
      d2 <- matrix(rep(log(thisrho),nterms),nrow=nterms,byrow=TRUE) -
          t(matrix(rep(logn*(k-j+thisparam$b),nrho),nrow=nrho,byrow=
              TRUE))
      d3 <- t(matrix(rep(thisparam$a,nrho),nrow=nrho,byrow=TRUE))
      thisG <- thisG + colSums(d1*(d2^d3))
    }
    # the 10 lines above implement equation (8) in HEB
    G[iii] <- thisG
  }

  pvalue <- G/n^k
  return(pvalue)
}

###################################
#
# updateparam
#
# Description
#
# This subroutine updates the current set of parameters to make sure
    that the parameters
# corresponding to k replicates and the j'th interval are included.
#
# Arguments
#
# param   a matrix of lists, where each element of param is a list
    with values for the
#         parameters a through e; these parameters specify the
    functional form of the bound;
#         a, b, and c are all vectors of unknown length, d and e are
    scalars.
# n       the number of molecules.
# k       the number of replicates for which we need to compute the
    corresponding parameters.
# j       the index of the interval for which we need to compute the
    corresponding parameters.
# Delta   0 for the lower bound and 1 for the upper bound.
#
# Value
```

```
#
# A possibly updated set of parameters, at least including those corresponding to (k,j).
#
# Details
#
# This subroutine make sure that the parameters corresponding to k replicates and a rank product
# within the j'th interval are included. If they already are (because calculated before), it
# does not compute anything. Otherwise, it recursively computes all parameters
# that are needed to arrive at the parameters for (k,j).
#
# Note
#
# This implementation closely follows HEB, in particular equations (9) through (11).

updateparam <- function(param,n,k,j,Delta) {

  k1 <- 1+k
  j1 <- 1+j

  if(length(param[[k1,j1]]$e) == 0) {  # apparently empty, so needs to be calculated

    if(j == 0) {   # initializing G_{k0}

      param[[k1,j1]]$e <- n^k
      param[[k1,j1]]$d <- 0
      # the 2 lines above implement equation (11) in HEB

    }
    else {
      k0 <- k1-1
      j0 <- j1-1
      param <- updateparam(param,n,k-1,j-1,Delta)
      # checking that the parameters for (k-1,j-1) that are needed to compute the
      # parameters for (k,j) are indeed available; if not, they are themselves computed
      param00 = param[[k0,j0]]
      newa0 = param00$a+1
      newb0 = param00$b
      newc0 = param00$c/newa0
      param11 = param00
      # the 5 lines above predefine some parameters common to equations (9) and (10) in HEB

      if(k == j){ # updates for G_{kk}

        param11$e <- (1-Delta)*(1-param00$e)
        param11$d <- Delta*param00$d+param00$e
        param11$a <- c(1,param00$a,newa0)
```

```
223           param11$b <- c(0,param00$b,newb0)
224           param11$c <- c(param00$d,Delta*param00$c,newc0)
225           # the 5 lines above implement equation (10) in HEB
226         }
227         else {  # updates for G_{kj}, j < k
228           param <- updateparam(param,n,k-1,j,Delta)
229           # checking that the parameters for (k-1,j) that are needed to
                compute the
230           # parameters for (k,j) are indeed available; if not, they are
                themselves computed
231           param01 <- param[[k0,j1]]
232
233           logn <- log(n)
234           lognnkj <- (k-j)*logn
235           newa1 <- param01$a+1
236           newa <- c(newa0,newa1)
237           newb <- c(newb0,param01$b)
238           newc <- c(newc0,-param01$c/newa1)
239           param11$e <- n*param01$e + (Delta-1)*(param00$e-param01$e)
240           lognminb <- c(-1*param00$b * logn,(1-param01$b)*logn)
241           param11$d <- Delta*param00$d + (1-Delta)*param01$d/n +
242             (param00$e-param01$e)/exp(lognnkj) -
243             sum(newc*(lognminb^newa))
244           param11$a <- c(1,1,param00$a,param01$a,newa)
245           param11$b <- c(0,1,param00$b,param01$b,newb)
246           param11$c <- c(param00$d,-param01$d,
247                          Delta*param00$c,(1-Delta)*param01$c/n,newc)
248           # the 15 lines above implement equation (9) in HEB
249         }
250         param[[k1,j1]] <- makeunique(param11)
251         # although not strictly necessary, the a, b and c vectors can
              possibly be shortened by
252         # restricting oneselves to unique combinations of a and b values
253       }
254     }
255     return(param)
256   }
257
258   ##################################
259   #
260   # makeunique
261   #
262   # Description
263   #
264   # This subroutine updates the parameters for a specific number of
        replicates and interval
265   # such that it contains only unique combinations of the parameters a
        and b.
266   #
267   # Arguments
268   #
269   # param   a single list with values for the parameters a through e;
        these parameters
270   #         specify the functional form of the bound; a, b, and c are
        all vectors of
```

```
271 #          unknown length, d and e are scalars.
272 #
273 # Value
274 #
275 # A possibly updated and then more concise set of parameters
      containing only unique
276 # combinations of the parameters a and b.
277 #
278 # Details
279 #
280 # While updating the vectors a and b, one may end up with the exact
      same combinations of
281 # a and b. Given the functional form of the bound, the representation
      can then be made more
282 # concise by simply adding the corresponding elements of c.
283
284 makeunique <- function(param) {
285
286   ab <- t(rbind(param$a,param$b))
287   uniqueab <- unique(ab)
288   nunique <- dim(uniqueab)[1]
289   param$a <- t(uniqueab[,1])
290   param$b <- t(uniqueab[,2])
291   newc <- rep(0,nunique)
292   for(i in 1:nunique) {
293     iii <- intersect(which(ab[,1]==uniqueab[i,1]),which(ab[,2]==
          uniqueab[i,2]))
294     newc[i] <- sum(param$c[iii])
295   }
296   param$c <- newc
297
298   return(param)
299
300 }
```

Bibliography

Ackermann, M., Liebhaber, S., Klusmann, J.H., Lachmann, N., 2015. Lost in translation: pluripotent stem cell-derived hematopoiesis. EMBO Mol. Med. 7, 1388–402.

Ajami, B., Bennett, J.L., Krieger, C., McNagny, K.M., Rossi, F.M.V., 2011. Infiltrating monocytes trigger EAE progression, but do not contribute to the resident microglia pool. Nat. Neurosci. 14, 1142–1149.

Ajami, B., Bennett, J.L., Krieger, C., Tetzlaff, W., Rossi, F.M.V., 2007. Local self-renewal can sustain CNS microglia maintenance and function throughout adult life. Nat. Neurosci. 10, 1538–43.

Alasoo, K., Martinez, F.O., Hale, C., Gordon, S., Powrie, F., Dougan, G., Mukhopadhyay, S., Gaffney, D.J., 2015. Transcriptional profiling of macrophages derived from monocytes and iPS cells identifies a conserved response to LPS and novel alternative transcription. Sci. Rep. 5, 12524.

Anderson, J.S., Bandi, S., Kaufman, D.S., Akkina, R., 2006. Derivation of normal macrophages from human embryonic stem (hES) cells for applications in HIV gene therapy. Retrovirology 3, 24.

Anderson, K.L., Smith, K.A., Conners, K., Mckercher, S.R., Maki, R.A., Bruce, E., Anderson, B.K.L., Torbett, B.E., 1998. Myeloid Development Is Selectively Disrupted in PU.1 Null Mice Karen. Blood 91, 3702–3710.

Back, J., Dierich, A., Bronn, C., Kastner, P., Chan, S., Dc, W., 2004. PU . 1 determines the self-renewal capacity of erythroid progenitor cells Plenary paper PU . 1 determines the self-renewal capacity of erythroid progenitor cells. Blood 103, 3615–3623.

Bain, C.C., Bravo-Blas, A., Scott, C.L., Gomez Perdiguero, E., Geissmann, F., Henri, S., Malissen, B., Osborne, L.C., Artis, D., Mowat, A.M., 2014. Constant replenishment from circulating monocytes maintains the macrophage pool in the intestine of adult mice. Nat. Immunol. 15, 929–37.

Bain, C.C., Scott, C.L., Uronen-Hansson, H., Gudjonsson, S., Jansson, O., Grip, O., Guilliams, M., Malissen, B., Agace, W.W., Mowat, a.M., 2013. Resident and pro-inflammatory macrophages in the colon represent alternative context-dependent fates of the same Ly6C(hi) monocyte precursors. Mucosal Immunol. 6, 498–510.

Belhareth, R., 2015. Macrophage populations and self-renewal: Changing the paradigm. World J. Immunol. 5, 131.

Bertrand, J.Y., Jalil, A., Klaine, M., Jung, S., Cumano, A., Godin, I., 2005. Three pathways to mature macrophages in the early mouse yolk sac. Blood 106, 3004–11.

Bigley, V., Haniffa, M., Doulatov, S., Wang, X.N., Dickinson, R., McGovern, N., Jardine, L., Pagan, S., Dimmick, I., Chua, I., Wallis, J., Lordan, J., Morgan, C., Kumararatne, D.S., Doffinger, R., van der Burg, M., van Dongen, J., Cant, A.,

Dick, J.E., Hambleton, S., Collin, M., 2011. The human syndrome of dendritic cell, monocyte, B and NK lymphoid deficiency. J. Exp. Med. 208, 227–34.

Blohmke, C.J., Darton, T.C., Jones, C., Suarez, N.M., Waddington, C.S., Angus, B., Zhou, L., Hill, J., Clare, S., Kane, L., Mukhopadhyay, S., Schreiber, F., Duque-Correa, M.A., Wright, J.C., Roumeliotis, T.I., Yu, L., Choudhary, J.S., Mejias, A., Ramilo, O., Shanyinde, M., Sztein, M.B., Kingsley, R.A., Lockhart, S., Levine, M.M., Lynn, D.J., Dougan, G., Pollard, A.J., 2016. Interferon-driven alterations of the host's amino acid metabolism in the pathogenesis of typhoid fever. J. Exp. Med. , jem.20151025.

Bloom, W., Bartelmez, G.W., 1940. Hematopoiesis in young human embryos. Am. J. Anat. 67, 21–53.

Böiers, C., Carrelha, J., Lutteropp, M., Luc, S., Green, J., Azzoni, E., Woll, P., Mead, A., Hultquist, A., Swiers, G., Perdiguero, E.G., Macaulay, I., Melchiori, L., Luis, T., Kharazi, S., Bouriez-Jones, T., Deng, Q., Ponten, A., Atkinson, D., Jensen, C., Sitnicka, E., Geissmann, F., Godin, I., Sandberg, R., De Bruijn, M., Jacobsen, S.E., 2013. Lymphomyeloid Contribution of an Immune-Restricted Progenitor Emerging Prior to Definitive Hematopoietic Stem Cells. Cell Stem Cell , 535–548.

Bolstad, B., Irizarry, R., Astrand, M., Speed, T., 2003. A comparison of normalization methods for high density oligonucleotide array data based on variance and bias. Bioinformatics 19, 185–193.

Boyle, W.J., Simonet, W.S., Lacey, D.L., 2003. Osteoclast differentiation and activation. Nature 423, 337–42.

Breitling, R., Armengaud, P., Amtmann, A., Herzyk, P., 2004. Rank products: A simple, yet powerful, new method to detect differentially regulated genes in replicated microarray experiments. FEBS Lett. 573, 83–92.

Brogna, S., Wen, J., 2009. Nonsense-mediated mRNA decay (NMD) mechanisms. Nat. Struct. Mol. Biol. 16, 107–13.

Broxmeyer, H.E., Sherry, B., Lu, L., Cooper, S., Carow, C., Wolpe, S.D., Cerami, A., 1989a. Myelopoietic enhancing effects of murine macrophage inflammatory proteins 1 and 2 on colony formation in vitro by murine and human bone marrow granulocyte/macrophage progenitor cells. J. Exp. Med. 170, 1583–1593.

Broxmeyer, H.E., Sherry, B., Lu, L., Cooper, S., Carow, C., Wolpe, S.D., Cerami, A., 1989b. Myelopoietic enhancing effects of murine macrophage inflammatory proteins 1 and 2 on colony formation in vitro by murine and human bone marrow granulocyte/macrophage progenitor cells. J. Exp. Med. 170, 1583–1593.

Bruttger, J., Karram, K., Wörtge, S., Regen, T., Marini, F., Hoppmann, N., Klein, M., Blank, T., Yona, S., Wolf, Y., Mack, M., Pinteaux, E., Müller, W., Zipp, F., Binder, H., Bopp, T., Prinz, M., Jung, S., Waisman, A., 2015. Genetic Cell Ablation Reveals Clusters of Local Self-Renewing Microglia in the Mammalian Central Nervous System. Immunity 43, 92–107.

Buchrieser, J., James, W., Moore, M.D., 2017. Human Induced Pluripotent Stem Cell-Derived Macrophages Share Ontogeny with MYB-Independent Tissue-Resident Macrophages. Stem Cell Reports 8.

Butko, E., Pouget, C., Traver, D., 2015. Complex regulation of HSC emergence by the Notch signaling pathway. Dev. Biol. 409, 129–138.

Butovsky, O., Jedrychowski, M.P., Moore, C.S., Cialic, R., Lanser, A.J., Gabriely, G., Koeglsperger, T., Dake, B., Wu, P.M., Doykan, C.E., Fanek, Z., Liu, L., Chen, Z., Rothstein, J.D., Ransohoff, R.M., Gygi, S.P., Antel, J.P., Weiner, H.L., 2014. Identification of a unique TGF-β-dependent molecular and functional signature in microglia. Nat. Neurosci. 17, 131–43.

Chang, K.H., Nelson, A.M., Cao, H., Wang, L., Nakamoto, B., Ware, C.B., Papayannopoulou, T., 2006. Definitive-like erythroid cells derived from human embryonic stem cells coexpress high levels of embryonic and fetal globins with little or no adult globin. Blood 108, 1515–23.

Charbord, B.P., Tavian, M., Humeau, L., Peault, B., 1996. Early Ontogeny of the Human Marrow From Long Bones: An Immunohistochemical Study of Hematopoiesis and Its Microenvironment. Blood 10, 4109–4119.

Chawla, A., Nguyen, K.D., Goh, Y.P.S., 2011. Macrophage-mediated inflammation in metabolic disease. Nat. Rev. Immunol. 11, 738–49.

Chen, M.J., Yokomizo, T., Zeigler, B.M., Dzierzak, E., Speck, N.a., 2009. Runx1 is required for the endothelial to haematopoietic cell transition but not thereafter. Nature 457, 887–91.

Chia, R., Achilli, F., Festing, M.F., Fisher, E.M., 2005. The origins and uses of mouse outbred stocks. Nat Genet 37, 1181–1186.

Choi, K., Kennedy, M., Kazarov, a., Papadimitriou, J.C., Keller, G., 1998. A common precursor for hematopoietic and endothelial cells. Development 125, 725–732.

Choi, K.D., Vodyanik, M., Slukvin, I.I., 2011. Hematopoietic differentiation and production of mature myeloid cells from human pluripotent stem cells. Nat. Protoc. 6, 296–313.

Choi, K.D., Vodyanik, M.A., Slukvin, I.I., 2009. Generation of mature human myelomonocytic cells through expansion and differentiation of pluripotent stem cell-derived lin-CD34+CD43 +CD45+ progenitors. J. Clin. Invest. 119, 2818–2829.

Choi, K.D., Vodyanik, M.a., Togarrati, P.P., Suknuntha, K., Kumar, A., Samarjeet, F., Probasco, M.D., Tian, S., Stewart, R., Thomson, J.a., Slukvin, I.I., 2012. Identification of the hemogenic endothelial progenitor and its direct precursor in human pluripotent stem cell differentiation cultures. Cell Rep. 2, 553–67.

Chorro, L., Sarde, A., Li, M., Woollard, K.J., Chambon, P., Malissen, B., Kissenpfennig, A., Barbaroux, J.B., Groves, R., Geissmann, F., 2009. Langerhans cell (LC) proliferation mediates neonatal development, homeostasis, and inflammation-associated expansion of the epidermal LC network. J. Exp. Med. 206, 3089–100.

Chow, A., Lucas, D., Hidalgo, A., Méndez-Ferrer, S., Hashimoto, D., Scheiermann, C., Battista, M., Leboeuf, M., Prophete, C., van Rooijen, N., Tanaka, M., Merad, M., Frenette, P.S., 2011. Bone marrow CD169+ macrophages promote the retention of hematopoietic stem and progenitor cells in the mesenchymal stem cell niche. J. Exp. Med. 208, 261–71.

Ciau-Uitz, A., Monteiro, R., Kirmizitas, A., Patient, R., 2014. Developmental hematopoiesis: Ontogeny, genetic programming and conservation. Exp. Hematol. 42, 669–683.

Clarke, D., Vegiopoulos, a., Crawford, a., Mucenski, M., Bonifer, C., Frampton, J., 2000. In vitro differentiation of c-myb(-/-) ES cells reveals that the colony forming capacity of unilineage macrophage precursors and myeloid progenitor commitment are c-Myb independent. Oncogene 19, 3343–51.

Cong, L., Ran, F.A., Cox, D., Lin, S., Barretto, R., Habib, N., Hsu, P.D., Wu, X., Jiang, W., Marraffini, L.A., Zhang, F., 2013. Multiplex Genome Engineering Using CRISPR/Cas System. Science (80-.). 339, 403–406. 20.

Consortium, T.G.O., 2000. Gene ontology: Tool for the identification of biology. Nat. Genet. 25, 25–29.

Cook, D.N., 1996. The role of MIP-1 alpha in inflammation and hematopoiesis. J. Leukoc. Biol. 59, 61–66.

Cowan, C.A., Klimanskaya, I., Mcmahon, J., Atienza, J., Witmyer, J., Zucker, J.P., Wang, S., Morton, C.C., Mcmahon, A.P., Powers, D., Melton, D.A., 2004. Derivation of Embryonic Stem-Cell Lines from Human Blastocysts. N Engl J Med 350, 1353–1356.

Cowley, S.A., Karlsson, K.R., Pelchen-matthews, A., Miller, J., Moore, M.D., James, W., 2012. Macrophages from Human Pluripotent Stem Cells. Handb. Macrophages 44.

Cumano, A., Godin, I., 2007. The Ontogeny of the Hematopoietic System. Annu. Rev. Immunol. , 745–85.

Daley, G.Q., 2012. The promise and perils of stem cell therapeutics. Cell Stem Cell 10, 740–9.

Daniel, M.G., Pereira, C.F., Lemischka, I.R., Moore, K.a., 2015. Making a Hematopoietic Stem Cell. Trends Cell Biol. xx, 1–13.

Davies, L.C., Jenkins, S.J., Allen, J.E., Taylor, P.R., 2013a. Tissue-resident macrophages. Nat. Immunol. 14, 986–95.

Davies, L.C., Rosas, M., Jenkins, S.J., Liao, C.T., Scurr, M.J., Brombacher, F., Fraser, D.J., Allen, J.E., Jones, S.a., Taylor, P.R., 2013b. Distinct bone marrow-derived and tissue-resident macrophage lineages proliferate at key stages during inflammation. Nat. Commun. 4, 1886.

Davis, R.P., Ng, E.S., Costa, M., Mossman, A.K., Sourris, K., Elefanty, A.G., Stanley, E.G., 2008. Targeting a GFP reporter gene to the MIXL1 locus of human embryonic stem cells identifies human primitive streak-like cells and enables isolation of primitive hematopoietic precursors. Blood 111, 1876–84.

Dias, J., Gumenyuk, M., Kang, H., Vodyanik, M., Yu, J., Thomson, J.a., Slukvin, I.I., 2011. Generation of red blood cells from human induced pluripotent stem cells. Stem Cells Dev. 20, 1639–47.

Ditadi, A., Sturgeon, C.M., Tober, J., Awong, G., Kennedy, M., Yzaguirre, A.D., Azzola, L., Ng, E.S., Stanley, E.G., French, D.L., Cheng, X., Gadue, P., Speck, N.A., Elefanty, A.G., Keller, G., 2015. Human definitive haemogenic endothelium and arterial vascular endothelium represent distinct lineages. Nat. Cell Biol. 17, 580–91.

Doetschman, T.C., Eistetter, H., Katz, M., Schmidt, W., Kemler, R., 1985. The in vitro development of blastocyst-derived embryonic stem cell lines: formation of visceral yolk sac, blood islands and myocardium. J. Embryol. Exp. Morphol. 87, 27–45.

Dommergues, M., Aubény, E., Dumez, Y., Durandy, A., Coulombel, L., 1992. Hematopoiesis in the human yolk sac: quantitation of erythroid and granulopoietic progenitors between 3.5 and 8 weeks of development. Bone Marrow Transplant. , 23–27.

Drabsch, Y., Hugo, H., Zhang, R., Dowhan, D.H., Miao, Y.R., Gewirtz, A.M., Barry, S.C., Ramsay, R.G., Gonda, T.J., 2007. Mechanism of and requirement for estrogen-regulated MYB expression in estrogen-receptor-positive breast cancer cells. Proc. Natl. Acad. Sci. U. S. A. 104, 13762–7.

Durafourt, B.A., Moore, C.S., Blain, M., Antel, J.P., 2013. Isolating, Culturing, and Polarizing Primary Human Adult and Fetal Microglia. Microglia Methods Protoc. 1041, 199–211.

Eilken, H.M., Nishikawa, S.I., Schroeder, T., 2009. Continuous single-cell imaging of blood generation from haemogenic endothelium. Nature 457, 896–900.

Ellis, E.L., Delbrück, M., 1939. THE GROWTH OF BACTERIOPHAGE. J. Gen. Physiol. 22, 365–384.

England, S.J., McGrath, K.E., Frame, J.M., Palis, J., 2011. Immature erythroblasts with extensive ex vivo self-renewal capacity emerge from the early mammalian fetus. Blood 117, 2708–2717.

Epelman, S., Lavine, K.J., Beaudin, A.E., Sojka, D.K., Carrero, J.a., Calderon, B., Brija, T., Gautier, E.L., Ivanov, S., Satpathy, A.T., Schilling, J.D., Schwendener, R., Sergin, I., Razani, B., Forsberg, E.C., Yokoyama, W.M., Unanue, E.R., Colonna, M., Randolph, G.J., Mann, D.L., 2014. Embryonic and adult-derived resident cardiac macrophages are maintained through distinct mechanisms at steady state and during inflammation. Immunity 40, 91–104.

Eroğlu, a., Demirci, S., Akbulut, H., Sever, N., Demirer, S., Unal, a.E., 2002. Effect of granulocyte-macrophage colony-stimulating factor on hepatic regeneration after 70% hepatectomy in normal and cirrhotic rats. HPB (Oxford). 4, 67–73.

Etemad, S., Zamin, R.M., Ruitenberg, M.J., Filgueira, L., 2012. A novel in vitro human microglia model: Characterization of human monocyte-derived microglia. J. Neurosci. Methods 209, 79–89.

Evans, M.J., Kaufman, M.H., 1981. Establishment in culture of pluripotential cells from mouse embryos.

Fehling, H.J., 2003. Tracking mesoderm induction and its specification to the hemangioblast during embryonic stem cell differentiation. Development 130, 4217–4227.

Feng, Q., Shabrani, N., Thon, J.N., Huo, H., Thiel, A., Machlus, K.R., Kim, K., Brooks, J., Li, F., Luo, C., Kimbrel, E.A., Wang, J., Kim, K.S., Italiano, J., Cho, J., Lu, S.J., Lanza, R., 2014. Scalable generation of universal platelets from human induced pluripotent stem cells. Stem Cell Reports 3, 817–831.

Ferrell, P.I., Xi, J., Ma, C., Adlakha, M., Kaufman, D.S., 2015. The RUNX1 +24 enhancer and P1 promoter identify a unique subpopulation of hematopoietic progenitor cells derived from human pluripotent stem cells. Stem Cells 33, 37–54.

Flynn, R., Grundmann, A., Renz, P., Hänseler, W., James, W.S., Cowley, S.A., Moore, M.D., 2015. CRISPR-mediated genotypic and phenotypic correction of a chronic granulomatous disease mutation in human iPS cells. Exp. Hematol. 43, 838–848.

Frame, J.M., McGrath, K.E., Palis, J., 2013. Erythro-myeloid progenitors: "Definitive" hematopoiesis in the conceptus prior to the emergence of hematopoietic stem cells. Blood Cells, Mol. Dis. 51, 220–225.

French, A., Yang, C.T., Taylor, S., Watt, S.M., Carpenter, L., 2015. Human Induced Pluripotent Stem Cell-Derived B Lymphocytes Express sIgM and Can be Generated via a Hemogenic Endothelium Intermediate. Stem Cells Dev. 00, 150225071446008.

Fukuda, T., 1973. Fetal Hemopoiesis. I. Electron Microscopic Studies on Human Yolk Sac Hemopoiesis. Virchows Arch B Cell Pathol 14, 197–213.

van Furth, R., Cohn, Z.a., 1968. The origin and kinetics of mononuclear phagocytes. J. Exp. Med. 128, 415–35.

van Furth, R., Cohn, Z.A., Hirsch, J.G., Humphrey, J.H., Spector, W.G., Langevoort, H.L., 1972. The mononuclear phagocyte system: a new classification of macrophages, monocytes, and their precursor cells. Bull. World Health Organ. 46, 845–852.

Garcia-Alegria, E., Menegatti, S., Batta, K., Cuvertino, S., Florkowska, M., Kouskoff, V., 2016. Emerging concepts for the in vitro derivation of murine hematopoietic stem and progenitor cells. FEBS Lett. , 1–10.

Gardner, R.L., 1982. Investigation of cell lineage and differentiation in the extraembryonic endoderm of the mouse embryo. J. Embryol. Exp. Morphol. 68, 175–198.

Gekas, C., Dieterlen-lièvre, F., Orkin, S.H., Mikkola, H.K.A., Marne, N.s., 2005. Hematopoietic Stem Cells. Am. J. Pathol. 8, 365–375.

Gentek, R., Sieweke, M.H., 2014. Tissue macrophage identity and self renewal. Immunol Rev 262, 56–73.

Ghigo, C., Mondor, I., Jorquera, A., Nowak, J., Wienert, S., Zahner, S.P., Clausen, B.E., Luche, H., Malissen, B., Klauschen, F., Bajénoff, M., 2013. Multicolor fate mapping of Langerhans cell homeostasis. J. Exp. Med. 210, 1657–64.

Gibbings, S.L., Goyal, R., Desch, A.N., Leach, S.M., Prabagar, M., Atif, S.M., Bratton, D.L., Janssen, W., Jakubzick, C.V., 2015. Transcriptome analysis highlights the conserved difference between embryonic and postnatal-derived alveolar macrophages. Blood 126, 1357–1366.

Ginhoux, F., Greter, M., Leboeuf, M., Nandi, S., See, P., Gokhan, S., Mehler, M.F., Conway, S.J., Ng, L.G., Stanley, E.R., Samokhvalov, I.M., Merad, M., 2010. Fate mapping analysis reveals that adult microglia derive from primitive macrophages. Science (80-.). 330, 841–5.

Ginhoux, F., Guilliams, M., 2016. Tissue-Resident Macrophage Ontogeny and Homeostasis. Immunity 44, 439–449.

Godin, I., Cumano, A., 2002. The hare and the tortoise: an embryonic haematopoietic race. Nat. Rev. Immunol. 2, 593–604.

Gomez Perdiguero, E., Klapproth, K., Schulz, C., Busch, K., de Bruijn, M., Rodewald, H.R., Geissmann, F., 2015. The Origin of Tissue-Resident Macrophages: When an Erythro-myeloid Progenitor Is an Erythro-myeloid Progenitor. Immunity 43, 1023–1024.

Gordon, S., Pluddemann, A., Martinez Estrada, F., 2014. Macrophage heterogeneity in tissues: Phenotypic diversity and functions. Immunol. Rev. 262, 36–55.

Greter, M., Lelios, I., Pelczar, P., Hoeffel, G., Price, J., Leboeuf, M., Kündig, T.M., Frei, K., Ginhoux, F., Merad, M., Becher, B., 2012. Stroma-Derived Interleukin-34 Controls the Development and Maintenance of Langerhans Cells and the Maintenance of Microglia. Immunity 37, 1050–1060.

Guilliams, M., De Kleer, I., Henri, S., Post, S., Vanhoutte, L., De Prijck, S., Deswarte, K., Malissen, B., Hammad, H., Lambrecht, B.N., 2013. Alveolar macrophages develop from fetal monocytes that differentiate into long-lived cells in the first week of life via GM-CSF. J. Exp. Med. 210, 1977–92.

Gutierrez-Ramos, J.C., Palacios, R., 1992. In vitro differentiation of embryonic stem cells into lymphocyte precursors able to generate T and B lymphocytes in vivo. Proc. Natl. Acad. Sci. U. S. A. 89, 9171–5.

Haga, E., Endo, Y., Haruta, M., Koba, C., Matsumura, K., Takamatsu, K., Ikeda, T., Nishimura, Y., Senju, S., 2014. Therapy of Peritoneally Disseminated Colon Cancer by TAP-Deficient Embryonic Stem Cell-Derived Macrophages in Allogeneic Recipients. J. Immunol. 193, 2024–2033.

Hale, C., Yeung, A., Goulding, D., Pickard, D., Alasoo, K., Powrie, F., Dougan, G., Mukhopadhyay, S., 2015. Induced pluripotent stem cell derived macrophages as a cellular system to study Salmonella and other pathogens. PLoS One 10, 1–20.

Hamann, J., Koning, N., Pouwels, W., Ulfman, L.H., van Eijk, M., Stacey, M., Lin, H.H., Gordon, S., Kwakkenbos, M.J., 2007. EMR1, the human homolog of F4/80, is an eosinophil-specific receptor. Eur. J. Immunol. 37, 2797–2802.

Hambleton, S., Salem, S., Bustamante, J., Bigley, V., Boisson-Dupuis, S., Azevedo, J., Fortin, A., Haniffa, M., Ceron-Gutierrez, L., Bacon, C.M., Menon, G., Trouillet, C., McDonald, D., Carey, P., Ginhoux, F., Alsina, L., Zumwalt, T.J., Kong, X.F., Kumararatne, D., Butler, K., Hubeau, M., Feinberg, J., Al-Muhsen, S., Cant, A., Abel, L., Chaussabel, D., Doffinger, R., Talesnik, E., Grumach, A., Duarte, A., Abarca, K., Moraes-Vasconcelos, D., Burk, D., Berghuis, A., Geissmann, F., Collin, M., Casanova, J.L., Gros, P., 2011. IRF8 Mutations and Human Dendritic-Cell Immunodeficiency. N. Engl. J. Med. 365, 127–138.

Haniffa, M., Ginhoux, F., Wang, X., Bigley, V., Abel, M., Dimmick, I., Bullock, S., Grisotto, M., Booth, T., Taub, P., Hilkens, C., Merad, M., Collin, M., 2009. Differential rates of replacement of human dermal dendritic cells and macrophages during hematopoietic stem cell transplantation. J. Exp. Med. 206, 371–85.

Hannon, G.J., Rossi, J.J., 2004. Unlocking the potential of the human genome with RNA interference. Nature 431, 371–378.

Hashimoto, D., Chow, A., Noizat, C., Teo, P., Beasley, M.B., Leboeuf, M., Becker, C.D., See, P., Price, J., Lucas, D., Greter, M., Mortha, A., Boyer, S.W., Forsberg, E.C., Tanaka, M., van Rooijen, N., García-Sastre, A., Stanley, E.R., Ginhoux, F., Frenette, P.S., Merad, M., 2013. Tissue-resident macrophages self-maintain locally throughout adult life with minimal contribution from circulating monocytes. Immunity 38, 792–804.

Heskes, T., Eisinga, R., Breitling, R., 2014. A fast algorithm for determining bounds and accurate approximate p -values of the rank product statistic for replicate experiments. BMC Bioinformatics 15, 367.

Hoeffel, G., Chen, J., Lavin, Y., Low, D., Almeida, F.F., See, P., Beaudin, A.E., Lum, J., Low, I., Forsberg, E.C., Poidinger, M., Zolezzi, F., Larbi, A., Ng, L.G., Chan, J.K.Y., Greter, M., Becher, B., Samokhvalov, I.M., Merad, M., Ginhoux, F., 2015. C-Myb⁺ Erythro-Myeloid Progenitor-Derived Fetal Monocytes Give Rise to Adult Tissue-Resident Macrophages. Immunity 42, 665–678.

Hoeffel, G., Wang, Y., Greter, M., See, P., Teo, P., Malleret, B., Leboeuf, M., Low, D., Oller, G., Almeida, F., Choy, S.H.Y., Grisotto, M., Renia, L., Conway, S.J., Stanley, E.R., Chan, J.K.Y., Ng, L.G., Samokhvalov, I.M., Merad, M., Ginhoux, F., 2012. Adult Langerhans cells derive predominantly from embryonic fetal liver monocytes with a minor contribution of yolk sac-derived macrophages. J. Exp. Med. 209, 1167–81.

Hu, C., Fan, L., Cen, P., Chen, E., Jiang, Z., Li, L., 2016. Energy metabolism plays a critical role in stem cell maintenance and differentiation. Int. J. Mol. Sci. 17.

Hume, D.A., MacDonald, K.P.A., 2012. Therapeutic applications of macrophage colony-stimulating factor-1 (CSF-1) and antagonists of CSF-1 receptor (CSF-1R) signaling. Blood 119, 1810–1820.

Huyhn, a., Dommergues, M., Izac, B., Croisille, L., Katz, a., Vainchenker, W., Coulombel, L., 1995. Characterization of hematopoietic progenitors from human yolk sacs and embryos. Blood 86, 4474–85.

Ito, Y., 1999. Molecular basis of tissue-specific gene expression mediated by the runt domain transcription factor PEBP2/CBF. Genes Cells 4, 685–96.

Itskovitz-Eldor, J., Schuldiner, M., Karsenti, D., Eden, a., Yanuka, O., Amit, M., Soreq, H., Benvenisty, N., 2000. Differentiation of human embryonic stem cells into embryoid bodies compromising the three embryonic germ layers. Mol. Med. 6, 88–95.

Ivanovs, A., Rybtsov, S., Welch, L., Anderson, R.a., Turner, M.L., Medvinsky, A., 2011. Highly potent human hematopoietic stem cells first emerge in the intraembryonic aorta-gonad-mesonephros region. J. Exp. Med. 208, 2417–27.

Jackson, M., Axton, R.A., Taylor, A.H., Wilson, J.A., Gordon-Keylock, S.A.M., Kokkaliaris, K.D., Brickman, J.M., Schulz, H., Hummel, O., Hubner, N., Forrester, L.M., 2012. HOXB4 can enhance the differentiation of embryonic stem cells by modulating the hematopoietic niche. Stem Cells 30, 150–160.

Jaffredo, T., Richard, C., Pouget, C., Teillet, M.A., Bollérot, K., Gautier, R., Drevon, C., 2010. Aortic remodelling during hemogenesis: is the chicken paradigm unique? Int. J. Dev. Biol. 54, 1045–54.

Jagannathan-Bogdan, M., Zon, L.I., 2013. Hematopoiesis. Development 140, 2463–2467.

Jeffery, I.B., Higgins, D.G., Culhane, A.C., 2006. Comparison and evaluation of methods for generating differentially expressed gene lists from microarray data. BMC Bioinformatics 7, 359.

Jenkins, S.J., Ruckerl, D., Cook, P.C., Jones, L.H., Finkelman, F.D., van Rooijen, N., MacDonald, A.S., Allen, J.E., 2011. Local macrophage proliferation, rather than recruitment from the blood, is a signature of TH2 inflammation. Science 332, 1284–8.

Jenkins, S.J., Ruckerl, D., Thomas, G.D., Hewitson, J.P., Duncan, S., Brombacher, F., Maizels, R.M., Hume, D.A., Allen, J.E., 2013a. IL-4 directly signals tissue-resident macrophages to proliferate beyond homeostatic levels controlled by CSF-1. J. Exp. Med. 210, 2477–91.

Jenkins, S.J., Ruckerl, D., Thomas, G.D., Hewitson, J.P., Duncan, S., Brombacher, F., Maizels, R.M., Hume, D.a., Allen, J.E., 2013b. IL-4 directly signals tissue-resident macrophages to proliferate beyond homeostatic levels controlled by CSF-1. J. Exp. Med. 210, 2477–2491.

Jieping, C., Clarke, D., Bonifer, C., 2007. Reduced c-myb expression levels affect hematopoietic development in vitro. Int. J. Hematol. 85, 312–6.

Kambal, A., Mitchell, G., Cary, W., Gruenloh, W., Jung, Y., Kalomoiris, S., Nacey, C., McGee, J., Lindsey, M., Fury, B., Bauer, G., Nolta, J.a., Anderson, J.S., 2011. Generation of HIV-1 resistant and functional macrophages from hematopoietic stem cell-derived induced pluripotent stem cells. Mol. Ther. 19, 584–93.

Kanitakis, J., Morelon, E., Petruzzo, P., Badet, L., Dubernard, J.M., 2011. Self-renewal capacity of human epidermal Langerhans cells: Observations made on a composite tissue allograft. Exp. Dermatol. 20, 145–146.

Karlsson, K.R., Cowley, S., Martinez, F.O., Shaw, M., Minger, S.L., James, W., 2008. Homogeneous monocytes and macrophages from human embryonic stem cells following coculture-free differentiation in M-CSF and IL-3. Exp. Hematol. 36, 1167–75.

Keller, G., Kennedy, M., Papayannopoulou, T., Wiles, M.V., 1993. Hematopoietic commitment during embryonic stem cell differentiation in culture. Mol. Cell. Biol. 13, 473–486.

Kelly, B., O'Neill, L.A., 2015. Metabolic reprogramming in macrophages and dendritic cells in innate immunity. Cell Res. 25, 771–84.

Kennedy, M., Awong, G., Sturgeon, C.M., Ditadi, A., LaMotte-Mohs, R., Zúñiga-Pflücker, J.C., Keller, G., 2012. T lymphocyte potential marks the emergence of definitive hematopoietic progenitors in human pluripotent stem cell differentiation cultures. Cell Rep. 2, 1722–35.

Kennedy, M., D'Souza, S.L., Lynch-Kattman, M., Schwantz, S., Keller, G., 2007. Development of the hemangioblast defines the onset of hematopoiesis in human ES cell differentiation cultures. Blood 109, 2679–87.

Kierdorf, K., Erny, D., Goldmann, T., Sander, V., Schulz, C., Perdiguero, E.G., Wieghofer, P., Heinrich, A., Riemke, P., Hölscher, C., Müller, D.N., Luckow, B., Brocker, T., Debowski, K., Fritz, G., Opdenakker, G., Diefenbach, A., Biber, K., Heikenwalder, M., Geissmann, F., Rosenbauer, F., Prinz, M., 2013. Microglia emerge from erythromyeloid precursors via Pu.1- and Irf8-dependent pathways. Nat. Neurosci. 16, 273–80.

Kirouac, D.C., Madlambayan, G.J., Yu, M., Sykes, E.A., Ito, C., Zandstra, P.W., 2009. Cell-cell interaction networks regulate blood stem and progenitor cell fate. Mol. Syst. Biol. 5, 293.

Kitajima, K., Minehata, K.i., Sakimura, K., Nakano, T., Hara, T., Kitajima, K., Minehata, K.i., Sakimura, K., Nakano, T., Hara, T., 2011. In vitro generation of HSC-like cells from murine ESCs/iPSCs by enforced expression of LIM-homeobox transcription factor Lhx2. Blood 117, 3748–3758.

Klepper, A., Branch, A.D., 2015. Macrophages and the Viral Dissemination Super Highway. EC Microbiol. 6, 356–372.

Klimchenko, O., Di Stefano, A., Geoerger, B., Hamidi, S., Opolon, P., Robert, T., Routhier, M., El-Benna, J., Delezoide, A.L., Boukour, S., Lescure, B., Solary, E., Vainchenker, W., Norol, F., 2011. Monocytic cells derived from human embryonic stem cells and fetal liver share common differentiation pathways and homeostatic functions. Blood 117, 3065–75.

Kobayashi, M., Shelley, W.C., Seo, W., Vemula, S., Lin, Y., Liu, Y., Kapur, R., Taniuchi, I., Yoshimoto, M., 2014. Functional B-1 progenitor cells are present in the hematopoietic stem cell-deficient embryo and depend on Cbfβ for their development. Proc. Natl. Acad. Sci. U. S. A. 111, 12151–6.

Kownatzki, E., Kapp, a., Uhrich, S., 1986. Novel neutrophil chemotactic factor derived from human peripheral blood mononuclear leucocytes. Clin. Exp. Immunol. 64, 214–22.

Kyba, M., Perlingeiro, R.C.R., Daley, G.Q., 2002. HoxB4 confers definitive lymphoid-myeloid engraftment potential on embryonic stem cell and yolk sac hematopoietic progenitors. Cell 109, 29–37.

Van de laar, L., Saelens, W., De Prijck, S., Martens, L., Scott, C.L., Van Isterdael, G., Hoffmann, E., Beyaert, R., Saeys, Y., Lambrecht, B.N., Guilliams, M., 2016. Yolk Sac Macrophages, Fetal Liver, and Adult Monocytes Can Colonize an Empty Niche and Develop into Functional Tissue-Resident Macrophages. Immunity 44, 755–768.

Lachmann, N., Ackermann, M., Frenzel, E., Liebhaber, S., Brennig, S., Happle, C., Hoffmann, D., Klimenkova, O., Lüttge, D., Buchegger, T., Kühnel, M.P., Schambach, A., Janciauskiene, S., Figueiredo, C., Hansen, G., Skokowa, J., Moritz, T., 2015. Large-scale hematopoietic differentiation of human induced pluripotent stem cells provides granulocytes or macrophages for cell replacement therapies. Stem Cell Reports 4, 282–296.

Lahmar, Q., Keirsse, J., Laoui, D., Movahedi, K., Van Overmeire, E., Van Ginderachter, J.a., 2015. Tissue-resident versus monocyte-derived macrophages in the tumor microenvironment. Biochim. Biophys. Acta - Rev. Cancer 1865, 23–34.

Lancrin, C., Sroczynska, P., Stephenson, C., Allen, T., Kouskoff, V., Lacaud, G., 2009. The haemangioblast generates haematopoietic cells through a haemogenic endothelium stage. Nature 457, 892–5.

Laterveer, L., Lindley, I.J., Heemskerk, D.P., Camps, J.a., Pauwels, E.K., Willemze, R., Fibbe, W.E., 1996. Rapid mobilization of hematopoietic progenitor cells in rhesus monkeys by a single intravenous injection of interleukin-8. Blood 87, 781–8.

Lee, P.Y., Wang, J.X., Parisini, E., Dascher, C.C., Nigrovic, P.a., 2013. Ly6 family proteins in neutrophil biology. J. Leukoc. Biol. 94, 585–94.

Lei, W., Rushton, J.J., Davis, L.M., Liu, F., Ness, S.A., 2004. Positive and negative determinants of target gene specificity Myb transcription factors. J. Biol. Chem. 279, 29519–29527.

Lieu, Y.K., Reddy, E.P., 2009. Conditional c-myb knockout in adult hematopoietic stem cells leads to loss of self-renewal due to impaired proliferation and accelerated differentiation. Proc. Natl. Acad. Sci. U. S. A. 106, 21689–94.

Lin, Y., Yoder, M.C., Yoshimoto, M., 2014. Lymphoid progenitor emergence in the murine embryo and yolk sac precedes stem cell detection. Stem Cells Dev. 23, 1168–77.

Lin, Y.C., Kuo, M.W., Yu, J., Kuo, H.H., Lin, R.J., Lo, W.L., Yu, A.L., 2008. c-Myb is an evolutionary conserved miR-150 target and miR-150/c-Myb interaction is important for embryonic development. Mol. Biol. Evol. 25, 2189–2198.

Linde, L., Boelz, S., Neu-Yilik, G., Kulozik, A.E., Kerem, B., 2007. The efficiency of nonsense-mediated mRNA decay is an inherent character and varies among different cells. Eur. J. Hum. Genet. 15, 1156–1162.

Lindenbaum, M.H., Grosveld, F., 1990. An in vitro globin gene switching model based on differentiated embryonic stem cells. Genes Dev. 4, 2075–2085.

Litvack, M.L., Wigle, T.J., Lee, J., Wang, J., Ackerley, C., Grunebaum, E., Post, M., 2016. Alveolar-like Stem Cell-derived Myb(neg) Macrophages Promote Recovery and Survival in Airway Disease. Am. J. Respir. Crit. Care Med. , 1–69.

Lu, S.J., Li, F., Vida, L., Honig, G.R., 2004. CD34+CD38- hematopoietic precursors derived from human embryonic stem cells exhibit an embryonic gene expression pattern. Blood 103, 4134–4141.

Lu, S.J., Li, F., Yin, H., Feng, Q., Kimbrel, E.a., Hahm, E., Thon, J.N., Wang, W., Italiano, J.E., Cho, J., Lanza, R., 2011. Platelets generated from human embryonic stem cells are functional in vitro and in the microcirculation of living mice. Cell Res. 21, 530–545.

Luban, J., Bossolt, K.L., Franke, E.K., Kalpana, G.V., Goff, S.P., 1993. Human immunodeficiency virus type 1 Gag protein binds to cyclophilins A and B. Cell 73, 1067–1078.

Luckett, W.P., 1978. Origin and differentiation of yolk-sac and extraembryonic mesoderm in presomite human and rhesus-monkey embryos. Am. J. Anat. 152, 59–97.

Lund, R.J., Närvä, E., Lahesmaa, R., 2012. Genetic and epigenetic stability of human pluripotent stem cells. Nat. Rev. Genet. 13, 732–744.

M, R., Saule, S., C, L., H, R., H, G., D, S., 1979. Three new types of viral oncogene of cellular origin specific for hematopoietic cell transformation. Nature 281, 452–455.

Ma, F., Ebihara, Y., Umeda, K., Sakai, H., Hanada, S., Zhang, H., Zaike, Y., Tsuchida, E., Nakahata, T., Nakauchi, H., Tsuji, K., 2008. Generation of functional erythrocytes from human embryonic stem cell-derived definitive hematopoiesis. Proc. Natl. Acad. Sci. United States Am. F., Ebihara, Y., Umeda, K., Sakai, H., Hanada, S., Zhang, H., ... Tsuji, K. (2008). Gener. Funct. erythrocytes from Hum. embryonic stem cell-derived Defin. he 105, 13087–13092.

Martin, G.R., 1981. Isolation of a pluripotent cell line from early mouse embryos cultured in medium conditioned by teratocarcinoma stem cells. Proc. Natl. Acad. Sci. U. S. A. 78, 7634–7638.

McGovern, N., Schlitzer, A., Gunawan, M., Jardine, L., Shin, A., Poyner, E., Green, K., Dickinson, R., Wang, X.N., Low, D., Best, K., Covins, S., Milne, P., Pagan, S., Aljefri, K., Windebank, M., Saavedra, D.M., Larbi, A., Wasan, P.S., Duan, K., Poidinger, M., Bigley, V., Ginhoux, F., Collin, M., Haniffa, M., 2014. Human dermal CD14+ cells are a transient population of monocyte-derived macrophages. Immunity 41, 465–477.

McGrath, K.E., Frame, J.M., Fegan, K.H., Bowen, J.R., Conway, S.J., Catherman, S.C., Kingsley, P.D., Koniski, A.D., Palis, J., 2015a. Distinct Sources of Hematopoietic Progenitors Emerge before HSCs and Provide Functional Blood Cells in the Mammalian Embryo. Cell Rep. 11, 1892–1904.

McGrath, K.E., Frame, J.M., Palis, J., 2015b. Early hematopoiesis and macrophage development. Semin. Immunol. 27, 379–387.

McKercher, S.R., Torbett, B.E., Anderson, K.L., Henkel, G.W., Vestal, D.J., Baribault, H., Klemsz, M., Feeney, a.J., Wu, G.E., Paige, C.J., Maki, R.a., 1996. Targeted disruption of the PU.1 gene results in multiple hematopoietic abnormalities. EMBO J. 15, 5647–5658.

Melief, J., Koning, N., Schuurman, K.G., Van De Garde, M.D.B., Smolders, J., Hoek, R.M., Van Eijk, M., Hamann, J., Huitinga, I., 2012. Phenotyping primary human microglia: Tight regulation of LPS responsiveness. Glia 60, 1506–1517.

Merad, M., Manz, M.G., Karsunky, H., Wagers, A., Peters, W., Charo, I., Weissman, I.L., Cyster, J.G., Engleman, E.G., 2002. Langerhans cells renew in the skin throughout life under steady-state conditions. Nat. Immunol. 3, 1135–1141.

Migliaccio, G., Migliaccio, A.R., Petti, S., Mavilio, F., Russo, G., Lazzaro, D., Testa, U., Marinucci, M., Peschle, C., 1986. Human Embryonic Hemopoiesis. J Clin Invest 78, 51–60.

Mikkola, H.K.a., Fujiwara, Y., Schlaeger, T.M., Traver, D., Orkin, S.H., 2003. Expression of CD41 marks the initiation of definitive hematopoiesis in the mouse embryo. Blood 101, 508–16.

Mildner, A., Schmidt, H., Nitsche, M., Merkler, D., Hanisch, U.K., Mack, M., Heikenwalder, M., Brück, W., Priller, J., Prinz, M., 2007. Microglia in the adult brain arise from Ly-6ChiCCR2+ monocytes only under defined host conditions. Nat. Neurosci. 10, 1544–53.

Milner, J.D., Orekov, T., Ward, J.M., Cheng, L., Torres-Velez, F., Junttila, I., Sun, G., Buller, M., Morris, S.C., Finkelman, F.D., Paul, W.E., 2010. Sustained IL-4 exposure leads to a novel pathway for hemophagocytosis, inflammation, and tissue macrophage accumulation. Blood 116, 2476–2483.

Molawi, K., Wolf, Y., Kandalla, P.K., Favret, J., Hagemeyer, N., Frenzel, K., Pinto, A.R., Klapproth, K., Henri, S., Malissen, B., Rodewald, H.R., Rosenthal, N.A., Bajenoff, M., Prinz, M., Jung, S., Sieweke, M.H., 2014. Progressive replacement of embryo-derived cardiac macrophages with age. J. Exp. Med. 211, 2151–8.

Moore, K.J., Tabas, I., 2011. Macrophages in the pathogenesis of atherosclerosis. Cell 145, 341–355.

Moore, M.A.S., 2009. The Ontogeny of the Hematopoietic System. Essentials Stem Cell Biol. , 199–209.

Moreau-Gachelin, F., Ray, D., Mattei, M., Tambourin, P., Tavitian, A., 1989. The putative oncogene Spi-1: murine chromosomal localization and transcriptional activation in murine acute erythroleukemias. Oncogene 4, 1449–1456.

Moreau-Gachelin, F., Ray, D., Tambourin, P., Tavitian, A., Klemsz, M.J., McKercher, S.R., Celada, A., Van Beveren, C., Maki, R.A., 1990. The PU.1 transcription factor is the product of the putative oncogene Spi-1. Cell 61, 1166.

Moreau-Gachelin, F., Tavitian, A., Tambourin, P., 1988. Spi-1 is a putative oncogene in virally induced murine erythroleukaemias. Nature 336, 403–405.

Moscovici, C., 1975. Leukemic Transformation with Avian Myeloblastosis Virus: Present Status. Curr. Top. Microbiol. Immunol. 71, 79–101.

Mucenski, M.L., McLain, K., Kier, a.B., Swerdlow, S.H., Schreiner, C.M., Miller, T.a., Pietryga, D.W., Scott, W.J., Potter, S.S., 1991. A functional c-myb gene is required for normal murine fetal hepatic hematopoiesis. Cell 65, 677–89.

Muffat, J., Li, Y., Mitalipova, M., Omer, A., Corcoran, S., Bakiasi, G., Tsai, L.H., Aubourg, P., Ransohoff, R.M., Jaenisch, R., 2016. Derivation of microglia-like cells from human pluripotent stem cells. Nat. Med. .

Müller, a.M., Dzierzak, E.a., 1993. ES cells have only a limited lymphopoietic potential after adoptive transfer into mouse recipients. Development 118, 1343–1351.

Murray, P.J., Allen, J.E., Biswas, S.K., Fisher, E.A., Gilroy, D.W., Goerdt, S., Gordon, S., Hamilton, J.A., Ivashkiv, L.B., Lawrence, T., Locati, M., Mantovani, A., Martinez, F.O., Mege, J.L., Mosser, D.M., Natoli, G., Saeij, J.P., Schultze, J.L., Shirey, K.A., Sica, A., Suttles, J., Udalova, I., van Ginderachter, J.A., Vogel, S.N., Wynn, T.A., 2014. Macrophage Activation and Polarization: Nomenclature and Experimental Guidelines. Immunity 41, 14–20.

Naito, M., Yamamura, F., Nishikawa, S., Takahashi, K., 1989. Development, differentiation, and maturation of fetal mouse yolk sac macrophages in cultures. J. Leukoc. Biol. 46, 1–10.

Nguyen, L.S., Wilkinson, M.F., Gecz, J., 2014. Nonsense-mediated mRNA decay: Inter-individual variability and human disease. Neurosci. Biobehav. Rev. 46, 175–186.

Nishikawa, S.I., Nishikawa, S., Hirashima, M., Matsuyoshi, N., Kodama, H., 1998. Progressive lineage analysis by cell sorting and culture identifies FLK1+VE-cadherin+ cells at a diverging point of endothelial and hemopoietic lineages. Development 125, 1747–1757.

Nisitani, S., Tsubata, T., Honjo, T., 1994. Lineage Marker-Negative Lymphocyte Precursors Derived From Embryonic Stem-Cells in-Vitro Differentiate Into Mature Lymphocytes in-Vivo. Int. Immunol. 6, 909–916.

Niwa, A., Heike, T., Umeda, K., Oshima, K., Kato, I., Sakai, H., Suemori, H., Nakahata, T., Saito, M.K., 2011. A novel Serum-Free monolayer culture for orderly hematopoietic differentiation of human pluripotent cells via mesodermal progenitors. PLoS One 6.

Noy, R., Pollard, J.W., 2014. Tumor-Associated Macrophages: From Mechanisms to Therapy. Immunity 41, 49–61.

Ohgidani, M., Kato, T.A., Setoyama, D., Sagata, N., Hashimoto, R., Shigenobu, K., Yoshida, T., Hayakawa, K., Shimokawa, N., Miura, D., Utsumi, H., Kanba, S., 2014. Direct induction of ramified microglia-like cells from human monocytes: dynamic microglial dysfunction in Nasu-Hakola disease. Sci. Rep. 4, 4957.

Okabe, Y., Medzhitov, R., 2015. Tissue biology perspective on macrophages. Nat. Immunol. 17, 9–17.

Okada, H., Watanabe, T., Niki, M., Takano, H., Chiba, N., Yanai, N., Tani, K., Hibino, H., Asano, S., Mucenski, M.L., Ito, Y., Noda, T., Satake, M., 1998. AML1(-/-) embryos do not express certain hematopoiesis-related gene transcripts including those of the PU.1 gene. Oncogene 17, 2287–2293.

Okuda, T., Van Deursen, J., Hiebert, S.W., Grosveld, G., Downing, J.R., 1996. AML1, the target of multiple chromosomal translocations in human leukemia, is essential for normal fetal liver hematopoiesis. Cell 84, 321–330.

Olefsky, J.M., Glass, C.K., 2010. Macrophages, Inflammation, and Insulin Resistance. Annu. Rev. Physiol. , 1–28.

Olivier, E.N., Marenah, L., Mccahill, A., Condie, A., Cowan, S., C.Mountford, J., 2016. Tissue Engineering and Regenerative Medicine High-Efficiency Serum-Free Feeder-Free Erythroid Differentiation of Human Pluripotent Stem Cells Using Small Molecules. Stem Cells Transl. Med. 5, 1–12.

Olivier, E.N., Qiu, C., Velho, M., Hirsch, R.E., Bouhassira, E.E., 2006. Large-scale production of embryonic red blood cells from human embryonic stem cells. Exp. Hematol. 34, 1635–1642.

Orkin, S.H., Zon, L.I., 2008. Hematopoiesis: an evolving paradigm for stem cell biology. Cell 132, 631–44.

O'Rourke, J.P., Ness, S.a., 2008. Alternative RNA splicing produces multiple forms of c-Myb with unique transcriptional activities. Mol. Cell. Biol. 28, 2091–101.

Osato, M., 2014. An unsung runt 6e isoform for HSC expansion. Blood 123, 3684–3686.

Padrón-barthe, L., Temiño, S., Villa, C., Carramolino, L., Isern, J., Torres, M., Temin, S., 2014. Clonal analysis identifies hemogenic endothelium as the source of the blood-endothelial common lineage in the mouse embryo. Blood 124, 2523–2532.

Palis, J., Chan, R.J., Koniski, a., Patel, R., Starr, M., Yoder, M.C., 2001. Spatial and temporal emergence of high proliferative potential hematopoietic precursors during murine embryogenesis. Proc. Natl. Acad. Sci. U. S. A. 98, 4528–33.

Palis, J., Robertson, S., Kennedy, M., Wall, C., Keller, G., 1999. Development of erythroid and myeloid progenitors in the yolk sac and embryo proper of the mouse. Development 126, 5073–5084.

Palis, J., Yoder, M.C., 2001. Yolk-sac hematopoiesis: The first blood cells of mouse and man. Exp. Hematol. 29, 927–936.

Panopoulos, A.D., Yanes, O., Ruiz, S., Kida, Y.S., Diep, D., Tautenhahn, R., Herrerias, A., Batchelder, E.M., Plongthongkum, N., Lutz, M., Berggren, W.T., Zhang, K., Evans, R.M., Siuzdak, G., Izpisua Belmonte, J.C., 2012. The metabolome of induced pluripotent stem cells reveals metabolic changes occurring in somatic cell reprogramming. Cell Res. 22, 168–177.

Perdiguero, E.G., Geissmann, F., 2015. The development and maintenance of resident macrophages. Nat. Immunol. 17, 2–8.

Pereira, L.a., Wong, M.S., Mossman, A.K., Sourris, K., Janes, M.E., Knezevic, K., Hirst, C.E., Lim, S.M., Pimanda, J.E., Stanley, E.G., Elefanty, A.G., 2012. Pdgfrα and Flk1 are direct target genes of Mixl1 in differentiating embryonic stem cells. Stem Cell Res. 8, 165–79.

Pick, M., Azzola, L., Osborne, E., Stanley, E.G., Elefanty, A.G., 2013. Generation of Megakaryocytic Progenitors from Human Embryonic Stem Cells in a Feeder- and Serum-Free Medium. PLoS One 8, 1–11.

Pinto, A.R., Godwin, J.W., Chandran, A., Hersey, L., Ilinykh, A., Debuque, R., Wang, L., Rosenthal, N.A., 2014. Age-related changes in tissue macrophages precede cardiac functional impairment. Aging (Albany. NY). 6, 399–413.

Pollard, J.W., 2009. Trophic macrophages in development and disease. Nat. Rev. Immunol. 9, 259–70.

Potocnik, a.J., Kohler, H., Eichmann, K., 1997. Hemato-lymphoid in vivo reconstitution potential of subpopulations derived from in vitro differentiated embryonic stem cells. Proc. Natl. Acad. Sci. U. S. A. 94, 10295–300.

Price, J.G., Idoyaga, J., Salmon, H., Hogstad, B., Bigarella, C.L., Ghaffari, S., Leboeuf, M., Merad, M., 2015. CDKN1A regulates Langerhans cell survival and promotes Treg cell generation upon exposure to ionizing irradiation. Nat. Neurosci. 16, 1060–8.

Qiu, C., Hanson, E., Olivier, E., Inada, M., Kaufman, D.S., Gupta, S., Bouhassira, E.E., 2005. Differentiation of human embryonic stem cells into hematopoietic cells by coculture with human fetal liver cells recapitulates the globin switch that occurs early in development. Exp. Hematol. 33, 1450–8.

Quintana, A.M., Zhou, Y.E., Pena, J.J., O'Rourke, J.P., Ness, S.A., 2011. Dramatic repositioning of c-Myb to different promoters during the cell cycle observed by combining cell sorting with chromatin immunoprecipitation. PLoS One 6.

Rafii, S., Kloss, C.C., Butler, J.M., Ginsberg, M., Gars, E., Lis, R., Zhan, Q., Josipovic, P., Ding, B.S.S., Xiang, J., Elemento, O., Zaninovic, N., Rosenwaks, Z., Sadelain, M., Rafii, J.A., James, D., 2013. Human ESC-derived hemogenic endothelial cells undergo distinct waves of endothelial to hematopoietic transition. Blood 121, 770–780.

Ramsay, R.G., Gonda, T.J., 2008. MYB function in normal and cancer cells. Nat. Rev. Cancer 8, 523–34.

Ran, F.A., Hsu, P.D., Lin, C.Y., Gootenberg, J.S., Konermann, S., Trevino, A.E., Scott, D.A., Inoue, A., Matoba, S., Zhang, Y., Zhang, F., 2013. Double nicking by RNA-guided CRISPR cas9 for enhanced genome editing specificity. Cell 154, 1380–1389.

Reubinoff, B.E., Pera, M.F., Fong, C.Y., Trounson, a., Bongso, a., 2000. Embryonic stem cell lines from human blastocysts: somatic differentiation in vitro. Nat. Biotechnol. 18, 399–404.

Robb, L., 2007. Cytokine receptors and hematopoietic differentiation. Oncogene 26, 6715–23.

Rossant, B.J., Gardner, R.L., Alexandre, H.L., 1978. Investigation of the potency of cells from the postimplantation mouse embryo by blastocyst injection : a preliminary report. J. Embryol. exp. Morph. 48, 239–247.

Rowe, R.G., Mandelbaum, J., Zon, L.I., Daley, G.Q., 2016. Engineering Hematopoietic Stem Cells: Lessons from Development. Cell Stem Cell 18, 707–720.

Rückerl, D., Allen, J.E., 2014. Macrophage proliferation, provenance, and plasticity in macroparasite infection. Immunol. Rev. 262, 113–133.

Rybalko, V., Hsieh, P.L., Merscham-Banda, M., Suggs, L.J., Farrar, R.P., 2015. The development of macrophage-mediated cell therapy to improve skeletal muscle function after injury. PLoS One 10, 1–19.

Saeki, K., Saeki, K., Nakahara, M., Matsuyama, S., Nakamura, N., Yogiashi, Y., Yoneda, A., Koyanagi, M., Kondo, Y., Yuo, A., 2009. A feeder-free and efficient production of functional neutrophils from human embryonic stem cells. Stem Cells 27, 59–67.

Samokhvalov, I.M., Samokhvalova, N.I., Nishikawa, S.i., 2007. Cell tracing shows the contribution of the yolk sac to adult haematopoiesis. Nature 446, 1056–61.

Sanjana, N.E., Shalem, O., Zhang, F., 2014. Improved vectors and genome-wide libraries for CRISPR screening. Nat. Methods 11, 783–784.

Schaller, T., Ocwieja, K.E., Rasaiyaah, J., Price, A.J., Brady, T.L., Roth, S.L., Hue, S., Fletcher, A.J., Lee, K., KewalRamani, V.N., Noursadeghi, M., Jenner, R.G., James, L.C., Bushman, F.D., Towers, G.J., 2011. HIV-1 capsid-cyclophilin interactions determine nuclear import pathway, integration targeting and replication efficiency. PLoS Pathog. 7.

Schulz, C., Gomez Perdiguero, E., Chorro, L., Szabo-Rogers, H., Cagnard, N., Kierdorf, K., Prinz, M., Wu, B., Jacobsen, S.E.W., Pollard, J.W., Frampton, J., Liu, K.J., Geissmann, F., 2012. A lineage of myeloid cells independent of Myb and hematopoietic stem cells. Science (80-.). 336, 86–90.

Scott, C.L., Zheng, F., De Baetselier, P., Martens, L., Saeys, Y., De Prijck, S., Lippens, S., Abels, C., Schoonooghe, S., Raes, G., Devoogdt, N., Lambrecht, B.N., Beschin, A., Guilliams, M., 2016. Bone marrow-derived monocytes give rise to self-renewing and fully differentiated Kupffer cells. Nat. Commun. 7, 10321.

Scott, E.W., Simon, M.C., Anastasi, J., Singh, H., 1994. Requirement of transcription factor PU.1 in the development of multiple hematopietic lineages. Science (80-.). 265, 1573–1577.

Senju, S., Haruta, M., Matsumura, K., Matsunaga, Y., Fukushima, S., Ikeda, T., Takamatsu, K., Irie, a., Nishimura, Y., 2011. Generation of dendritic cells and macrophages from human induced pluripotent stem cells aiming at cell therapy. Gene Ther. 18, 874–83.

Shalem, O., Sanjana, E.N., Hartenian, E., Zhang, F., 2014. Genome-Scale CRISPR-Cas9 Knockout. Science (80-.). 343, 84–88.

Sharif, O., Bolshakov, V.N., Raines, S., Newham, P., Perkins, N.D., 2007. Transcriptional profiling of the LPS induced NF-kappaB response in macrophages. BMC Immunol. 8, 1–17.

Sheng, J., Ruedl, C., Karjalainen, K., 2015. Most Tissue-Resident Macrophages Except Microglia Are Derived from Fetal Hematopoietic Stem Cells. Immunity 43, 382–393.

Shibata, Y., Berclaz, P.Y., Chroneos, Z.C., Yoshida, M., Whitsett, J.A., Trapnell, B.C., 2001. GM-CSF regulates alveolar macrophage differentiation and innate immunity in the lung through PU.1. Immunity 15, 557–567.

Shyh-Chang, N., Daley, G.Q., Cantley, L.C., 2013. Stem cell metabolism in tissue development and aging. Development 140, 2535–47.

Sica, A., Mantovani, A., 2012. Macrophage plasticity and polarization: in vivo veritas. J. Clin. Invest. 122, 787–795.

Slukvin, I.I., Vodyanik, M.a., Thomson, J.a., Gumenyuk, M.E., Choi, K.D., 2006. Directed Differentiation of Human Embryonic Stem Cells into Functional Dendritic Cells through the Myeloid Pathway. J. Immunol. 176, 2924–2932.

Smith, A.M., Gibbons, H.M., Lill, C., Faull, R.L.M., Dragunow, M., 2013. solation and Culture of Adult Human Microglia Within Mixed Glial Cultures for Functional Experimentation and High-Content Analysis. Methods Mol. Biol. 1041, 41–51.

Soza-ried, C., Hess, I., Netuschil, N., Schorpp, M., Boehm, T., 2010. Essential role of c-myb in definitive hematopoiesis is evolutionarily conserved. PNAS 107, 17304–17308.

Sturgeon, C.M., Ditadi, A., Awong, G., Kennedy, M., Keller, G., 2014. Wnt signaling controls the specification of definitive and primitive hematopoiesis from human pluripotent stem cells. Nat. Biotechnol. 32, 554–61.

Su, Z., Frye, C., Bae, K.M., Kelley, V., Vieweg, J., 2008. Differentiation of human embryonic stem cells into immunostimulatory dendritic cells under feeder-free culture conditions. Clin. cancer Res. 14, 6207–6217.

Subramanian, A., Guo, B., Marsden, M.D., Galic, Z., Kitchen, S., Kacena, A., Brown, H.J., Cheng, G., Zack, J.A., 2009. Macrophage differentiation from embryoid bodies derived from human embryonic stem cells. J. Stem Cells 4, 29–45.

Subramanian, A., Tamayo, P., Mootha, V.K., Mukherjee, S., Ebert, B.L., Gillette, M.a., Paulovich, A., Pomeroy, S.L., Golub, T.R., Lander, E.S., Mesirov, J.P., 2005. Gene set enrichment analysis: a knowledge-based approach for interpreting genome-wide expression profiles. Proc. Natl. Acad. Sci. U. S. A. 102, 15545–50.

Sumner, R., Crawford, a., Mucenski, M., Frampton, J., 2000. Initiation of adult myelopoiesis can occur in the absence of c-Myb whereas subsequent development is strictly dependent on the transcription factor. Oncogene 19, 3335–42.

Swiers, G., Baumann, C., O'Rourke, J., Giannoulatou, E., Taylor, S., Joshi, A., Moignard, V., Pina, C., Bee, T., Kokkaliaris, K.D., Yoshimoto, M., Yoder, M.C., Frampton, J., Schroeder, T., Enver, T., Göttgens, B., de Bruijn, M.F.T.R., 2013. Early dynamic fate changes in haemogenic endothelium characterized at the single-cell level. Nat. Commun. 4, 2924.

Tagliani, E., Shi, C., Nancy, P., Tay, C.S., Pamer, E.G., Erlebacher, A., 2011. Coordinate regulation of tissue macrophage and dendritic cell population dynamics by CSF-1. J. Exp. Med. 208, 1901–1916.

Takahashi, K., Tanabe, K., Ohnuki, M., Narita, M., Ichisaka, T., Tomoda, K., Yamanaka, S., 2007. Induction of pluripotent stem cells from adult human fibroblasts by defined factors. Cell 131, 861–72.

Takahashi, K., Yamamura, F., Naito, M., 1989. Differentiation , Maturation , and Proliferation Macrophages in the Mouse Yolk Sac : A Light-Microscopic, Enzyme-Cytochimical, Immunohistochemical, and Ultrastructural Study. J. Leukoc. Biol. 45, 87–96.

Tamoutounour, S., Guilliams, M., MontananaSanchis, F., Liu, H., Terhorst, D., Malosse, C., Pollet, E., Ardouin, L., Luche, H., Sanchez, C., Dalod, M., Malissen, B., Henri, S., 2013. Origins and functional specialization of macrophages and of conventional and monocyte-derived dendritic cells in mouse skin. Immunity 39, 925–938.

Tavian, M., Hallais, M.F., Péault, B., 1999. Emergence of intraembryonic hematopoietic precursors in the pre-liver human embryo. Development 126, 793–803.

Tavian, M., Péault, B., 2005. Embryonic development of the human hematopoietic system. Int. J. Dev. Biol. 49, 243–50.

Thi, E.P., Lambertz, U., Reiner, N.E., 2012. Sleeping with the enemy: How intracellular pathogens cope with a macrophage lifestyle. PLoS Pathog. 8, 1–4.

Thomson, J.a., 1998. Embryonic Stem Cell Lines Derived from Human Blastocysts. Science (80-.). 282, 1145–1147.

Timmermans, F., Velghe, I., Vanwalleghem, L., De Smedt, M., Van Coppernolle, S., Taghon, T., Moore, H.D., Leclercq, G., Langerak, A.W., Kerre, T., Plum, J., Vandekerckhove, B., 2009. Generation of T cells from human embryonic stem cell-derived hematopoietic zones. J. Immunol. 182, 6879–6888.

Tober, J., Koniski, A., McGrath, K.E., Vemishetti, R., Emerson, R., Mesy-bentley, K.K.L.D., Waugh, R., Palis, J., De Mesy-Bentley, K.K.L., Waugh, R., Palis, J., 2007. The megakaryocyte lineage originates from hemangioblast precursors and is an integral component both of primitive and of definitive hematopoiesis. Blood 109, 1433–1441.

Tseng, S.Y., Nishimoto, K.P., Silk, K.M., Majumdar, A.S., Dawes, G.N., Waldmann, H., Fairchild, P.J., Lebkowski, J.S., Reddy, A., 2009. Generation of immunogenic dendritic cells from human embryonic stem cells without serum and feeder cells. Regen. Med. 4, 513–526.

Uenishi, G., Theisen, D., Lee, J.H., Kumar, A., Raymond, M., Vodyanik, M., Swanson, S., Stewart, R., Thomson, J., Slukvin, I., 2014. Tenascin C promotes hematoendothelial development and T lymphoid commitment from human pluripotent stem cells in chemically defined conditions. Stem Cell Reports 3, 1073–1084.

Ueno, H., Weissman, I.L., 2006. Clonal Analysis of Mouse Development Reveals a Polyclonal Origin for Yolk Sac Blood Islands. Dev. Cell 11, 519–533.

Van Wilgenburg, B., Moore, M.D., James, W.S., Cowley, S.A., 2014. The productive entry pathway of HIV-1 in macrophages is dependent on endocytosis through lipid rafts containing CD4. PLoS One 9, 1–14.

Vanhee, S., De Mulder, K., Van Caeneghem, Y., Verstichel, G., Van Roy, N., Menten, B., Velghe, I., Philippe, J., De Bleser, D., Lambrecht, B.N., Taghon, T., Leclercq, G., Kerre, T., Vandekerckhove, B., 2015. In vitro human embryonic stem cell hematopoiesis mimics MYB-independent yolk sac hematopoiesis. Haematologica 100, 157–166.

Vo, L.T., Daley, G.Q., 2015. De novo generation of HSCs from somatic and pluripotent stem cell sources. Blood 125, 2641–2648.

Vodyanik, M.a., Bork, J.a., Thomson, J.a., Slukvin, I.I., 2005. Human embryonic stem cell-derived CD34+ cells: efficient production in the coculture with OP9 stromal cells and analysis of lymphohematopoietic potential. Blood 105, 617–26.

Vodyanik, M.a., Yu, J., Zhang, X., Tian, S., Stewart, R., Thomson, J.a., Slukvin, I.I., 2010. A mesoderm-derived precursor for mesenchymal stem and endothelial cells. Cell Stem Cell 7, 718–29.

Wang, L., Li, L., Shojaei, F., Levac, K., Cerdan, C., Menendez, P., Martin, T., Rouleau, A., Bhatia, M., 2004. Endothelial and hematopoietic cell fate of human embryonic stem cells originates from primitive endothelium with hemangioblastic properties. Immunity 21, 31–41.

Wang, L., Menendez, P., Shojaei, F., Li, L., Mazurier, F., Dick, J.E., Cerdan, C., Levac, K., Bhatia, M., 2005a. Generation of hematopoietic repopulating cells from human embryonic stem cells independent of ectopic HOXB4 expression. J. Exp. Med. 201, 1603–14.

Wang, Q., Stacy, T., Bindert, M., Marin-padillat, M., Sharpe, A.H., Speck, N.A., 1996. Disruption of the Cbfa2 gene causes necrosis and hemorrhaging in the central nervous system and blocks definitive hematopoiesis. PNAS 93, 3444–3449.

Wang, Y., Szretter, K.J., Vermi, W., Gilfillan, S., Rossini, C., Cella, M., Barrow, A.D., Diamond, M.S., Colonna, M., 2014. IL-34 is a tissue-restricted ligand of CSF1R required for the development of Langerhans cells and microglia. Nat Immunol. 13, 753–760.

Wang, Y., Yates, F., Naveiras, O., Ernst, P., Daley, G.Q., 2005b. Embryonic stem cell-derived hematopoietic stem cells. Proc Natl Acad Sci U S A 102, 19081–19086.

Watanabe, K., Ueno, M., Kamiya, D., Nishiyama, A., Matsumura, M., Wataya, T., Takahashi, J.B., Nishikawa, S., Nishikawa, S.i., Muguruma, K., Sasai, Y., 2007. A ROCK inhibitor permits survival of dissociated human embryonic stem cells. Nat. Biotechnol. 25, 681–6.

Wiles, M.V., Keller, G., 1991. Multiple haematopoietic lineages develop from embryonic stem (ES) cells in culture. Development 111, 259–267.

van Wilgenburg, B., Browne, C., Vowles, J., Cowley, S.a., 2013. Efficient, long term production of monocyte-derived macrophages from human pluripotent stem cells under partly-defined and fully-defined conditions. PLoS One 8, e71098.

van Wilgenburg, B., Scherwitzl, I., Hutchinson, E.C., Leng, T., Kurioka, A., Kulicke, C., de Lara, C., Cole, S., Vasanawathana, S., Limpitikul, W., Malasit, P., Young, D., Denney, L., Consortium, S.H., Moore, M.D., Fabris, P., Giordani, M.T., Oo, Y.H., Laidlaw, S.M., Dustin, L.B., Ho, L.P., Thompson, F.M., Ramamurthy, N., Mongkolsapaya, J., Willberg, C.B., Screaton, G.R., Klenerman, P., 2016. MAIT cells are activated during human viral infections. Nat. Commun. 7.

Woll, P.S., Martin, C.H., Miller, J.S., Kaufman, D.S., 2005. Human Embryonic Stem Cell-Derived NK Cells Acquire Functional Receptors and Cytolytic Activity. J. Immunol. 175, 5095–5103.

Wynn, T.a., Chawla, A., Pollard, J.W., 2013. Macrophage biology in development, homeostasis and disease. Nature 496, 445–455.

Wynn, T.a., Ph, D., Barron, L., 2011. Macrophages: Master Regulators of Inflammation and Fibrosis. Semin Liver Dis. 30, 245–257.

Xu M, J., Matsuoka, S., Yang, F.C., Ebihara, Y., Manabe, a., Tanaka, R., Eguchi, M., Asano, S., Nakahata, T., Tsuji, K., 2001. Evidence for the presence of murine primitive megakaryocytopoiesis in the early yolk sac. Blood 97, 2016–2022.

Yokomizo, T., Hasegawa, K., Ishitobi, H., Osato, M., Ema, M., Ito, Y., Yamamoto, M., Takahashi, S., 2008. Runx1 is involved in primitive erythropoiesis in the mouse. Blood 111, 4075–80.

Yokoyama, Y., Suzuki, T., Sakata-yanagimoto, M., Kumano, K., Higashi, K., 2009. Derivation of functional mature neutrophils from human embryonic stem cells. Blood 113, 6584–6592.

Yona, S., Kim, K.W., Wolf, Y., Mildner, A., Varol, D., Breker, M., Strauss-Ayali, D., Viukov, S., Guilliams, M., Misharin, A., Hume, D.A., Perlman, H., Malissen, B., Zelzer, E., Jung, S., 2013. Fate Mapping Reveals Origins and Dynamics of Monocytes and Tissue Macrophages under Homeostasis. Immunity 38, 79–91.

Yoshimoto, M., Montecino-rodriguez, E., Ferkowicz, M.J., Porayette, P., Shelley, W.C., Conway, S.J., Dorshkind, K., Yoder, M.C., 2010. Embryonic day 9 yolk sac and intra-embryonic hemogenic endothelium independently generate a B-1 and marginal zone progenitor lacking B-2 potential. PNAS 108, 1468–1473.

Yoshimoto, M., Porayette, P., Glosson, N.L., Conway, S.J., Carlesso, N., Cardoso, A.a., Kaplan, M.H., Yoder, M.C., 2012. Autonomous murine T-cell progenitor production in the extra-embryonic yolk sac before HSC emergence. Blood 119, 5706–14.

Yu, J., Vodyanik, M.a., Smuga-Otto, K., Antosiewicz-Bourget, J., Frane, J.L., Tian, S., Nie, J., Jonsdottir, G.a., Ruotti, V., Stewart, R., Slukvin, I.I., Thomson, J.a., 2007. Induced pluripotent stem cell lines derived from human somatic cells. Science (80-.). 318, 1917–20.

Yung, E., Sorin, M., Pal, a., Craig, E., Morozov, a., Delattre, O., Kappes, J., Ott, D., Kalpana, G.V., 2001. Inhibition of HIV-1 virion production by a transdominant mutant of integrase interactor 1. Nat. Med. 7, 920–6.

Zakrzewska, A., Cui, C., Stockhammer, O.W., Benard, E.L., Spaink, H.P., Meijer, A.H., 2010. Macrophage-specific gene functions in Spi1-directed innate immunity. Blood 116, e1–11.

Zambidis, E.T., Park, T.S., Yu, W., Tam, A., Levine, M., Yuan, X., Pryzhkova, M., Péault, B., 2008. Expression of angiotensin-converting enzyme (CD143) identifies and regulates primitive hemangioblasts derived from human pluripotent stem cells. Blood 112, 3601–14.

Zetoune, A.B., Fontanière, S., Magnin, D., Anczuków, O., Buisson, M., Zhang, C.X., Mazoyer, S., 2008. Comparison of nonsense-mediated mRNA decay efficiency in various murine tissues. BMC Genet. 9, 83.

Zigmond, E., Bernshtein, B., Friedlander, G., Walker, C.R., Yona, S., Kim, K.W., Brenner, O., Krauthgamer, R., Varol, C., Muller, W., Jung, S., 2014. Macrophage-restricted interleukin-10 receptor deficiency, but not IL-10 deficiency, causes severe spontaneous colitis. Immunity 40, 720–733.

Zigmond, E., Jung, S., 2013. Intestinal macrophages: Well educated exceptions from the rule. Trends Immunol. 34, 162–168.